THE SECOND INTERNATIONAL CONFERENCE ON MARS POLAR SCIENCE AND EXPLORATION

REYKJAVÍK, ICELAND
AUGUST 21–25, 2000

SECOND INTERNATIONAL CONFERENCE ON MARS POLAR SCIENCE AND EXPLORATION

Hosted by

University of Iceland

Sponsored by

Geological Survey of Canada
International Glaciological Society
Lunar and Planetary Institute
National Aeronautics and Space Administration
Reykjavík — European City of Culture in the Year 2000
University of Iceland

Conveners

Helgi Björnsson, Science Institute, University of Iceland
Stephen Clifford, Lunar and Planetary Institute
David Paige, University of California, Los Angeles
Thorsteinn Thorsteinsson, Alfred Wegener Institute and University of Iceland

LPI Contribution No. 1057

Compiled in 2000 by
LUNAR AND PLANETARY INSTITUTE

The Institute is operated by the Universities Space Research Association under Contract No. NASW-4574 with the National Aeronautics and Space Administration.

Abstracts in this volume may be cited as

Author A. B. (2000) Title of abstract. In *Second International Conference on Mars Polar Science and Exploration*, p. xx. LPI Contribution No. 1057, Lunar and Planetary Institute, Houston.

This report is distributed by

ORDER DEPARTMENT
Lunar and Planetary Institute
3600 Bay Area Boulevard
Houston TX 77058-1113
Phone: 281-486-2172
Fax: 281-486-2186
E-mail: order@lpi.usra.edu

Mail order requestors will be invoiced for the cost of shipping and handling.

Preface

This volume contains abstracts that have been accepted for presentation at the Second International Conference on Mars Polar Science and Exploration, August 21–25, 2000. The Scientific Organizing Committee consisted of Terrestrial Members Nobuhiko Azuma *(Nagaoka University of Technology)*, Dorthe Dahl-Jensen *(University of Copenhagen)*, David Fisher *(Geological Survey of Canada)*, Ralf Greve *(Darmstadt University of Technology)*, Einar H. Gudmundsson *(University of Iceland)*, Magnus T. Gudmundsson *(University of Iceland)*, Sigfus Johnsen *(University of Copenhagen)*, Thor Jakobsson *(Icelandic Meteorological Office)*, Werner Kuhs *(University of Göttingen)*, Heinz Miller *(Alfred Wegener Institute)*, Valerie Masson *(Laboratory of Climate and Environmental Sciences)*, John Nye *(University of Bristol)*, Helgi Torfason *(National Energy Authority, Iceland)*, and David Wynn-Williams *(British Antarctic Survey)*. Planetary Members included Wendy Calvin *(U.S. Geological Survey, Flagstaff)*, Michael Carr *(U.S. Geological Survey, Menlo Park)*, David Crisp *(Jet Propulsion Laboratory)*, James Cutts *(Jet Propulsion Laboratory)*, William Durham *(Lawrence Livermore National Laboratory)*, Fraser Fanale *(University of Hawai'i)*, Jack Farmer *(Arizona State University)*, James Garvin *(NASA Goddard Space Flight Center)*, Rejean Grard *(European Space Agency/ESTEC)*, Robert Haberle *(NASA Ames Research Center)*, Ken Herkenhoff *(U.S. Geological Survey, Flagstaff)*, Alan Howard *(University of Virginia)*, Hugh Kieffer *(U.S. Geological Survey, Flagstaff)*, Ralph Lorenz *(Lunar and Planetary Laboratory)*, Daniel McCleese *(NASA Jet Propulsion Laboratory)*, Michael Malin *(Malin Space Science Systems)*, James W. Rice Jr. *(University of Arizona)*, David Smith *(NASA Goddard Space Flight Center)*, Carol Stoker *(NASA Ames Research Center)*, Susan Smrekar *(NASA Jet Propulsion Laboratory)*, Peter Thomas *(Cornell University)*, Aaron Zent *(NASA Ames Research Center)*, and Maria Zuber *(Massachusetts Institute of Technology)*.

Logistical, administrative, and publications support were provided by the Publications and Program Services Department of the Lunar and Planetary Institute.

Contents

DETERMINATION OF MARTIAN NORTHERN POLAR INSOLATION LEVELS USING A GEODETIC ELEVATION MODEL. J. R. Arrell[1] and M. T. Zuber[1,2], [1]Department of Earth, Atmospheric and Planetary Sciences, Massachusetts Institute of Technology, Cambridge, MA 02139-4307 and [2]Laboratory for Terrestrial Physics, Code 920, NASA/Goddard Space Flight Center, Greenbelt, MD 20771; rarrell@mit.edu, zuber@tharsis.gsfc.nasa.gov.

Introduction. Solar insolation levels at the Martian polar caps bear significantly on the seasonal and climatic cycling of volatiles on that planet [1, 2]. In the northern hemisphere, the Martian surface slopes downhill from the equator to the pole [3, 4] such that the north polar cap is situated in a 5-km-deep hemispheric-scale depression. This large-scale topographic setting plays an important role in the insolation of the northern polar cap. Elevations measured by the Mars Orbiter Laser Alimeter (MOLA) [5] provide comprehensive, high-accuracy topographical information required to precisely determine polar insolation. In this study, we employ a geodetic elevation model to quantify the north polar insolation and consider implications for seasonal and climatic changes [3, 4].

Geodetic Elevation Model. The primary model used in this study is a geodetic elevation model (GEM) derived from MOLA data of the northern hemisphere [6]. The GEM is a topographical model that accounts for the curvature of the planet with minimal distortion.

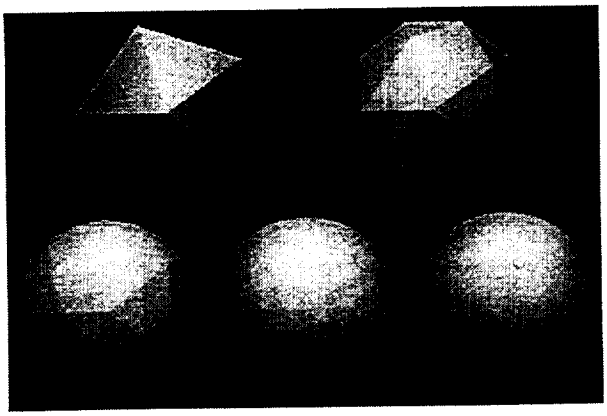

Fig. 1. Five trianglular meshes used for GEMs with increasing levels of resolution.

The GEM begins as an equilateral triangular grid wrapped around a sphere. Higher resolutions are achieved by repeatedly subdividing the triangles into four smaller triangles as shown in Fig. 1.

The final model is not necessarily spherical, even though the original grid is developed on a sphere. The radii are sampled, and the grid vertices are relocated to conform with the MOLA-derived radii of the planet. Fig. 2 shows an ellipsoid modeled by the GEM. Note that there is no evidence of spherical distortion. Some minor distortion is caused by morphing a spherical grid into to an arbitrary shape. However, by increasing the resolution of the grid, the effect of the distortion can be reduced until it is smaller than a single pixel.

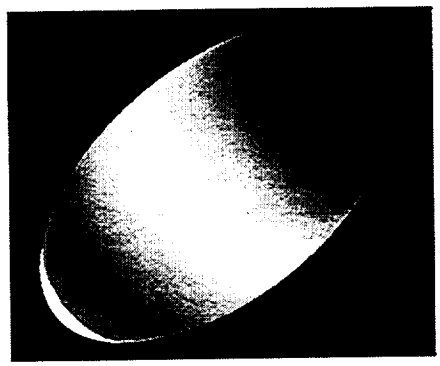

Fig. 2. Ellipsoid modeled with a GEM.

We incorporated the MOLA radii into the GEM to produce an accurate three-dimensional depiction of Mars from which solar lighting conditions can be accurately calculated. Fig. 3 shows several false color images of the shape of Mars during the northern summer solstice from the point of view of the sun.

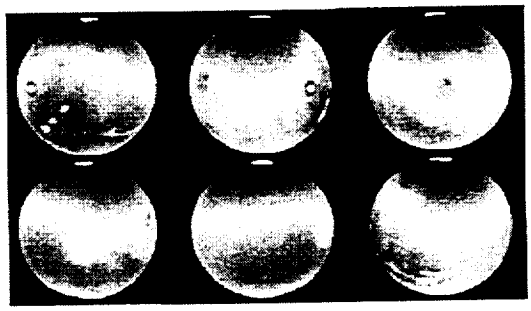

Fig. 3. Six false color images of the shape of Mars generated using the GEM.

Insolation and Seasons. Initial modeling quantifies the seasonal variability of polar insolation. The northern ice cap receives sunlight for only 45% of the Martian year, or just under 300 Martian days out of the 669-Mars day year. This is ~10% less than the 335 days that would be expected if Mars were spherical and smooth. This result implies that Mars' shape has a non-neglible effect on polar insolation. Fig. 4 shows a graph of the polar insolation levels for half the Martian

year, starting at peak insolation during the northern summer solstice.

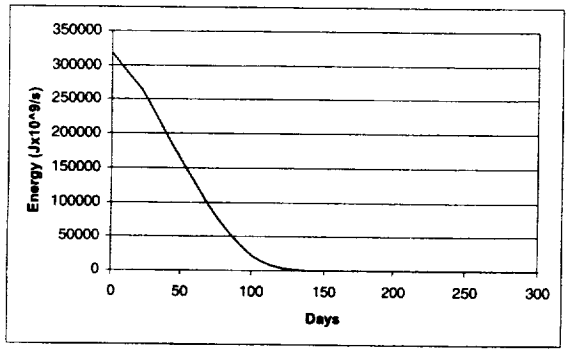

Fig. 4. Graph of solar energy input into the northern ice deposits during half the Martian year.

The amount of insolation drops off quickly, reaching 10% of the peak value after only 100 Martian days. Any climatic forcing that results from the increased insolation levels can only be active for a fraction of the Martian year.

These results are based on the amount of sunlight hitting the visible ice cap. In the northern hemisphere there is a strong correlation between visible ice deposits and elevation [7, 3]. There exists a 3-km elevation difference between the top of the ice deposits and the surrounding terrain [3]. This topography has an important effect on the amount of overall solar radiation reaching the ice deposits. Fig. 5 shows the polar insolation levels over the course of an entire day.

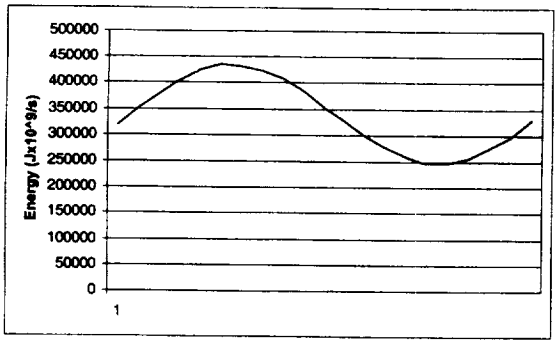

Fig. 5. Graph of solar energy input into the northern ice deposits during the course of a Martian day.

One of the primary causes of the daily variation in polar insolation is the asymmetry of the ice cap, illustrated in Fig. 6 [6]. Note that the ice reaches much farther south along the 0° E meridian than along the 180° E meridian.

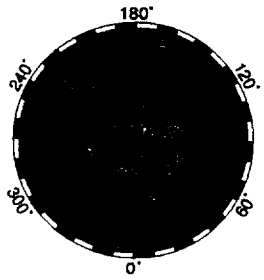

Fig. 6. Topographical map of the north pole of Mars, highlighting assymetry of ice deposits.

Insolation and Obliquity. The Martian surface contains a wealth of evidence pointing to the past presence of liquid water [8]. The fact that liquid water is unstable on Mars today represents evidence for a significantly different climate earlier in Martian history. A key factor in understanding the history of climate on Mars is quantifying the effect of varying the planetary obliquity on the volatile inventory. While the current obluquity of Mars (25.2°) is similar to that for Earth, in the past 10 Ma, the Martian obliquity is believed to have been as high as 45° [9]. Such a large planetary tilt would have significantly increased the amount of sunlight hitting the Martian poles, and would have had profound effects on the Martian climate [1, 2]. Using the MOLA data, we are calculating the polar insolation for a wide range of possible obliquities. In addition, we are modeling the insolation levels on the southern ice cap. This process is significantly more labor intensive, because, unlike the northern ice deposits, the presence of ice deposits in the south does not correlate with elevation [4].

It is hoped that this work will produce a comprehensive dataset of Mars' polar insolation levels that can be used in future studies of the past and present climatological and hydrological processes.

References: [1.] Leighton R.B. and B.C. Murray (1966) *Science, 153,* 136-144. [2.] Fanale, F. et al. (1992) in *Mars*, ed. H. Kieffer, B. Jakosky, C. Snyder, & M. Matthews, Univ. Ariz. Press, 1135-1179. [3.] Zuber M. T. et al., (1998) *Science, 282,* 2053-2060. [4.] Smith D. E. et al. (1999) *Science, 284,* 1421-1576. [5.] Zuber M. T. et al. (1992) *JGR, 97,* 7781-7797. [6.] Zuber M. T. et al. (2000) *Science, 287,* 1788-1793. [7.] Thomas P. et al. (1992) in *Mars*, ed. H. Kieffer, B. Jakosky, C. Snyder, & M. Matthews, Univ. Ariz. Press, 767-795. [8.] Carr, M. H. (1996) *Water on Mars,* Oxford Univ. Press. [9.] Touma J. and J. Wisdom (1993) *Science, 259,* 1294-1297.

ICE-RICH DEBRIS APRONS AND LOBATE CRATER : DIGITAL ELEVATION MODELING DERIVED FROM VIKING IMAGES. D. Baratoux[1], C. Delacourt[1], N. Mangold[2] and P. Allemand[1], [1]Laboratoire des sciences de la Terre UMR 5570,CNRS, Université C. Bernard Lyon I et ENS-Lyon, 43 Bd du 11 Novembre 69 622 Villeurbanne CEDEX, France, baratoux@univ-lyon1.fr, [2]Equipe planétologie, UMR 8616, CNRS Univ. Paris-Sud, 91405 Orsay CEDEX, France, mangold@geol-u.psud.fr

Introduction: We present a new method to derive Digital Elevation Model (D.E.M.) from Viking images and two applications for ice supply studies in the Martian soil. Our objectives has been defined in respect of the knowledge of the Martian topography. While Mola provide extremely well-controlled and high-precise topographic data over the whole surface of Mars, resolution is limited by the distance between ground tracks. Even if improvements were made in removing severe offset in cartographic products [1] data consistency between different missions is still a problem. The method has been divided in two steps : the correlation algorithm and camera adjustment for D.E.M. processing.

Image correlation : According to the expected vertical precision map from Viking images computed by R. Kirk [2], sub-pixel accuracy is required in image correlation to provide significant results. The phase-correlation algorithm [3,4], based on Fourier transform has been adapted to overcome several difficulties in the case of Viking imagery. For instance, resampling and local geometric transformation of images has been applied because of different resolution and geometry. Ground seasonal changes and Vidicon camera properties produce a noisy correlation signal that has been removed by band pass filtering. Selection of homologous points results in a data set of points that density depends on roughness and topography of the area (fig. 1). Flat and smooth area are difficult to correlate because of a near constant grey level over the surface. Interpolation in these area can compensate the lack of points.

Camera adjustment : In a second step, camera angles and positions must be adjusted and this has been achieved by relative orientation method [5]. Not enough accurate ground control points are available and even if control points were provided, a sub-pixel registration of images would be required to update camera angles and position which is difficult to realize. The relative orientation method takeS advantage of sub-pixel accuracy of our correlation algorithm and is only based on the coplaneity relation. This mathematical equation expresses the fact that two vectors on homologous rays are in the same plane. No control points are needed at this step.

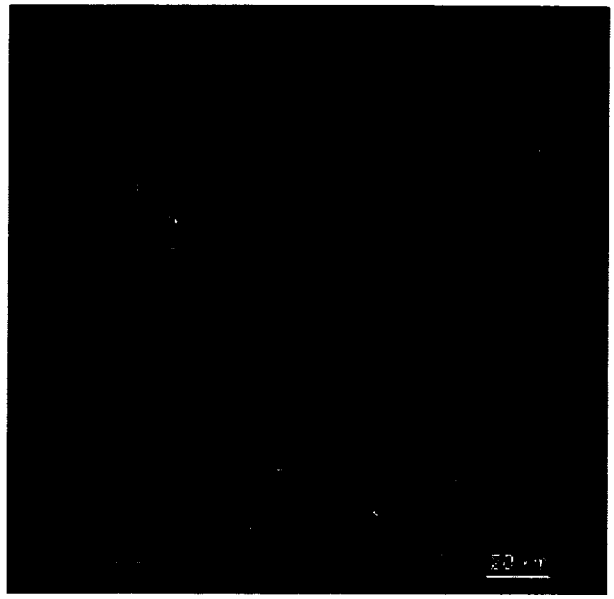

Figure 1 : Map of points used for processing the D.E.M. from images 529a05 and 675b62. A strong difference in roughness between mesa and low-elevation area is detected by the correlation algorithm.

The key of this technique is the choice of the best correlated points from the data set of homologous points. This is achieved by fitting coplaneity values along the lines of the image when camera angles and positions contain small errors. The improvement at the end of this adjustment can be estimated from the intersection distance (fig. 2) between lines of sight in both images (which is equal to 0 for each point when correlation values are exact). 5 from the 12 unknown orientation parameters (three coordinates for the position and three angles for each camera) are solved at the end of the relative orientation. The D.E.M. is processed at this step in a unknown frame and has to be transformed by rotation, translation and scale factors : the 7 parameters of this geometric transformation have to be computed from control points extracted with the MDIM files, altitude can be estimated from Mola topographic profile in the neighborhood. Consequently, the expected vertical precision can be attained in relative height. Errors in absolute altimetry and planimetry are only connected with accuracy and number of control points. A more accurate absolute adjustment will be processed when new Mola data will be available.

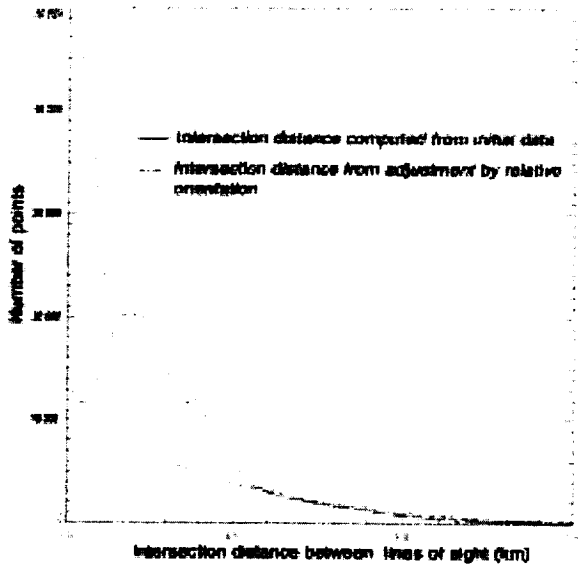

Figure 2 : Histogram of intersection distance before and after relative orientation of images. The relative orientation has been computed from 42 selected points in images 529a05 and 675b62.

Discussions : Validation of the method has been done by comparison with Mola data [6]. This technics has been applied to the interesting area of Deuteronilus Mensae in which the relief is due to glacial processes. These results are presented in a companion paper [7]. Topographic data from Mola in this area (fig. 3) does not allow direct comparison because no mola track are available on the overlaping area at present time. However, altitude range of mesa obtained by both method are in good agreement (fig. 4).

According to most of the recent studies of lobate crater and since these craters was first obseved from Viking images[8], ejecta emplacement is interpreted by debris-flow processes and sub-surface volatiles. We think that detailed topographic data are required to elaborate physical models, and to obtain new insights into sub-surface properties. We present a D.E.M. computed for a lobate crater as an other example of the usefulness of our D.E.M. processing method from Viking images.

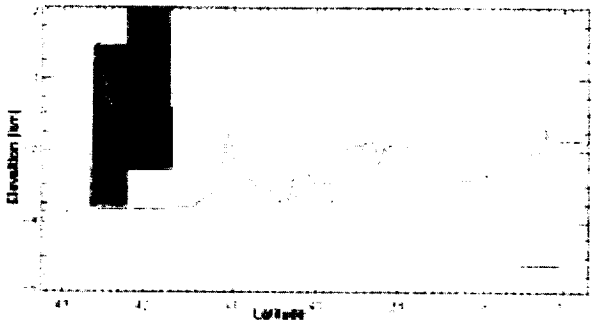

Figure 3 : Topographic data from Mola track ap00253

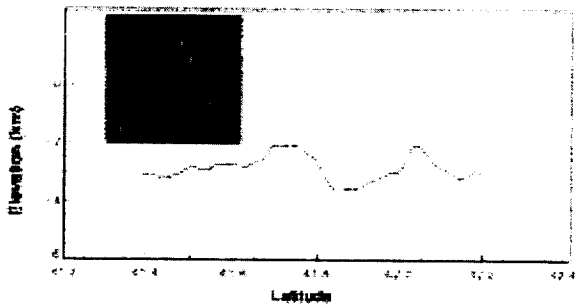

Figure 4 : Topographic profile extracted from the D.E.M.

References:

[1] Zeitler W. and Oberst J. (1999) J.Geophys.Res., 104, 14,051-14,063

[2] Kirk R. (1999) Fifth international conference on Mars, Pasadena, California.

[3] Schaum A. and McHugh M. (1991) NRL report 9298.

[4] Michel R. PhD Thesis (1997), Univ. Paris XI

[5] Kraus K. and Waldhaüsl (1998), Manual of photogrammetry, Hermes.

[6] Baratoux D., Allemand P., Delacourt . Martian Digital Elevation Model derived from Viking images, submitted to J. Geophys. Res.

[7] Frey V. Baratoux D., Mangold N., this volume

[8] M.H. Carr, L.S. Crumper, J.A. Cutts, R. Greeley, J. E. Guest and H. Masursky (1977), J. Geophys. Res., 82, 4055-4065

THE CURRENT ATMOSPHERIC CIRCULATION AND CLIMATE OF MARS: THE POLAR REGIONS. J. R. Barnes, College of Oceanic and Atmospheric Sciences, Oregon State University, Corvallis, OR, 97331, barnes@oce.orst.edu.

New data from MGS and a host of modeling investigations are significantly expanding our understanding of the current atmospheric circulation and climate of Mars. The determination of an accurate global topography by the MOLA Experiment and improved observations of surface thermal inertia and visual albedo by the TES Experiment are extremely important for this progress, as are of course the TES and RS thermal and compositional data. The MOC imagery are providing an unprecedented visual view of various dynamic phenomena, especially in the polar regions.

The current Mars atmospheric circulation is fundamentally similar in nature to that on the Earth, accounting for the absence of oceans. The latter simplifies the climate system considerably, particularly for variations on interannual time scales. However, the presence of two multiple-phase atmospheric constituents, water and carbon dioxide, is an added complexity, as is the presence of suspended dust that can dramatically alter the global atmospheric circulation on very short time scales. Our understanding of the current climate system points to key roles for carbon dioxide, water, and dust, with the interactions both in the atmosphere and on the surface between the three being very complex. The importance of surface-atmosphere interactions for these three species, along with the role of microphysical processes in the atmosphere, makes regional and small-scale processes potentially critical to the system. This makes the climate modeling challenge a formidable one, with modelers only just now beginning to attack the problems of fully-coupled dust, water, and carbon dioxide processes, and problems of smaller-scale circulation systems and processes. The latter may be especially crucial to understanding the polar regions.

Various aspects of our present understanding of the atmospheric circulation and climate system of Mars and the polar regions will be discussed, with an emphasis on the new data and the new modeling efforts. Key problems, issues, and areas for future study will be highlighted.

THE CONTRIBUTION OF WATER ICE CLOUDS TO THE WATER CYCLE IN THE NORTH POLAR REGION OF MARS: PRELIMINARY ANALYSIS. D. S. Bass[1] and L. K. Tamppari[2], [1]Southwest Research Institute, P.O. Drawer 28510, San Antonio, TX, 78228-0510, USA, dsb@kronos.space.swri.edu, [2]Jet Propulsion Laboratory, M/S 264-538, 4800 Oak Grove Dr., Pasadena, CA 91109, USA, leslie.tamppari@jpl.nasa.gov.

While it has long been known that Mars' north residual polar cap and the Martian regolith are significant sources of atmospheric water vapor, the amount of water vapor observed in the northern spring season by the Viking Mars Atmospheric Water Detector instrument (MAWD) cannot be attributed to cap and regolith sources alone [1]. [2] suggested that ice hazes may be the mechanism by which additional water is supplied to the Martian atmosphere. Additionally, a significant decrease in atmospheric water vapor was observed in the late northern summer that could not be correlated with the return of the cold seasonal CO_2 ice. While the detection of water ice clouds on Mars [e. g., 3] indicate that water exists in Mars' atmosphere in several different phases, the extent to which water ice clouds play a role in moving water through the Martian atmosphere remains uncertain.

Work by [4] suggested that the time dependence of water ice cap seasonal variability and the increase in atmospheric water vapor depended on the polar cap center reaching 200K, the night time saturation temperature (Figure 1). Additionally, they demonstrated that a decrease in atmospheric water vapor may be attributed to deposition of water ice onto the surface of the polar cap (Figure 2); temperatures were still too warm at this time in the summer for the deposition of carbon dioxide. However, whether water ice clouds contribute significantly to this variability is unknown.

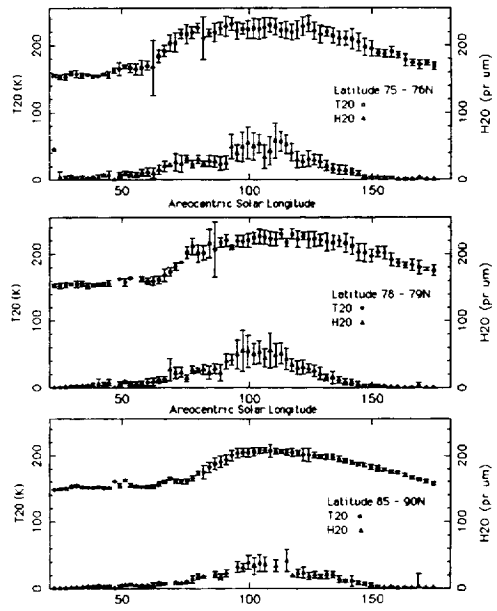

Figure 1. Viking IRTM T_{20} data and Viking MAWD atmospheric water vapor data. Note the peak of water vapor occurs at the same time in the summer regardless of the latitude. There is no gradual increase of water vapor in the atmosphere as the carbon dioxide cap sublimes (by L_s = 81.55) as would be expected if the source of water were directly associated with the regolith. Both datasets were binned in intervals of five Julian days and those dates were converted to areocentric solar longitude. Both datasets were binned in intervals of five Julian days and those dates were converted to areocentric solar longitude. Average values are plotted with error bars of plus and minus one standard deviation. Top graph shows zonally averaged latitude band 75 - 76N. Middle graph shows averaged latitude band chosen to cover only the dark polar sand sea--region is 78 - 79N, 265 - 330W. Bottom graph shows zonally averaged latitude band 85- 90N.

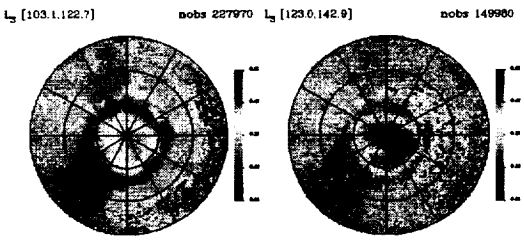

Figure 2. IRTM albedo maps showing increase in brighteness of northern residual water ice cap as summer season progresses. "Nobs" refers to the number of observations present in each map. Maps show data binned in increments of 40 Julian days and those dates are converted to areocentric solar longitude. Data are binned in 2 degree by 2-degree intervals. Albedos range from 0.12 (blue) to 0.60 (red).

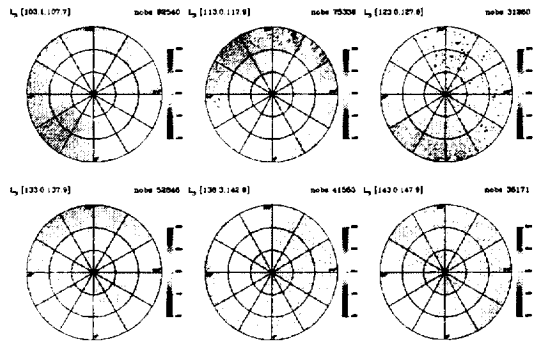

Figure 3. Six IRTM T_{20} surface temperature polar maps showing decreasing temperatures as summer season ends. Maps show all data binned in increments of 10 Julian days and those dates are converted to areocentric solar longitude. Each particular map shown was chosen to represent the data closest to the areocentric solar longitudes of the images in Part I: Fig. 2. "Nobs" refers to the number of observations present in each map. Temperatures range from 100 K (blue) to 300 K (red).

In a companion abstract, we describe our technique for identifying water ice clouds in the north polar region of Mars and present the resulting water ice cloud maps [5]. Here, we present preliminary results of a correlative study of Viking Orbiter imaging observations, Infrared Thermal Mapper (IRTM) and Mars Atmospheric Water Detector (MAWD) data of the north residual polar cap to provide additional constraints on Mars' water cycle.

For example, water ice clouds near the periphery of the residual north polar cap have been observed in Viking Orbiter IRTM data in the late summer season (Figure 4).

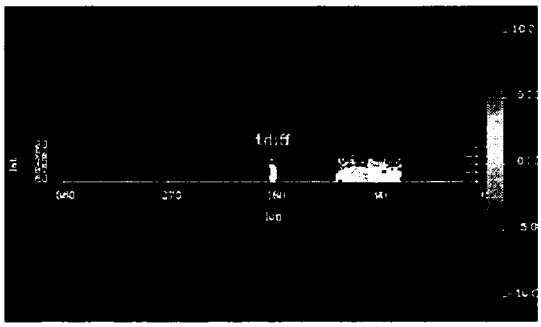

Figure 4. Water-ice clouds in the north polar cap region for L_s ~117°. West longitude is shown along the x-axis and latitude from 60-90°N is shown along the y-axis. Black indicates no data were present and white indicates where data were present, but no water-ice clouds were present. The cloud signature is shown in blues according to the temperature scale on the right. This signature is the result of differencing the 11 and 20 μm channel data after removing the surface spectral emissivity surface. Darker blues imply a thicker or colder water-ice cloud.

We have located Viking imaging data that show clouds in the northern summer season, providing ground-truth for cloud identification (Figure 5) [6]. Additional results will be presented.

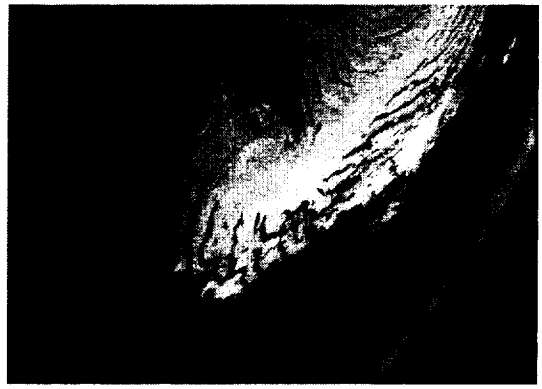

Figure 5. Viking Orbiter wide angle image (811A01) acquired with red filter. Clouds appear over the south east portion of the cap. A linear contrast stretch was employed.

[1] Jakosky, B. M. (1983) *Icarus 55*, 19-39. [2] Kahn, R. (1990) *J. Geophys. Res. 95(B9)*, 14677-14693. [3] Ibid; Tamppari, L. K. et. al. (2000) *J. Geophys. Res. 105(E2)*, 4087-4107. [4] Bass, D. S. *et. al.* (2000) *Icarus, 144*, 382-396; Bass, D. S. and D. A. Paige (2000) *Icarus 144*, 397-409. [5] Tamppari, L. K. and D. S. Bass (2000) 2nd International Conference on Mars Polar Science and Exploration, Aug. 21-25. [6] Tamppari, L. K. et. al. (2000) *J. Geophys. Res. 105(E2)*, 4087-4107.

JÖKULHLAUPS IN ICELAND: CHARACTERISTICS AND IMPACT. H. Björnsson, Science Institute, Department of Geophysics, University of Iceland, Hofsvallagötu 53, IS-107 Reykjavík, Iceland. E-mail: hb@raunvis.hi.is

Introduction: Glacier outburst floods, jökulhlaups, are frequent in Iceland. They can be traced to three types of sources: to subglacial lakes at geothermal areas, to meltwater drained during volcanic eruptions and to marginal ice dammed lakes. Jökulhlaups are major events; they may profoundly affect landscape and they threaten human life and property. In Iceland, jökulhlaups have caused loss of lives, ruined farms and cultivated land, and devastated large vegetated areas. They threaten roads, bridges and hydroelectric power plants on glacier-fed rivers. Their effects on landscape are seen in the erosion of large canyons and in the transport and deposition of sediments over sandur deltas. The present lecture gives an overview of jökulhlaups in Iceland, their sources, triggering and drainage [1].

Volcanically Triggered Floods: Since the time of the settlement of Iceland (870 A.D.), at least 80 subglacial volcanic eruptions have been reported, many of them causing tremendous jökulhlaups. The peak discharge of the largest floods (from Katla beneath the Mýrdalsjökull ice cap) has been estimated at the order of 100-300,000 $m^3 s^{-1}$, duration was 3 -5 days and the total volume of the order of 1-8 km^3. Some of the floods may have consisted of a hyperconcentrated fluid-sediment mixture. The potentially largest and most catastrophic jökulhlaups may be caused by eruptions in the voluminous ice-filled calderas in northern Vatnajökull (of Bárdarbunga and Kverkfjöll). They may be the source of prehistoric jökulhlaups, with estimated peak discharge of 400,000 $m^3 s^{-1}$.

Subglacial Lakes: A few of the volcanoes contain geothermal systems maintaining permanent depressions, underlain by subglacial lakes that drain periodically in outburst floods. The best known depressions at geothermal areas are the Grímsvötn depression and the Skaftá cauldrons. Ice drains toward the Grímsvötn depression from an area of 160 km^2 where a geothermal system continuously melts ice at the rate of 0.2-0.5 $km^3 a^{-1}$ during normal times. The meltwater is trapped in a lake at the bed and normally the 250 m thick ice cover that floats on the lake rises 10-15 m per year. The seal is broken when the lake level has risen typically 80-150 m and the water flows 50 km beneath the glacier down to the Skeidarársandur outwash plain. Outburst floods from Grímsvötn have occurred at 1 to 10 year intervals, with a peak discharge of 600 to 40,000 $m^3 s^{-1}$ at the glacier margin, a duration of 2 days to 4 weeks and a total volume of 0.5 to 4.0 km^3. Typically the discharge increases approximately exponentially but having reached the peak, the discharge falls more rapidly. General models of discharge of jökulhlaups give in many respects satisfactory simulations for jökulhlaups from Grímsvötn. The best fit is obtained for the Manning roughness coefficients n = 0.08-0.09 $m^{-1/3}$ s. An empirical power law relationship is obtained between peak discharge and total volume of the jökulhlaups from Grímsvötn; $Q_{max} = K V_t^b$, where Q_{max} is measured in $m^3 s^{-1}$, V_t in $10^6 m^3$, $K = 4.15\ 10^{-3}\ s^{-1}\ m^{-2.52}$ and b = 1.84.

The two Skaftá cauldrons are situated at geothermal systems, 10-15 km to the northwest of Grímsvötn. Since 1955, at least thirty jökulhlaups have drained from the cauldrons to the river Skaftá. The ice cauldrons are approximately circular. The centre of the eastern cauldron subsides by about 100-150 m in a jökulhlaup draining a volume of 0.2-0.4 km^3 of water; the other cauldron by 50-100 m and drains a volume of 0.05-0.16 km^3. The period between these drainage events is about 2 to 3 years for each cauldron. The ice drainage area of the western and the eastern cauldrons have been estimated at 33 km^2 and 58 km^2, respectively. Typically the discharge risers rapidly and recedes slowly; form is in that respect a mirror image of the typical Grímsvötn hydrograph. The reservoir water temperature may be well above the melting point (10-20 °C) and the flowing water seems not to be confined to a tunnel but spread out beneath the glacier and later gradually collected back to conduits.

Marginal Lakes: At present, jökulhlaups originate from some fifteen marginal ice-dammed lakes in Iceland. Typical values for peak discharges are 1,000-3,000 m^3/s, duration 2-5 days and total volumes of 2,000 x 10^6 m^3. Hydro-graphs for jökulhlaups from marginal lakes have a shape similar to those of the typical Grímsvötn jökulhlaup.

References: [1] Björnsson, H. *Ann. Glaciol.* 16, 95-106.

THE KATLA SUBGLACIAL VOLCANO: TOPOGRAPHY AND FLOW PATHS OF JÖKULHLAUPS. H. Björnsson, F. Pálsson and M.T. Gudmundsson, Science Institute, Department of Geophysics, University of Iceland, Hofsvallagötu 53, IS-107 Reykjavík, Iceland. E-mail: hb@raunvis.hi.is

The bedrock topography of the Myrdalsjökull ice cap has been mapped with radio echo-soundings. The ice cap is located at the southern tip of the eastern volcanic zone in Iceland, which is propagating southwards. The ice cap is underlain by a huge caldera that has erupted 20 times during the last 1100 years. The rims of the caldera encircle an area of 110 km^2. The caldera is 600 to 750 m deep; the lowest elevation of the floor is 650 m a. s. l. and the highest rims rise to 1400 m. Three outlet glaciers have eroded 300 to 500 m deep breaches in the crater rim. The difference in morphology between the northern and southern caldera floor may reflect the level of subglacial volcanic activity. The northern floor is deeper and more level (an area of 25 km^2 below 800 m) whereas the southern floor is more rugged and elevated (subglacial ridges and mounts rise above 1100 m surrounded by depressions down to 750 m). A row of craters, trending NNW, is seen 2 km within the eastern rim of the caldera. The last eruption site (of 1918 A.D.) is situated at the eastern part of the caldera, beneath 400 m thick ice. A number of ridges radiate out from the caldera, however, none towards south. One ridge strikes W towards the neighbouring volcano Eyjafjallajökull and a second ridge strikes E from the eastern rim of the caldera. Ridges also radiate towards NW, N, and NE from the caldera. A linear depression, bounded by steep slopes, 150 m deep and 1.5 km wide, strikes NE towards the volcanic fissure Eldgjá which produced a lavaflow of 14 km^3 in 930 A.D. Presently, geothermal activity is displayed by twelve small depressions in the glacier surface (of diameter up to 1 km). Meltwater is accumulated beneath two or three of these cauldrons and frequently drained in small outburst floods (jökulhlaups). From an area of 70 km^2 within the caldera, meltwater is drained down to Myrdalssandur, as did 18 of 20 recorded jökulhlaups in historical times; from 20 km^2 down to Solheimasandur as 2 of the jökulhlaups; the third route was taken by a jökulhaup in 1600 B.P.

References: H. Björnsson, F. Pálsson & M.T. Gudmundsson (1994) *EOS Trans.* 74 (16).

SCIENTIFIC OBJECTIVES OF THE MARS SURVEYOR 2001 GAMMA-RAY SPECTROMETER. W.V. Boynton[1], W.C. Feldman[5], J.I. Trombka[4], C. d'Uston[2], I. Mitrofanov[6], J.R.Arnold[3], Englert P.A.J., Metzger A.E.[7], R.C. Reedy[5], S.W. Squyres[8], H. Wänke[9], S.H. Bailey[1], J. Brückner[9], L.G.Evans[4], D. Hamara[1], R. Starr[4], and C. W. Fellows[1]. [1]Lunar and Planetary laboratory, University of Arizona, Tucson, Arizona, [2]Centre d'Etude Spatiale des Rayonnements, CNRS/UPS, Toulouse, France, [3]Department of Chemistry, University of California, San Diego, La Jolla, [4]NASA Goddard Space Flight Center, Greenbelt, Maryland, [5]Los Alamos national Laboratory, Los Alamos, New Mexico, [6]Cosmic Research Institute (IKI), Moscow, Russia, [7]Jet Propulsion Laboratory, California Institute of Technology, Pasadena, [8]Center for Radiophysics and Space Research, Cornell University, Ithaca, New York, [9]Max Planck Institute für Chemie, Mainz, Federal Republic of Germany.

Introduction: The Gamma-Ray Spectrometer (GRS) is one of the instruments on the Mars Surveyor 2001 Orbiter, which is part of NASA's Mars-Surveyor program. The GRS is really an instrument suite consisting of the GRS, a neutron spectrometer (NS) and a high-energy neutron detector (HEND). Each of these instruments/sensors are remotely mounted at different locations on the spacecraft and connect to a central electronics box. The GRS will achieve global mapping of the elemental composition of the surface and the abundance of hydrogen in the shallow subsurface. It is an updated design using the same technology as the lost Mars Observer mission (Boynton et al., 1992).

The Martian surface is continuously bombarded by cosmic ray particles; their interactions with the constituents of the soil produces nuclear reaction cascades with fast neutrons being the main secondaries. Those neutrons interact in turn with the nuclei of the elements that make up the soil and they eventually get slowed to thermal energies. In this process they leave the nuclei in an excited state that decays via the emission of characteristic gamma rays. All these processes are precisely known (Reedy, 1978) and have been simulated by means of numerical models (Masarik and Reedy, 1994; Drake et al., 1994; Gasnault and d'Uston, 1999). Thus, remote gamma-ray spectroscopy is a useful method for quantitatively measuring the geochemical composition of the surface down to a few 10s of g/cm^2 (Evans et al. 1993).

Scientific objectives: The major scientific goal of the GRS set of instruments is to determine quantitatively the elemental abundances of the Martian surface. The elements that the gamma-ray spectrometer will measure are those that are naturally radioactive (Th, U, K) and all those that are excited by neutrons and produce a significant flux of gamma rays (H, O, C, Si, Mg, Cl, Fe, Ca, S,...). The neutron spectrum is sensitive to carbon and hydrogen, elements which are particularly effective at slowing the neutrons, and on iron, titanium and some rare-earth elements, which capture the thermal neutrons. Using both gamma-ray data, which determines H over a depth of about 15cm, and neutron data, which determine H over a depth of about 1meter, the amount of ice and its depth of burial will be derived.

The resulting geochemical composition will be mapped over the entire planet surface with a spatial resolution up to 300km. In addition to mapping elemental abundances, the distribution of water and its near surface stratigraphy will be determined, and the depth of the seasonal polar caps and their variation with time will be evaluated. Because the gamma-ray flux is very weak, ranging between 0.01 to 0.0001 photons/cm^2/s, we are statistics limited. For the weakest gamma-ray emissions, our spatial resolution will be degraded in order to build up better statistics over a larger area on the surface.

This investigation will contribute to understanding the origin of the planet, its geologic evolution and its current state in particular in terms of distribution of volatiles.

- Because K, Th and U are incompatible elements that do not change ratios with geochemical processes, and given the fact that K is volatile and Th is not, then the K/U ratio is indicative of the temperature of the materials that formed Mars and will provide constraints on the origin of the planet.

- Concerning the evolution of the planet, the major element analysis of the main geologic regions of the planet will allow us to define what compositional characteristics distinguish the highlands from the lowlands in relation with the Martian North-South dichotomy. This analysis of the chemical composition of the volcanic terrains is related to the erupted magmas and can be used to probe the interior of the planet.

- Measurements of H and C will lead to determine the distribution of H_2O and CO_2 ices in terms of location, superficial extent, depth and time (Evans and Squyres, 1987).

- The seasonal polar cap thickness will be determined up to about 2 meters, which will significantly contribute to the evaluation of the sinks and sources of these volatile species and constrain the atmospheric circulation models.

- Questions on past history of volatiles will be addressed by searching for ancient salt deposits of nitrates or chlorides if they existed.

- In relation with the inventory of past volatiles and their present fate, Martian carbonates deposits will also be detected owing to the combination of gamma ray and neutron measurements (Feldman and Jakosky, 1991).

Instrument description: As noted earlier, the GRS instrument suite consists of 4 main subsystems : the gamma-ray spectrometer sensor head, the neutron spectrometer (NS), the high energy neutron detector (HEND) and the central electronics box (CEB).

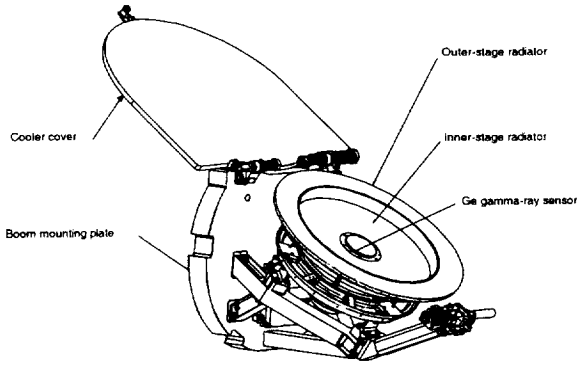

Fig. 1. Gamma-Ray Sensor Head

The gamma-ray sensor head is mounted on a 6.3 meter boom in order to minimize the interference of the signal from the spacecraft. The sensor is based on a large (67 mm long x 67 mm diameter) high-purity n-type germanium detector (HPGe). The sensor is a germanium crystal, encapsulated in a sealed titanium canister, made by EURISYS MESURES Company in Strasbourg (France) . Chemically pure titanium has been selected in order to minimize interferences with aluminum measurements since aluminum, which is also a common alloying element used with titanium, would otherwise be the classical choice for building such a canister. This type of detector provides unequaled high energy resolution of ≤2.3 keV @ 1.33MeV; its large volume results in the necessary high detection efficiency (≥54% efficiency relative to a 3"x3" NaI detector). The first stage electronics with pulse preamplifier, the test pulse driver and the pulse shaping amplifier is located in close vicinity of the detector canister. The rest of the analog pulse processing system together with high voltage power supply are part of the CEB mounted in the spacecraft. This detector must operate at temperatures below 130K, nominally at ~85K. This low temperature is achieved by means of a two stage passive cooler that was manufactured for us by A.D. Little Company of Cambridge (Mass.). An annealing capability is implemented in order to remove the expected energy resolution degradation that will arise due to radiation damage from the long exposure in space (Brückner et al., 1991). Also included in the design is a door to cover the radiator. The door, when opened, allows the cooling surfaces to radiate to space; when closed, the door allows the sensor to be heated for annealing. This mechanism was provided by Swales Aerospace of Beltsville (Maryland). The total mass of the sensor head on the end of the boom is 14.2 kg.

The neutron spectrometer consists of 4 borated plastic scintillators and photomultipliers. The scintillators are arranged so that the orientation of the faces relative to the spacecraft velocity vector will be fixed throughout the mapping orbit. Because the Mars Surveyor spacecraft will travel faster than a thermal neutron, it will be possible to use the Doppler filter technique to separate thermal and epithermal neutrons (Feldman and Drake, 1986). The Doppler filter spectroscopy will provide 3 filters and correlated double-interaction events will provide 16 energy channels for fast neutrons. This instrument also consist of preamplifiers, support electronics, signal processing, and a high voltage power supply for the photomultiplier tubes. Its total mass is 3.7 kg and it will be mounted on a small platform to give it a clear field of view. The neutron spectrometer is fabricated by the Los Alamos National Laboratory.

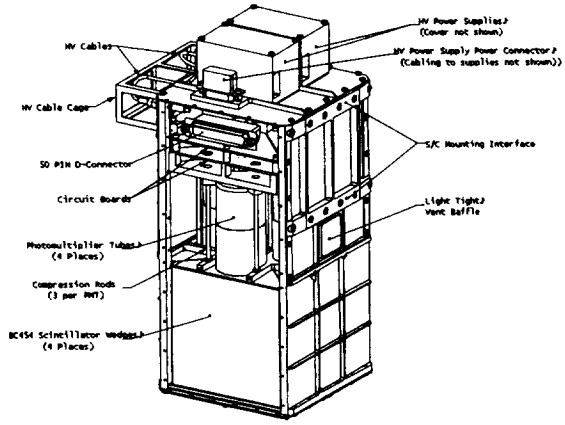

Fig. 2. Neutron Spectrometer Sensor Head

The High energy neutron detector (HEND) consists of 4 sensors . The first three are ^{3}He counters, two of which are surrounded by polyethylene moderators, and take neutron measurements in the range 10^{-2} to 1 eV, 1 to 10^3 eV, and 1 to 10^3 keV. A forth sensor made of stilben scintillator will measure high energy neutrons in the range 1 to 10 MeV. A fast photomultiplier provides the capacity to distinguish between counts from neutrons and counts from photons by pulse-shape discrimination. An outer CsI scintillator associated to a photomultiplier serves as an active anticoincidence detector to reject charged particle contribution to the neutron counts. This also serves the purpose of a back-up measure of the gamma ray spectrum. With its electronics, the mass of this instrument is 3.6 kg; it will be mounted on the instrument deck of the spacecraft. HEND is provided by the Cosmic Research Institute of Moscow.

References: Boynton W. V. et al., J. Geophys. Res., 97, 7681-7698 (1992). Brückner J. et al., IEEE Trans. Nucl. Sci., NS-38, 209-217 (1991), Drake D. M. et al., Nucl. Instrum. Methods Phys. Res.,B84, 337-356 (1994), D'Uston C. et al ., Nature, 341, 598-600 (1989), Evans L. G. and Squyres S. W., J. Geophys. Res., 92, 9153-9167 (1987), Evans L. G., Reedy R. C., Trombka J.I., in *Remote Geochemical Analysis: Elemental and Mineralogical Composition*, ed. C. Pieters and P. Englert, Cambridge University Press, 167-196 (1993), Feldman W.C. and Drake D.M., Nucl. Instrum. Meth. Phys. Res., A245, 182-190 (1986), Feldman W. C. and Jakosky B. M., J. Geophys. Res., 96, 15589-15598 (1991), Gasnault O. and d'Uston C., Mars Exploration Symposium, Paris, (Feb, 1999), Masarik J. and Reedy R.C., In LPSC 25, Lunar and Planetary Institute, Houston, 845-846 (1994), Reedy R. C., In LPSC 9, Pergamon Press, 2961-2984 (1978), Surkov Yu. A. et al., Cosmic Research, 18, 453-460 (1981), Surkov Yu. A. et al., Nature, 341, 595-598 (1989), Trombka J. I. et al., In LPSC 22, Lunar and Planetary Institute, Houston, 23-29 (1992).

LARGE GROOVES IN THE SOUTH POLAR LAYERED DEPOSITS: INSIGHTS FROM SPACECRAFT DATA AND TERRESTRIAL ANALOGS. N. T. Bridges[1] and K. E. Herkenhoff[2], [1]Jet Propulsion Laboratory 183-501, California Institute of Technology, 4800 Oak Grove Drive, Pasadena, CA 91109 (Nathan.Bridges@jpl.nasa.gov), [2]U. S. Geological Survey, 2255 N. Gemini Drive, Flagstaff, AZ 86001 (kherkenhoff@usgs.gov)

Introduction: The Martian polar layered deposits (PLD) are probably the best source of information about the recent climate history of Mars [1-8], but their origin and the mechanisms of accumulation are still a mystery [9]. The polar layers are sedimentary deposits that most planetary scientists believe are composed of water ice and varying amounts of wind-blown dust [3-5], although their composition is poorly constrained [10]. Interpretation of the observed polar stratigraphy in terms of global climate changes is complicated by the significant difference in surface ages between the north and south PLD inferred from crater statistics [2,8,11].

The study reported here was undertaken as part of the landing site selection effort for the Mars Polar Lander (MPL) and Deep Space 2 (DS2) missions that made use of all available data. We used Mariner 9, Viking, and Mars Global Surveyor images of the south PLD in the area accessible to MPL and DS2 to evaluate the topography and morphology of grooves, terraced layers, and other features. Here we report on results from grooves that appear to have been carved by strong winds. Because these features are found throughout the interior of the PLD, where MPL and DS2 were targeted to land, their topographic characteristics were judged as important input for landing site safety assessment. The characteristics of the grooves also provide constraints and insights into aeolian processes in the polar regions and the effects these have on PLD ablation. Our results indicate that these grooves do not represent landing hazards at the scale of the images (~80 m/pixel). Their topography and shape do not seem correlated with south PLD layering. No Earth analog of suitable scale exists, although the grooves bear some resemblance to smaller terrestrial deflation hollows found in soft sediment and ice.

Method: Our most mature analysis of the available spacecraft data is for Mariner 9 images. At 72-99 m/pixel, the resolution of these frames is superior to that from Viking and, by using photoclinometry, they provide higher spatial sampling of topography than that available from MOLA. The Mariner 9 image inventory was searched for frames within the MPL landing zone (72° - 78° S, 190° - 230° W). Twenty-two narrow-angle images (minus blue filter) were found, of which five contained topographic features of interest. The selected images were processed using the USGS Planetary Image Cartography System (PICS) to remove noise spikes and apply radiometric calibration [12]. The images were geometrically controlled using the USGS Mars Digital Image Mosaic and projected to a polar stereographic projection. The PICS routine TVPROF was then used to calculate topographic profiles, using estimates of atmospheric scattering or "haze" derived from measurements of shadows in the images or nearby images taken during the same orbit. Areas of the images that appeared level were used to measure the reflectance of the "flat" surface, then this value was adjusted in TVPROF to produce profiles with reasonable overall relief (less than 1 km). Surface photometry was modeled using a Minnaert function and the Minnaert index, k, was computed as a function of incidence angle from the red filter values of Thorpe [13]. Parameters used for each image are shown in Table 1. Presently, MOLA data are being used to constrain the overall relief of the profiles.

The photoclinometric routine used here assumes that the albedo of the surface is constant. Because this assumption is not valid in general, albedo variations result in long-scale slope changes in the derived profiles. As shown in Figure 1, such effects were corrected by subtracting a linear fit in certain sections of some of the profiles.

Results: Although some regional, and perhaps artificial, slopes remain after detrending, the general profiles seem fairly realistic and correlate with apparent albedo variations in the images. The grooves are 10s of km long, up to 1-2 km wide, 10s of m deep, and have V-shaped profiles. The slope distribution for the profiles is shown in Figure 2, with the number of slopes in each profile normalized to 100%. Slopes greater than 10°, the limit that the MPL was designed to survive, comprise only 1% of all slopes. For the two profiles with the greatest number of large slopes (181B8P1 and 189B2P1), slopes greater than 10° make up 5% of the topography, with the rest of the profiles containing <1% or no slopes of this magnitude. We found that variations in k, "haze", and "flat" values within the uncertainty expected within the images resulted in negligible differences in topographic slopes, once profiles were detrended.

Discussion and conclusions: The grooves are typically V-shaped and symmetrical, consistent with an aeolian origin. Slumping of the walls of the grooves is

not observed but may not be resolved in these images. The depth of the grooves (up to 100 m) is somewhat variable, suggesting that the depth of erosion is not controlled by stratigraphic variations in layer competence or resistance.

Some grooves studied here, such as in Figure 1, are oriented approximately perpendicular to local slope [14]. Although this is inconsistent with downslope winds and could argue for an extensional origin, the grooves' V-shaped cross-sections and linearity are indicative of a wind origin. In addition, many other grooves have orientations consistent with off-cap winds, commonly curved in the direction expected for deflection by the Coriolis force.

A perfect terrestrial analog for these features has not been identified. Wind deflation hollows are found in loess deposits and Antarctic ice (P. Lee, personal communication, 2000), but these features are not as linear nor as large as those on Mars. The long time scales over which aeolian deflation can occur on Mars, combined with the relative lack of other erosive processes that could subsequently erase depressions, may account for the large size of the south polar grooves.

The relative absence of >10° slopes over ~80 m lengthscales indicates that these areas would probably not have been hazardous to MPL or DS2, but steeper slopes at the scale of the spacecraft cannot be ruled out using these data. Therefore, the grooved terrain was not selected as a potential MPL/DS2 landing site. These data, combined with further analysis of MOLA altimetry, should greatly increase our understanding of the south PLD topography both for scientific and landing site safety purposes.

References: [1] Murray, B. C., (1972). *Icarus* **17**, 328-345. [2] Cutts, J. A., *et al.* (1976). *Science* **194**, 1329-1337. [3] Cutts, J. A., *et al.* (1979). *J. Geophys. Res.* **84**, 2975-2994. [4] Squyres, S. W. (1979). *Icarus* **40**, 244-261. [5] Toon, O. B., *et al.* (1980). *Icarus* **44**, 552-607. [6] Carr, M. H. (1982). *Icarus* **50**, 129-139. [7] Howard, A. D., *et al.* (1982). *Icarus* **50**, 161-215. [8] Plaut, J. J., *et al.* (1988). *Icarus* **76**, 357-377. [9] Thomas, P., *et al.* (1992). In *Mars*, University of Arizona Press, Tucson, pp. 767-795. [10] Malin, M. C. (1986). *Geophys. Res. Lett.* **13**, 444-447. [11] Herkenhoff, K. E. and Plaut, J. J. (2000). *Icarus* (in press). [12] Herkenhoff, K. E. *et al.* (1988). *Icarus* **75**, 133-145. [13] Thorpe, T. E. (1977). *J. Geophys. Res.* **82**, 4161-4165. [14] Vasavada, A.R., *et al.*, (2000). *J. Geophys. Res.* **105**, 6961-6969.

TABLE 1. Image Parameters for Photoclinometry

Image	*g*	*i*	*k*	Haze	Flat
181B07	48.52	70.02	0.64	533	830
181B08	42.37	71.34	0.62	533	830
183B06	43.98	62.96	0.98	601	775
187B05	47.40	72.42	0.64	523	710
189B02	62.47	77.35	0.69	436	510

g = phase angle, i = incidence angle, k = Minnaert index

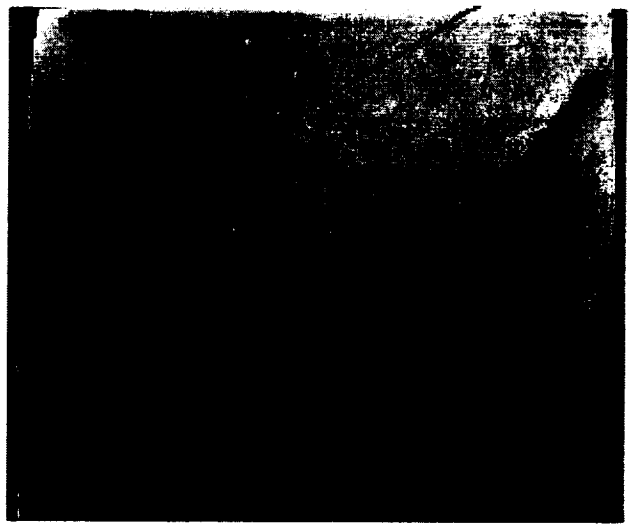

Figure 1: Mariner 9 image 181B07 with superimposed photoclinometric profiles. Red lines are originally derived values. Black line is the slope upon which detrending was made and green is the resulting detrended profile.

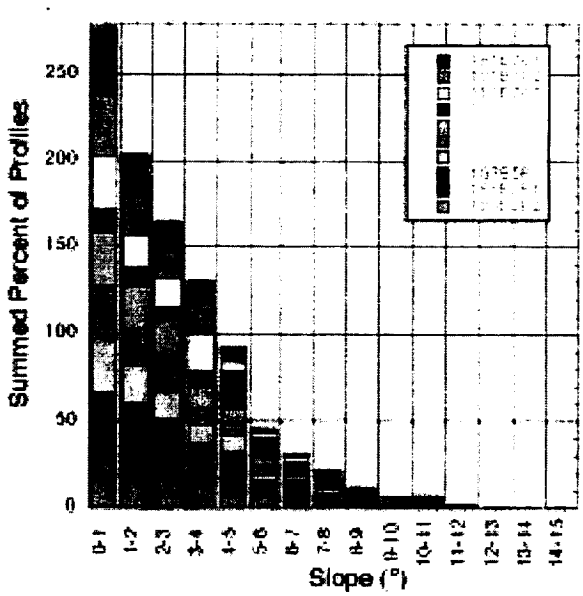

Figure 2: Histogram of slopes in all profiles.

A NOVEL APPROACH TO EXPLORING THE MARS POLAR CAPS. J. R. Brophy[1], F. D. Carsey[2], D. H. Rodgers[3], L. A. Soderblom[4], and B. H. Wilcox[5], [1]Jet Propulsion Laboratory, 4800 Oak Grove Drive, Pasadena, CA 91109, USA, John.R.Brophy@jpl.nasa.gov, [2]Jet Propulsion Laboratory, 4800 Oak Grove Drive, Pasadena, CA 91109, USA, Frank.D.Carsey@jpl.nasa.gov, [3]Jet Propulsion Laboratory, 4800 Oak Grove Drive, Pasadena, CA 91109, USA, David.H.Rodgers@jpl.nasa.gov, [4]United States Geological Survey, Bldg. #1, 2255 North Gemini Drive, Flagstaff, AZ, 86002, USA, lsoderblom@flagmail.wr.usgs.gov, [5]Jet Propulsion Laboratory, 4800 Oak Grove Drive, Pasadena, CA 91109, USA, Brian.H.Wilcox@jpl.nasa.gov.

Introduction: The Martian polar caps contain some of the most important scientific sites on the planet. There is much interest in exploring them with a view to understanding their role in the Mars climate system. By gaining access to the stratigraphy of the polar terrain, it is probable that one can access the climate history of the planet. Additionally, investigations aimed at localizing subsurface water—liquid or solid—are not only of great scientific interest but are also germane to the long-term interests of the manned space flight program.

A major difficulty with polar exploration is access. Current techniques using chemical propulsion, Holman transfers, and direct-entry landers with aeroshells have limited capability to access the polar terrain. For the near term the authors propose a new approach to solving this transportation issue by using Solar Electric Propulsion (SEP), recently flight demonstrated on NASA's DS1 Mission to an asteroid and a comet. For a longer-term approach there are additional ways in which access to Mars, as well as other planets, can be significantly improved. These include the use of Chaos orbit theory to enable transportation between LaGrange points in the solar system, gossamer structures enabling very low-mass mobility, and advanced ascent vehicles.

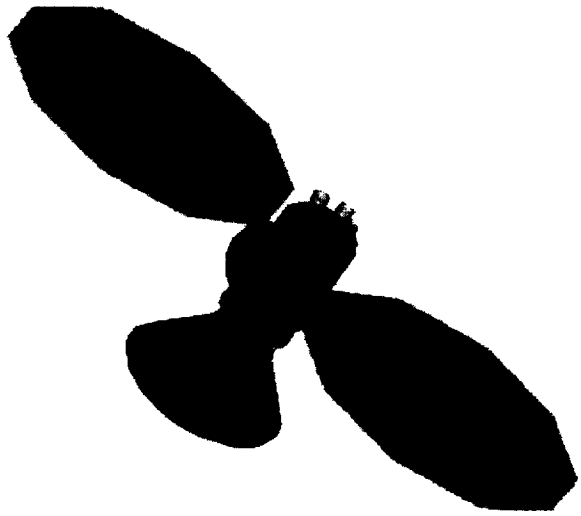

Concept of SEP System with 1700 kG Lander

In this paper the authors describe how a 1000-kG payload can be transported to the surface of Mars and a polar sample obtained and returned to Earth in less than 5 years using SEP. A vision of how this approach can be integrated into a long-term Mars exploration strategy building toward the future is also discussed.

RADAR REFLECTIVITY OF THE MARTIAN POLAR REGIONS. B. J. Butler, *National Radio Astronomy Observatory, Socorro, NM, (bbutler@nrao.edu)*, M. A. Slade, *Jet Propulsion Labratory, Pasadena, CA*, D. O. Muhleman, *California Institute of Technology, Pasadena, CA.*

Radar experiments provide a unique method of probing the surfaces and subsurfaces of planetary bodies. Information on surface and subsurface structures and properties can be extracted from radar data. There is a well developed history of radar investigations of the planet Mars, beginning in with the first reports of variation of scattering properties as a function of martian longitude in the mid-1960's. Because of the rapid rotation of Mars, the standard technique of delay–doppler mapping cannot be used as effectively as it is on Mercury and Venus, making it a more difficult radar target. Techniques have been developed to overcome this difficulty, including an inversion technique to combine many doppler-only (CW) experiments from different viewing geometries into a map of surface reflectivity, and new random long-code techniques. These techniques still suffer from ambiguities, however. A third technique which does not suffer from these ambiguities is the combination of the powerful Goldstone transmitter with the VLA as the receiving instrument to create a combined radar imaging instrument. We have used this combined radar instrument to image the surface of Mars in 3.5-cm radar reflectivity during the 1988, 1992/93, and 1999 oppositions. Figure 1 shows a map of radar reflectivity from the surface of Mars obtained during the 1988 opposition.

During the 1988 experiments, the residual south polar ice cap (RSPIC) was the brightest radar reflector on the planet - intrinsically brighter than even the Tharsis lava flows. This was quite an unexpected result. In contrast, during the 1992/93 experiments, the residual north polar ice cap (RNPIC) was not nearly so bright, and in fact showed no enhancement at all. This was puzzling, given the 1988 results for the RSPIC. We attributed the lack of a radar reflection enhancement to a combination of three effects: the geometry was different; the season was different; and the intrinsic scattering from the residual ice caps was different.

The 1999 experiments provided a chance to test the relative importance of these three effects, since the RNPIC would be visible in a geometry very similar to the RSPIC in 1988, and the season would also be very similar. Preliminary reduction of the data taken in 1999 shows that the RNPIC did in fact show a radar reflectivity enhancement (see Figure 2), but that it was still not as bright as the RSPIC in 1988.

Details regarding the radar reflectivity of the residual ice caps, as well as the surrounding polar layered terrains (in light of our radar reflectivity data) will be discussed.

Figure 1. Snapshot image of the 3.5-cm radar reflectivity of Mars obtained in a joint Goldstone/VLA radar experiment in 1988. Darker shades are higher reflectivity. The residual south polar ice cap is the spot at the bottom. The Tharsis volcanic region is prominent in the center of the image, as is the "Stealth" region, stretching to the west of Tharsis.

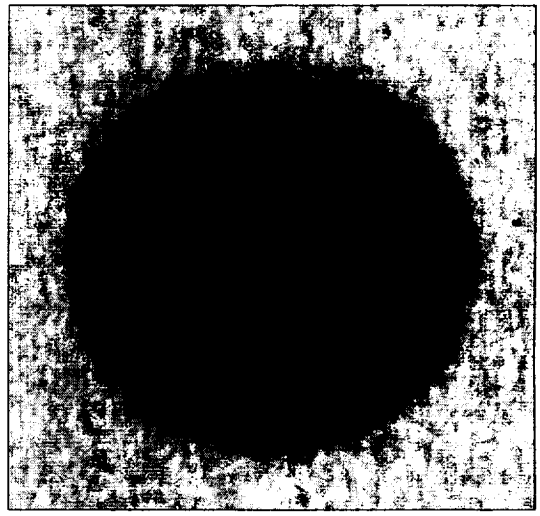

Figure 2. Averaged martian radar reflectivity in the north polar regions - data taken 24Jun1999. The spot at the top is the reflection from the north polar residual ice cap, and is surrounded by the very radar-dark sand sea.

SUBLIMATION MODEL FOR FORMATION OF RESIDUAL CAP DEPRESSIONS. S. Byrne[1] and A.P. Ingersoll[1]. [1]Division of Geological and Planetary Sciences, Caltech, 1200 E. California Blvd., Pasadena, CA 91125, US. Correspondence Email: shane@gps.caltech.edu

Introduction: The Mars Global Surveyor (MGS) spacecraft, through the Mars Orbital Camera (MOC), has provided unprecedented views at high resolution of the southern residual polar cap. Since the orbit is not quite polar (3° off) there is a ring at 87 south which the spacecraft must pass tangent to in every revolution about the planet. Hence there is an extremely well imaged ring at this latitude that intersects the residual cap. Several terrain types unique to this area are apparent [1]. Some of the most unusual geomorphic features revealed are circular/quasi-circular depressions which are steep walled and flat floored, with a characteristic depth of ~10m [1] and a broad range of lateral sizes. We have developed a sublimation driven model to explain the formation of these features.

Observations: An example of this terrain is shown in figure 1. Characteristics of these features were discussed by Thomas et al [1].

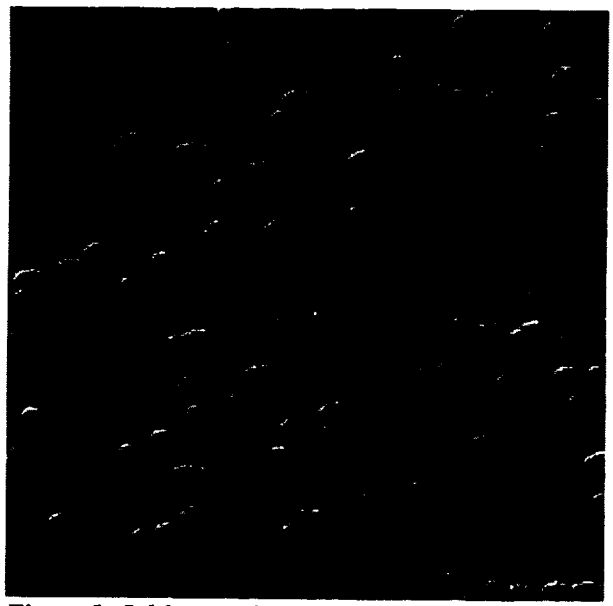

***Figure 1**: Subframe of M07-02823 taken at 11 meters per pixel, 87 S, 6 W. The scene here is approximately 3 Km across, sunlight is from the bottom right, north is to the left. Several depressions are visible in this image, some have merged to form larger non-circular shapes.*

In general, as discussed above, they have circular or near circular shapes, flat floors and steep walls. They appear only on the residual cap itself (as mapped by Viking [2]). They show no noticeable changes as the southern summer season progresses. Each depression appears to have an interior moat of constant width. The moat width is independent of the lateral size of the depression. Inside the moat, at the center of the depressions, are elevated areas approximately 2 meters above moat level, which are possibly lag deposits remaining after sublimation of the interior [1]. One of the most intriguing observed properties is the existence of four or more layers within the medium in which the depressions are incised [1]. Figure 2 (as shown in the Thomas et al [1] article) shows a more detailed view of the layering, each layer is roughly two meters thick and so when slopes are this steep can only be discerned in the highest resolution MOC images.

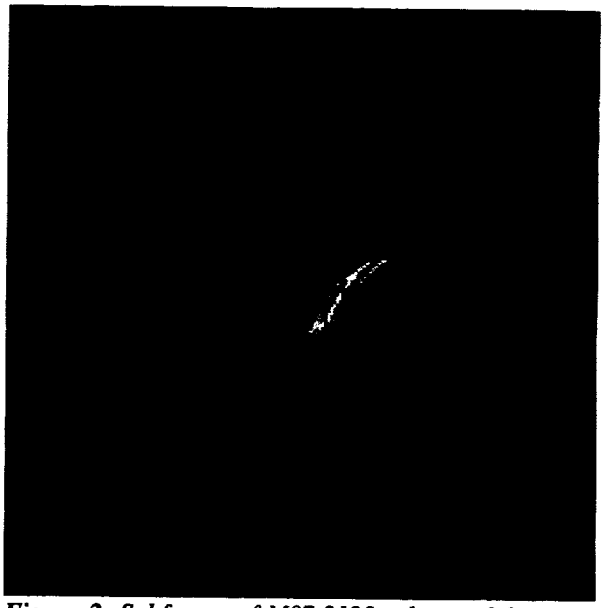

***Figure 2**: Subframe of M07-2129 taken at 2.2 meters per pixel, 87 S, 78 W. The scene here is approximately 500 meters across, sunlight is from the bottom right, north is to the left. The layers in the sidewalls are just visible.*

These layers are observed in other images within the walls of the depressions. The layers are not perfectly parallel and appear to branch, merge and get pinched out. It is possible that there are thinner layers which are not being resolved and which are responsible for this irregular behavior.

Sublimation Model for Formation of Residual Cap Depressions: S. Byrne and A.P. Ingersoll

Model: Our model assumes cylindrical symmetry. The sun circles each day at a constant height above the horizon (which varies as a function of season). This would be true if one were exactly at the pole and provides a very good approximation at a latitude of 87 degrees. The medium in which the depressions form can have horizontal layering incorporating changes in albedo, thermodynamic properties, composition and density as a function of depth. The model is started with some small depression and run forward to examine the evolution of its shape. This model accounts for the effects of incident sunlight, reflected sunlight within the depression, emitted thermal radiation within the depression, reflected thermal radiation and the effects of partial shadowing due to low sun elevations. The surface temperature is fixed at the sublimation temperature of CO_2. Sublimation and redeposition of frost occurs depending on the difference between incoming and outgoing radiation. The rates of these processes may differ across the depression. This model should be sensitive to events occurring on timescales as short as 1° of L_s, even though there is no evidence for change this rapid. This model is the first step in a larger modeling effort to explain the full asymmetrical nature of these features.

Discussion: We investigate the conditions necessary to form features similar to those observed in the MOC data. The possibility of significant amounts of water ice and variations in dust fractions from layer to layer are also considered. We will report on our findings and their implications.

References: [1] Thomas P.C. et al., (2000), Nature, 404, 161-164. [2] James P.B. et al (1979), J. Geophys. Res., 84, 2889-2922.

HIGH-LATITUDE MARTIAN IMPACT PALEOLAKES: THE POSSIBLE CONTRIBUTION OF SNOWFALL AND ANCIENT GLACIERS IN THE LACUSTRINE ACTIVITY ASSOCIATED TO ARGYRE AND HELLAS . N. A. Cabrol and E. A. Grin. SETI Institute. NASA Ames Research Center.

Introduction: Hellas and Argyre show impact crater paleolakes, which morphologies could have been associated to glacial and sub-glacial processes, implying the existence of snowfall and ancient glaciers. Some of them show as well a hydrothermal contribution related to the presence of volcanic centers.

Argyre: The Argyre group counts 8 members, that were supplied by the Doanus Vallis system. Some of them display spectacular fluvio-lacustrine structures (e.g., deltas, sedimentary terraces), and evidence of several episodes of flow or one sustained long episode. The material deposited both on the channel lakebed floor shows a small population of superimposed impact craters (1 to 5 over areas ranging from 10,000 to nearly 15,000 km^2). Many craters are subdued or partially filled by this unit. The best estimate would give a Middle Amazonian age to this unit (Cabrol and Grin, 2000)), placing it in climate conditions close to what Mars is experiencing today. Although the crater sample is small and the area reduced, the worst case estimate still puts this geological unit at the fringe of the Upper Hesperian and Lower Amazonian.

One of the most striking systems of the Argyre group is centered 57°S and 18°W. A valley network enters the *Darwin Crater* from the East rim. Bright deposits are visible on the top of local crests near the east rim of the crater. This Viking image was taken during the extended mission by the Orbiter 2 on February 1978 during orbit 533 with Ls≈42°. It was Spring in the northern hemisphere, and fall in the southern hemisphere. The south polar CO_2 ice cap was growing. The latitude of the edge of the south cap at Ls=42° would have been very close to 56°S. latitude. So its possible that the bright deposit is CO_2 ice beginning to deposit on the regional crests. The Viking image shows also material in the valleys that enters Darwin downslope. This material is different from debris slope material. It finds its source on cirque-like depressions, and flows down, as shown by sinuosities, junctions, and erosional forms associated with the flow in Darwin crater. The combination of observations could be consistent with a the remnants of an ancient glacier-like feature. To form a glacier, precipitation of snow is required. We will see that recent martian climate modeling by Haberle et al., (2000) shows that such precipitation were likely to happen repetitively in Argyre through time.

In addition to the recent lakes associated with the filling of craters by potential basal melt in glacier, more recently Parker et al., (2000), basing their observation on MOLA, MOC and TES data have shown the potential for the complete filling of the Argyre basin by a large body of water that would have overtopped the northern rim of the basin during the Noachian. Therefore, Argyre itself should account for another large impact basin paleolake.

Hellas: The Hellas region is covered by extended lava flows from Hadriaca Patera that resurfaced most of the preexisting units surrounding the volcano on the basin rim (Potter 1976). The Hellas basin itself seems to have been the locus of substantial lacustrine activity late in its history. Successive lakes may have been associated with the activity of Dao, Harmakhis and Reull Valles, as shown by clear terrace morphologies and smooth deposits that could indicate the presence of a shoeline. The latest lava flow episodes were proposed to be at the margin of the Hesperian and Amazonian periods (Greeley and Guest, 1987). The three channels cut these deposits and therefore could be more recent. They could be also contemporary to these lava flows and triggered by the volcanic activity. The very few number of superimposed craters on the channel material could support the hypothesis that the channel activity lasted long enough after the cessation of the volcanic activity. The nature of the material that en-

tered the Hellas basin from these channels resembles the lineated material of the fretted terrain, which is assumed to be ice/water rich.

Three smaller impact basins experienced ponding probably during the same period. In some places, lava flows interact with the channels that enter the three crater basins. We assume then that ponding might have occurred in these basins at the same time as the latest volcanic activity. The morphological evidence does not point toward long-sustained lacustrine activity at geological scale, but rather short ponding associated with possible limited hydrothermal activity. One crater basin is located 500 km of Hadriaca Patera, on the northwestern flank of the volcano. The channel that supplied this crater can be traced 400 km upstream and disappears. The morphological evidence left is not conclusive enough to tell if this upstream point is the source of the channel, or only one segment overtopped by a lava flow. In the crater itself, the morphology of the deposits does not resemble that of a lava flow, and some terracing and deposits can be observed. For these reasons, we would favor temporary ponding of water instead of filling from fluid lava.

On the east flank of Hadriaca Patera, two communicating smaller craters located between 39°S and 40°S latitude and 260°W longitude form an open system. The channel supplying them starts in the mountain units at the junction of Reull Vallis and Harmakhis Vallis. The southern crater basin is breached and material is deposited into Reull Vallis. The morphology of the deposits suggests a highly-loaded, mud-like flow. The stratigraphic age of the channel supplying these two basins is comparable to the latest lava flows, and support the potential interaction between volcanic activity and ground ice, as proposed by the previous work of Squyres et al., (1987) about this region.

Secchi- At 58° S and 260°W, the 200-km diameter Secchi crater shows clear evidence of flowing and deposition in its north and west parts. In its case, the timing of such events is difficult to establish. The Secchi basin is a Noachian basin. However, we could not find one truly superimposed impact crater ≥2 km-diameter on the 5000 km^2 deposits left by the valley networks, but only four smaller impacts (≤1.5 km-diameter with large lobate ejecta). This could indicate a recent setting, and/or a recently exhumed deposit. The source region of the valley networks is located on the northwest and west rims of Secchi. One system is centrifugal and heads north, while the other is entering Secchi. The source area is very limited but the valley networks are well-developed and preserved, favoring the hypothesis of a relatively recent activity. Plausible source of water supply include emergence of groundwater and melting of snow packs.

MARTIAN DUST STORMS: 1999 MOC OBSERVATIONS. B. A. Cantor[1], P. B. James[1], M. Caplinger[2], M. C. Malin[2], and K. S. Edgett[2], [1]Department of Physics and Astronomy, The University of Toledo, Toledo, OH. 43606-3390 (bcantor@astro1.panet.utoledo.edu), [2]Malin Space Science Systems, Post Office Box 910148, San Diego CA 92191-0148.

Introduction: The Mars Orbiter Camera on board the Mars Global Surveyor from March 9, 1999 (L_s=107.27°, the areocentric longitude of the Sun measured in degrees from Mars' northern spring equinox) to December 14,1999 (L_s=262.78°) has obtained daily global maps of the Martian surface at a resolution of 7.5 km/pixel in two wavelength bands: violet (400-450 nm) and red (575-625 nm). Visual inspection of these maps during the 1999 dust storm season has resulted in the detection of 764 dust storms, ranging in size from "local" (>10^2 km^2) to "regional" (>$10^6$$km^2$) storms. Of the 764 dust storms, 237 (31%) were observed at a latitude ≥ |57°| (103 in the north and 136 in the south). The MOC images scans that makeup the polar sections of these maps are exceptional due to the polar orbit of MGS which allowes for the monitoring of the northern and southern polar caps about every two hours. This has allowed us to observe for the first time the evolution of a local north polar dust storm (see Figure 1).

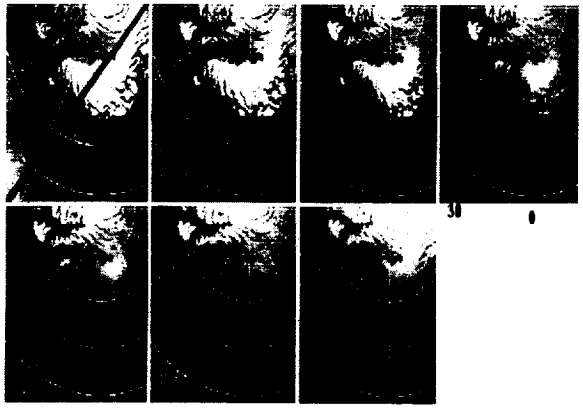

Figure 1. Evolution of a north polar local dust storm observed with the MOC WA-Red Filter on L_s = 136°.

Not only have local dust storms been observed in the polar regions during the 1999 dust storm season but four regional storms were observed to emanated from or near the northern and southern polar caps (see Table 1)

TABLE 1
1999 Regional Polar Dust Storms

	Central			Mass	
L_s	LAT	LONG	Area (km^2)	Loading (g/cm^2)	Length (Days)
163	74.63N	322.88	5.6E+6	3.0E-4	14
183	68.75N	309.63	1.7E+6	3.0E-4	9
227	59.50S	134.25	2.4E+6	2.6E-4	9
234	66.41S	201.51	1.8E+6	2.6E-4	8

Measurements of the sizes of these storms along with modeling the dust opacities (τ_d = 1.1 - > 2.0) has allowed for the estimation of the sedimentation rate due only to polar dust storms. What is found is that the sedimentation rate is about an order of magnitude less than that suggested by global dust storms (see Table 1) [1]. MOC observations suggest that the erosional rate for the south polar region and the depositional rate in the north polar region are variable on a yearly basis and are highly dependent on global and regional dust storm activity.

References: [1]Pollack et al. (1979) *JGR, 84,2929-2945.*

EXAMINATION OF A DEEP SUBSURFACE MARS POLAR CAP MISSION TO ADDRESS CLIMATE HISTORY F. D. Carsey, K. Nock, G. Bearman, D. Kossakovski, and B. Wilcox, all at California Institute of Technology Jet Propulsion Laboratory, Pasadena CA 91109 (fcarsey@jpl.nasa.gov).

Introduction: We have examined the technological readiness of a mission to the Mars north polar area for the science objective of developing a climate history. We argue that the polar regions are scientifically extremely important mission sites from the perspectives of both climate history and astrobiology and that a polar deep subsurface mission would constitute a serious challenge and significant accomplishment. Thus a key question is: What is the technical readiness status of such a mission?

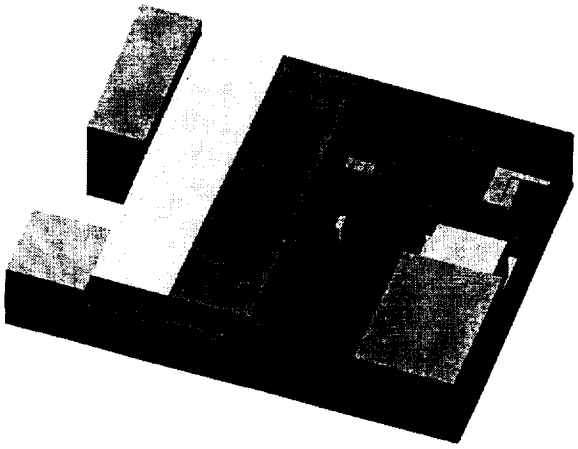

Fig. 1 The layout of a Mars surface analysis laboratory. Particles from the subsurface explorer would be moved in a capillary filled with high-pressure gas through a suite of instruments.

Mission Overview: We have taken the 2009 flight opportunity as a working launch period. To enhance geographic access and reduce costs, the mission profile is a Delta 2 or 3 launch with a 5 kW SEP cruise stage, involving about 2.5 years of flight, arriving at the Mars North Pole in November, 2011, resulting in > 100 days with the sun > 5° above the horizon for a site in the 85°-87°N latitude. The latitude selection is driven by our ability to drill the Polar Layered Deposits (PLD) and the time for which there is adequate insolation. Telecommunications from the site are planned to be direct to Earth, but orbital relay is seen as a good contingency. We note that landing-location accuracy is required, and that hazard avoidance may be called for according to recently published images.

Science: The overall topic of climate history was chosen. An alternate and very interesting mission could be focussed on life detection in the contact of the PLD and its basement, but uncertainties in the nature and scope of science instrumentation were seen to be significant. A strawman instrument set includes a mass spectrometer, microscopes at 1 and 10 micron resolutions, ground-penetrating radar for subsurface survey and for tracking the subsurface explorer, Raman, Moessbauer and electron paramagnetic spectrometer for mineralogic information, and a luminescence dater.

Chronometry remains a crucial scientific technology. Our approach, which is not firmly established, is to consider luminescence dating as a technique to establish a 150,000-year baseline against which other schemes, e.g. 3he/He abundances, stable and/or radioactive isotopes, etc., can be compared in order to construct a longer-term calendar for the deeper ice.

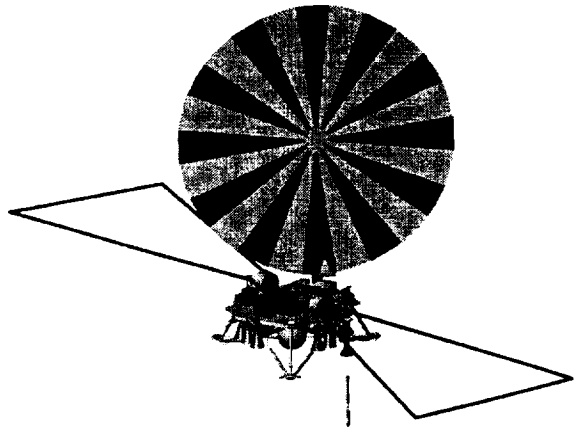

Fig. 2. The MCHM lander with its large round solar collector, bow-tie sounding radar antenna, and subsurface explorer, deployed, at lower center.

Subsurface Explorer: Another key technology is the subsurface explorer; in this study the percussive drill has been used to gain access to the ice at depth. This device will be discussed elsewhere at this conference. The percussive drill acquires samples at depth by capturing material ground up by the drill and moving small particles (< 100 microns) to the surface through a capillary. In the 100 days of good sunlight at the North Pole, the subsurface explorer can drill through somewhat more than 1 km.

Summary: We conclude from our analysis that the deep subsurface exploration of a site such as the Mars PLD is within reach, a remarkable and exciting idea. Scientific analysis of the pulverized material from the drill can be addressed with quite good expectations. Developments are called for in the areas of precision landing site location and hazard avoidance, Chronometry of the PLD material, subsurface access methods, sample handling for scientific analysis, and scientific instrumentation.

TES OBSERVATIONS OF THE MARTIAN SURFACE AND ATMOSPHERE. P.R. Christensen[1], H.H. Kieffer[2], J.C. Pearl[3], B. Conrath[3], M.C. Malin[4], R.C. Clark[5], R. V. Morris[6], J. L. Bandfield[1], and M. D. Lane[7], M.D. Smith[3], V. E. Hamilton[1], R.O. Kuzmin, [1]Department of Geology, Arizona State University, Tempe, AZ, [2]U.S. Geological Survey, Flagstaff, AZ, [3]Goddard Space Flight Center, Greenbelt, MD, [4]Malin Space Science Systems, San Diego, CA, [5]U.S. Geological Survey, Denver, CO, [6]NASA Johnson Space Center, Houston, TX.

Introduction: The TES instrument is a Fourier transform Michelson interferometer operating with 10 or 5 cm^{-1} sampling in the thermal infrared spectral region from 1700 to 200 cm^{-1} (~6 to 50 μm) where virtually all minerals have characteristic fundamental vibrational absorption bands (1, 2, 3, 4, 5, 6, 7, 8). The TES data used in this paper are among the $6x10^7$ spectra collected during the early mapping phase of the MGS mission from southern hemisphere winter to early summer (aerocentric longitude, L_s, 107° to 297°. The methodology for separating the surface and atmospheric components of the radiance from Mars, which allows detailed analysis and interpretation of surface mineralogy (9, 10), is described in previous papers (10, 11).

Atmospheric Properties: Between September 1997 and September 1998 when the final aerobraking phase of the mission began, the TES acquired an extensive data set spanning approximately half of a Martian year. Nadir-viewing measurements provided information on both structure and composition of the Martian atmosphere.

Dynamics. Spectral measurements from this data set within the 15-μm CO2 absorption band are inverted to obtain atmospheric temperature profiles from the surface up to about the 0.1 mbar level. Mean meridional cross sections of thermal structure are calculated for periods of time near northern hemisphere fall equinox, winter solstice, and spring equinox, as well as for a time interval immediately following the onset of the Noachis Terra dust storm. Gradient thermal wind cross-sections are calculated from the thermal structure. Regions of possible wave activity are identified using cross sections of rms temperature deviations from the mean (12).

Aerosols. The nadir-viewing measurements contain the distinct spectral signature of atmospheric dust, allowing measurement of dust opacity. In the early stages of the mission, the 9-μm dust opacity at mid-southern latitudes was low. TES observed several large regional dust storms as the season advanced through southern spring and summer, where peak opacities approached or exceeded unity, as well as smaller local storms. Over the time scale of a day, both large and small dust storms exhibited notable change in spatial coverage and intensity. The region at the edge of the retreating southern seasonal polar ice cap was observed to be consistently more dusty than other latitudes(13).

Surface Composition: The composition of the surface has been derived from atmosphere-removed spectra in Cimmeria. These spectra do not match terrestrial high-silica igneous rocks (granite and rhyolite), ultramafic igneous rocks, limestone, nor quartz- and clay-rich sandstone and siltstone. A particulate (sand-sized) sample of terrestrial flood basalt does provide an excellent match in both spectral shape and band depth to the Cimmeria spectrum over the entire TES spectral range. The identification of basalt is consistent with previous indications of pyroxene and basalt-like compositions from visible / near-infrared and thermal-infrared spectral measurements. A linear spectral deconvolution model was applied to both surface-only Cimmeria spectra using a library of 60 minerals to determine the composition and abundance of the component minerals. Plagioclase feldspar (45%; 53%) and clinopyroxene (26%; 19%) were positively identified above an estimated detection threshold of 10-15% for these minerals. The TES observations provide the first identification of feldspars on Mars. The Cimmeria spectra are not well matched by any one SNC meteorite spectrum, indicating that this region is not characterized by a single SNC lithology. The occurrence of unweathered feldspar and pyroxene in Cimmeria, together with the inferred presence of pyroxene and unweathered basalts in other dark regions and at the Viking and Pathfinder landing sites, provides evidence that extensive global chemical weathering of materials currently exposed on Martian surface has not occurred (9).

The TES has discovered a remarkable accumulation of crystalline hematite (α-Fe_2O_3) that covers an area with very sharp boundaries approximately 350 by 350-750 km in size centered near 2°S latitude between 0 and 5° W longitude (Sinus Meridiani). Crystalline hematite is uniquely identified by the presence of fundamental vibrational absorption features centered near 300, 450, and >525 cm^{-1}, and by the absence of silicate fundamentals in the 1000 cm^{-1} region. The spectrally-derived areal abundance of hematite varies with particle size from ~10% (>30 μm

diameter) to 40-60% (10 ∝m diameter). The hematite in Sinus Meridiani is thus distinct from the fine-grained (diameter <5-10 μm), red, crystalline hematite considered, on the basis of visible, near-IR data, to be a minor spectral component in Martian bright regions like Olympus-Amazonis. Sinus Meridiani hematite is closely associated with a smooth, layered, friable surface that is interpreted to be sedimentary in origin. We prefer chemical precipitation models and favor precipitation from Fe-rich water based on the probable association with sedimentary materials, large geographic size, distance from a regional heat source, and lack of evidence for extensive groundwater processes elsewhere on Mars. The TES results thus provide mineralogic evidence for probable large-scale water interactions (14).

References:

1. R. J. P. Lyon, *Stanf. Res. Inst. Final Rep. Contract NASr* 49(04) (1962).

2. A. N. Lazerev, *Vibrational spectra and structure of silicates* (Consultants Bureau, N.Y., 1972).

3. V. C. Farmer, *The Infrared Spectra of Minerals* (Mineralogical Society, London, 1974).

4. J. W. Salisbury, L. S. Walter, N. Vergo, *U.S.G.S., Open File Report* , 87-263 (1987).

5. J. W. Salisbury, in *Remote Geochemical Analysis: Elemental and Mineralogical Composition* C. Pieters, P. Englert, Eds. (Cambridge University Press, Cambridge, 1993) pp. Ch. 4.

6. M. D. Lane, P. R. Christensen, *J. Geophys. Res.* 102, 25,581-25,592 (1997).

7. V. E. Hamilton, *J. Geophys. Res.* (in press).

8. P. R. Christensen, et al., J. Geophys. Res. (in press).

9. P. R. Christensen, J. L. Bandfield, M. D. Smith, V. E. Hamilton, R. N. Clark, *J. Geophys. Res.* (in press).

10. J. L. Bandfield, M. D. Smith, P. R. Christensen, *J. Geophys. Res.* (in press).

11. M. D. Smith, J. L. Bandfield, P. R. Christensen, *J. Geophys. Res.* (in press).

12. B. J. Conrath, et al., *J. Geophys. Res.* (in press).

13. M. Smith, B. Conrath, J. Pearl, P. R. Christensen, *J. Geophys. Res.* (in press).

14. P. R. Christensen, et al., *J. Geophys. Res.* (in press).

CONTRIBUTION OF VOLCANIC OUTGASSING TO THE MARTIAN POLAR LAYERED DEPOSITS. *Robert A. Craddock*[1] *and Ronald Greeley*[2], [1]Center for Earth and Planetary Studies, National Air and Space Museum, Smithsonian Institution, Washington, D.C. 20560; [2]Department of Geology, Arizona State University, Tempe, Arizona 85287

While it is generally believed that the polar layered deposits are the result of astronomical variations causing adsorbed volatiles to be cyclically released from the regolith [e.g., 1], an important component may be volatiles released from volcanic outgassing. MOC images reveal that martian volcanism continued nearly up to the present day [2], which coincides with the young age of the polar layered deposits [3]. Depending on the magnitude and duration of eruption episodes, the amount of volatiles released into the martian atmosphere from volcanic outgassing may have been significant. To date, however, the contribution this process has made to the total volatile inventory on Mars as well as the amount that may have been sequestered in the polar caps has not been fully explored. Our estimates suggest that the amount of volatiles released from volcanic outgassing through time is easily accounted for in the martian polar layered deposits, undermining the need for an astronomical mechanism.

Volcanism has been a dominant geologic process on Mars throughout much of its history [4], but only recently have estimates been made of the total volume of volcanic material erupted through time [5]. Because most martian volcanic material is believed to be basaltic [4, 5], our model is based on measurements of gas constituents made from Hawaiian lavas [6]. Short-lived atmospheric pressures as high as ~0.3-0.5 bars may have occurred during the Hesperian. Because most of the modeled gases accompanying these pressure increases were greenhouse gases (i.e., CO_2 and SO_2) warmer surface temperatures may also be possible. The estimates presented here are important for assessing the total volatile inventory of the planet, determining martian paleoclimatic conditions, understanding the types of chemical weathering and surface alteration of materials which may have taken place, and in determining whether life developed on Mars.

Several lines of evidence indicate that most martian volcanic materials are basaltic [7]. Morphometric analyses of individual flows suggest that the composition of martian lavas is basaltic andesite [e.g., 8], which would have ~0.5 wt % H_20 [9]. Typical values for Hawaiian lavas, however, are •0.5 wt % [6], which agree with the values determined for individual minerals in SNC meteorites [10]. Because the morphology of ancient highland patera suggests they were erupted explosively while younger flows appear to have erupted effusively, the volatile content of the martian mantle may have changed with time [11]. For simplicity, a reasonable estimate of the water content of martian lavas is 0.5 wt % H_2O. Taking into account the other gas constituents, the total amount of volatile material outgassed during an eruption on Mars is modeled to be ~0.76 wt %. Not included in our calculations are gases released during periods of quiescence, specifically carbon dioxide and sulfur dioxide. Based on terrestrial volcanoes, the amount of carbon dioxide released during periods of quiescence may be a factor of 10 greater than what is released during the actual eruption [12]. Similarly, the amount of sulfur dioxide released just prior to an eruption has been observed to be a factor of 7 greater [13].

The total amount of water released from volcanic outgassing is found to be equal to a layer only 8 m deep distributed over the entire planet. This is a factor of 6 less than original estimates [6]. The total mass of carbon dioxide is equivalent to 317 mbar of atmospheric pressure. This roughly accounts for the CO_2 currently in the martian atmosphere (~2.5 x 10^{16} kg) as well as the amount possibly contained in the southern polar cap (5 x 10^{17} kg). Sulfur dioxide is the most

abundant gas released through volcanism, but its influence on atmospheric pressure would only be on the order of ~3 martian years [14]. However, based on original erupted magma volumes [7], *Postawko and Fanale* [15] suggested that 1 wt % SO_2 would be capable of warming the martian atmosphere by as much as 10°K, with a more pronounced effect near the eruption. Including gas released during periods of quiescence, our effective wt % SO_2 is 1.4, which suggests even higher episodic temperatures. The released SO_2 would quickly form sulfuric acid vapor (H_2SO_4) which would nucleate and precipitate as acid rain [14]. We estimate that 3-21 m of H_2SO_4 may have precipitated on Mars. *Settle* [14] suggested that SO_2 released from volcanic eruptions could be dispersed globally and trigger leaching of surface materials upon deposition, thus explaining the high sulfur content of the soil and duricrust measured at both landing sites [16]. If the warmer atmospheric temperatures accompanying volcanic eruptions were high enough to decouple the Jeans escape of hydrogen from the nonthermal escape of oxygen, the hydrogen flux from degassing may explain the martian atmospheric D/H ratio. Minor gas constituents (HF, HCl, and H_2S) would have formed hydroxyl salts on surface materials. *Malin* [17] suggested that under current martian conditions these salts would continually recrystallize, resulting in physical weathering of geologic materials. It may also be possible that emitted hydrogen fluoride dissolved small amounts of quartz sand, if present on the surface.

Table 1. Mass (10^{15} kg) of Martian Volcanic Gases Released Through Time.

Epoch	Constituents								
	H_2O	SO_2 [1]	CO_2 [1]	H_2S	H_2	N_2	HCl	HF	CO
Late Amazonian	35.0	14.7	2.25	0.95	0.03	0.12	0.07	0.05	0.03
Middle Amazonian	140	58.7	8.99	3.78	0.13	0.50	0.27	0.22	0.14
Early Amazonian	260	109	16.7	7.02	0.24	0.92	0.51	0.41	0.25
Late Hesperian	258	108	16.6	6.96	0.23	0.92	0.50	0.40	0.25
Early Hesperian	291	122	18.7	7.85	0.26	1.03	0.57	0.46	0.28
Late Noachian	128	53.6	8.22	3.45	0.12	0.45	0.25	0.20	0.12
Middle Noachian	23.0	9.64	1.48	0.62	0.02	0.08	0.04	0.04	0.02
Early Noachian	?	?	?	?	?	?	?	?	?
Minimum Total Est.	1135	476	72.9	30.6	1.03	4.03	1.82	2.21	1.10

[1]Does not include gases released during periods of quiescence, which may be a factor of 7 more for SO_2 and an order of magnitude more for CO_2.

References: [1] Toon, O.B., *et al., Icarus, 44*, 552-607, 1980. [2] Hartmann, W.K., *et al., Nature, 397*, 586-589, 1999. [3] Plaut, J.J., *et al., Icarus, 75*, 357-377, 1988. [4] Greeley, R., and P.D. Spudis, *Rev. Geophys. Space Phys., 19*, 13-41, 1981. [5] Greeley, R., and B.D. Schneid, *Science, 254*, 996-998, 1991. [6] Greenland, L.P., in *Volcanism in Hawaii*, Vol. 1, Chap. 29, U.S. Geol. Surv. Prof. Pap. 1350, 759-770, U.S. Gov. Printing Office, Washington, 1987. [7] Greeley, R., *Science, 236*, 1653-1654, 1987. [8] Zimbelman, J.R., *Proc. Lunar Planet. Sci. Conf. 16th*, Part 1, *J. Geophys. Res., 90*, suppl., D157-D162, 1985. [9] Williams, H., and A.R. McBirney, *Volcanology*, 397 pp., Freeman, Cooper, & Co., San Francisco, 1979. [10] Watson, L.L. *et al., Science, 265*, 86-90, 1994. [11] Schubert G., et al., in *Origin and Evolution of Planetary and Satellite Atmospheres*, 450-483, Univ. Arizona, 1989. [12] Greenland, L.P., in *Volcanism in Hawaii*, Vol. 1, Chap. 30, U.S. Geol. Surv. Prof. Pap. 1350, 781-790, U.S. Gov. Printing Office, Washington, 1987. [13] Stoiber, R.E., and A. Jepsen, *Science, 182*, 577-578, 1973. [14] Settle, M., *J. Geophys. Res., 84*, 8343-8354, 1979. [15] Postawko, S.E., and F.P. Fanale, Workshop on the Martian Surface and Atmosphere Through Time, Lunar and Planet. Inst. Tech. Rept. No. 92-02, 24-25, Lunar and Planet. Inst., Houston, Tex., 1992. [16] Toulmin, P., *et al., J. Geophys. Res., 82*, 4625-4634, 1977. [17] Malin, M.C. *J. Geophys. Res., 79*, 3888-3894, 1974.

NORTHWESTERN THARSIS LATENT OUTFLOW ACTIVITY MARS. J.M. Dohm[1], R.C. Anderson[2], V.R. Baker[1], J.C. Ferris[1], T.M. Hare[3], R.G. Strom[1], L. Rudd[1], J.W. Rice, Jr.[1], D.H. Scott[4] [1]Department of Hydrology and Water Resources, University of Arizona, Tucson, AZ, 85721,jmd@hwr.arizona.edu; [2]Jet Propulsion Laboratory, Pasadena, CA; [3] U.S. Geological Survey, Flagstaff, AZ; [4]Private.

INTRODUCTION. Previously defined outflow channels, which are indicated by relict landforms similar to those observed on Earth, signify ancient catastrophic flood events on Mars [e.g., 1-5]. These conspicuous geomorphic features are some of the most remarkable yet profound discoveries made by geologists to date. These outflow channels, which debouched tremendous volumes of water into topographic lows such as Chryse, Utopia, Elysium, and Hellas Planitiae, may represent the beginning of warmer and wetter climatic periods unlike the present-day cold and dry Mars [e.g., 6-7]. In addition to the previously identified outflow channels [e.g., 4, 8-10], observations permitted by the newly acquired MOLA data have revealed a system of gigantic valleys, referred to as the northwestern slope valleys (NSV; Figure 1), that are located to the northwest of a huge shield volcano, Arsia Mons, western hemisphere of Mars. These features generally correspond spatially to gravity lows similar to the eastern-most, circum-Chryse outflow channel systems [e.g., 11]. Geologic investigations of the Tharsis region suggest that the large valley system pre-dates the construction of Arsia Mons and its extensive associated lava flows of mainly Late Hesperian and Amazonian age and coincides stratigraphically with the early development of the circum-Chryse outflow channel systems that debouch into Chryse Planitia [e.g., 12-14](**Figure 1**). This newly identified system, the NSV, potentially signifies the largest flood event(s) ever recorded for the solar system (**Table 1**).

DISCUSSION. The NSV was previously obscured to the trained eye using Mariner and Viking data by veneers of lava flows and volcanic air fall deposits and putative ash flow deposits [e.g., 8]. The veneers suppress evidence (e.g., relict features) making it difficult to rule out modes of valley formation. In addition to volcanic modification, local eolian, fluvial, and mass movement processes further obscure clues that would otherwise aid in better understanding the origin of the valleys.

Following careful consideration of the stratigraphic, geomorphic, paleotectonic, topographic (using MOLA data), and geophysical data, catastrophic fluvial activity best explains the formation of the NSV. We emphasize, however, that other possible activities including glaciation, tectonism, wind erosion, and mass wasting cannot be ruled out as contributors to the NSV. In the case of catastrophic flooding, conservative estimates of the capacity to discharge water northwestward towards the Amazonis Planitia place the NSV at nearly half the volumetric potential of all the other martian outflow channels combined calculated from valley geometries (present-day and estimated post-carved valley profiles--Table 1); a total peak discharge perhaps equivalent to 50,000 times the output of the Amazon River.

IMPLICATIONS. Since the NSV (1) may be the largest fluvial system ever documented for the solar system and (2) could represent a significant source of water for the northern plains ocean when placed in context with other martian outflow channels, efforts should focus on the potential source region(s), which includes attempts to help explain the tremendous quantities of water that would be necessary to form the valley geometries of the NSV. We our currently performing such work, which includes paleotopographic reconstruction using stratigraphic [e.g., 8, 13-18], paleotectonic [20-26], paleoerosional [e.g., 8, 12-14, 27- 31], and paleohdrological information (e.g., **Table 1**).

REFERENCES. [1] Bretz, J H., 1969, *J. Geology, 77*, 505-543. [2] Baker, V.R. and Milton, D.J., 1974, *Icarus, 23*, 27-41. [3] Baker, V.R., 1978, *Science, 202*, 1249-1256. [4] Baker, V.R., 1982, *Univ. of Texas Press, Austin*, 198 pp. [5] Mars Channel Working Group, 1983, *Geol. Soc. Amer. Bull., 94*, 1035-1054. [6] Baker, V.R., et al., 1991, *Nature 352*, 589-594. [7] Baker, V.R., et al., 2000, *Lunar Planet. Sci., XXXI.* [8] Scott, D.H., and Tanaka, K.L., 1986, *USGS I-Map 1802A.* [9] Greeley, R., and Guest, J.E., 1987, *USGS I-Map 1802B.* [10] Carr, M.H., 1979, *J. Geophys. Res., 84*, 2995-3007. [11] Phillips, R.J., et al., 2000, *Lunar Planet. Sci., XXXI.* [12] Chapman, M.G., and Tanaka, K.L., 1996, *USGS I- Map 2398.* [13] Rotto, S.L., and Tanaka, K.L., 1995, *USGS I-Map 2441.* [14] Nelson, D.M., and Greeley, R., 1999, *J. Geophys. Res., 104*, 8653-8669. [15] Scott, D.H., et al., 1998, *USGS I-Map 2561.* [16] Scott, D.H., and Zimbelman, J.R., et al., 1995, *USGS I-Map 2480.* [17] Scott, D.H., and Chapman, M.G., 1991, *USGS I-Map 2084.* [18] Witbeck, N.E., et al., 1991, *USGS I-Map 2010.* [19] Morris, E.C., 1991, *USGS I-Map 2001.* [20] Tanaka, K.L., and Davis, P.A., 1988, *J. Geophys. Res., 93*, 14,893-14,917. [21] Anderson, R.C., et al., 1997, *Lunar Planet. Sci., XXVIII.* [22] Anderson, R.C., et al., 1998, *Lunar Planet. Sci., XXIX.* [23] Anderson, R.C., et al., 1999, *Lunar Planet. Sci., XXX.* [24] Anderson, R.C., et al., 2000, *Lunar Planet. Sci., XXXI.* [25] Dohm, J.M., et al., 1998, *Astron. & Geophys., 39*, 3.20-3.22. [26] Dohm, J.M., and Tanaka, K.L., 1999, *Planet. & Space Sci. 47*, 411-431. [27] Scott, D.H., et al., 1995, *USGS I-Map 2461.* [28] Zimbelman, J.R., et al., 1994, *USGS I-Map 2402.* [29] Craddock, R.A., and Greeley, R., 1994, *USGS I-Map 2310.* [30] Chapman, M.G., and Tanaka, K.L., 1993, *USGS I-Map 2294.* [31] Carr, M.H., and Chuang, F.C.,1997, *J. Geophys. Res., 102*, 9145-9152. [32] Komar, P.D., 1979. *Icarus, 37*, 156-181. [33] Komatsu, G. and Baker, V.R., 1997, *J. Geophys. Res., 162*, 4151-4160. [34] Robinson, M.S., and Tanaka, K.L., 1990, *Geology, 18*, 902-905.

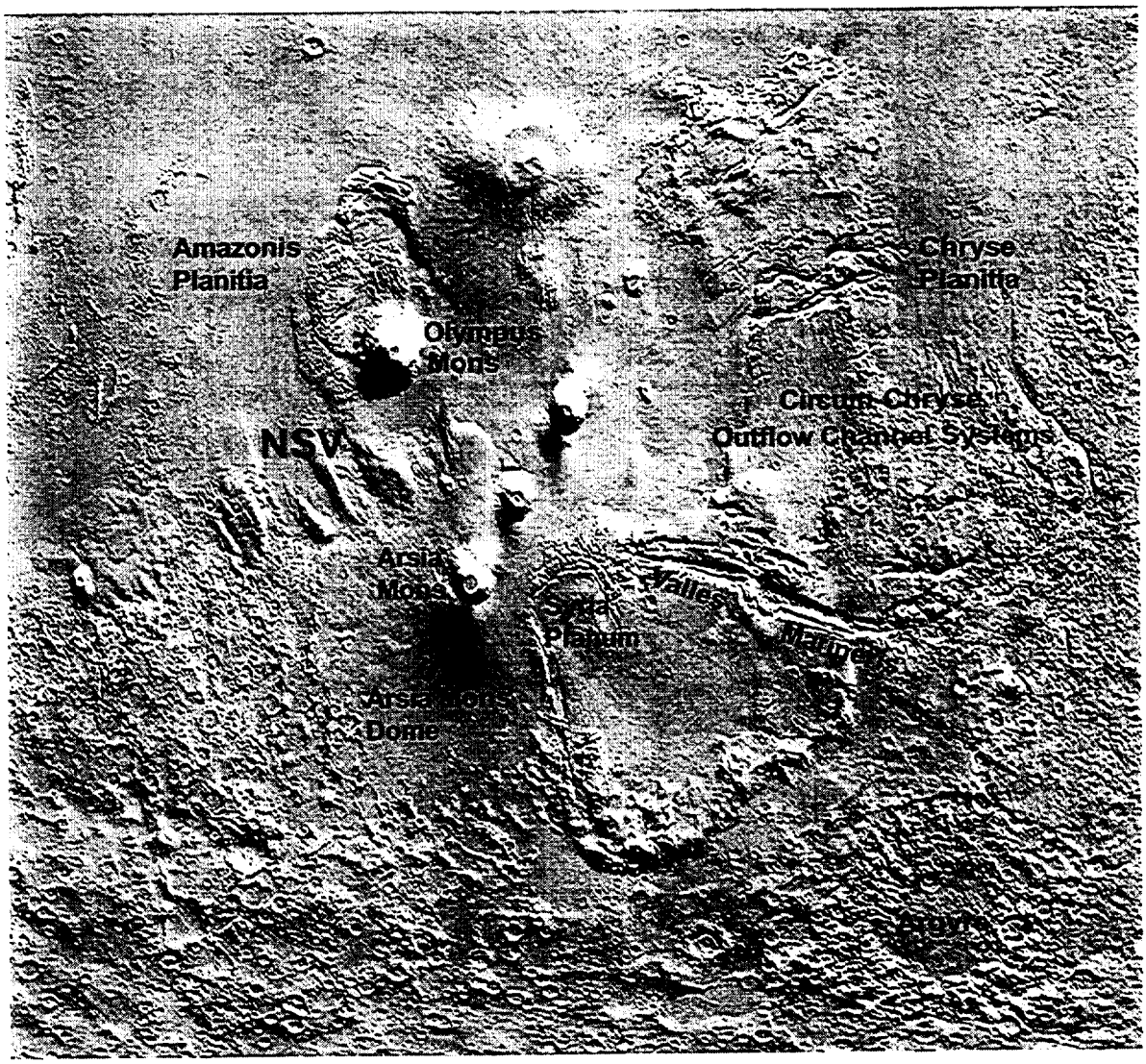

Figure 1. MOLA shaded relief map (MOLA Science Team). Newly identified northwestern slope valleys.

Reference	Channel	D(m)	W(km)	S	V (m/s)	Q (m^3/sec)
Komar (1979) [32]	Mangala	100	14	0.003	15	2×10^{7}
Baker (1982) [4]	Maja	100	80	0.02	38	3×10^{8}
Komatsu and Baker (1997) [33]	Ares	500 - 1000	25	0.02 - 0.0001	25 -150	5×10^{8}
Robinson and Tanaka (1990) [34]	Kasei	400 - 1300	80	0.009	30 - 75	$1\text{-}2 \times 10^{9}$
Dohm et al. (2000)	NSV	1200 - 2400	100 - 700	0.004 - 0.005	30 - 40	$2\text{-}3 \times 10^{10}$

Table 1. A comparative analysis between some of the previously defined martian outflow valley systems and the newly defined northwestern slope valleys (NSV).

COMPARATIVE RHEOLOGIES OF SOLID H_2O, CO_2, AND CO_2 CLATHRATE HYDRATE. W. B. Durham[1], S. H. Kirby[2], and L. A. Stern[2], [1]UCLLNL (P.O. Box 808, Livermore, CA 94550; durham1@llnl.gov), [2]USGS (Menlo Park, CA 94025).

Introduction: Water ice, CO_2 ice, and CO_2 clathrate hydrate are the principal ices expected to be present in the polar ice caps of Mars and in Martian soil. Laboratory experiments are now giving us well resolved information on the strength of these ices under ductile flow conditions, such as during the slow spreading of an ice sheet under the influence of gravitational forces. The purpose of this abstract is to present the current state of knowledge of the rheologies of these ices.

Background: Laboratory experimentation on ices is aimed at providing a constitutive rheological law, typically of the form

$$\dot{\varepsilon} = A\sigma^n \exp(-Q/RT) \quad (1)$$

where $\dot{\varepsilon}$ is the ductile (permanent, volume conservative) strain rate, σ is differential stress, T is temperature, R is the gas constant, and the three parameters A, n, and Q are material-specific constants. It is possible to duplicate Martian temperatures and Martian differential stresses in the laboratory, but it is not possible to duplicate them simultaneously because the resulting Martian strain rates will be too low to measure on the laboratory time scale. While we endeavor to reach ever finer levels of resolution, the current limit on laboratory strain rates, about 2×10^{-8} s^{-1}, is still several orders of magnitude faster than strain rates in the spreading Martian polar caps.

Recent results [1, 2] have shown that the three pure phases have very distinct rheologies. The clathrate hydrate is extremely strong and can be considered almost undeformable in comparison with other ices. CO_2 in contrast is exceedingly weak and will dominate the behavior of icy mixtures of which it is a component. The strength of water ice is intermediate to that of the other two ices. (A convenient and semi-quantitative way to picture the strengths of these ices is that the strengths of mild stainless steel, clathrate hydrate, water, and co2 are about equally spaced on a logarithmic scale.) Despite uncertainties about the age and topography of the Martian polar caps, the weakness of CO_2 ice is so pronounced that we can already say with confidence that it cannot be present as a major component of the Martian polar caps [3].

New results: Figure 1 shows the present state of knowledge of the rheologies of the three ices. We can report here two changes since our most recent publication of laboratory results [1].

Firstly, in new experiments on methane clathrate, which we take as a proxy for CO_2 clathrate, the strength appears higher at Martian temperatures than we predicted earlier. Measurements on methane hydrate have now been performed to temperatures as high as 287 K, and improved methods for removing free water from samples have shown that earlier strengths had been measurably influenced by small amounts of water.

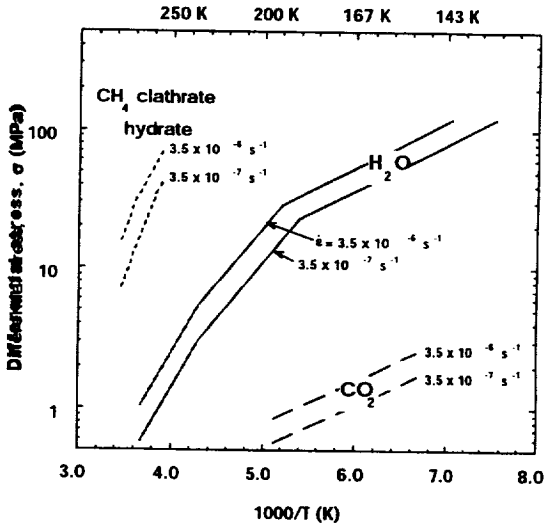

Figure 1. Laboratory results for the steady-state flow of three ices. Each line plots flow stress vs inverse temperature for a given value of strain rate $\dot{\varepsilon}$. Flow stresses are shown for two different strain rates for each of the ices to illustrate their respective strain-rate sensitivity. Data for methane clathrate hydrate are limited to warm temperatures because the exceedingly high strength of the material puts it beyond the limits of the testing apparatus at $T < 260$ K.

The other piece of new information that we want to contribute to the understanding of the flow of Martian ices is the relative contributions of dislocation creep and grain size dependent creep to the deformation of water ice. In terms of the constitutive law (Eq. 1), the two mechanisms have separate sets of material constants A, n, and Q, and the preexponential A for grain size dependent creep varies inversely (to the power 1.4) with grain size [4]. The two mechanisms act simultaneously and independently in any crystal-

line material, but in ice of "reasonable" grain sizes of 0.1 – 10 mm, the two mechanisms will contribute comparable amounts of strain rate at Martian stresses and temperatures (Figure 2). The same appears true at conditions of terrestrial glaciers and ice caps and in the interiors (but not on the surfaces) of the large icy satellites of the outer solar system. The message is, then, that models for the flow of water ice in most planetary applications must account for both dislocation creep and grain size dependent creep.

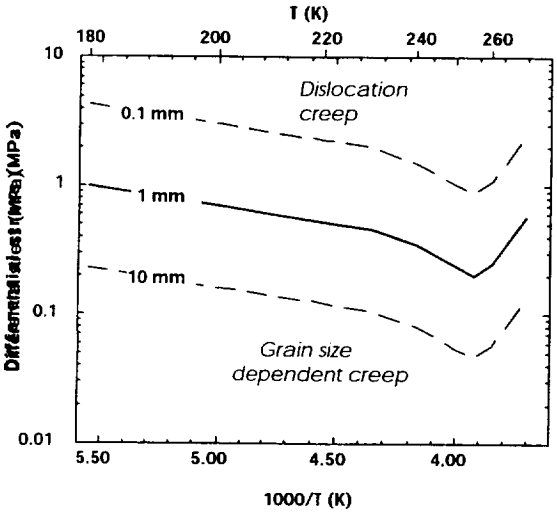

Figure 2. Deformation map for water ice showing the boundary between dislocation creep domination and grain size dependent creep domination at a grain size of 1 mm (solid line) and at grain sizes 0.1 and 10 mm (dashed lines). Grain size dependent creep data are from [4].

References: [1] Durham W. B. et al. (1999) *Abstracts, Intl. Workshop on the Martian Ice Caps, Copenhagen.* [2] Durham W. B. et al. (1999) *Geophys. Res. Lett. 26*, 3493-3496. [3] Nye J. F. et al. (2000, in press) *Icarus, Mars Polar Conf. Special volume.* [4] Goldsby D. L. and Kohlstedt D. L. (1997) *Scripta Mater., 37*, 1399–1406.

AN ASSESSMENT OF THE NORTH POLAR MAGNETIC ANOMALY: IMPLICATIONS FOR BASAL MELTING AND POLAR WANDER. J. T. Eckberg, Physics Department, Montana State University, EPS 264, Bozeman, MT, 59717, eckberg@montana.edu.

Introduction: Measurements taken by the magnetometers aboard MGS during aerobreaking have provided the most spatially complete mapping of the radial magnetic field (B_r) in the Mars North Polar Region (NPR) available to date. The subsequent map made of this complete coverage [1,fig 1], depicts an anomalous region of relatively strong field intensity (~+/- 40nT) in addition to the more isotropically distributed regions of (~+/- 10nT). This analysis explores the possible connection between liquid water environments in the NPR and reinforcement of magnetized regions.

Martian Paleomagnetism: The B_r magnitude observed in the NPR is much weaker (~40x) than the lineated B_r structures in Terra Cimmeria and Terra Sirenum that have received the majority of the attention to date [2]. This is believed to be the result of large impacts [16] and high heat flux [3,9] in the Noachian, both of which raised the temperature of the magnetic region above the Currie temperature (T_c) and randomizing the once coherent domains of a magnetized layer believed to lie in a layer roughly 25-35 km beneath the surface [4]. While the large impact structures undoubtedly removed any trace of magnetization in their affected radius, the heating of the crust appears to have significantly thinned the remnant layer without completely removing it. The existence and location of the NPR anomaly is then suggestive of a mechanism that produced the observed fields after the cessation of the Martian dynamo.

Oceanus Borealis: The recent debate over the existence of liquid water in Vastitas Borealis proposed by Parker et al. [5], supported by MOLA topographic analysis [6], and disputed by MOC tests [7] appears to have found a plausible solution in the proposal of a "mud ocean" by Tanaka et al. [8] as the true nature of Oceanus Borealis. The mud in question was material that by fluvial erosion in the outflow channels has been transported with the water and deposited in the low lying northern plains. This assessment is supported by radio-Doppler gravity data that reveal the continuation of the Chryse outflow channel well into Acidalia planitia by negative gravity lineations not otherwise visible [9].

Clifford et al. have connected these Hesperian outflows with basal melting under a once larger and thicker north polar ice cap. As the northern ocean cooled to freezing temperatures, more and more of the water became trapped at the poles due to the instability of ice at the lower latitudes. The thickening of the polar ice cap resulted in basal melting and suffusion of the crust beneath the cap with liquid water [10].

Paleomagnetization: Crystallization remnant magnetization (CRM, sometimes referred to as chemical remnant magnetism) is a process by which a magnetic mineral forms in the presence of an external magnetic field. [11] The magnetic field in this case is proposed to come not from an early dynamo but rather iron-rich regions in the crust that became magnetized by the dynamo. The proposed mineral in this case is magnetite (Fe_3O_4) and possibly maghemite (γ–Fe_2O_3) , which can precipitate in a low temperature, aqueous solution of dissolved Fe^{2+} with the stipulation that the oxidation must occur slowly [12]. On Earth, this is not the case and as a result the weakly magnetic mineral hematite (α-Fe_2O_3) is formed. Fe^{2+} ions dissolve into water as it comes into contact with iron phases of pyroxene and olivine, probable constituents of the Martian crust [15].

CRM occurs as the magnetic particle size grows past the superparamagnetic scale, (d<10nm) to the single domain (SD) scale in an external magnetic field. The coherent magnetization of a particle decreases as the growth continues into the pseudo-single domain (PSD) and multi-domain (MD) scales for the mineral. In the case of the proposed region, this process should be continuous up to the point the water began to freeze and therefore, all particle sizes would be present in their relative abundances (dependant upon Ph, Fe ion content, etc.) [12]. As this watery environment became frozen, the chemical precipitation of magnetic particles effectively ceased and the average magnetic alignment would become fixed in the direction parallel to the external field.

Another process could have assisted in the magnetization of the region if the flow of the basal melt was at some point vigorous enough to disrupt the alignment of CRM formed particles. Post depositional remnant magnetism (PDRM) is the result of the magnetic torque(1) upon a particle with a significant magnetic moment relative to the size of the particle.

$$\mathbf{N}_B = \mathbf{m} \times \mathbf{B}$$

Figure 1. Magnetic torque is the curl of the particle magnetic moment with the magnetic field.

This would tend to insure that all free particles would eventually become aligned with the external field. PDRM however, would only become viable in the case where the torque on the particle is larger than the drag force the particle would feel in a flow. Another detri-

ment to PDRM is the effect Brownian motion has on the alignment of the particle moment [11]. This is however temperature dependent and would cease to be significant previous to freezing.

Polar Wander: The offset of the magnetic anomaly from the north polar cap promotes the notion that the spin-axis of Mars may have sometime in the past wandered to the location observed today. Assuming the footprint of the pole covered the observed anomaly then this would imply a paleo-pole location of roughly 340°W longitude by 75°N latitude (2), if the shift occurred after most of the cap-induced magnetization was completed. This seems to be the case as there is no significant magnetic signature centered about the current pole. Transport of water into the crust by basal melt undoubtedly diminished the volume of the cap significantly by the time the liquid phase had ceased. The shift apparently had the effect of consolidating the remaining surface water ice about the new pole in a thicker arrangement, now incapable of basal melting due to the cooler interior.

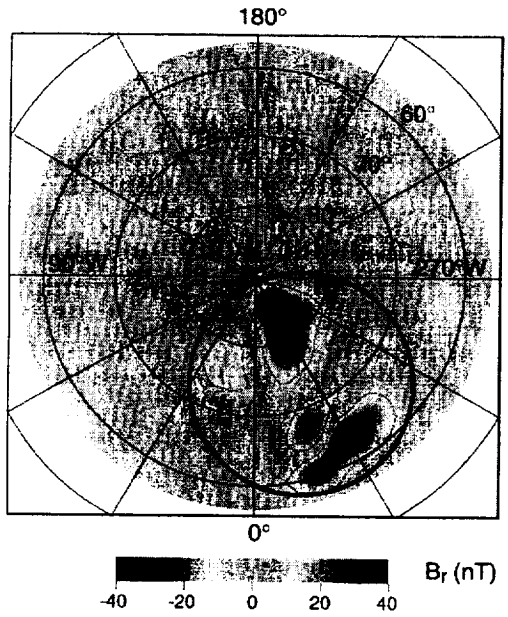

Figure 2. The proposed minimum polar cap footprint required for basal melt derived CRM.

Additional, possibly circumstantial evidence appears to support this theory. The shift in position of the paleo-pole is in roughly the direction expected from displacement of large masses of material from Tharsis and Elysium volcanism assuming Tharsis originated at higher southern latitude [16]. Also, the location and asymmetry of circumpolar deposits about the northern ice cap [14, fig 1 & 3] possibly suggest the effect of a pole drift related mechanism.

Conclusions: The location and intensity of magnetization of the NPR magnetic anomaly is consistent with a mechanism by which basal melting supplied the liquid water for crystalline remnant magnetism and possibly post-depositional remnant magnetism to occur underneath the north polar ice cap. This would have occurred not in the present location of the ice cap but in the region overlying the NPR magnetic anomaly mapped by MGS during aerobreaking. The proposed paleo-cap location is suggestive of an epoch previous to significant Tharsis distension and spin axis adjustment.

References:[1] Acuna, M.H. et al., (1999) *Science* **284**, 790. [2] Connery J.E.P. et al., (1999) *Science* **284**, 794. [3] Schubert, G. et al., (1992), in *MARS* 147-183, U.Ariz. Press. [4] Gilmore et al., (2000) *LPSC* **XXXI,** Abstract #2003 LPI Houston (CD-ROM). [5] Parker T.J. et al., (1989) *Icarus* **82**, 111. [6] Head J.W. et al., (1999) *Science* **286,** 2134 [7] Malin, M. and Edgett, K. *GRL.* **26**, 3049 (1999). [8] Tanaka K.L. et al., (2000) *LPSC* **XXXI,** Abstract #2041, LPI Houston (CD-ROM). [9] Zuber M.T. et al., (2000) *Science* **287**, 1788. [10] Clifford S.M. et al. (1999) *MARS V*, Abstract #6236, LPI Houston (CD-ROM). [11] Dunlop and Ozdemir (1997) Rock Magnetism: Fundamentals and frontiers, Cambridge Press [12] Pick, T. and Tauxe, L. (1991) *JGR.* **96**, No. B6, 9925-9936. [13] Griffiths (1999) Intro. to Electrodynamics, Prentice Hall.[14]Thomas, P et al.,(1992), in *MARS* 767-795, U.Ariz. Press. [15] Longhi J. et al., (1992), in *MARS* 184-208, U.Ariz. Press. [16] Banert, W.B. et al., (1992), in *MARS* 249-297, U.Ariz. Press. [17] For an animation of impact demagnetization, visit the site: http://mgs-mager.gsfc.nasa.gov/animation/mars_impact.html.

THE MARTIAN NORTH POLAR CAP: SEDIMENTARY ASPECTS. K. S. Edgett and M. C. Malin, Malin Space Science Systems, P. O. Box 910148, San Diego CA 92191-0148, USA.

Synopsis: The polar layered terrains of Mars exhibit many of the characteristics common to sedimentary rocks and deposits on Earth, including groups of similar beds (*i.e.*, 'formations'), continuity of beds over 100s of kilometers distance, beds of differing thickness and resistance to erosion, deformed beds, and erosional unconformities. Many of these features are readily apparent in the north polar cap, the subject of this brief report, in 1.5–12 m/pixel images acquired by the Mars Global Surveyor (MGS) Mars Orbiter Camera (MOC) in the past 2 years. The sedimentary and stratigraphic properties described here attest to the presence of a complex geologic record that, with adequate field work, could one day be deciphered.

Introduction: 'Laminated terrain' or 'polar layered deposits' have been known since the Mariner 9 mission. The layered nature of the polar material led to immediate speculation that these units are a type of sedimentary deposit, most likely a mixture of silicates (largely in the form of dust settled from atmospheric suspension) and, owing to their presence near the poles, ice. The layered expression was interpreted to indicate that a record of past climate change is present, as changes in the depositional environment, processes, and/or materials would lead to changes in bedding style and properties. The apparent similar thickness and repeatability of layers visible in Mariner 9 and Viking orbiter images suggested that these might be the result of climate-induced control on a cyclic or episodic basis. Here we report on new observations regarding the sedimentological character of polar layers; earlier MOC images and discussions were described in [1].

Data: MGS has been orbiting Mars since September 1997. Because of the spacecraft aerobraking schedule and seasonal darkness (*i.e*, winter), the north polar region has only been adequately viewed by MOC in July–September 1998 and March–August 1999. The focus here is upon the properties of layers exposed in the broad, shallow slopes of troughs or 'dark lanes' within the Planum Boreum (residual north polar cap). MOC has viewed these surfaces from orbit in a nadir-pointed orientation, thus each image represents a vantage point "looking straight down" upon a banded slope in the north polar terrain.

More Beds; Beds of Differing Properties; and Unconformable Beds: Figure 1 shows a slope in a north polar trough that has dozens of layers and groups of layers of differing thickness and resistance to erosion. Layers that form ridges are more resistant than those that are recessed. The layers in Fig. 1 include a set in the upper 1/4 of the image that appears to pinch-out from left to right, perhaps representing the location of an erosional unconformity. As was suspected before the MGS mission, MOC images reveal that there are many more—and thinner—beds than were visible in Viking and Mariner 9 orbiter images. This observation suggests that there could be even thinner beds, down to scales of centimeters or less, and that such beds would be accessible to landed spacecraft.

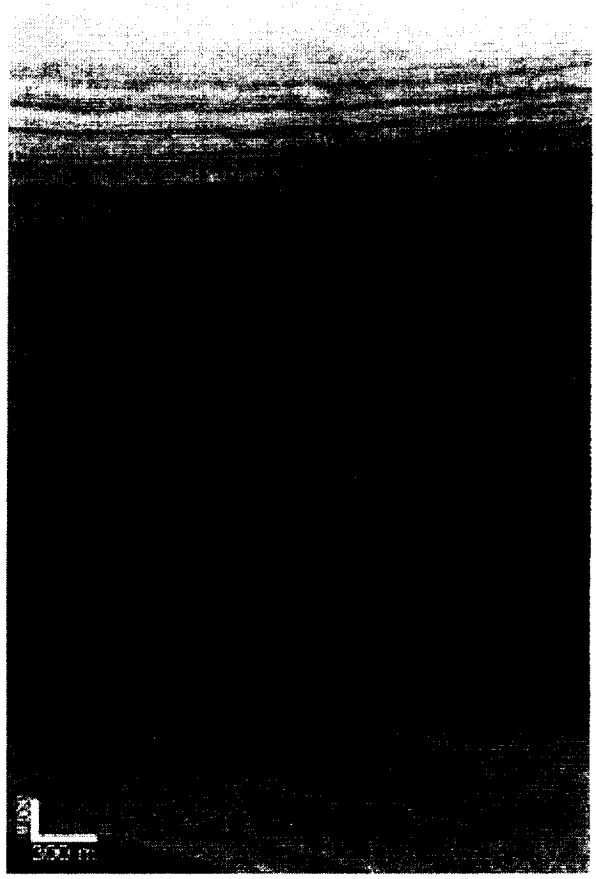

Figure 1. North polar layer outcrop. Sub-frame of MOC image M02-04374, near 81.1°N, 287.4°W, illuminated from top/upper right, acquired 27 June 1999.

Stratigraphy and Continuity: Individual beds within the north polar cap can be traced over distances greater than 100 km, and whole groupings of beds—perhaps better described as geologic 'formations'—can be traced over 100s of kilometers, as well. Figure 2 shows three views of the walls of a single trough; each image is spaced 10s of km from the other, yet many beds can be seen to be continuous over this distance. The feature labeled "MB" in Fig. 2 is a

marker bed that is also found in other troughs throughout the north polar region and will perhaps be useful in the stratigraphic correlation efforts that are just beginning. Figure 3 also exhibits the promise of stratigraphic studies in the north polar region. The two images in Fig. 3 are located on escarpments located ~280 km apart in different polar troughs, yet they have the same stratigraphic sequence including a slightly jumbled, platy, dark terraced unit overlain by a lighter-toned, thick, flat-lying, evenly-bedded unit. The contact between the two units might be an unconformity.

Deformed Beds: Several examples of folded or otherwise deformed beds have been identified in the north polar strata; Fig. 4 provides one example, others were shown in [1]. The folded beds in this case might represent soft-sediment deformation rather than a tectonic process, because they are bounded above and below by more regular, horizontal beds with no apparent unconformity between them.

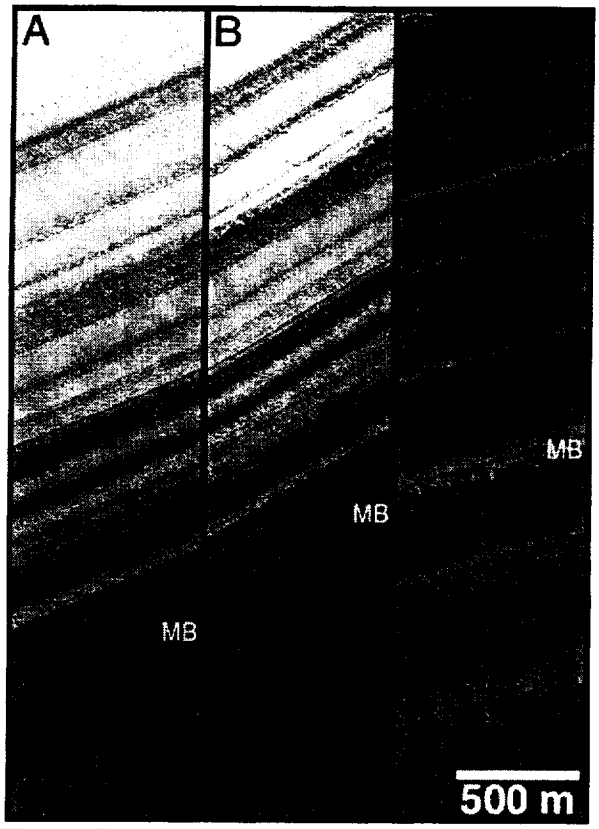

Figure 2. Continuity of polar layers over >100 km distance. Sub-frames of MOC images (A) M00-01754 near 86.5°N, 281.5°W, (B) M00-02100 near 86.4°N, 278.7°W, and (C) M00-02072 near 85.9°N, 257.9°W. All illuminated from the upper right, all acquired in April 1999.

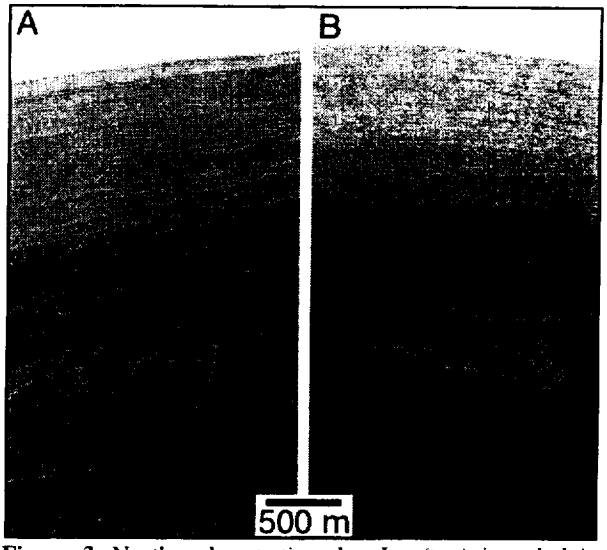

Figure 3. North polar stratigraphy. Ice (top) is underlain in both cases by a sequence of light-toned, horizontally-bedded material, which itself is underlain by a darker, platy layered unit. The images are located ~280 km from each other on two different escarpments. (A) Sub-frame of M02-01676 near 85.4°N, 167.9°W, illuminated from the right, 14 June 1999. (B) Sub-frame of M03-04769 near 85.0°N, 357.7°W, illuminated from top/upper right, 24 July 1999. Both scenes are partly obscured by late-summer haze.

Figure 4. Deformed beds in a north polar trough slope (upper 1/4 of image). Sub-frame of M00-01925 near 81.4°N, 273.1°W, illuminated from the upper right, 12 April 1999.

Reference: [1] Edgett K. S. and Malin M. C. (2000) *LPS XXXI*, abstract #1068.

SPRING DEFROSTING OF MARTIAN POLAR REGIONS: MARS GLOBAL SURVEYOR MOC AND TES MONITORING OF THE RICHARDSON CRATER DUNE FIELD, 1999–2000.

K. S. Edgett, K. D. Supulver, and M. C. Malin, Malin Space Science Systems, P.O. Box 910148, San Diego, CA 92191-0148, USA.

Synopsis: Changes in the appearance of a defrosting dune field in the martian southern hemisphere are tracked from late winter into early summer. Changes become noticeable shortly after the dune field emerges into sunlight as winter transitions to spring. These changes, in the form of small dark spots formed on and along the base of the dunes, occur while surface temperatures are still around the freezing point of CO_2 (~148 K). Most of the changes occur over the course of spring, while temperatures are transitioning from those of frozen CO_2 toward the H_2O freezing point (~273 K). Late spring and early summer views acquired ~2 a.m. local time exhibit higher albedos than ~2 p.m. views obtained during the same period, suggesting that frost forms on these surfaces as the sun dips toward the horizon during early morning hours in these seasons.

Introduction: Mars Global Surveyor (MGS) Mars Orbiter Camera (MOC) images have shown that dune fields in the polar regions of Mars are the first surfaces to show signs of becoming frosted in autumn and defrosted in spring [1]. Repeated observations of the same dune field by both MOC and the MGS Thermal Emission Spectrometer (TES) provide a record of visual change as a function of temperature and season. In this preliminary study, we look at the dune field in Richardson Crater, located at 72.4°S, 180.0°W, as it was observed by MOC and TES between L_s 150° (June 1999) and L_s 310° (Feb. 2000).

Observations/Discussion: Figure 1 has 21 sub-frames of MOC images of the Richardson Crater dune field acquired between late winter and early summer. Each picture is shown at the same scale, covers an area approximately 2.2 by 3.4 km, and is oriented such that north is up. Figure 2 shows the size and location of each MOC sub-frame relative to a Viking orbiter view of the dune field. Although the sub-frames cover different portions of the dune field, each sample is presumed to be representative of what the entire dune field looked like—in terms of seasonal frost patterns—on the basis of other MOC observations of frosted dune fields which show that one area is fairly representative of the whole (*e.g.*, images in [1]). In general, the MOC images in Figure 1 show a slow transition from a dune field that is completely covered with seasonal frost at L_s 150° (Fig. 1A) to one that has no frost at L_s 306° (Fig. 1U). The L_s 150° and 164° views were obtained while the dune field was still in winter darkness—sufficient light was scattered over the horizon to allow images to be obtained. The summer views (Figs. 1S–1U) show that the dunes are darker than the substrate upon which they occur. The albedo contrast between the dunes and substrate does not become obvious until late spring (Figs. 1P–1R), which suggests that frost reduces this contrast until at least ~L_s 250°. During the middle spring period (Figs. 1I–1Q), a combination of dark- and light-toned spots and streaks are evident (note that the two long, wide dark surfaces in Fig. 1J are caused by underexposure in shadowed areas, not albedo). As of this writing we do not know what these bright and dark spots represent—perhaps the dark ones are patches of low albedo sand that have become exposed by defrosting, while light spots are patches of water frost formed by outgassing of the dunes as they begin to warm up. Alternatively, the bright and dark spots might all represent changes in the particle size and/or physical state of surface-covering frosts. Particle size is a suspect because these materials form streaks in response to local winds, and are thus thought to either have saltated (particle size) or settled to the surface (from outgassing at point sources on the dune surfaces).

Figure 3 shows changes in albedo and temperature as a function of L_s in the Richardson Crater dune field. All data used here were obtained at the same times that MOC images in Figure 1 were acquired. Filled circles represent data obtained at local time ~2 p.m., open circles are data from ~2 a.m. The temperatures are derived from the TES thermal bolometer (5.5–100 μm single band), the albedos from the TES visual bolometer (0.3–2.7 μm). The dunes in late winter are at temperatures consistent with frozen CO_2. Temperatures rise toward that of frozen H_2O throughout the spring, corresponding to the period in which the varied spots and streaks are observed. By late spring, temperatures reach ~273 K and all visual evidence for frost disappears—except in early morning images such as Fig. 1T, which has a corresponding albedo of 0.22 while the dune field and substrate typically have an afternoon albedo of 0.14.

Reference: [1] Malin M. C. and Edgett K. S. (2000) *LPS XXXI*, abstract #1056.

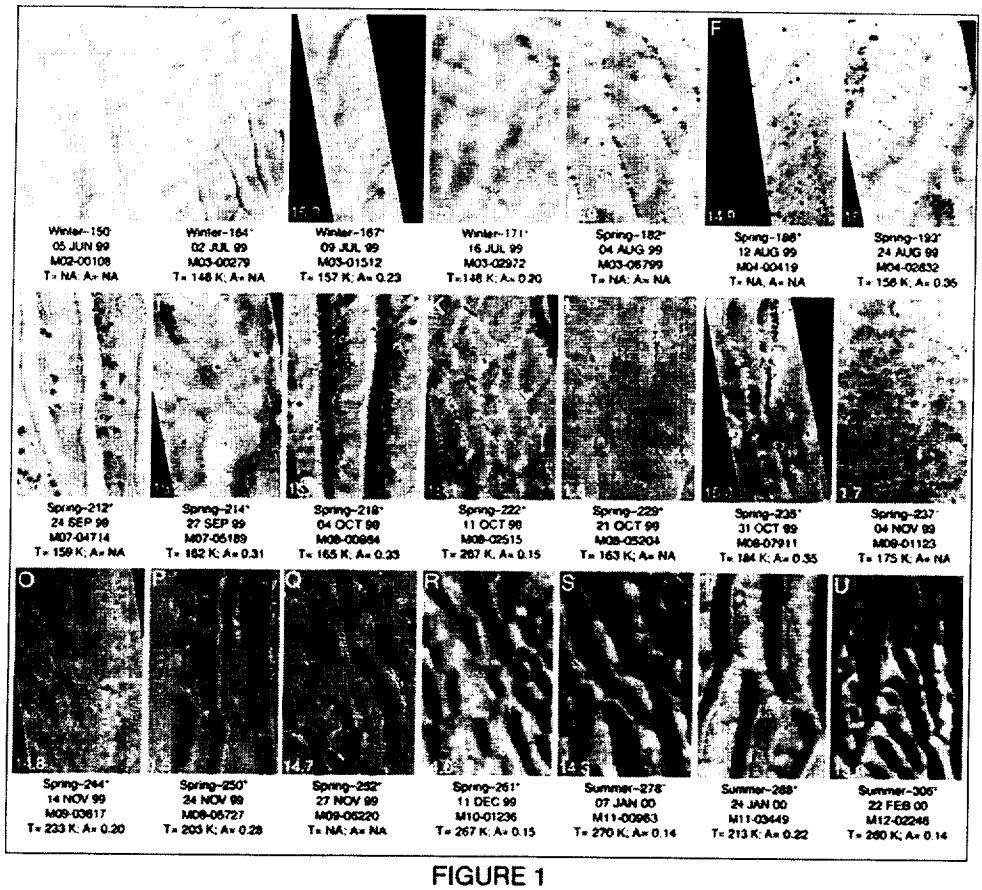

FIGURE 1

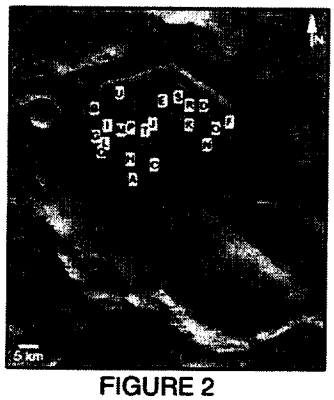

FIGURE 2

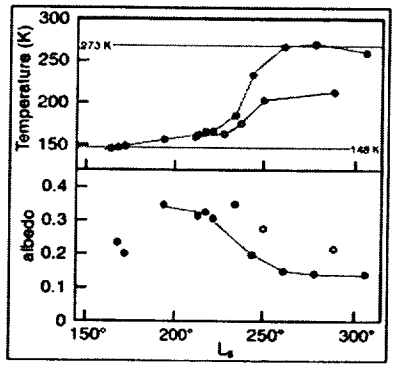

FIGURE 3

Figure 1: MGS MOC views of Richardson Crater dune field, L_s 150°–306°. Local time of day is given in lower left corner of each. See text for additional details. **Figure 2:** Context of each MOC image sub-frame in Figure 1. White boxes are same size (2.2 by 3.4 km) as Figure 1 images. **Figure 3:** MGS TES thermal bolometer temperatures and visual bolometer albedos obtained at the same time as MOC images in Figure 1. Filled circles are at ~2 p.m. local time, open circles ~2 a.m.

THE KATLA SUBGLACIAL VOLCANO: EARTHQUAKES AND EVIDENCE FOR CRUSTAL MAGMA CHAMBERS. Páll Einarsson and Bryndís Brandsdóttir, Science Institute, University of Iceland, Hofsvallagata 53, 107 Reykjavík, Iceland (palli@raunvis.hi.is, bryndis@raunvis.hi.is)

Seismological methods can be used effectively to study the internal structure and dynamics of volcanoes. Hypocenters of earthquakes provide information on the location of physical events, focal mechanism studies give information on their nature. Seismic waves that have propagated through the roots of volcanoes carry information on the physical state of the material there, e. g. location of magma chambers. Eruptive activity is usually accompanied by seismic activity which can give invaluable information on processes in the crust s.a. magma migration. Several of the Icelandic central volcanoes, including the subglacial Katla volcano in South Iceland, are the source of persistent seismic activity in spite of little other apparent signs of volcanic unrest [1], [2]. Several physical processes can cause these earthquakes, s. a. slow inflation or deflation of a shallow-level magma chamber, intrusion of magma into the shallow crust, or thermal cracking due to heating or cooling of brittle crustal material.

The Katla volcano is an off-rift volcano, covered by the glacier Mýrdalsjökull, and located in the volcanic flank zone in South Iceland. It has produced mainly transitional alkalic basalt lavas and tephra [3], [4], but more silicic rocks are known from nunataks in the glacier [5]. A caldera, 10 km x 13 km in diameter, mapped beneath the glacier by radio echo sounding (Björnsson et al., this conference), is underlain by a zone of low P-velocity and high S-wave attenuation interpreted as a magma chamber at a depth of less than 3 km [6]. The Eldgjá fissure to the north is structurally connected to the Katla volcano, and the similarity of the chemistry of Katla and Eldgjá lavas has led to the suggestion that Eldgjá eruptions were fed by lateral flow from the Katla magma chamber [7]. The Eyjafjallajökull volcano to the west of Katla has a distinct, E-W striking fissure swarm that merges with the radial fissure system of Katla. The volcanoes thus appear to be tectonically connected.

Katla eruptions during the last 1100 years are relatively well known from historical records [8]. At least 17 eruptions occurred in this time, the latest large ones in 1823, 1860 and 1918. These eruptions were accompanied by substantial jökulhlaups from the glacier. Small subglacial eruptions appear to have occurred in 1955 and 1999 as suggested by seismicity, both earthquakes and volcanic tremor recorded prior to small jökulhlaups. No eruption was visible but subsidence cauldrons were formed in the ice within the caldera on both occasions.

The most dramatic evidence for prehistoric activity of Katla is a layer from about 12 000 ybp found in the GRIP ice core, thought to correspond to Ash Zone 1 in Atlantic sediment cores and a deposit formed by lahars, ash fall and surges on the south flank of the volcano [9], [10]. Ash layers from Katla have also been identified in the GRIP core at 75 400 and 77 500 ice core years [9].

Katla and the surrounding volcanic area has shown persistent high seismic activity for more than four decades. No volcanic activity has been detected during this time, however, with the exception of probable small subglacial eruptions in 1955 and 1999. Seismic data of the period 1978-1985 are anlysed here. Epicenters of this period fall into two distinct clusters under the Mýrdalsjökull glacier. One cluster is located within the caldera of the Katla volcano, the other is centered in the Goðabunga area, west of the caldera and beneath the western caldera rim. All available data are consistent with hypocentral depths of 0-4 km. Earthquakes of both clusters have distinct characteristics of volcanic earthquakes, i. e. emergent P-waves and poor S-waves. These characteristics are more pronounced for the Goðabunga cluster. The coincidence of the Katla cluster with the caldera and an area of S-wave shadowing suggests that it is related to an active magma chamber of the Katla volcano. Similarly we take the Goðabunga cluster as an indicator of the existance of a second magma chamber. It is a matter of definition whether this chamber represents a separate central volcano or a second magma chamber of the Katla volcano. The two clusters together with the Eyjafjallajökull volcano to the west and its fissure swarm form a pronounced E-W structure and appear to be mechanically coupled. Two historical eruptions of Eyjafjallajökull are temporally related to Katla eruptions. Earthquakes under Goðabunga show a clear seasonal correlation. Earthquakes are several times more likely to happen in the latter half of the year than in the first [11]. Two factors are likely to be effective here, the load of the glacier ice and the pore pressure in the crust beneath the glacier. Both factors would tend to reduce the friction on fault planes in the autumn when melt water seeps into the crust and increases the pore pressure. We argue that the pore pressure produces a larger effect than the change in the ice load.

References: [1] Tryggvason, E. (1973) *Bull. Seismol. Soc. Am., 63*, 1327-1348. [2] Einarsson, P. (1991) *Tectonophys., 189*, 261-279. [3] Jakobsson, S. P. (1979) *Acta Nat. Isl., 26*, 103 pp. [4] Steinþórsson, S. et al. (1985) *JGR, 90*, 10,027-10,042. [5] Jóhannesson, H. et al. (1982) *Museum of Nat. Hist. and Iceland Geod. Surv.* [6] Guðmundsson, Ó. et al. (1994) *Geophys. J. Int., 119*, 277-296. [7] Sigurdsson, H., and S. Sparks (1978) *Nature, 274*, 126-130. [8] Þórarinsson, S. (1975) *Ferðafélag Íslands, Árbók*, 125-149. [9] Grönvold, K. et al. (1995) *Earth Planet. Sci. Lett., 135*, 149-155. [10] Lacasse, C. et al. (1995) *Bull. Volcanol., 57*, 18-32. [11] Brandsdóttir, B., and Einarsson, P. (1992) *In: Volcanic Seismology* (eds. P. Gasparini and K. Aki), Springer Verlag, 212-222.

CURRENT ISSUES IN MARS POLAR RESEARCH: USING MOLA DATA TO COMPARE THE MARTIAN POLAR CAPS Kathryn E. Fishbaugh[1] and James W. Head III[1], [1]Brown University Box 1846, Providence, RI 02912, kathryn_fishbaugh@brown.edu, james_head_III@brown.edu

Introduction

New high-resolution data from the Mars Orbiter Laser Altimeter (MOLA) [1,2] has allowed detailed topographic mapping of the north [3] and south polar regions, following earlier comparisons using Viking data [4-6]. These new data allow one to compare the overall topography and geologic histories [7] of the two polar regions and to highlight some specific outstanding issues in Mars polar studies.

Observations

Polar cap shape. In plan, the south polar cap (including the polar residual ice and layered terrain) has a more irregular shape than the north polar cap. Both caps are asymmetrical about the current rotational poles. In the north, this has been interpreted to be due to retreat of the cap from the 180°W direction [3]. Hesperian retreat may also have played a role in asymmetry of the southern cap [8,9]. The centers of the caps are offset a few degrees from the present rotational poles in antipodal directions. The caps have similar cross-sectional shapes [2], but the south polar cap has a larger volume (~2-3 x 10^6 km^3 [2]) compared to the north cap (1.2-1.7 x 10^6 km^3[1]).

Topography of circumpolar regions. The south polar cap does not lie within a depression as does the north polar cap [1,3], but instead the surrounding topography slopes away from the south polar cap. Much of the southern circumpolar topography (and thus the subcap topography) is older and rougher (influenced by Hellas, Argyre and Prometheus) than the northern circumpolar deposits which are some of the smoothest terrains on Mars [10].

Geology and stratigraphy: The circumpolar deposits in the north consist mostly of the very smooth and extensive Hesperian Vastitas Borealis Formation (VB) [7]. Amazonian mantling material, thought to partly be derived from erosion of Apl [4,3], overlies VB and surrounds and (in some places) mantled the cap itself. The Late Amazonian cap [7] overlies the VB. In the south, heavily cratered Noachian terrains (Npl, Npld) generally underlie the Hesperian Dorsa Argentea Formation (Hd) [e.g., 6,7] and ridged (Hr) and undivided material (HNu). The Late Amazonian [7] polar cap (Apl, Api) overlies the Hesperian and Noachian terrain.

Polar cap ages. The northern and southern caps are mapped as late Amazonian in age [7]. Based on crater counts from high resolution Viking images covering ~80% of the layered deposits, Plaut et al. [5] estimated the southern cap to be a few 100 Myr (Early to Mid Amazonian). This age was later revised to 7 - 15 Myr (Late Amazonian) based upon a revised recent Martian cratering flux [11]. Based on crater counts [12], the estimates of the age of the north polar deposits range from <100 Kyr [13,14] to <10 Myr [4]. Thus, the southern cap appears to have a much older surface age. An older southern cap is supported by the fact that the northern cap was deposited after whatever resurfaced the northern plains and by models of the Martian hydrological cycle [15]. There is evidence in both polar regions of once more extensive caps.

Evidence for formerly larger polar caps. Blanketing of portions of the north polar cap at Olympia Planitia and evidence for depressions interpreted as kettles just south of this area show that the Amazonian-aged cap was once more extensive [3,16]. In the south there is extensive evidence (esker-like ridges, extensive development of cavi, chasmae, channels draining the deposits, etc.) that the Hesperian-aged Dorsa Argentea Formation and related units represent older water ice-rich polar deposits below the Amazonian Api/Apl and that they underwent extensive melting and retreat [8,13,17].

Melting of polar materials. There is evidence for melting having occurred at both caps. The best examples of this evidence are Chasma Boreale [18-21] in the north and Chasma Australe [22] in the south which are compared in [9]. Both caps also contain smaller chasmae similar to Boreale [20, 21] and Australe. The South polar region also contains other varieties of melting features (such as eskers and cavi [8,13]). The greater variety of southern melting features could be due to the greater variation in basal topography in the south or differences in substrate properties between the north and south [8,9].

This evidence for melting strongly implies that similar thermal conditions must have existed at both caps at the time(s) of melting.

Outstanding issues

1) Asymmetry: Both caps are asymmetrical about the current rotational poles and are presently offset from the rotational poles by a few degrees in antipodal directions. Some asymmetry is plausibly interpreted as due to retreat of portions of the caps. Could the antipodal offset be due to polar wander [23]? What is the relative timing of the retreat of both caps? What mechanism(s) could provide a physically plausible means of causing the amount of retreat we observe? Was retreat of the caps smoothly continuous or episodic?

2) Sub-polar cap topography: The northern cap lies within a broad, unusually smooth depression, while the southern circumpolar topography slopes away from the cap. The underlying topography in the south is much rougher, more heavily cratered, and slopes away from the pole. Could substrate differences between the two caps be responsible for differences in basal melting features? Could variations in the subcap topography between the two caps influence cap flow and the storage capacity of meltwater?

3) Chronology: The Southern Late Amazonian cap is

surrounded by and partially overlies Hesperian deposits, some of which (Hd, HNu) are interpreted to be volatile-rich, polar-like deposits [8]. The Northern Late Amazonian cap overlies Hesperian deposits (VB), implying a hiatus in deposition between the Late Hesperian and Late Amazonian. These observations lead to questions about the chronology of geologic activity in both regions.

Are the polar cap deposits entirely of Late Amazonian age? If so, what geological activity was occurring during the time between deposition of the surrounding Hesperian deposits and the deposition of the Late Amazonian polar deposits (e.g., polar wander? [23])? Or are at least part of the layered deposits of both caps actually Late Hesperian in age, as suggested by their close connection with the surrounding terrain? If these deposits are in part Late Hesperian, then some process (e.g., ice cap movement and crater obliteration [24]) may be destroying the cratering record within the caps, and this process may be operating more efficiently in the northern cap. Is the geologic record at the poles continuous or discontinuous, and is there evidence for processes of active crater removal [24]? Do the southern Hesperian deposits (Hd) represent ancient polar deposits [8]? Where is the equivalent unit in the north? Could the southern polar deposits be related to a former standing body of water in the north [25]?

5) The significance of basal melting: Numerous examples of features related to basal melting exist near both poles. Among the possible scenarios permitting melting are: 1) local sub-cap volcanic eruptions [19], 2) a higher geothermal heat flux in the past [13], 3) much thicker caps [18], 4) climate change, 5) obliquity change, 6) polar wander, or 5) inclusion of clathrates, salts, more dust, etc. within the layered deposits. Crustal thickness differences between the northern and southern hemispheres [26] suggest that geothermal heat flux would likely be different beneath the two caps and thus that melting by this method would not be contemporaneous at the two poles. Topography does not appear to suggest formerly larger caps with volumes sufficient to induce melting at the base of the cap by a shallowing of the current geotherm within the crust [e.g., 13,18]. Climate change, obliquity change, and polar wander would affect both caps in a similar manner, and their effects need to be quantified. The north polar cap may have entrained evaporites since it may overlie oceanic deposits [3], whereas the south polar cap may have more CO_2 clathrates [13, 27] both of which would lower the ice melting point. This strongly suggests similar thermal conditions at both caps. What is the cause(s) of this extensive melting? Were the causes different at both poles? Was it contemporaneous at both poles?

References [1] Zuber, M. et al. (1998), *Science*, 282, 2053-2060. [2] Smith, D. et al., *Science*, 279, 1686-1692, 1998. [3] Fishbaugh, K. & J. Head (2000), *J. Geophys. Res.*, in review. [4] Thomas, P., et al. (1992), in *Mars*, H. Kieffer et al., eds., University of AZ Press, Tucson, 767-795 [5] Plaut, J., et al. (1988), *Icarus*, 76, 357-377. [6] Schenk, P. & J. Moore (1999), *LPS 30*, #1819. [7] Tanaka, K. & D. Scott (1987), *U.S. Geol. Surv. Misc. Inv. Series Map I-1802-C*. [8] Head, J. (2000), *LPS 31*, #1116-1119, #1121. [9] Fishbaugh, K., et al. (2000), *LPS 31* #1206. [10] Kreslavsky, M. & J. Head (1999), *J. Geophys. Res.*, 104, 21911-21924. [11] Herkenhoff, K. & J. Plaut (2000), *Icarus*, in press. [12] Cutts, J., et al. (1976), *Science*, 194, 1329-1337. [13] Clifford, S. et al. (2000), *Icarus*, in press. [14] Herkenhoff, K. et al. (1997), *LPS 28*, 551. [15] Clifford, S. & Parker, T. (2000), *Icarus*, in press. [16] Fishbaugh, K. & J. Head (2000), *LPS 31*, #1271. [17] Kargel, J. (1993), *LPS 24*, 753-754. [18] Clifford, S. (1987), *J. Geophys. Res.*, 92, 9135-9152. [19] Benito, G., et al. (1997), *Icarus*, 129. [20] Fishbaugh, K & J. Head (1999), *5th Int. Conf. Mars*, LPI, Pasadena, #6187. [21] Fishbaugh, K. and J. Head (2000), The morphology of Chasma Boreale, Mars using MOLA data: Investigating formation by melting, *in prep.* [22] Anguita, F., et al. (1998), *LPI Contribution No. 953*, LPI, Houston, 1. [23] Scultz, P. & A. Lutz (1988), *Icarus*, 73, 91-141. [24] Head, J. (2000), LPS 31, #2036. [25] Parker, T. (1989), *Icarus*, 82, 111. [26] Zuber, M. et al. (1999), *Eos, Transactions*, AGU 80, F602. [27] Nye, J. et al. (2000), *Icarus*, in press.

NORTH POLAR REGION OF MARS: EVIDENCE FOR RESIDUAL CAP RETREAT AND BASAL MELTING Kathryn E. Fishbaugh[1] and James W. Head III[1], [1]Brown University, Dept. of Geological Sciences, Box 1846, Providence, RI 02912, kathryn_fishbaugh@brown.edu, james_head@brown.edu.

Abstract:

We present evidence for asymmetric retreat of the north polar cap (consisting of polar layered terrain and polar residual ice) of Mars. This evidence exists in the form of the Olympia Lobe (a portion of the cap now covered by dunes), outlying polar material remnants, and depressions interpreted to be kettles. Several possible causes of this retreat include: 1) a decrease in accumulation, 2) an increase in ablation rates, and 3) melting of polar material. Evidence of past melting exists in the form of Chasma Boreale and other, smaller chasmae. These features are interpreted to have been formed by the basal outflow of meltwater and consequent collapse of polar materials.

Polar residual ice remnants and kettles

High albedo patches south of and concentric to Olympia Planitia were identified [1,2] using Viking Orbiter and Mariner 9 images. These have been postulated to be remnants of polar residual ice [1], remnants of the seasonal CO_2 frost cap [3], and outlying mesas of ice, frost, or polar layered materials [2]. We have now identified more of these features and have better constrained their characteristics using MOLA data (Fig. 1) and Viking images. The irregular topography of these features can be contrasted with the surrounding cratered plains in Fig. 1. We propose that the prominent mesas and irregular depressions represent remnants of polar material and kettle-like features, respectively. In profile, in addition to the kettles and prominent remnants, some mapped bright patches exhibit a flat topography and are thus probably frost patches. Viking images also show some bright outliers to be associated with the bowls and rims of craters. We propose that the mapped [1,2] high albedo patches represent a mix of: 1) frost and/or residual ice - filled craters, 2) frost patches, 3) polar material remnants, and 4) kettles.

The Olympia Lobe and the previous extent of the polar cap

Olympia Planitia (situated poleward of and concentric to the polar material remnants and kettles) is dune-covered and not flat as previously thought. It has a positive, convex topography, contiguous with the polar cap as shown in Fig. 1. On the basis of this topography, we propose that Olympia Planitia represents an extension of the polar cap, now covered by dunes.

We suggest that, together, Olympia Planitia and the polar material outliers and kettles represent remnant morphology of a once larger northern cap (Fig. 2). We have termed this former extension the Olympia Lobe. Assuming cone shapes delineated by the slope from the top of the cap to the furthest extent of Olympia Planitia and by the slope from the top of the cap to 77°N (see Fig. 2), we have estimated the minimum missing volume of polar material. This volume estimate of $3x10^5$ km^3 constitutes 25% of the minimum volume estimate of the entire current cap [4]. Assuming 40% sediment content in the layered terrain [5], this yields 250 times the amount of sediment estimated [6] to be in the north polar ergs. Thus, ablation of the cap could easily provide enough material for the dunes covering Olympia Planitia and for part if not all of the surrounding Amazonian mantling [1,2] deposits. This may imply that the current estimations [e.g. 5] of the volume percentage of dust in the north polar layered deposits need to be revised.

Though the evidence presented points towards an asymmetrical retreat of the polar cap in that it has occurred predominantly from the 180°W direction, Howard et al. [8] have noted ridges parallel to the cap and visible in Viking images up to 20 km beyond the cap edge in the 300-360°W direction which may represent a former cap extent.

The topography of Olympia Planitia and the presence of remnants of polar material and depressions interpreted to be kettles concentric to and just south of this region suggest that the cap has retreated and that this retreat has been predominantly from the 180°W direction. The configuration of the formerly larger cap is illustrated in Fig. 2. There are several possible causes for retreat of the cap, and these may have acted in some combination.

Possible causes of retreat

1) Decrease in accumulation: This could cause an imbalance between accumulation and ablation. The decrease could be caused by a number of factors, including: a) a decrease in H_2O supply due to inclusion of surface water into the regolith or due to low obliquity [e.g. 7,9] or b) a decrease in dust supply available for nucleation due to high obliquity [e.g. 7,9].

2) An increase in the ablation rates: This could be caused by, among other possibilities, a) an increase in obliquity, b) polar wander [10] and consequent movement of parts of the cap to more southerly latitudes, or c) deposition of volcanic ash from Alba Patera.

3) Melting of polar materials: The best evidence of melting exists in the form of chasmae in the 40-90°W direction. While these chasmae do not lie within the former Olympia Lobe, their presence strongly suggests melting in the past history of the cap.

Evidence of melting

Several origins have been proposed for the formation of Chasma Boreale. Howard [11] proposed that the chasma was carved by concentration of katabatic winds created by cold air flowing from the top of the cap down a topographic low. Evidence for this included the presence of yardangs, dunes, and erosional scarps within the Chasma. Zuber et al. [4] have supported this conclusion.

Other authors [e.g. 12,13] have proposed formation by catastrophic outflow of meltwater, analogous to a terrestrial jokulhlaup, citing similarities with a Martian outflow channel, Ravi Valles [12], and the presence of fluvial bedforms [13].

New high-resolution topography from MOLA allows us to better characterize the morphology of Chasma Boreale. It shows that the floor is relatively flat and lies close to the elevation of the surrounding plains. We propose that Chasma Boreale was formed initially by outflow of meltwater in sub/englacial tunnels and subsequent collapse of the polar materials. Eolian processes (including katabatic winds) and sublimation, the principle agents of ablation at this time, have since modified the

chasma.

In our analysis [14,15] we interpret the data to mean that the flow began near the deep, enclosed depression at the beginning of the chasma. The meltwater then tunneled through or beneath the ice (and was thus able at some points to flow upslope) until it broke out at the cap periphery. Polar materials then collapsed as a result of the flow and removal of material, forming a reentrant. During the outflow, layered material sediments and ice were deposited in the form of the lobate, delta-like structure at the chasma mouth, subduing the underlying polygonal terrain. Channel-like topographic lows were also carved beyond the lobate deposits.

As the outflow waned, the flow followed the lowest floor topography, eroding the eastern side of the lobe, following the earlier carved channels, and depositing a few meters of sediment in the lowest parts of the adjacent north polar basin.

Two smaller chasmae to the west of Chasma Boreale also show evidence of channel-like features carved at their mouths. These chasmae have opposing curvature, arguing against a genetic relationship with the nearby polar cap troughs.

Summary and future work

We have presented evidence (in the form of recessional morphology, including polar material remnants and kettles) for asymmetric retreat of the north polar cap of Mars. This missing portion of the cap, termed the Olympia Lobe, has a volume sufficient to provide more than enough sediment (assuming 40 volume% sediment content) for the north polar ergs and part if not all of the surrounding mantling deposits. Retreat may be caused by several factors, including melting (which we propose formed Chasma Boreale).

Future work will include further investigation into the causes of retreat, using MOC and MOLA data, the timing of retreat, and similarities with terrestrial ice sheet retreat. We also plan to investigate the relative ages of the chasmae, polar cap troughs, and the portion of the Olympia Lobe still in existence.

References: [1] Dial, A. (1984), *USGS Map I-1640*. [2] Tanaka, K. & D. Scott (1987), *USGS Map I-1802-C*. [3] Thomas, P. et al. (1992), in *Mars*, H. Kiffer et al., eds., UA Press, Tucson, 767-795. [4] Zuber et al. (1998), *Science*, 282, 2053-2060. [5] Herkenhoff, K. (1998) *LPI Contrib. 953*, LPI, Houston, 18-19. [6] Greeley et al. (1992), in *Mars*, H. Kiffer et al., eds., UA Press, Tucson, 730-766. [7] Clifford et al. (2000), *Icarus*, in press. [8] Howard, A. et al. (1982), *Icarus*, 50, 161-215. [9] Toon et al. (1980), *Icarus*, 44, 552-607. [10] Ward (1992) in *Mars*, H. Kieffer et al., eds., UA Press, Tucson, 317-320. [11] Howard, A. (1980), *NASA Tech. Mem.* 82385, 333-335. [12] Clifford, S. (1987), *JGR*, 92, 9135-9152. [13] Benito, G. et al. (1997), *Icarus*, 129. [14] Fishbaugh, K. and J. Head (1999) *5th Int. Conf. Mars*, LPI, Pasadena, Abstract #6187. [15] Fishbaugh, K. and J. Head (2000), The morphology of Chasma Boreale, Mars using MOLA data: Investigating formation by melting, *in prep*.

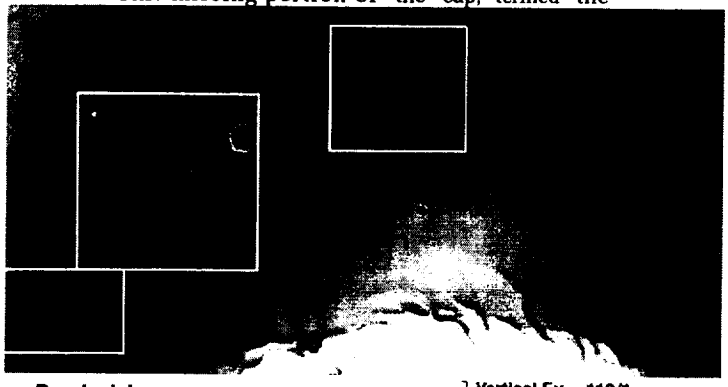

Fig. 1 Topographic map enhanced to show details of Olympia Planitia and the remnant arc region. Black is low and, white is high. The large depression in the middle box is about 250 m deep.

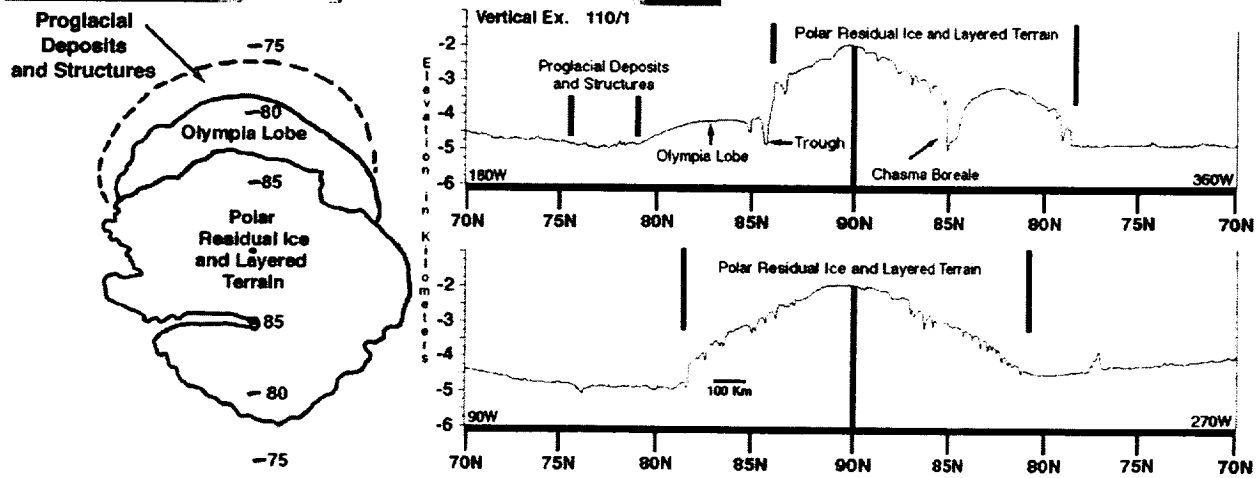

Fig. 2 The figure on the left shows the configuration of the once larger cap. The dotted line shows the extent of the kettles and polar material remnants and extends out to about 77°N. Topographic profiles show the relationships of the distal deposits (interpreted to be proglacial deposits and structures), the Olympia Lobe (interpreted to be a large-scale equivalent of an ice-cored moraine), and the main cap (residual ice and layered terrain).

CONTINUING MEASUREMENTS OF CO_2 CRYSTALS WITH A HAND-HELD 35 GHZ RADIOMETER. J. Foster[1], A.Chang[1], D. Hall[1], A. Tait[2], W. Wergin[3], and E. Erbe[3], [1]NASA/GSFC Hydrological Sciences Branch, Laboratory of Hydrospheric Processes, Greenbelt, MD, USA 20771 Email: jfoster@glacier.gsfc.nasa.gov, Phone: 301-614-5769, Fax: 301-614-5808, [2]U. S. Research Associates, Greenbelt, MD, USA 20770, [3]USDA/Agricultural Research Service, Electron Microscope Laboratory, Beltsville, MD, USA, 20705.

Abstract: In order to increase our knowledge of the Martian polar caps, an improved understanding of the behavior of both frozen H_2O and CO_2 in different parts of the electromagnetic spectrum is needed. The thermal microwave part of the spectrum has received relatively little attention compared to the visible and infrared wavelengths. A simple experiment to measure the brightness temperature of frozen CO_2 was first performed in the winter of 1998 using a 35 GHz radiometer. In experiments performed during the winter of 1999 and 2000, passive microwave radiation emanating from within layers of manufactured CO_2 (dry ice) crystals was again measured with a 35 GHz hand-held radiometer. Both large (0.8 cm) and small (0.3 cm) cylindrical-shaped dry ice pellets, at a temperature of 197 K (–76 degrees C), were measured. A 1 m^2 plate of aluminum sheet metal was positioned beneath the dry ice so that microwave emissions from the underlying soil layers would be minimized. Non-absorbing foam was positioned around the sides of the plate in order to keep the dry ice in place and to assure that the incremental deposits were level. 35 GHz measurements of this plate were made through the dry ice deposits in the following way. Layers of dry ice were built up and measurements were repeated for the increasing CO_2 pack. First, 7 cm of large CO_2 pellets were poured onto the sheet metal plate, then an additional 7 cm were added, and finally, 12 cm were added on top of the 14 cm base. Hand-held 35 GHz measurements were made each time the thickness of the deposit was increased. The same process was repeated for the smaller grain pellets. Furthermore, during the past winter, 35 GHz measurements were taken of a 25 kg (27 cm x 27 cm x 27 cm) solid cube of CO_2, which was cut in half and then re-measured.

After the above-described series of measurements was made, the CO_2 crystals were then placed on top of a melting snowpack, and as before, measurements were made using the 35 GHz radiometer. As a final part of this experiment, soil particles were spread on top of the dry ice, and once again, microwave measurements were made with the 35 GHz radiometer.

Compared to the natural snow crystals, results for the dry ice layers exhibit considerably lower microwave brightness temperatures for similar thicknesses, regardless of the incidence angle of the radiometer. For example, with a covering of 7 cm of small dry ice pellets, the 35 GHz brightness temperature at an incidence angle of 60° H (horizontal polarization) was 90 K. For natural snow having a thickness of 7 cm or so, a brightness temperature of about 220 K would be expected. The lower brightness temperatures are due primarily to a combination of the lower physical temperature and the larger crystal sizes of the commercial CO_2 crystals compared to natural snow crystals. As the crystal size approaches the size of the microwave wavelength, it scatters microwave radiation more effectively. The dry ice crystals in this experiment were about an order of magnitude larger than the natural snow crystals.

In general, the larger dry ice grains scattered slightly more radiation than did the smaller grains. For a thickness of less than 10 cm, the difference is about 15%, but for a thickness of 26 cm, the difference was only 2%.

For the solid block of dry ice, there was no increase in scattering when the thickness of the block was doubled. At a thickness of 10 cm the scattering was comparable to that of the grains. The thicker dry ice cube actually showed a slight decrease in scattering, perhaps because the dense ice was emitting more radiation than it was scattering.

When the dry ice grains were mixed with wet snow (from a nearby drift), the brightness temperature dropped from 277 K to 227 K. A minute later the temperature plummeted to 182 K, and a minute after this it fell to 176 K, at which time it then became stable. The reason believed for the initial precipitous drop in brightness temperature and then the gradual leveling off is that the very cold dry ice was freezing the free water inbetween the snow crystals. Once nearly all of the liquid water was solidified, the now-refrozen snow, mixed with the considerably colder dry ice, emitted microwave energy at a much lower temperature.

Spreading soil on the mixture of dry ice and snow had no apparent effect on the brightness temperatures.

TROUGHS IN ICE SHEETS AND OTHER ICY DEPOSITS ON MARS: ANALYSIS OF THEIR RADIATIVE BALANCE. A. Fountain, J. Kargel, K. Lewis, D. MacAyeal, T. Pfeffer, and J. Zwally.

It has long been known (e.g., Pfeffer and Bretherton, 1987) that groove-like structures in glaciers and ice sheets can trap more incoming solar radiation than is the case for a "normal" flat, smooth surface. In this presentation, we shall describe the radiative regimes of typical scarps and troughs on icy surfaces of Mars, and suggest how these features originate and evolve through time. The basis of our analysis is the radiation balance model presented by Pfeffer and Bretherton (1987). Their model considers the visible band radiation regime of a V-shaped groove on a terrestrial ice surface, and shows that absorbed energy can be enhanced by up to 50% for grooves with small opening angles and with typical polar values of the solar zenith angle. Our work extends this model by considering: (a) departures from V-shaped geometry, (b) both englacial and surficial dust and debris, and (c) the infrared spectrum. We apply the extended model to various features on the Martian surface, including the spiral-like scarps on the Northern and Southern ice sheets, the large-scale chasms (e.g., Chasm Borealis), and groove-like lineations on valley floors thought to be filled with mixtures of dust and icy substances. In conjunction with study of valley-closure experiments (see the companion abstract), we suggest that spiral-like scarps and chasms are stable features of the Martian climate regime. We also suggest that further study of scarps and chasms may shed light on the composition (i.e., relative proportions of water ice, carbon-dioxide ice and dust) of the Martian ice sheets and valley fills.

TROUGHS ON MARTIAN ICE SHEETS: ANALYSIS OF THEIR CLOSURE AND MASS BALANCE. A. Fountain, J. Kargel, K. Lewis, D. MacAyeal, T. Pfeffer, and J. Zwally.

At the Copenhagen workshop on Martian polar processes, Ralf Greve commented that the flow regime surrounding scarps and troughs of the Martian polar ice sheets cannot be modeled using traditional "plan view" ice-sheet models. Such models are inadequate because they typically use reduced equations that embody certain simplifications applicable only to terrestrial ice sheets where the upper ice sheet surface is smooth. In response to this suggestion, we have constructed a 2-dimensional, time dependent "side view" (two spatial dimensions: one horizontal, one vertical) model of scarp closure that is designed to overcome the difficulties described by Greve. The purpose of the model is to evaluate the scales of stress variation and styles of flow closure so as to estimate errors that may be encountered by "plan view" models. We show that there may be avenues whereby the complications associated with scarp closure can be overcome in "plan view" models through appropriate parameterizations of 3-dimensional effects. Following this, we apply the flow model to simulate the evolution of a typical scarp on the North Polar Cap of Mars. Our simulations investigate: (a) the role of "radiation trapping" (see our companion abstract) in creating and maintaining "spiral-like" scarps on the ice sheet, (b) the consequences of different flow-laws and ice compositions on scarp evolution and, in particular, scarp age, and (c) the role of dust and debris in scarp evolution.

RADAR SOUNDING OF LAYERING IN POLAR ICE SHEETS : POSSIBILITIES AND LIMITATIONS CONSIDERING THE DIELECTRIC PROPERTIES OF ICE CRYSTALS. Shuji Fujita, Department of Applied Physics, Graduate School of Engineering, Hokkaido University, N13-W8, Sapporo, 060-8628 Japan TEL&FAX: +81-11-706-7331 E-mail: sfujita@nd-ap.eng.hokudai.ac.jp

Abstract: RF radar sounding is now an essential part of methodology to observe the ice sheets on polar continents. We can detect physical conditions within the several-thousand-meters-thick ice sheets using proper platforms such as ground-based vehicles or airplanes. We can also extend information of ice-core data from a drilling point to wider regions of polar ice sheets. Ice sounding technique has its basis in the high-frequency dielectric properties of the target object, that is, ice and snow. In the past decade, new progress has appeared in understanding of the high-frequency electrical properties of water ice (Ih) through laboratory measurements (reviewed in ref. [1]). This progress consequently brought about significant progress in interpretation of the radar data from Antarctica [2, 3]. In particular, using multiple frequencies, we can distinguish reflections due to changes in dielectric permittivity and due to changes in electrical conductivity. Through this discrimination, we can deduce that what factor (density, impurity or crystal orientation fabrics) cause electromagnetic scattering. We introduce the physical principles of the ice-radar-data interpretation using actual data from a traverse line Dome F region to marginal area in Antarctica, and present knowledge of the dielectric properties of ice and its limitations. We mainly put stress on the knowledge of water ice and data from Antarctic ice sheet, considering application and extension of the knowledge to the Mars polar region.

References: [1] Fujita, S., et al., A summary of the complex dielectric permittivity of ice in the megahertz range and its applications for radar sounding, in Physics of Ice Core Records. 2000, Hokkaido University Press: Sapporo. [2] Fujita, S., et al., Nature of radio echo layering in the Antarctic ice sheet detected by a two-frequency experiment. JGR, 1999. 104(B6): p. 13013-13024. [3] Fujita, S. and S. Mae, Causes and nature of ice sheet radio-echo intenal reflections estimated from the dielectric properties of ice. Ann. Glaciol., 1994. 20: p. 80-86.

INTERACTIONS OF INTRUSIVE VOLCANISM WITH PERMAFROST ON MARS. E. J. Gaidos, *Geological and Planetary Sciences, California Institute of Technology, Pasadena CA 91125, USA, (gaidos@gps.caltech.edu)*, F. Nimmo, *Bullard Laboratories, Department of Earth Sciences, Cambridge University, Cambridge UK (nimmo@esc.cam.ac.uk).*

Martian dike formation may have created swarms of linear faults and accompanied uplift and lithospheric extension, particularly around the Tharsis plateau. A model of dike emplacement and graben formation in the permafrost-capped crust showed that sufficient volumes of melt water could be generated to explain episodes of catastrophic flooding of Mars [1] . The geologic youth of certain volcanic terrains from crater counts [2] and the young radiometric ages of some SNC meteorites [3] suggests that volcanism, and thus dike formation may be a global, ongoing occurrence on Mars, although surface expression may be subtle because of depth of intrusion or obscuration by subsequent deposition. The interaction of intrusive magmatic bodies and permafrost or ice is a complex, poorly studied process [4] with few known terrestrial analogs [5,6]. There is limited morphological evidence for cryomagmatic activity on Mars [7]. However, ice-magma interactions may have played an important role in the subsurface chemical alteration of the crust, as suggested by the presence of weathering products in the SNC meteorites [8]. In the absence of a catastrophic release, subsurface melt water above dikes was shown to persist for 10 Myr before refreezing [1] and thus is also of potential exobiological interest.

We examine dike intrusion and the formation of melt water bodies under conditions of varying permafrost thickness, ice fraction, and dike intrusion depth. Shallow events may lead to phreaomagmatic eruptions and the formation of maars, rather than grabens. We also consider the subsequent physical and chemical evolution of the ice-water system after dike emplacement and graben formation. Extensional faulting of the country rock above the dike and cracking of cooling, newly-formed igneous rock will allow water to percolate towards the magma body, initiating hydrothermal circulation. This will result in more rapid cooling of the dike and generation of (the same) melt water volume. Convection will continue as long as the thermal gradient exceeds the critical value given by $4.2 \times 10^{-10} k^{-1} b^{-2}$ K m^{-1} [9], where k is the permeability and b is the thickness of the permeable layer in meters. For $k \sim 10^{-14}$ m^2 and b = 1 km the required heat flow is 80 mW m^{-1}, comparable to modern terrestrial oceanic crust and several times higher than the estimated Martian mean. The convective velocity in the buoyant plume of water in the hydrothermal system is $v = k\rho\alpha g \Delta T \mu^{-1}$ [9] which will be of order 10^{-7} m s^{-1} for ΔT = 500 K. The entire volume of melt could be circulated through the hydrothermal system in only $\sim$ 100 yr. It is more likely that conduction of heat through an impermeable lid on the freezing dike will limit the amount of heat flow that can be transferred to the hydrothermal system and that heat transfer and flow rates will be smaller. The total amount of hydrothermal circulation that could be driven by the cooling dike, assuming that the temperature differential between inflow and outflow is 5°C, considered a typical average value along the axis of mid-ocean ridges [10], giving a heat flow per mass flow of 20 kJ kg^{-1}. The heat given off by the cooling dike in melting the ice is the latent heat of fusion (325 kJ kg^{-1}) indicating that the entire water body could circulate through the hydrothermal system several times.

Hydrothermal activity in a basaltic rock will result in the leaching of ferrous iron and manganese. High temperature alteration also results in stripping of Ca from the rock and its replacement by Mg. We predict that a ferrous, acidic, and Ca-rich brine will be produced. Cooling of the water body after a few million years will result in refreezing. Rejection of solutes from the freezing front will result in concentration of the brine. A $CaCl_2$ brine will have a eutectic point at -55°C [11] and will be stable at depths greater than 400-800 m, assuming a mean surface temperature of 214 K, a thermal conductivity of 2 W m^{-1} K^{-1}, and a present-day heat flow of 10-20 mW m^{-2}. The concentration of Ca in modern terrestrial hydrothermal fluids is 30 mM kg^{-1} [10], while the eutectic concentration is several molar. Thus the residual brine volume would be less than 1% of the original volume, but this still may be several tens of km^3 [1]. Precipitation of the iron as sulfides or ferrihydroxides, depending on fluid chemistry, will form iron deposits that might resemble either ophiolitic ore deposits or banded iron formations on Earth. Such deposits may have local magnetic signatures [12] . Gases from the water body may vent to the atmosphere through the normal faults bounding the graben. If the graben depth exceeds the permafrost depth the graben may flood and could lead to draining of the subsurface [1]. At current surface temperatures this would form an ice-covered lake which would eventually be removed by sublimation or buried by mass wasting of the graben walls. Alternatively annealing of the permafrost on the Myr-timescale of graben formation could seal the system.

Subsurface hydrothermal systems are predicted to be able to support ecosystems independent of sunlight [13,14] although lack of a supply of surface oxidants will limit the available energy [15,16]. However, for Martian organisms to take advantage of this refuge a mechanism for "seeding" the water bodies is required. Certain terrestrial prokaryotes may be able to lie dormant for $\sim$1 million years in permafrost [17], but preservation of viable organisms for billions of years in the Martian crust in the absence of prior evolutionary selection for fitness seems implausible.

References: [1] D. McKenzie and F. Nimmo (1999) *Nature* 397, 231. [2] W. Hartmann *et al.* (1999) *Nature* 397, 586. [3] E. Jagoutz (1991) *Space Sci. Rev.* 56, 13. [4] S. W. Squyres, D. E. Wilhelms, and A. C. Moosman (1987) *Icarus* 70, 385. [5] J. E. Beget, D. M. Hopkins, and S. D. Charron (1996) *Arctic* 49, 62. [6] M. T. Gudmundsson, F. Sigmundsson, and H. Bjornsson (1997) *Nature* 389, 954. [7] M. W. Carruthers and G. E. McGill (1998) *J. Geophys. Res.* 103, 31433. [8] H. Y. McSween (1994) *Meteorit.* 29, 757.

[9] D. L. Turcotte and G. Schubert (1982) *Geodynamics*, New York: Wiley, p. 405. [10] H. Elderfield and A. Schultz (1996) *Annu. Rev. Earth Planet Sci.* 24, 191. [11] G. W. Brass 1980 *Icarus* 42, 20. [12] C. Ramarao *et al.* (1991) *Geoexploration* 28, 121. [13] P. Boston, M. Ivanov, and C. P. McKay (1992) *Icarus* 95, 300. [14] E. L. Shock (1997) *J. Geophys. Res.* 102, 23687. [15] B. Jakosky and E. L. Shock (1998) *J. Geophys. Res.* 103, 19359. [16] E. J. Gaidos, K. H. Nealson, and J. L. Kirschvink (1999) *Science* 284, 1631. [17] E. Vorobyova et al. (1997) *FEMS Microb. Rev.* 20, 277.

VERTICAL ROUGHNESS OF THE POLAR REGIONS OF MARS FROM MARS ORBITER LASER ALTIMETER PULSE-WIDTH MEASUREMENTS. J. B. Garvin[1], J. J. Frawley[2] , and S. E. H. Sakimoto[3]; [1](NASA's GSFC, Code 921, Greenbelt, MD 20771 USA; garvin@denali.gsfc.nasa.gov), [2](Raytheon-STX and Herring Bay Geophysics, at NASA's GSFC, Code 921), [3] (USRA at NASA's GSFC, Code 921).

Introduction: The sub-kilometer scale vertical roughness of the martian surface in the polar regions can be investigated using calibrated, optical pulse width data provided by the Mars Orbiter Laser Altimeter (MOLA). Garvin and others [1] have previously discussed initial observations of what we have called "total vertical roughness" or TVR, as derived from MOLA optical pulse width observations acquired during the pre-mapping phases of the Mars Global Surveyor (MGS) mission. Here we present the first assessment of the Mars polar region properties of the TVR parameter from more than nine months of continuous mapping by MOLA as part of the MGS mapping mission. Other than meter-scale surface properties directly inferred from Mars Orbiter Camera (MOC) images, MOLA measurements of footprint-scale TVR represent the only direct measurements of the local vertical structure of the martian surface at ~ 150 m length scales. These types of data have previously been shown to correlate with geologic process histories for terrestrial desert surfaces on the basis of Shuttle Laser Altimeter (SLA) observations [2].

MOLA Observations: The MOLA measurement of pulse dilation is notoriously sensitive to receiver saturation, which induces ambiguities in the instrument's measurement of the received pulse width. As part of our initial assessment of MOLA's optical pulse width parameter, we observed a correlation between ambiguous measurements and pulse energy saturation. The suspicion is that MOLA detector saturation induces a ringing in the backscattered echo which is recorded by the instrument as a distinctly wider pulse. During the first few months of MGS mapping (March 1999 to late June 1999), the threshold settings within the MOLA instrument favored strong surface signals that subsequently saturated the detector. The resulting measurements of pulse energy (a proxy for surface reflectivity) and pulse width were unusable due to corruption of their absolute magnitudes. By adjusting the threshold settings within MOLA, however, saturation was partially avoided and more robust measurements of pulse width became possible, as of July 3, 1999. Since that time, we have tracked the behavior of the calibrated, optical pulse width parameter, and it appears to be reproducible to within 10 % in the martian polar regions where there are abundant cross-overs. We have screened all optical pulse width measurements by first filtering out any measurements for which the corresponding received pulse energy was saturated. In addition, whenever the raw, electronic pulse width is saturated, we ignore such footprints. A majority of the measurements since the threshold adjustments of July 3, 1999 are unsaturated and have been considered in the assembly of maps of the derived TVR parameter. The action that was taken increased the threshold of the channel one to its maximal level to minimize saturation, increase dynamic range of the pulse width measurements, and to decrease the false-alarm rate [J. Abshire, pers. communication, 1999].

Vertical Roughness. Once unsaturated pulses are identified, the optical pulse width must be converted to a more physically meaningful parameter. Garvin and others [2] have shown that the total width of orbital laser echoes (above threshold) is a measure of the total vertical roughness or TVR of the area within the illuminated laser footprint. In cases where the within-footprint relief variation is dominated by a footprint-scale tilt, TVR is a measure of the local slope. In other circumstances, TVR is sensitive to vertical elements at the scale of meters within MOLA's footprint, but only in the terms of the dominant modes in the local surface height distribution. Our experience with SLA measurements of unvegetated terrestrial surfaces gives us confidence in this interpretation [2]. We can take the optical pulse width and convert it to TVR using an approach first discussed in [1,2]. Essentially, we must correct the optical pulse width for the effect of local slopes. Gardner [3] developed an approach for estimating the amount of within-footprint laser pulse spreading. We have used this method together with the polar region MOLA-based topography [4] to derive sub-kilometer-scale slopes and correct each TVR measurement for slope-induced pulse spreading. The results are consistent, yet we recognize the limitations associated with independent assessment of 150m scale slopes imposed by the MOLA pulse repetition rate. The dynamic range of the resulting TVR parameter extends from ~ 0.3 m (the limit of our ability to discriminate differences) to over 8 m. The TVR parameter is an RMS value, and does not fully capture the possible local extremes of small-scale roughness.

Global Statistics: On the basis of all unsaturated pulse width data up through March 2000 (i.e., more than 200 million measurements), we have constructed a 0.25 x 0.25 degree global TVR map for Mars. Much finer resolution data (i.e., 500 m spatial) is available

for the polar regions. We have taken all of the point TVR data and examined the global statistical patterns. The mean global TVR is 2.1 m RMS, with a standard deviation of ~ 2.0 m. The data are bimodal with the primary mode at 1.5 m RMS. Less than 1% of all values occur in excess of 10 m, and these are restricted to the flanks of the uplands, canyons, and some larger crater rims. In comparison, the north and south polar latitudes (i.e., those areas north or south of 65 degrees latitude) display a pattern very similar to that for all of Mars, with a mean TVR of 2.01 m RMS. In contrast, those terrestrial deserts sampled by the Shuttle Laser Altimeter (SLA) during its flights in 1996 and 1997, suggest a mean TVR of 4.4 m (RMS), with a sigma of 3.7 m [2]. Terrestrial deserts exhibit a very unimodal pattern of vertical roughness, with less than 1% of all observed values having magnitudes > 6 m RMS. Polar layered terrains in the vicinity of the anticipated Mars Polar Lander landing site display mean TVR values of 1.4–1.5 m, with a more unimodal pattern, attesting to their minimal vertical structure at 150 m length scales.

Global Spatial Patterns. We have developed the first global maps of TVR for Mars at sufficient spatial resolution to establish regional surface units. There are essentially 5 global TVR units, although the polar latitudes display some evidence of time-variable behavior associated with the occurrence of surface frosts. The lowest TVR unit (0.3 to 1.1 m RMS) dominates the northern lowland plains and characterizes much of the Vastitis Borealis formation in this region. The interior of Isidis and portions of the smooth intercrater plains in the southern uplands also display this smooth character. Portions of the interiors of Argyre and Hellas are also within this unit. A transitional unit with TVR just above 1.1 m RMS is most prevalent at the boundary of the Vastitis Borealis, and this type of surface appears to correlate with more than 50% of the putative "C2" shoreline contour at –3700 m elevation [5]. A large fraction of the northern volcanic plains, including areas around Elysium and into Amazonis, fall into a TVR unit that extends from ~ 1.3 m to 1.7 m (RMS). Sections of Sinai Planum and Lunae Planum are also characteristic of this surface. As one nears the 2.0 m RMS threshold, impact crater ejecta blankets and inner cavity walls appear to dominate, as well many of the minor Tharsis region volcanic surfaces. Most of Tharsis falls into a narrow TVR unit from ~ 2 m RMS to 2.5 m, as do the more elevated portions of Elysium, and the CO_2 frost-covered South Polar icecap. The Olympia Planitia dunes and the more rugged sections of the uplands adjacent to the crustal dichotomy region display TVR values in the 2.2 to 3.0 m RMS range. Dune covered margins of the North polar ice cap are similar to the average uplands in terms of their TVR magnitudes, at least on a regional basis. The rim of the Argyre impact basin is very distinctive in terms of its elevated TVR properties, in contrast with Hellas, whose rim is less rough at MOLA footprint scales. The most elevated TVR values on Mars are clustered in a few distinctive areas, including the interior of Valles Marineris, the Olympus Mons aureole (over 7 m RMS), and parts of the south polar icecap, which may have been CO_2 frost covered during initial observations. These areas are as rugged as tree-covered surfaces on Earth at 150 m length scales.

Conclusions: What is most striking about the global TVR patterns is the dramatic transition that occurs in the northern lowland plains. TVR values in the 1.2–1.5 m RMS interval appear to correlate with the –3700 m elevation contour for 60% of the boundary, and follow the crustal dichotomy boundary equally as well. More than 50% of the lowermost TVR values on Mars fall within the Northern Lowland plains, although an interconnected quiltwork of this unit is observed in the southern mid-latitudes. Another striking regional boundary separates the crustal dichotomy region from the lowland plains to the north from Arabia to Daedalia Planum. Whatever the local cause, TVR is highly correlated with major physiographic and geology boundaries on Mars. We are continuing to calibrate the TVR maps so that more specific unit correlations can be examined and process links established.

In the North Polar region, after removing all effects of slope-induced pulse spreading, the TVR statistics indicate that all of the dune-related surfaces are 3-4 times rougher than other surface units. Such dune surfaces are rougher (in terms of TVR) than the inner cavity walls of fresh impact craters, as well as the margin of N. polar icecap. In contrast, the South Polar region is almost uniformly smooth as observed with the MOLA-based TVR parameter. Frost-cover associated with higher-standing topography is more rugged, but not as much as the polar dune deposits in the North. We are in the process of unraveling the temporal aspects of the TVR parameter for the polar regions, which appears to reflect a 0.5 to 1.0 m RMS shift with martian seasons. {We strongly acknowledge the support of the MOLA PI, D. E. Smith, the Instrument Engineer J. B. Abshire, J. Bryan Blair, and Greg Neumann in this work}.

References: [1] Garvin J. B. et al. (1999) *GRL, 26,* 381-384. [2] Garvin J. B. et al. (1998) *Physics and Chem. of Earth, 23,* 1053-1068. [3] Gardner C. (1992) *IEEE Trans. Geosci. Rem. Sensing, 30,* 1061-1072. [4] Smith D. E. et al. (1999) *Science 286,* 1495-1503. [5] Head J. W. et al. (1999) *Science 286,* 2134-2137.

ICE FLOW, ISOSTASY AND GRAVITY ANOMALY OF THE PERMANENT NORTH POLAR H_2O ICE CAP OF MARS. R. Greve, *Institut für Mechanik III, Technische Universität Darmstadt, D-64289 Darmstadt, Germany (greve@mechanik.tu-darmstadt.de)*, V. Klemann, *Institut für Planetologie, Universität Münster, D-48149 Münster, Germany*, D. Wolf, *Kinematik und Dynamik der Erde, GeoForschungsZentrum Potsdam, D-14473 Potsdam, Germany.*

Modelling Approach: The flow of the permanent north polar H_2O ice cap of Mars and the isostatic depression of the underlying bedrock are investigated with the 3-d dynamic/thermodynamic ice-sheet model SICOPOLIS [1] coupled to a two-layer visco-elastic model for the lithosphere/mantle system [2,3]. SICOPOLIS describes the ice as a density-preserving, heat-conducting power-law fluid with thermo-mechanical coupling due to the strong temperature dependence of the ice viscosity [4], and computes three-dimensionally the temporal evolution of ice extent, thickness, temperature, water content and age as a response to external forcing. The latter must be specified by (i) the mean annual air temperature above the ice, (ii) the surface mass balance (ice accumulation minus melting and evaporation), (iii) the global sea level (not relevant for Martian applications) and (iv) the geothermal heat flux from below into the ice body. However, owing to the now well-known surface topography [5] on the one hand, but the shortage of information about the surface mass balance on the other, here the inverse strategy of prescribing the topography and computing the surface mass balance required to sustain the topography is pursuited [4]. Following further the approach of [4], we use a conceptional, paraboloid-like ice cap, growing and shrinking between the present minimum extent within 80.5°N and an assumed past maximum extent southward to 75°N with a period of 1.3 Myr (first modulation of obliquity cycle), vary the surface temperature with the same period between its measured present distribution and a 30°C warming coinciding with the maximum ice extent, and apply a geothermal heat flux of $35\,\mathrm{mW\,m^{-2}}$.

The lithosphere/mantle model displace comprises an elastic lithosphere of constant thickness, underlain by a Maxwell-viscoelastic half-space mantle. Both layers are treated as incompressible, and we apply terrestrial standard values for the rheological parameters: density of the lithosphere and of the mantle $\rho_l = \rho_m = 3380\,\mathrm{kg\,m^{-3}}$, shear modulus of the lithosphere $\mu_l = 64\,\mathrm{GPa}$, shear modulus of the mantle $\mu_m = 145\,\mathrm{GPa}$, viscosity of the mantle $\eta_m = 10^{21}\,\mathrm{Pa\,s}$ [3]. The thickness of the lithosphere, H_l, which is the most crucial parameter of the lithosphere/mantle system, is varied between 50 and 400 km. The field equations of displacement, stress and gravity are solved in the Hankel-wavenumber, k, and Laplace-frequency, s, domain, where they are simply a system of ordinary differential equations in the remaining vertical coordinate, z, and the results are transformed back to the space-time domain by computing the inverse Laplace and Hankel transformations.

Simulations: We carry out four simulations with the coupled SICOPOLIS/displace model and lithosphere thicknesses of 50, 100, 200 and 400 km, referred to as displace (50, 100, 200, 400 km). Another simulation assumes a simple local-lithosphere-relaxing-asthenosphere (LLRA) model with an isostatic time lag of 3 kyr [6], representing maximum isostatic response, and the other extreme of no isostasy at all is investigated by a further simulation with rigid lithosphere. The model time is from 6.5 Myr before present until today, so that five 1.3-Myr cycles are covered and the results are not influenced by arbitrary initial conditions. Here only results for the simulated present ice cap will be discussed.

Results: Table 1 shows the vertical lithosphere displacements (positive downward) in the centre of the ice cap at the north pole, w_{max}, and at the ice margin at 80.5°N, w_{marg}, as well as the maximum surface-accumulation rate, S_{max}, for the six simulations. Evidently, w_{max} is decreasing in the order of the six simulations due to the increasing lithosphere rigidity, whereas w_{marg} has a maximum for $H_l = 100\,\mathrm{km}$ due to the counteracting increasing non-local response of the lithosphere. As discussed extensively by [4], surface accumulation and ablation rates are likely of the order of $0.1\,\mathrm{mm\,w.e.\,yr^{-1}}$ (w.e.: water equivalent), which, by comparison with the S_{max} values of Table 1, favours the last three simulations, that is, $H_l \geq 200\,\mathrm{km}$. This finding is in good agreement with independent estimates of the lithosphere thickness [7].

Simulation	w_{max} [m]	w_{marg} [m]	S_{max} [mm w.e. yr^{-1}]
LLRA	1142	0	4.246
displace (50 km)	848	158	1.810
displace (100 km)	568	171	0.734
displace (200 km)	278	137	0.333
displace (400 km)	124	80	0.268
Rigid lithosphere	0	0	0.244

Table 1: Results of simulations for the present ice cap. w_{max} is maximum vertical lithosphere displacement (taken at the north pole), w_{marg} vertical lithosphere displacement at the ice margin, S_{max} maximum surface-accumulation rate.

In Fig. 1 the velocity field for simulation displace (200 km) is depicted for a vertical transect across the north pole. As it is expected, the ice flow is downward and outward in the inner accumulation zone, and points towards the surface in the outer ablation zone. Flow velocities are of the order of some millimetres per year, so that the present ice cap is virtually stagnant, as was already found by [4]. The reason for the conspicuous upward-pointing velocity vectors close to the base is that the modelled ice cap was larger in the past, so that the lithosphere still experiences some uplift which raises the basal ice. Compared to a fully local compensation of the ice load like in simulation LLRA, the bedrock depression is rather small, but the increase in ice thickness is still sufficient to produce a ca. 50% larger ice flow as in the case of a rigid lithosphere.

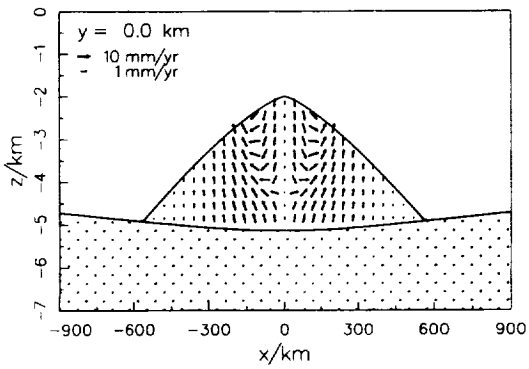

Figure 1: Transect across the north pole at $x = y = 0$ (x, y span the horizontal plane) for present ice cap of simulation displace (200 km): Topography of ice and lithosphere surface, ice-velocity field.

The computed spectrum of relaxation times of the lithosphere/mantle system for simulation displace (200 km) given in Fig. 2 shows two different modes, M0 and L0, due to the two-layered model. M0 is the buoyancy mode, mainly responsible for vertical displacements of the lithosphere, whereas the viscoelastic mode L0 is less significant [2,3]. It is most important that the relaxation times in both modes for any wavenumber (inverse size) of the ice load do not exceed 10 kyr, whereas the period for changes in the ice extent is 1.3 Myr in the simulation. Significant changes on shorter time scales were found to be very unlikely [4]. As a consequence, the lithosphere/mantle system is nearly in steady state with the ice load at any time of the cycle. Therefore, the viscoelastic properties of the mantle (ρ_m, μ_m, η_m) do not influence the results, and the only important parameters of the ground model are the lithosphere thickness, H_l, and, to a lesser extent, the density, ρ_l, and the shear modulus, μ_l, of the lithosphere. This finding, even though demonstrated only for simulation displace (200 km), remains equally valid for the other simulations.

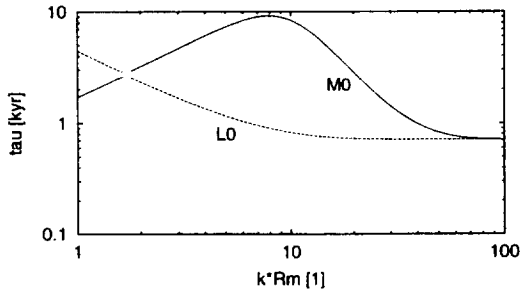

Figure 2: Relaxation time, τ, vs. Hankel wavenumber of the ice load, k, normalized with the mean Martian radius, R_m, for simulation displace (200 km).

The ice cap and the corresponding isostatic depression of the ground go along with a gravity anomaly, which can in principle be detected by orbiting space probes. Fig. 3 displays the vertical displacement of the geoid, h_g (positive upward), for the four simulations displace (50, 100, 200, 400 km). As the signal vanishes in the limit case of fully local isostatic compensation like in simulation LLRA, it is the more pronounced the less isostatic depression takes place, that is, the thicker the lithosphere is. For 200 km thickness, the geoid displacement is 45 m in the centre of the ice cap (north pole), reaches zero approximately at the ice margin, and takes negative values of up to -5.5 m in the adjacent ice-free region due to the non-local lithosphere depression. Compared to the gravity anomalies of major features of the Martian surface, such as the Tharsis rise with $h_g \sim 1400$ m and the Argyre basin with $h_g \sim -400$ m [8], the signal of the ice cap is rather small, but should still be discernible by satellite gravimetry.

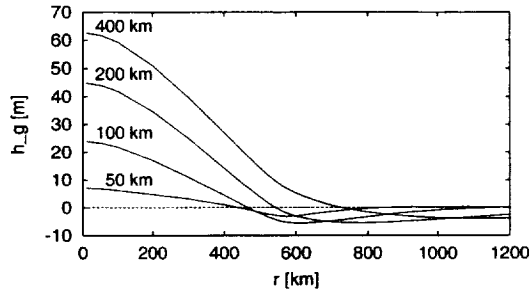

Figure 3: Vertical geoid displacement, h_g, vs. radial distance from the north pole, r, for simulations displace (50, 100, 200, 400 km).

Conclusions: Comparison of the simulated flow of the north polar permanent ice cap with accumulation rates feasible from the point of view of atmosphere physics indicates a thickness of the Martian lithosphere of at least 200 km. For 200 km, the isostatic depression in the centre of the ice cap is approximately 25% of the fully local isostatic compensation, and maximum ice-flow velocities are of the order of some millimetres per year. Relaxation times for the lithosphere/mantle system are less than 10 kyr, much smaller than significant changes of the ice load, so that the ground depression follows the ice-load history in a quasi-static fashion. The vertical geoid displacement due to the combined ice load and ground depression is of the order of some 10 m.

References: [1] Greve R. (1997) *J. Climate*, **10** (5), 901-918. [2] Wolf D. (1985) *J. Geophys.*, **57**, 106-117. [3] Klemann V. and Wolf D. (1999) *Geophys. J. Int.*, **139**, 216-226. [4] Greve R. (2000) *Icarus*, Mars Polar Science Special Issue (in press). [5] Zuber M. T. et al. (1998) *Science*, **282**, 2053-2060. [6] LeMeur E. and Huybrechts P. (1996) *Ann. Glaciol.*, **23**, 309-317. [7] Schubert G. et al. (1992) in *Mars*, eds. H. H. Kieffer et al., Univ. of Arizona Press, Tucson, 147-183. [8] Esposito P. et al. (1992) in *Mars*, eds. H. H. Kieffer et al., Univ. of Arizona Press, Tucson, 209-248.

THE ERUPTION AT GJÁLP, VATNAJÖKULL IN 1996 - LESSONS ON SUBGLACIAL ERUPTIONS.
Magnús T. Gudmundsson, Science Institute, University of Iceland (Hofsvallagata 53, 107 Reykjavík, Iceland, mtg@hi.is)

Introduction: Volcanism under the Pleistocene ice sheet has had a profound effect on landscape in Iceland. Fissure eruptions typically produced hyaloclastite ridges and, in some cases, the higher and more voluminous tuyas. These landforms are today conspicuous features of the active volcanic zones. Volcanic eruptions have been numerous within the present ice caps, notably where the active volcanic zone is covered by the Vatnajökull ice cap in central Iceland [1], and under the Mýrdalsjökull ice cap in south Iceland. However, despite the high frequency of eruptions within glaciers in Iceland, no such eruption had been monitored in any detail before the Gjálp eruption in October 1996. The reason for this was the unusually quiet volcanic period that occurred in Vatnajökull after 1938 and the fact that the last major eruption in Mýrdalsjökull occurred in 1918. Thus, the Gjálp eruption provided an unique opportunity to observe processes and measure their rates during a subglacial eruption.

Course of events: The eruption occurred in September-October 1996, midway between the large ice covered central volcanoes of Bárðarbunga in the north and Grímsvötn in the south. For monitoring purposes, the course of events was observed from the air when weather permitted [2]. The eruption started in the evening of September 30, under 500-600 m of ice, and on October 1, 100 m deep depressions were observed in the ice surface above the erupting fissure. A subaerial vent opened after 30 hours and tephra was spread over the glacier surface during the remaining 12 days of the eruption. However, the subaerial eruption was always a minor part of the activity; the main eruption was subglacial. By October 2, the erupting fissure had reached 6 km in length. The rate of melting, as witnessed by the increase in volume of the depressions in the ice above the erupting fissure, was about 0.5 km^3/day for the first four days, after which it declined. By the end of the eruption about 3 km^3 of ice had melted, and a further 1 km^3 was melted in the following six months. The observed melting rates suggest that the magma fragmented into small particles, resulting in highly efficient heat transfer from magma to ice. Thus, fragmentation into pyroclastic glass was the dominant style of activity; the expected melting rate for a pile of pillow lavas is about one order of magnitude lower than the observed rate.

Ice cap response: Apparently, the meltwater produced was drained away continuously, since no signs of subglacial water accumulation were observed at the eruption site during or after the eruption. Moreover, flow of ice into the depressions overlying the vents was confined to the depressions themselves. Although a progressively larger area of the ice cap was affected as the depressions gradually grew in width, the ice flow outside the depressions was not affected. This suggests that eruptions under temperate ice caps do not trigger ice cap instability. The depth of the ice depressions over the eruption site has decreased from 160-190 m at the end of the eruption to 80-100 m in 1999. The width of the affected area has at the same time increased from 4 km to 8 km. Simple estimates based on glacier mass balance and size of affected area suggest that the ice cap should regain its former profile in 25-40 years.

The volcanic edifice: The hyaloclastite ridge produced in the eruption is 6 km long and 0.5-2 km wide. The magma erupted was basalt andesite [3]. The ridge is apparently very narrow near its southern end, but is spread out in the northern end, where ice thickness was greatest. It has a volume of 0.6-0.8 km^3. A further 0.1 km^3 of material was transported by the meltwater into the Grímsvötn caldera-lake to the south of the eruption site. The ridge has a maximum relief of 450 m relative to the surrounding bedrock but is more typically 150-200 m high. The top of the edifice was visible for about a year, but was then covered by ice flowing in from the sides.

The future: At the present time two competing processes are at work in Gjálp. Firstly, there is alteration of the pyroclastic glass into palagonite. When inspected in June 1997, the exposed top of the edifice showed some signs of alteration and temperatures of the pile were 60-70 °C at 0.5 m depth. Secondly, there is compaction and erosion by the glacier. The rates of these processes in the glacial environment are unknown but Gjálp will be a natural laboratory where they can be monitored in future. Repeated measurements of the form and thermal state of the Gjálp

edifice should throw new light on the development of older hyaloclastite ridges, and how well they have preserved their original form and size.

References: [1] Larsen, G., Gudmundsson, M.T., Björnsson, H. (1998) *Geology*, 26, 943-946. [2] Gudmundsson, M.T., Sigmundsson, F., Björnsson, H. (1997) *Nature*, 389, 954-957. [3] Einarsson, P., Brandsdóttir, B., Gudmundsson, M.T., Björnsson, H., Grönvold, K., Sigmundsson, F. (1997) *Eos*, 78, 369, 374-375.

MAGNETIC PROPERTIES OF THE DUST ON MARS. H. P. Gunnlaugsson, *Institute for Physics and Astronomy, Ny Munkegade, DK-8000 Århus C, DENMARK, (hpg@ifa.au.dk).*

Introduction: The abstract summarizes the results from a new analysis of the data from the Magnetic Properties Experiment on Mars Pathfinder [1], regarding the magnetic properties of the dust.

The Mars Pathfinder lander carried two sets of the so–called Magnet Array (MA): an upper MA, placed on top of the electronics box, and a lower MA situated on the base petal between two of the solar-cell petals of the lander. Each MA consist of five "bulls eye" pattern magnets of various surface magnetic field strength. The detailed design of the MA is described in [2]. The Magnetic Properties Experiment on Mars Pathfinder is an extension of a similar experiment on the Viking Mission. One of the magnets of the Viking Magnetic Properties Experiment was exposed to airborne particles exclusively, the so–called RTC (Reference Test Chart) magnet [3,4]. This magnet was of similar strength as the strongest magnet of the MAs (magnet #1) of the Pathfinder mission. The MA contained additionally weaker magnets, labeled #2–#5 in order of decreasing strength. During the mission, these magnets collected magnetic dust particles suspended in the Martian atmosphere [5,6]. Pictures were taken of the magnets at regular intervals using various optical filters, and these data were used for the analysis. Figure 1 shows a picture of the lower MA taken on Sol 55. The bulls eye pattern on the strongest magnet

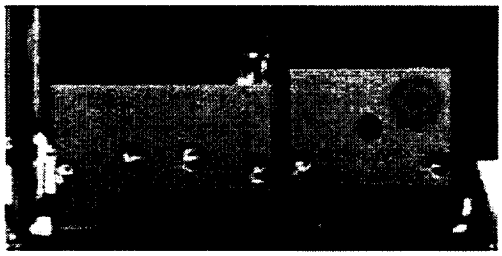

Figure 1: Pictures of the lower MA taken on Pathfinder sol 55, using the blue (443 nm) filter. Below the MA, one can see the color chips used for calibration.

is clearly visible and a similar pattern can be seen less clearly on the weaker magnets.

The fact that the magnets are not fully covered with dust allows one to find the amount of dust accumulated onto the magnets. Figure 2 shows the amount of dust on the strongest magnets of the upper and lower MAs as a function of Pathfinder sol. Two periods or instances, where dust has been removed from the MAs, can clearly be seen. The first between sol 23 and 26, and the second between sol 39 and 40. Schofield *et. al,* [7] reported that a dust devil passed through the Pathfinder landing site on sol 25, offering a possible explanation for the removal of dust between sols 23 and 26.

Analysis: Estimating the Magnetic properties of the dust is not a straightforward task due to the complicated adhering

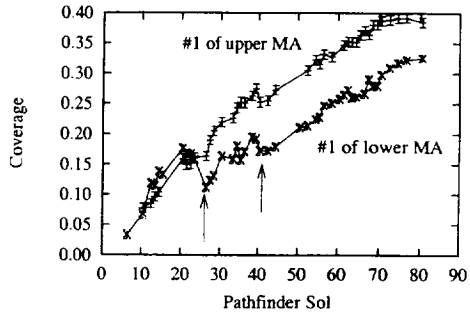

Figure 2: Coverage as a function of Pathfinder sol for the dust accumulated on the strongest magnet of the upper and lower MAs in the blue (443 nm filter). Error bars are not included for clarity, but the errors are on the average 0.007. The arrows indicate instances of dust removal from the magnets.

mechanism. This is related to the extremely small size of the particles suspended in the atmosphere on Mars (average particle diameter $3.2 - 3.4$ μm [8,9]) relative to the surface roughness of the MAs. This means that the physical intuition derived from working with terrestrial analogues, usually with larger particles, may give misleading information for the properties of the particles. Simple estimates, based on where dust is stable on the MAs, are inadequate as they depend on assumptions regarding the interactions between the surface of the targets and the dust which are not fulfilled. Estimates based on the rate of dust accumulation also become unreliable due to instances/periods of dust removal. Instead, one needs to look at the dust pattern in greater details and relate the dust amount at a particular location on the magnets to the magnets' ability to attract dust to that location. In the analysis the symmetry of the dust pattern has been utilized, and the coverage of dust as a function of distance from the centre of the "bulls-eye" pattern, i.e. the covering profile, has been found.

Results: Theoretical dust profiles for particles of given magnetic properties have been calculated. These profiles are compared to the measured profiles and the difference has been minimized. Figure 3 shows a comparison between the measured and calculated profile for the strongest magnet of the lower MA.

The results from the model optimization are summarized in Table 1. It is seen from the Table that there is a variation in the magnetisation of the material accumulated to the different magnets. This result is in conflict with the assumption that the dust is homogeneous. The Table also reflects some of the difficulties in studying this material by e.g. Mössbauer spectroscopy. To obtain large amounts of material, strong magnets are needed, but simultaneously one does not obtain the strongly magnetic component in large amounts. To obtain

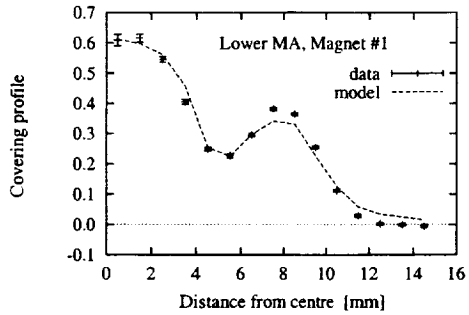

Figure 3: The covering profile for magnet #1 of the lower MA compared to the calculated profile.

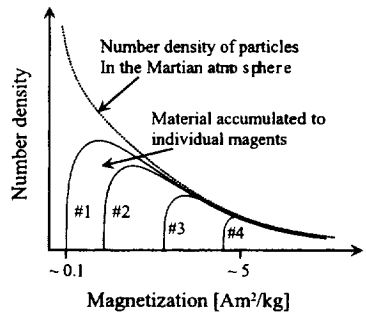

Figure 4: Illustration of the number density of particles as a function of magnetisation, and how the magnets have accumulated particles from this distribution.

Table 1: Average saturation magnetization of the dust accumulated to the different magnets, and the dust amount accumulated on sol 80 for the lower MA.

Magnet #	Average saturation magnetization (Am^2kg^{-1})	Dust accumulated on sol 80 (μgcm^{-2})
1	0.3	190
2	0.7	50
3	1.5	20
4	6	8
5	>6	<5

the highly magnetic material, weaker magnets are needed, but then some active mechanism may have to be deployed to accumulate enough material to allow any realistic study.

Discussion: The results summarized in Table 1 show that there is a considerable spread in saturation magnetisation of the dust suspended in the Martian Atmosphere. The results are consistent with the assumption that the number density of particles with a given magnetisation is a decreasing function of magnetisation. This view is illustrated in figure 4. The value of the highest saturation magnetization, 6 Am^2kg^{-1}, is of great importance since it significantly limits which mineral can be responsible for the magnetic properties of the dust. Not many iron oxides have such a high saturation magnetization. These results excludes the – perhaps – most probable mineral, hematite (α–Fe_2O_3). Other naturally occurring iron oxides with such a high saturation magnetisation are magnetite and maghemite. Based on the bright reddish colour of the dust, pure magnetite or titanomagnetite seem to be unattractive, while the possibility of maghemite seems attracting, and has been the favored interpretation [4-6].

Taking the SNC meteorites to represent the surface rocks on Mars, it is clear that they are not magnetic enough to explain the results obtained here [10]. Thus, some unknown oxidative mechanism has enhanced the magnetisation of the soil/dust on Mars. Due to the similar results obtained by both Viking landers and the Pathfinder lander, this process has worked on a global scale, and should be part of any model proposed for the origin of the Martian soil.

The best indications of what can be learned from the Magnetic Properties Experiment, comes from simulation experiments using terrestrial analogues. If the results of such experiments are to be compared with the data from Mars, great care has to be taken. If the material used does not show the same profiles or spread in magnetisation as observed on Mars, the results can not be compared directly to the results from Mars Pathfinder.

References: [1] H. P. Gunnlaugsson, (2000), *Planet. Space Sci.* submitted. [2] H. P. Gunnlaugsson *et al.*, (1998), *Planet. Space Sci.*, **46**, 449-459. [3] R. B. Hargraves *et al.*, (1977), *JGR*, **82**, 4547-4558. [4] R. B. Hargraves *et al.*, (1979), *JGR*, **84**(B12), 8379-8384. [5] S. F. Hviid *et al.*, (1997), *Science*, **278**, 1768-1770. [6] M. B. Madsen *et al.*, (1999), *JGR*, **104**(E4), 8761-8780. [7] J. T. Schofield *et al.*, (1997), *Science*, **278**, 1752-1758. [8] M. G. Tomasko *et al.*, (1999), *JGR*, **104**(E4), 8987-9008. [9] W. J. Markiewicz *et al.*, (1999), *JGR*, **104**(E4), 9009-9018. [10] R. B. Hargraves *et al.*, (2000), *JGR*, **105**(E1), 1819-1827.

OPTICAL PROPERTIES OF THE MAGNETIC DUST ON MARS. H. P. Gunnlaugsson, *Institute for Physics and Astronomy, University of Aarhus, Ny Munkegade, DK-8000 Århus C, DENMARK, (hpg@ifa.au.dk).*

Introduction: The abstract summarizes the results from a new analysis of the data from the Magnetic Properties Experiment on Mars Pathfinder [1], regarding the optical properties of the magnetic dust.

Among the remarkable results of the Viking mission was the discovery that the Martian dust/soil is highly magnetic, in the sense that the dust is attracted by small hand magnets [2,3]. Study of the properties of the magnetic dust is of importance, as it may contain invaluable clues on the surface processes that have shaped the planet, especially the role of water in these processes [4].

The Mars Pathfinder lander carried two sets of the so–called Magnet Array (MA): an upper MA, placed on top of the electronics box, and a lower MA situated on the base petal between two of the solar-cell petals of the lander. Each MA consists of five "bulls eye" pattern magnets of various surface magnetic field strength. The detailed design of the MA is described in [5]. During the mission, these magnets collected magnetic dust particles suspended in the Martian atmosphere [6,7]. Pictures were taken of the magnets at regular intervals using various optical filters, and these data were used for the analysis.

Analysis: The magnets are not fully covered with dust, and during the mission, the dust covering increased (see e.g. [8]). This means that the detected reflections found from the images, are composites of the reflection from the platinum coated surface of the MAs and the reflection from the magnetic dust. To obtain optical spectra of the magnetic dust of high S/N ratio, the observed signal has been decomposed into the time independent reflection from the magnetic dust of time dependent coverage. The resulting spectra depend slightly on necessary assumptions used in the analysis. Briefly, these effects can be described as a scaling and an offset in the spectra obtained, meaning that the absolute error is 20-30%.

Results: Figure 1 shows the diffuse reflection spectra obtained for the dust accumulated to the magnets indicated. As is seen from the figure, all curves are similar. The spectrum for the dust accumulated on magnet #2 indicates more crystalline features, but based on the error analysis this can not be claimed to be significant.

In figure 2 the spectra compiled in this work are compared with the spectra of different Martian soil/rocks types. All spectra show the characteristic near-UV absorption for ferric minerals [11,12]. However, the spectra of the magnetic dust differ significantly in the infrared part of the spectrum.

Discussion: The difference in the spectra of the magnetic dust and the reference spectra in the slope of the spectra above 750 nm is compelling. Several hypothesis have been suggested to account for this difference and what it may tell us about the surface on Mars. Below, some possibilities are discussed.

- There is a total lack of the absorption feature between 750 and 1000 nm. Morris *et al.*, [12,13] demonstrated that this feature could be caused by transitions in specific ferric minerals, and viewed this as a measure of the degree of crystallinity. This suggests small particle (nanophase) ferric oxide such as maghemite.

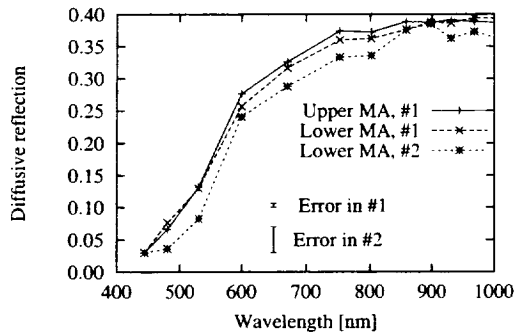

Figure 1: The diffuse reflection spectra of the dust accumulated on the strongest magnet (#1) of the upper and lower MAs and the second strongest magnet (#2) of the lower MA. The error bars indicate the statistical error in the data.

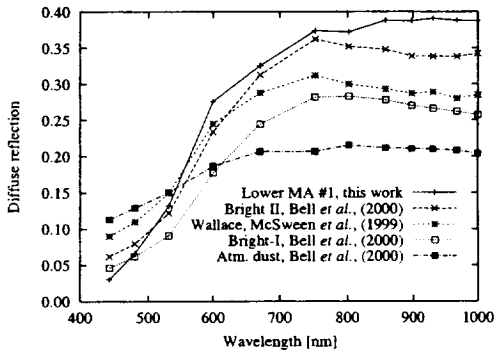

Figure 2: The diffuse reflection spectra of the dust accumulated to the strongest magnet of the lower MA compared to the spectra of two soil units and and atmospheric dust(data from [9]) and the spectrum of the rock Wallace (data from [10]).

- Morris *et al.* [14] have suggested that this difference is due to the fact that the magnetic dust does not contain pure ferric Fe, and suggested titanomagnetite. This seems to be in conflict with the rather bright reflection of the magnetic dust, but may be consistent with oxidized titanomagnetite, or titanomaghemite.

- The difference may be caused by a lack of mafic material in the magnetic dust. Bridges *et al.*, [15] and Greeley *et al.*, [16] reported the observations of ventifacts

and other aeolian features which illustrate that grinding of rock has taken place on Mars. Thus, the soil could consist of rock fragments, absorbing strongly in the infrared, and a dust component, which does not, and is the only component observed on the magnets. This would suggest that the rock fragments are either too large to be lifted into suspension or not magnetic enough to be captured by the magnets.

- An alternative possibility is that the observed difference is actually an artifact caused by the wavelength dependence of the extinction efficiency. This interpretation would demand that the magnetic particles had a size distribution with an average radius of $\bar{r} = 0.75\mu$m, considerably smaller than the values $\bar{r} \sim 1.5\mu$m obtained by [17] and [18] for the aerosols suspended in the Martian atmosphere.

It is clear from the discussion here that not all questions regarding the magnetic phase on Mars have been answered. The optical data show that the material accumulated to magnets is unique, a fact that should stimulate further efforts to study this material. Some of the questions raised here could be answered in an extended Magnetic Properties Experiment, utilizing the knowledge of how this material is accumulated to magnets. Simulation experiment, utilizing terrestrial analogues are a necessary tool to enhance the knowledge of what is actually observed on the magnets on Mars. The data presented here will contribute to how accurately such experiments describe the data from Mars.

References: [1] H. P. Gunnlaugsson, (2000), *Planet. Space Sci.*, submitted. [2] R. B. Hargraves *et al.*, (1977), *JGR*, **82**, 4547-4558. [3] R. B. Hargraves *et al.*, (1979), *JGR*, **84**(B12), 8379-8384. [4] M. B. Madsen *et al.*, (1995), *Hyp. Int.*, **95**, 291-304. [5] H. P. Gunnlaugsson *et al.*, (1998), *Planet. Space Sci.*, **46**, 449-459. [6] S. F. Hviid *et al.*, (1997), *Science*, **278**, 1768-1770. [7] M. B. Madsen *et al.*, (1999), *JGR*, **104**(E4), 8761-8780. [8] H. P. Gunnlaugsson, (2000), this conference. [9] J. F. Bell, III *et al.*, (2000), *JGR*, **105**(E1), 1721-1755. [10] H. Y. McSween, Jr. *et al.*, (1999), *JGR*, **104**(E4), 8679-8715. [11] D. M. Sherman *et al.*, (1982), *JGR*, **87**(B12), 10169-10180. [12] R. V. Morris *et al.*, (1985), *JGR*, **90**(B4), 3126-3144. [13] R. V. Morris and H. V. Lauer, Jr., (1990), *JGR*, **95**(B4), 5101-5109. [14] R. V. Morris *et al.*, (1999), *JGR*, **105**(E1), 1757-1817. [15] N. T. Bridges *et al.*, (1999), *JGR*, **104**(E4), 8595-8615. [16] R. Greeley *et al.*, (1999), *JGR*, **104**(E4), 8573-8584. [17] M. G. Tomasko *et al.*, (1999), *JGR*, **104**(E4), 8987-9007. [18] W. J. Markiewicz *et al.*, (1999), *JGR*, **104**(E4), 9009-9017.

MAGHEMITE ON MARS: POSSIBLE CLUES FROM TITANOMAGHEMITE IN ICELANDIC BASALT. H. P. Gunnlaugsson[1], G. Weyer[1] and Ö. Helgason[2], [1]Institute of Physics and Astronomy, Aarhus University, Ny Munkegade, DK-8000 Århus C, DENMARK, (hpg@ifa.au.dk), [2]Science Institute, University of Iceland, Dunhaga 3, IS-107, Reykjavík, ICELAND.

The Viking landers and the Pathfinder lander carried instrument packages to investigate the magnetic properties of the soil and dust on Mars [1,2]. The instruments consisted of small permanent magnets that accumulated magnetic dust particles suspended in the Martian atmosphere. From the results [3-5] we now know that there is a strongly magnetic mineral in the Martian soil and dust. The SNC meteorites, assumed to be Martian surface rocks, are not magnetic enough to explain the high magnetisation of the soil/dust on Mars observed by the Viking and Pathfinder landers [6]. It is therefore indicated that some (oxidative) mechanism has enhanced the magnetisation of the surface material. Based on the magnetic and optical properties of the accumulated dust, the magnetic phase has tentatively been identified as maghemite, γ-Fe_2O_3, present as cement in or stain on silicate agglomerates. It is, however, not possible to exclude that the magnetic phase is titanomagnetite ($Fe_{3-x}Ti_xO_4$) or titanomaghemite (γ-$Fe_{2-x}Ti_xO_3$) having been inherited directly from the bedrock [4].

The properties and the formation of this magnetic material are of considerable interest. It may give invaluable clues to answer questions about the role of water in the soil forming processes on Mars [7]. Has the formation of the red soil on Mars taken place predominantly via oxidation of Fe(II) in aqueous solution eons ago when Mars was warmer and wetter? Or is the soil forming process an ongoing process of breakdown and oxidation of surface rocks? The material can be studied by separating it from the soil/dust with magnets offering a unique opportunity to make comparative studies on robotic Mars missions. Finding terrestrial analogues is essential to gain insight into how to answer the above questions.

Titanomaghemite has been found to be common in mixtures with titanomagnetite in partially oxidised Icelandic basalt [8]. The titanomaghemite has been shown to exhibit unusual high temperature stability [9] and has been found to have Ti/Fe ratios close to 0.15 [10]. The formation process has been found to enhance the magnetisation of the rock by up to an order of a magnitude [11]. It is possible that the formation of titanomaghemite in basalt lava from Iceland is related to the formation of maghemite on Mars. Icelandic basalt is therefore an interesting analogue for the study of possible soil forming processes on Mars.

To study the iron oxides in Icelandic basalt, we have applied Mössbauer spectroscopy. It is a unique technique to characterise iron oxides in basalt, giving information on the valence state of Fe and on magnetic interactions. The Mössbauer spectrum of titanomagnetite is well known [12]. The spectrum of pure magnetite consists of two characteristic sextets, usually labelled A and B. The A sextet, assigned to Fe(III) on tetrahedral sites, has a hyperfine splitting of approximately 49 T. The B sextet, assigned to Fe(II) and Fe(III) on octahedral sites exchanging rapidly electrons, results in one unresolved sextet which has a hyperfine splitting of approximately 45.5 T. The area ratio between the A sextet and B sextets is close to ½. In titanomagnetite, characteristic changes in the hyperfine parameters allow for rough estimates of the amount of titanium in the magnetite. The spectrum of titanomaghemite, consists of one sextet, overlapping the A sextet of titanomagnetite.

Figure 1 shows selected Mössbauer spectra of samples from the LG-series.

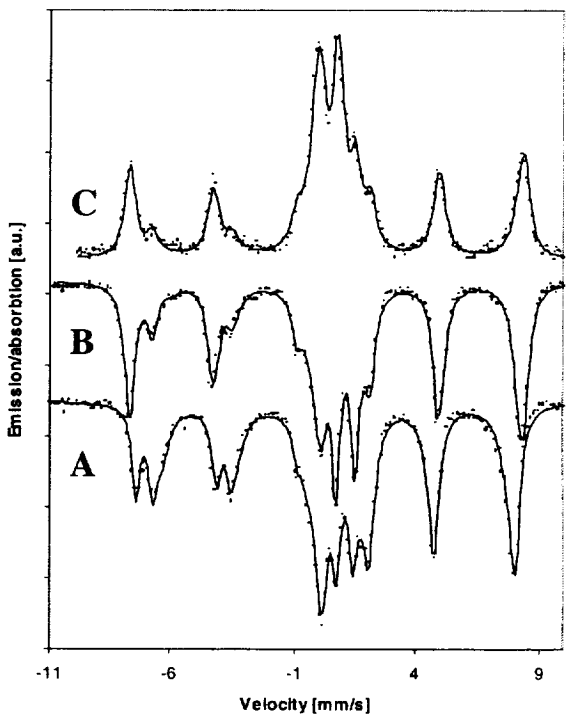

Figure 1: Mössbauer spectra of selected samples from the LG-series discussed in the text.

The LG-series (described in [11]) represent samples taken at regular intervals away from a dike intrusion. Far from the dike (> 1 m) the samples are unaltered by heat from the dike. The transmission Mössbauer (TM) spectra reveal titanomagnetite with x~0.2 and no detectable amount of titanomaghemite (see the spectrum marked A in figure 1). Close to the dike (< 1 m), oxidation and exolution of the titanomagnetite has taken place and the Mössbauer spectra reveal a mixture of titanomaghemite and titanomagnetite with x~0.05 (see spectrum B in figure 1). Conversion electrons released from the decay of ^{57}Fe penetrate of the order 0.25 μm of material. Since the size of the Fe-Ti oxide islands in the samples is in the range 20-200 μm [13], conversion electron Mössbauer spectroscopy (CEMS) is only sensitive to the surface of these grains (see spectrum C in figure 1). From the analysis of the spectra of LG-4 in figure 1 it was found that the area ratio between the titanomaghemite and the titanomagnetite sextets was 3.8 and 5.6 in the TM and CEM spectra, respectively, clearly indicating that the oxidation has predominantly taken place on the surface of the Fe-Ti oxide particles. The centre part of the spectra in figure 1 consists of lines from paramagnetic minerals. Lines from minerals containing Fe(II) dominate the centre part of the TM spectra, while lines from Fe(III) containing minerals dominate the centre part of the CEM spectrum.

Figure 2 shows a Scanning Electron Microscopy picture (SEM) taken in backscatter mode of a typical Fe-Ti oxide island in one of the samples obtained close to the dike intrusion.

Figure 2. SEM backscatter picture of a typical Fe-Ti oxide island in the sample LG-2, obtained 18 cm from the dike intrusion.

The SEM picture clearly shows fine exolution lamellae, with an intergrowth of the order 0.1 μm. These lamellae have been interpreted as the result of the titanomagnetite/titanomaghemite exolution, clearly showing why a separation of these phases has never been successful, neither physical nor by means of XRD and optical spectroscopy [7].

Maghemite in Icelandic basalt is formed upon thermal exolution of titanium rich magnetite and is always found in fine structured mixtures with magnetite. Thermal exolution on Mars seems an unattractive hypothesis due to the global formation of the maghemite, while impacts and volcanic activity are most likely to cause only local effects. Formation through photostimulated oxidation due to UV radiation [14,15] is perhaps more relevant. The extremely small particle size observed for the aerosols suspended in the Martian atmosphere suggests that one does not observe the whole Fe-Ti oxide particles, but only the oxidation products, titanomaghemite, knocked off from the original titanomagnetite grains as a result of transport over geological distances and timescales. The dark material eroding from the polar regions on Mars [16] may represent trapped material, an intermediate stage in the soil forming process.

If the magnetic phase on Mars is titanomaghemite, formed upon oxyexolution in titanomagnetite, the data presented here suggest that it would be associated with magnetite, easily identified by Mössbauer spectroscopy. Additionally, it should be mentioned that maghemite derived from oxidation of Fe(II) in aqueous solutions would not contain the element titanium.

References: [1] R. B. Hargraves *et al.*, (1977), *JGR*, **82**, 4547-4558. [2] H. P. Gunnlaugsson *et al.*, (1998), *Planet. Space Sci.*, **46**, 449-459. [3] S. F. Hviid *et al.*, (1997), *Science*, **278**, 1768-1770. [4] R. B. Hargraves *et al.*, (1979), *JGR*, **84**(B14), 8379-8384. [5] M. B. Madsen *et al.*, (1999), *JGR*, **104**(E4), 8761-8780. [6] R. B. Hargraves *et al.*, (2000), *JGR*, **105**(E1), 1819-1827. [7] M. B. Madsen *et al.*, (1995), *Hyp. Int.*, **95**(1-4), 291-304. [8] S. Steinthorsson *et al.*, (1992), *Min. Mag.*, **56**, 185-199. [9] Ö. Helgason *et al.*, (1992), *Hyp. Int.*, **70**, 981-984. [10] H. P. Gunnlaugsson *et al.*, (1996), In I. Ortalli (Ed.), Conf. Proc., **50**, 383-386. [11] L. Kristjansson (1985), *JGR*, **90**(B12), 10129-10135. [12] H. Tanaka and M. Kono (1987), *J. Geomag. Geoelectr.*, **39**, 463-475. [13] K. Grønvald, (1992), Univ. Iceland, privat comm. [14] R. L. Huguenin (1976), *Science*, **192**, 138-139. [15] R. L. Huguenin (1976), *Icarus*, **28**, 203-212. [16] P. Thomas *et al.*, (1992), In (H. H. Kieffer et al., Eds.) Mars, *Univ. Ariz. Press*, 767-798.

EXTENSIVE LAKES IN THE DRY VALLEYS (ANTARCTICA) DURING THE LAST GLACIAL MAXIMUM: IMPLICATIONS FOR PAST LAKES ON MARS. B. L. Hall, University of Maine, Orono, ME 04469-5790 USA, brendah@maine.maine.edu, and Woods Hole Oceanographic Institution, Woods Hole, MA 02543 USA.

Introduction: At the last glacial maximum (~10,000-20,000 years before present), the Dry Valleys of Antarctica (77°-78° S, 160°-164° E) supported huge closed-basin lakes (up to 212 km^2, 550 m deep), significantly larger than any lake that exists in the region today (<7 km^2, commonly <70 m deep) [1]. The existence, elevation, and volume of these former lakes have been determined by mapping widespread geomorphic features, such as deltas and shorelines. Chronology comes from over 500 accelerator mass spectrometry (AMS) radiocarbon dates of benthic algal mats preserved within the lacustrine deposits.

Climate Regime: At present, the Dry Valleys are a hyperarid environment with <10 mm (water equivalent) of annual precipitation [2]. Mean annual temperature at Vanda Station on the floor of Wright Valley (80 m elevation) is –20 °C, with annual extremes ranging from –57 to +10 °C. Under this present climate regime, glaciers are polar with basal temperatures well below freezing (-18 °C at Meserve Glacier)[3]. Over 90% of ablation is by sublimation [4]. Solar radiation penetrates the glacier and melts ice along crystal boundaries a few centimeters below the surface [5]. This meltwater converges into supraglacial streams that flow off the ice margin. Ice cliffs act as radiation traps and are also an important meltwater source. By these mechanisms, meltwater production is enhanced on clear, sunny days and can occur even if the air temperature is below freezing [6]. However, even a thin layer of snow on the glacier surface inhibits this melt mechanism and halts melting. Average flow of the Onyx River at Lake Vanda is 2 x 10^{15} m^3/yr [7], however, during 1977-78, the river never reached Lake Vanda, due to a late spring snowstorm that caused a cessation in meltwater production.

Landforms produced under these hyperarid conditions include small (<10 m high), coarse-grained moraines, sand and fine-gravel fans, sand dunes, small deltas, and shorelines [8]. Preservation is excellent, due to the near-lack of water erosion, long-term slope stability, and limited erosive capacity of cold-based glaciers.

At the last glacial maximum, the climate of the Dry Valleys region likely was even colder than it is now. Despite the polar, hyperarid climate, huge lakes formed, indicating volumes of meltwater up to 100 times greater than that of today. The implication is that the production of meltwater and hence the formation of the lakes is not related so much to temperature, but instead to changes in absorbed solar radiation, a conclusion which is supported by some modern observations [6]. The formation of the lakes in the Dry Valleys is thought to relate to an increase in the number of clear, cloudless days, coupled with a decrease in snowfall [9]. This climate situation likely came about because the adjacent ocean was filled with a large ice sheet during the last glacial maximum. Distance to open water was increased at least 500 km and storm tracks may have been altered.

Implications: Evidence from the Antarctic indicates that large volumes of meltwater can be produced, even where the mean annual temperature is well below zero and even if air temperature is below freezing. It also stresses the importance of the amount of absorbed solar radiation as a factor in controlling melt. The implication for Mars is that at least small quantities of meltwater may be able to form even if air temperatures never reach the melting point of water.

References: [1] Hall, B.L., and Denton, G.H. (2000) *Geogr. Ann.*, in press; Hall, B.L., and Denton, G.H. (1995) *Ant. J. U.S., 30*, 52-53. [2] Thompson, D.C. (1973) *NZ Geogr. Soc. Conf. Ser.,4*, 259-265. [3] Bull, C. and Carnein, C.R. (1968) *ISAGE Symp. Hanover, NH*, 429-446. [4] Chinn, T.J.H. (1980) *Proc. of Riederalp Workshop, IAHS-AISH*, 237-246. [5] Fountain, A. et al. (1998) *Ant. Res. Ser.,72*, 65-76; Hendy, C.H. (2000) *Geogr. Ann.*, in press. [6] Chinn, T.J.H. (1993) *Ant. Res. Ser.,59*, 1-51; Fountain, A. et al. (1999) *Biosc.,49*, 961-971. [7] Chinn, T.J.H. (1993) *Ant. Res. Ser., 59*, 1-51. [8] Hall, B.L. et al. (1997) *J. Geol., 105*, 285-294. [9] Hall, B.L. and Denton, G.H. (1995) *Ant. J. U.S., 30*, 52-53.

COMPOSITION AND ENERGY BALANCE OF THE MARS SEASONAL POLAR CAPS FROM MGS. G. B. Hansen, Hawaii Institute of Geophysics and Planetology, SOEST, University of Hawaii, 2525 Correa Road, Honolulu, HI 96822 ghansen@pgd.hawaii.edu.

Introduction: Remote sensing results from the Mars Global Surveyor (MGS) orbiter will be reported in a continuing project to analyze the surface composition, infrared emissivity, and solar albedo of the seasonal polar caps of Mars, with the goal of producing a detailed model of the heat balance for each polar cap. These properties will be inferred primarily from spectra and bolometric radiances from the thermal emission spectrometer (TES), but also reflectivity and cloud/surface detection from the Mars orbiter laser altimeter (MOLA) and images from the Mars orbiter camera (MOC). The shortwave measurements of the solar bolometer of TES and MOC images are available only for sunlit polar caps, while the 1-μm MOLA observations are available for polar night as well, albeit only for a limited range of spacecraft altitudes and geometries. The TES spectra and thermal bolometer are usable over a wide range of altitudes and all lighting conditions. A study has already been completed using MOLA brightness data and TES spectra from two of the first 36 orbits to estimate the composition and grain size of both seasonal polar caps [1].

Observation Details: Observations are currently available from the "assessment subphase" (revolutions 3–137, September 15, 1997 to February 19, 1998, seasonal dates L_S=181.2–277.8°), part or all of the "science phasing" orbits, in two parts, SPO-1 and SPO-2, before and after solar conjunction (SPO-1, revolutions 202–328, April 2 to May 28, 1998, L_S=304–335°, and SPO-2, revolutions 383–551, June 23 to September 13, 1998, L_S=349–3°), and part of the second aerobraking phase (revolutions 580–661, September 26 to October 29, 1998, L_S=35–49.5°). As of this writing, complete MOC images are available to the beginning of the mapping period (March 27, 1999), and complete MOLA data is available to the end of SPO-2.

TES: TES spectra are the primary tool for abundance, composition, and temperature determination. TES is composed of a Michelson interferometer measuring from 1650 to 200 cm^{-1} (~6–50 μm) with a finest spectral resolution of either 6 or 12 cm^{-1}, and a two-channel bolometric radiometer measuring solar (0.3–2.7 μm) and thermal (5.5–100 μm) spectral regions [2]. It is equipped with a pointing mirror that was used in the large, elliptical early orbits to construct of spectral images (at low spatial resolution, ~130 km) of the disk of Mars. The finest spatial resolution of TES measurements is <3 km [3]. Observations of the winter polar regions are useful only above 8–10 μm.

MOLA: MOLA is used for surface reflectance and surface/cloud location determination. The primary purpose of MOLA is to measure the planetary radius and topography using a pulsed laser system operating at a wavelength of 1.064 μm [4]. Secondary products include the backscattered energy, and limited information on the width of the returned pulse, related to surface slope and roughness, and atmospheric scattering. For relative topography, the surface along-track resolution is ~300 m and the vertical resolution is about 30 cm [5]. Optically thick clouds will generate a return near the cloud top, but the thin clouds typical of Mars will tend to scatter the pulse out of the forward direction, thus preventing a significant return.

MOC: MOC images will be used to determine the relative reflectance and distribution of seasonal deposits. Images in the mapping orbit have spatial resolutions of <2 m for the narrow-angle camera and >200 m for the wide-angle red and blue cameras [6]. The images in the elliptical orbits are of lower resolution, and are not typically concurrent with TES measurements [7].

Previous Work: The seasonal polar caps of Mars are composed primarily of solid CO_2, and the optical properties of CO_2 ice require that pure snow with a sufficiently small particle size has a high visible/near-infrared albedo and a low infrared emissivity in parts of the thermal infrared, particularly in the region between 20 and 50 μm. Dust mixed into or on top of the CO_2 ice will lower the visible albedo and bring the thermal infrared emissivity closer to 1. Water ice mixed with the CO_2 will have little effect in the visible and near-infrared to 1.4 μm but can raise the 20–50 μm emissivity if the particle size is >50 μm.

Observations of both seasonal polar caps during two of the assessment orbits of the Mars Global Surveyor spacecraft were used [1] to show that there is a strong correlation between visible brightness and low 20–50 μm emissivity. TES spectra from regions with low 20–50 μm brightness temperature are consistent with surface deposits of CO_2 with millimeter-sized grains and containing varying small amounts of dust, and they are not consistent with the expected signature of water ice or clouds. Large regions of low emissivity were seen in the spring south seasonal cap that had not been observed previously. They are correlated with visible bright regions (which are known to become brighter as the spring progresses) inferred from historical observations. In the north polar night, brightness is

inferred from MOLA measurements. The model of seasonal CO_2 caps with bright, low-emissivity regions agrees with previous visible observations of bright crater rims, streaks, and other bright areas within the polar caps, some of which may evolve into dark, high-emissivity sheet ice or may have evolved from dark, high-emissivity ice into brighter, fractured, fine-grained ice layers. It is also in agreement with models of the CO_2 cycle, which require average polar cap emissivities <0.9.

Our initial examination of the first available complete TES spectra and ancillary data (revolutions 214–268 in the Science Phasing Orbit 1 (SPO-1) sequence) revealed serious artifacts in the polar spectra which were difficult to correct. After considerable experimentation, a scheme was developed that produces much improved spectra from the PDS supplied dataset. This involves linearizing the response (radiance/DN) consistent with the much better behaved, warmer non-polar spectra, and determining a dark correction which includes high-frequency patterns that are repeated throughout the data. This has allowed for a fairly accurate determination of surface temperatures, which have been compared to models based on atmospheric pressure and altitude [8]. This also allows us to now move quickly into the remaining data and produce quality products. In revolution 214, the low emissivity spots appear to align mostly with steep equator-facing slopes, implying possible formation by transient or intermittent atmospheric condensation. No clouds are to be found in the MOLA data from this orbit, although they are abundant in other orbits [9]. Most of the CO_2 deposits in the winter are large grained, or may have up to 1% dust content, forming in either case a high emissivity and low albedo surface. The night-side fringe (up to 70°–75° N) of the polar cap in revolution 214 appears to include significant amounts of fine-grained (≤5 μm) water ice in the surface and/or in a slightly warmer atmospheric haze.

New Work: The goal of the new work is to apply these techniques to all of the available polar data. For example, in SPO-1, TES observes the north polar seasonal cap at near its maximum size and the south polar cap near its minimum residual (CO_2) size. The use of atmospheric models is necessary to separate the surface emission from that of the atmospheric gas and dust and to quantify the radiative contributions of the components to the whole.

Surface models: Simple radiative transfer codes are generally sufficient for modeling thermal emission. Optical constants for CO_2 ice and water ice are well enough known [1, and references therein], while those for dust can probably be improved from studies of dust in the atmosphere [10]. Intimate and spatial mixtures are easily modeled, while layered surface constructs require a more complex approach. The retrievable properties of the surface will include CO_2 grain size, amount of admixed dust or water ice, and surface temperature

Atmospheric models: A band model was developed for the earlier work [1] which is sufficient for modeling the 15-μm CO_2 band in a clear atmosphere. The properties of dust and water ice aerosols can be readily modeled in the non-absorbing regions of the spectrum (given adequate optical constants for the dust [10]). The first approach for modeling the overlap region will be to include an infinitesimal aerosol layer at some level in an otherwise clear absorbing atmosphere. A correlated-k model [11] is being developed to handle the three-dimensional problem of absorbing and scattering aerosols in an absorbing atmosphere. The typical optical depths of atmospheric gas and aerosols will allow for the estimation of the surface radiance over a wide spectral range, even in the dusty southern spring conditions. Clouds of significant optical depth will be detectable by MOLA, which will aid in the TES interpretations.

Other Data Sources: The solar channel of TES and the MOC images have yet to be incorporated in this analysis, and will be included next.

References:

[1] Hansen G. B. (1999) *JGR, 104*, 16471–16486. [2] Christensen P. R. *et al.* (1992) *JGR, 97*, 7719–7734. [3[Christensen P. R. *et al.* (1998) *Science, 279*, 1692–1698. [4] Zuber M. T. *et al.* (1992) *JGR, 97*, 7781–7797. [5] Smith D. E. *et al.* (1998) *Science, 279*, 1686–1692. [6] Malin M. C. *et al.* (1992) *JGR, 97*, 7699–7718. [7] Malin M. C. *et al.* (1998) *Science, 279*, 1681–1685. [8] Smith, D. E., and M. T. Zuber (1998), *Geophys. Res. Lett., 25*, 4397–4400. [9] Pettengill, G. H., and P. G. Ford (1998), *Trans. Amer. Geophys. U., 79*, F526; Ivanov, A. B., and D. O. Muhleman (1999), *Fifth International Conference on Mars*, Abstract #6166, LPI # 692, (CD-ROM). [10] Snook K. J. *et al.* (1998) *BAAS, 30*, 1034. [11] Lacis A. A. and V. Oinas (1991) *JGR, 96*, 9027–9063.

POLAR TERRAIN AND YOUTHFUL GEOLOGICAL PROCESSES ON MARS. W. K. Hartmann, Planetary Science Institute, 620 N. 6th Avenue, Tucson, Arizona 85705, hartmann@psi.edu

Increasing evidence suggests that Martian depositional and erosional, and even fluvial processes, are more active in current geologic time than had been thought a few years ago. The evidence includes the following: (1) Independently reported crystallization ages for shergottites at 100-700 Ma. (2) Dating of liquid water weathering of the nakhlite, Lafayette, at around 650 Ma by Swindle *et al.* [1]. (3) Dating of the youngest lava flows by Hartmann and Berman at less than 100 Ma [2,3,4]. (4) Suggestions of seeps in MGS/MOC frames (see Malin web site [5]), implying youthful aquifers. (5) Abundant dust drifts, layering, and stratification in non-polar terrains. Some of these have virtually no craters [6,7], suggesting ongoing erosion that is exposing the surfaces. Our cratering data also suggest that older surfaces have experimental production of some meters of regolith gardening by impact since their formation [8].

These and other MGS/MOC data suggest that large amounts of aqueous, wind, and impact erosion, deflation, and transport are moving massive amounts of material around Mars, even within the last few hundred Ma. Much of this may be continually dumped in layered polar strata. Correspondingly, these polar strata show extremely low crater counts and evidence of ongoing deposition that removes smaller craters. Crater counts on the polar layered units suggest many units with kilometer-scale craters lasting on the order of 100 Ma and 20-meter-scale craters lasting less than 0.1 Ma. Viking and MGS/MO photography also indicates flow deformation in some instances, including engulfing of older underlying craters. Evidence and interpretation of these processes will be presented.

The implication is that Martian polar layered surfaces are not only re-forming continually by deposition, but also de-forming, in very recent geologic time.

References: [1] Swindle T. *et al.* (2000) *Meteoritics & Planet. Sci., 35,* 107-116; [2] Hartmann W. K. *et al.* (1999) *Nature, 397,* 586; [3] Hartmann W. K. (1999) *Meteoritics & Planet. Sci., 34,* 159; [4] Hartmann W. K. & Berman D. C. (2000) *J. Geophys. Res.*, in press; [5] http://www.msss.com ; [6] Edgett K. (2000) *LPS XXXI*, abstract #1057; [7] Edgett K. (2000) *LPS XXXI*, abstract #1066; [8] Hartmann W. K., *et al.* (2000), submitted to *Icarus*; [9] Hartmann W. K. (1999) *Meteoritics & Planet. Sci., 34,* 167.

(a)

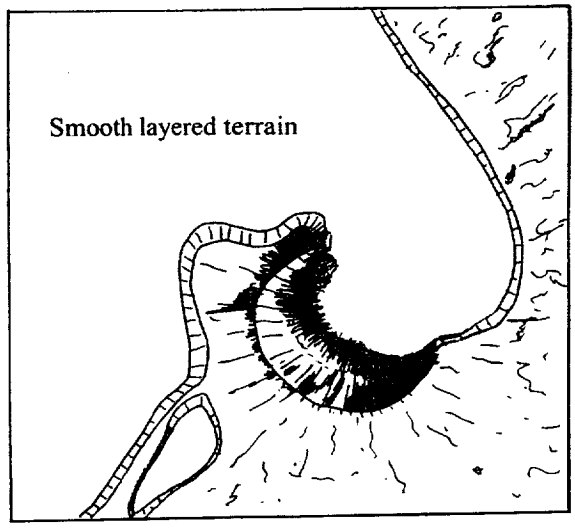

(b)

Figure 1. Evidence of flow of smooth terrain near south polar cap. **(a)** Viking mosaic near -80 S, 240 W, showing crater partly buried by overlapping smooth units. **(b)** Schematic interpretation of the same image. A lobe of the smooth terrain appears clearly to have spread over and engulfed an older impact crater.

POLAR TERRAIN AND YOUTHFUL GEOLOGICAL PROCESSES ON MARS: W. K. Hartmann

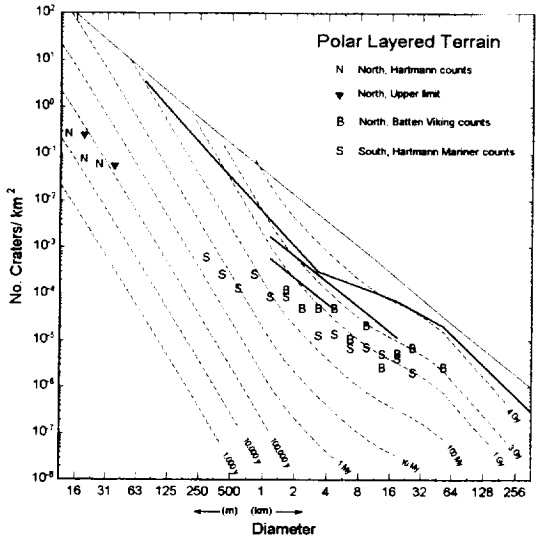

Figure 2. Crater counts diagram with isochrons deduced by Hartmann [9]. The data suggest small craters as rapidly removed, with km-scale craters lasting on the order of 100 Ma and 20-m-scale craters lasting < 0.1 Ma.

EVIDENCE FOR GEOLOGICALLY RECENT LATERAL MIGRATION OF VOLATILE-RICH POLAR LAYERED DEPOSITS. J. W. Head, Department of Geological Sciences, Brown University, Providence, RI 02912 (james_head_iii@brown.edu).

Abstract: An impact crater with pristine-appearing secondary crater chains is partly covered with more than a kilometer of polar layered terrain continuous with the main polar deposit. The observed relationships strongly suggest that the crater formed near the edge of the cap in late Amazonian time, was buried by polar cap advance, and that some retreat has occurred. This, together with evidence for ice streaming, suggests that portions of the cap may have been mobile in the past.

Introduction and Background: The south polar region is dominated by deposits of Amazonian-aged residual ice (Api) and layered terrain (Apl) [1], deposits that also occur at the north pole [1-3]. These are distinguished from seasonal deposits and the polar hood, which show distinctive annual variations in their distribution. A major question is the nature and mode of emplacement of the Mars polar layered deposits and their evolution [1-3]. Are they presently forming, stationary, or retreating? Is there any evidence for movement in the layered terrain, and if so, over what time scales? The very young ages of these polar deposits [1-3] could be interpreted to mean that deposition and/or movement has modified impact craters formed in the polar deposits, producing an abnormally young age. (e.g. [10]) New MOLA data have shown the characteristics of the polar deposits in considerable detail [e.g., 4-6], and revealed evidence for the possible retreat of a portion of the north polar cap in the Olympia Planitia area [7], and basal melting and retreat of volatile-rich deposits in the Hesperian units underlying the polar deposits at the south pole [e.g., 8]. On the basis of these questions we have been investigating the nature of margins of the south polar cap, particularly in areas such as the Prometheus basin, where significant basal melting is suspected to have taken place in the past. Here we report on the nature of a 50 km diameter impact crater with pristine-appearing secondary crater chains; the crater is partly covered with more than a km of polar layered terrain continuous with the main polar deposit. The observed relationships strongly suggest that the crater formed near the edge of the cap in late Amazonian time, was buried by polar cap advance, and that some retreat has occurred. We also describe a candidate area of ice streaming.

Description and Interpretation: Near the mouth of Chasma Australe on the floor of the Prometheus basin lies a 50 km diameter impact crater (Fig. 1) that is partly embayed by deposits of Apl [1, 11]. The crater occurs in Hdu, the Hesperian-aged Dorsa Argentea Formation. MOLA data show that the crater is about 1 km deep, has a very crisp rim standing several hundred meters above the surrounding floor, and has a depth that is anomalous for other adjacent craters. On the west and southwest of the crater interior and rim, occurs Apl, with a thickness in excess of one kilometer. On the distal part of the floor of Chasma Australe, adjacent to the lobe of Apl superposed on the crater rim, occurs a very well-developed set of linear and clustered pits (Fig. 1). Mapping of these in detail reveals that they have all of the attributes of secondary craters and crater clusters and that they are radial to the 50 km buried crater. Examined in the perspective provided by MOLA topography (Fig. 2) one observes that the secondary crater fields and chains radiate from the 50 km crater and that they emerge from underneath deposits of Apl. Mapping of the area due north of the crater also shows evidence for crater fields and clusters radial to the 50 km crater, providing convincing evidence that the craters are not polar collapse features or eolian deflation pits, but rather that they represent radial ejecta deposits associated with the formation of the 50 km crater.

If this interpretation is correct, then this crater must have formed prior to the emplacement of the polar layered deposits in its interior. The freshness of the secondary crater deposits implies a very young Amazonian age for a crater of this size. The preservation and superposition of secondary craters on deposits thought to be related to basal melting and flooding of the Prometheus basin [8,9] also supports a young age. This relationship also suggests that the secondaries were not formed much earlier, covered, and then exhumed. The crispness of their morphology also suggests that they are young and largely unmodified.

Figure 1. Viking orbiter frame 383850 showing the relationship of the 50 km diameter crater (left), the distal end of Chasma Australe and the secondary crater chains on its floor (center), and the lobe of polar layered terrain (Apl) covering the secondaries and apparently extruding into the crater (left middle).

Implications: The relationships outlined in this analysis strongly suggest that an impact crater formed on the floor of the Prometheus basin adjacent to the south polar layered terrain in the relatively recent geological past. A plausible scenario is that material flowed from the edge of the cap down into the floor of the newly formed crater, and over its western rim, covering the rim and portions of the secondary crater field (Fig. 2). This movement would have obliterated any evidence of secondary craters and related ejecta in the Apl unit. These observations support the idea that there was actual movement and flowage in the cap itself, and that this movement obliterated surface texture (e.g., crater ejecta and secondary deposits). This may help to account for the very young age estimates for much of the polar layered terrain on the basis of superposed impact craters [2,3].

An alternate hypothesis, that the crater was formed much earlier, covered by later deposits and protected, and

then exhumed recently, does not seem to be supported by the geological relationships and crispness and preservation of the delicate secondary crater deposits.

Detailed mapping of the northern rim of the crater and secondary crater deposit distribution supports the idea that some minimal amount of retreat of this lobe may have occurred in the most recent past. Further evidence for this type of advance is found in another slightly larger crater some 300 km to the east (Fig. 3 in [12]) which also has a lobe of Apl extending into the crater floor. Although this does not have the same type of preserved secondaries, its depth suggests that it too was a relatively young post-Hd crater into which Apl advanced in a lobe-like manner. Examination of several other craters in the region shows similar evidence for relatively recent advance.

We also see evidence for possible glacial streaming (Fig. 3). Here a range of linear features occur in a trough extending downslope toward the floor of the Prometheus Basin. The morphology and structure of this example is strikingly similar to glacial streaming features on Earth [13]. Glacial streaming features on Earth often initiate at zones of change in slope of underlying topography [13]. This example appears to initiate at a similar change in topography, the rim of the underlying Prometheus Basin.

References: [1] K. Tanaka and D. Scott, USGS Map I-1802C, 1987; [2] P. Thomas et al., in Mars, U. AZ Press, 767, 1992; [3] J. Plaut et al., Icarus, 75, 357, 1988; [4] M. Zuber et al., Science, 282, 2053, 1998; [5] D. Smith et al., Science, 279, 1686, 1998; Science, 284, 1495, 1999; [6] K. Fishbaugh and J. Head, LPSC 31, #1637, 2000; [7] K. Fishbaugh and J. Head, LPSC 31, #1271, 2000; [8] J. Head, LPSC 31, #1119, 2000; [9] K. Fishbaugh et al., LPSC 31, #1206, 2000. [10] A. Pathare and D. Paige, LPSC 31, #1571, 2000. [11] R. Kuzmin, Cryolithosphere of Mars, Nauka, Moscow, 144p., 1983. [12] J. Head, LPSC 31 #2036, 2000. [13] C. R. Bentley, J.G.R., 92, 8843, 1987.

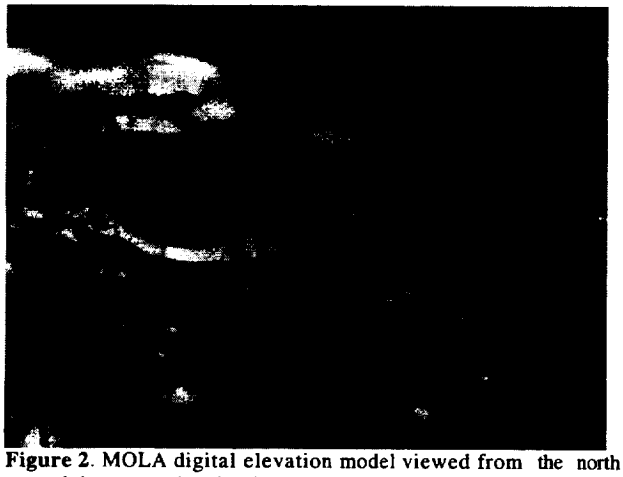

Figure 2. MOLA digital elevation model viewed from the north toward the crater, showing how the ejecta emerges from beneath the lobe of Apl (middle right). Yellow is high, purple (crater floor) is low, and blue is the background Dorsa Argentea Formation at intermediate elevations.

Figure 3. Ice stream-like features in the south polar deposits. Viking image 383B43, and USGS Map I-1647.

EVIDENCE FOR AN EXTENSIVE SOUTH POLAR ICE CAP IN MIDDLE MARS HISTORY. J. W. Head and K. Fishbaugh, Dept. of Geological Sciences, Brown University, Providence, RI 02912 (James_Head_III@brown.edu).

Abstract: MOLA local and regional topographic data support the presence of an extensive Hesperian-aged volatile-rich south polar deposit underlying the present Amazonian-aged cap; several lines of evidence for melting and subglacial flow indicate that the deposits underwent meltback and liquid water drainage into surrounding lows, including the Argyre basin.

Introduction: Present volatile-rich south polar cap deposits [1] are of Amazonian age [2], are areally [2] and topographically [3] centered near the present south rotational pole, consist of Api (residual ice) and Apl (layered terrain) [2] and are thought to be relatively young [4]. Comparison to the north polar cap shows some similarities and significant differences [2-5]. A number of researchers have proposed that the evolution of water on Mars must have involved more extensive polar ice deposits accumulating at a cold trap at the south pole in earlier Mars history [e.g., 6-11]. Specifically, Kargel and Storm [11] noted an abundance of anomalous landforms that they attributed to glaciation; the distribution of these features suggested the presence of large high-latitude ice sheets as late as the Middle Amazonian Period, perhaps covering a significant part of the southern high latitudes [7]. However, major questions and uncertainties exist about the nature and extent of such deposits [e.g., 13] and whether or not they would even accumulate at or near the present rotational pole [12]. The availability of new very high resolution altimetry data from the MOLA experiment [14] permits reassessment of the local topographic characteristics of individual features and regional topographic relationships of stratigraphic units related to these hypotheses.

South polar regional deposits and topography: The youngest extensive stratigraphic units [2] are Amazonian in age (Fig. 1): Api (polar ice deposits which form a residual high-albedo feature at the martian south polar summit and are offset about 200 km north from the pole position at 45W) and Apl (polar layered deposits which are smooth, sparsely cratered moderate-albedo material that forms Planum Australe; in places it is characterized by alternating light and dark layers tens of meters thick with the complete sequence as much as 3 km thick). Apl surrounds Api in a more extensive deposit and is topographically lower [3], with its base generally at about 1800 m elevation. Apl extends north almost continuously to about -80, and is asymmetrically distributed between -70 and -80 in the zone 140-245W. Lowest in the stratigraphic column are units of Noachian age associated with the Hellas and Argyre impact basins followed by several members of a heavily cratered plateau sequence, the youngest member of which extends into the Hesperian [2]. Stratigraphically between the Noachian heavily cratered units and the Amazonian polar deposits is the Hesperian Dorsa Argentea Formation (Hd) which forms polar plains which embay older highland rocks and ridged plains material. The Dorsa Argentea Formation is stratigraphically below Apl, and is predominantly topographically lower than Apl (about 1000-1800 m elevation). The areal distribution of Hd is significant; it is adjacent to Apl, extends northward, and forms a large deposit asymmetrical about the present pole in a direction (-83 to -57; 252-130 W) complementary to the asymmetrical distribution of Apl (Fig. 1). An additional unit (HNu) occurs largely surrounded by Hd and has been assigned a Noachian-Hesperian age [2]. HNu is undivided material composed of rough massive deposits exposed in walls and floors of large irregular pits (Angusti and Sisyphi Cavi) and forming closely spaced rounded hills a few km across [2]. HNu tends to form close to and abutting Apl and within Hd is generally closer to the pole than to the higher latitude margins of Hd. HNu has a large topographic range extending from lows less than 1000 m in the bottom of pits to elevations greater than 3000 m. A significant percentage of the outcrops of this unit occur at elevations in excess of 1800 m, the same elevations as Apl, the polar layered deposits.

In summary, on the basis of areal distribution, surface morphology, stratigraphic relationships, topographic relationships, and complementary asymmetry about the present pole, we conclude that of the units mapped in the south polar region [2], Hd and NHu represent the best candidates for ancient polar deposits (Fig. 1). We now proceed to assess the nature of associated features and their topographic distribution.

Structures associated with Hd and HNu: Several distinctive features and structures have been noted in these two units and these may provide insight into processes associated with the emplacement of the units; several have been investigated using MOLA data [15-18]. *Dorsa Argentea*: These are narrow sinuous ridges that lie in a broad linear depression extending from a high at the polar cap (in HNu) continuously down-slope to near the distal portion of Hd. The ridges occur in the lower parts of the valley and extend generally parallel to it. Detailed mapping of the individual ridges shows that they are sharp and distinctive in the distal parts of Hd, but that they become obscured and are overlain by the upper parts of Hd toward the polar cap. The new topographic data support the interpretation of these ridges as eskers [15 and references therein] and suggest that unit Hd was volatile-rich, and that significant melting, basal lateral liquid water transport, and extensive meltback occurred in the past in this area. *Angusti and Sisyphi Cavi*: These pits and depressions have been interpreted as eolian etching or basal melting of ice-rich deposits [16 and references therein]. Analysis of MOLA topography supports the interpretation that they represent basal melting of ice-rich deposits. In addition, volumetric considerations and to-

pographic lineations suggest that some of the basal melting occurred beneath regions presently occupied by Apl, and that some of the liquid water was deposited in lows distal to the polar deposits. *Chasmata*: Chasma Australe is a distinctive canyon in the polar layered terrain that has been interpreted to have formed by katabatic winds or basal melting [17 and references therein]. New MOLA data document at least two other significant chasmata in adjacent parts of Apl, and on the basis of these data, the analysis supports a basal melting and basal transport hypothesis for their origin and emplacement of adjacent deposits of Hd. Extensive melting within the Prometheus impact basin apparently caused buildup of water bodies and their rapid release and drainage into the portion of Prometheus not covered by polar deposits. MOLA data reveal subtle erosional patterns, evidence for flooding of the basin, and the channels where water was drained from the basin and was distributed into the surrounding lowlands [17]. In summary, taken together, all these features support the interpretation that Hd and HNu represent volatile-rich deposits and that they were once more volumetrically extensive than at present, having undergone meltback. Evidence for melting and basal transport is extensive and varied in its manifestation (eskers, collapse pits, chasmata) and differs in different parts of the deposit. In regions dominated by Hd and HNu (320-130W), basal melting is seen in esker-like ridges and cavi, while within Prometheus basin (200-320W) chasmata dominate. This difference could be related to the presence of the basin and factors favoring ponding of water, such as low-porosity impact melt sheets on the floor of the basin [17].

Discussion and interpretation: These data thus support the general concept that significant volatile-rich deposits formed earlier in Mars history at polar cold traps [e.g., 6-11]. Geologic evidence indicates a Hesperian age [2] for these deposits and topographic evidence suggests that the deposits underlie much of the present area of Amazonian-aged polar layered terrain. Parts of Hd and HNu lie at the same elevation as adjacent exposures of Apl, suggesting that there may be some lateral equivalence and possible overlap in time of these units. The associated geological features are consistent with volatile-rich materials, and their distribution suggests that such deposits extended to latitudes as low as about -57, and covered a surface area at least as large as the present layered terrain. Significant volatiles were lost when portions of the cap underwent meltback to approximately the present position of the edge of the layered terrain. That a significant part of these volatiles was water is supported by: 1) the presence of sinuous ridges plausibly interpreted as eskers, and marking the location of subglacial streams that drained much of the retreating polar cap, 2) chasmata interpreted as massive outflow of subglacial meltwater into the Prometheus Basin and out low points in the basin rim to surrounding low regions, and 3) cavi, the surface manifestation of subglacial melting and vertical and lateral movement of water. Where did the water go? Very deep cavi provide evidence that at least some water reentered the subpolar cap aquifer, but chasmata and esker-like ridges strongly suggest that much of the water migrated laterally to the edges of the deposits. An analysis of the distal parts of these deposits using MOLA data [18] shows that sinuous channels emerge from the distal margins of the circumpolar deposits and extend downslope over hundreds of km into adjacent lows, such as the Argyre basin. These channels are interpreted to result from drainage of water from the receding polar cap [18]. Continuity of the esker-like ridges and lack of abundant moraines suggests extensive stagnant-retreat, as opposed to active-retreat, implying a period of significant warming at these latitudes. Among the candidate causes for such warming are loading-induced basal melting, enhanced geothermal gradient, global climate change, or orbital variations. Finally, if polar deposits occurred here during the Hesperian and are so intimately associated with later Amazonian-aged layered deposits, it suggests that the present south pole has been a cold trap at least during significant parts of these two periods.

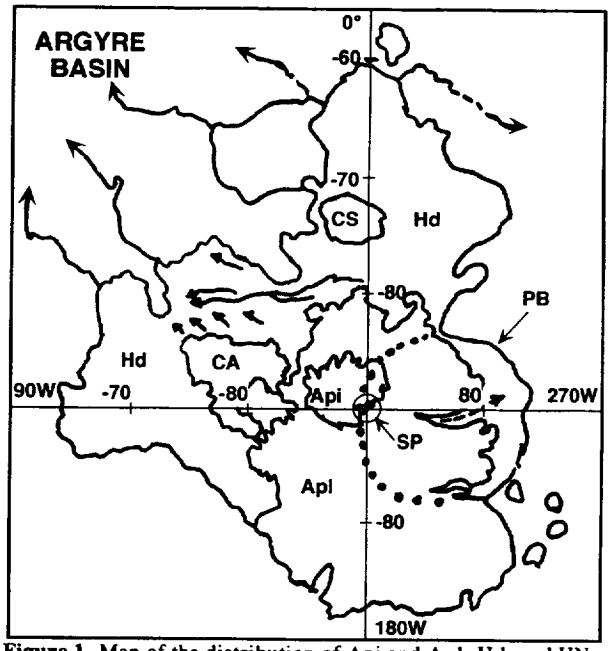

Figure 1. Map of the distribution of Api and Apl, Hd, and HNu and features associated with south polar deposits. SP, South Pole; PB, Prometheus Basin, dotted line shows extension under cap, dashed arrow shows chasma; CA, CS, Cavi Angusti, Sisyphi; arrows within Hd are Dorsa Argentea esker-like ridges; arrows outside Hd are channels draining Hd.

References: [1] P. Thomas et al., in *Mars*, U. AZ Press, 767, 1992; [2] K. Tanaka and D. Scott, *USGS Map I-1802C*, 1987; [3] M. Zuber et al., *Science*, *282*, 2053, 1998; [4] Plaut et al., *Icarus*, *75*, 357, 1988; [5] K. Fishbaugh and J. Head, *LPSC*, *31*, #1637, 2000; [6] F. Fanale et al., *Icarus*, *50*, 381, 1982; *Icarus*, *67*, 1, 1986; [7] V. Baker et al., *Nature*, *352*, 589, 1991; [8] S. Clifford, *JGR*, *92*, 9135, 1987; [9] S. Clifford, *JGR*, *98*, 10973, 1993; [10] S. Clifford and T. Parker, *Icarus*, in press, 2000; [11] J. Kargel and R. Strom, *Geology*, *20*, 3, 1992; [12] P. Schultz and A. Lutz, *Icarus*, *73*, 91, 1988. [13] M. Carr, *Water on Mars*, Oxford, 1996; [14] D. Smith et al., *Science*, *279*, 1686, 1998; *Science*, *284*, 1495, 1999; [15] J. Head, *LPSC*, *31*, #1116 and #1117, 2000; [16] J. Head, *LPSC*, *31*, #1118, 2000; [17] K. Fishbaugh et al., *LPSC*, *31*, #1206, 2000; [18] J. Head, *LPSC*, *31*, #1121, 2000.

CLASSIFICATION OF MARTIAN VOLCANOES ON BASIS OF VOLCANO GROUND ICE INTERACTION. J. Helgason, Ekra Geological Consulting, Thorsgata 24, IS-101 Reykjavik, Iceland, e-mail: jhelgason@simnet.is.

Most Martian volcanoes have common morphological features indicating mass wasting and erosion compatible with large scale break down of ground ice. While some features suggest the ground ice melted rapidly resulting in catastrophic erosive events, other features indicate a slow melting process (e.g sublimation) resulting in collapse structures.

To determine relative volcano age and activity on Mars it is suggested that volcano interactions with an overlying ice sheet may be helpful.

Examples of the various morphological features indicating volcano-ice interaction are drawn from the literature: a) valley formation that probably formed in response to jokulhlaups and subglacial volcanism (e.g. Arsia Mons, Pavonis Mons and Ascraeus Mons [1]), b) isolated thermocarst depressions probably formed by geothermal melting of ground ice, e.g. Hadriaca Patera, c) large scale sublimation of distal strata (e.g. Appollinaris Patera), d) small fluvial valleys (e.g. Hecatus Tholus), e) large scale failure of volcano flanks through aureole development (Olymp-us Mons [1]), f) rimless craters without ash collars (e.g. Arsia Mons), g) rampart craters on volcanoes (e.g. Ceraunius Tholus, Syria Planum, Appollinaris Patera), h) channels (e.g. Elysium Mons, i) mud flows or lahars (e.g. Arsia Mons, Elysium Mons).

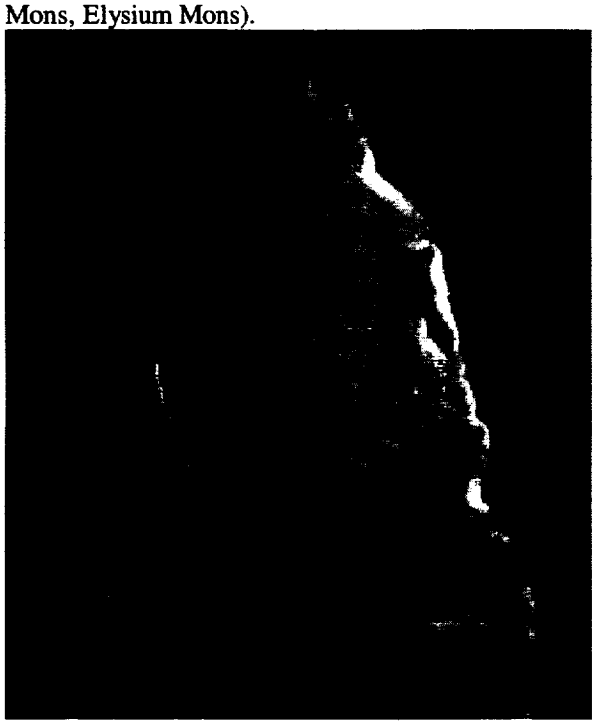

Viking Orbiter image (97A41) showing possible thermocarst landscape on the flank of the volcano Hadriaca Patera (Dao Vallis) [2].

Although various other explanations can account for some of these features they are all compatible with a ground ice-volcano interaction.

These features suggests that to an extent most Martian volcanoes are covered with sheet of ground ice of variable thickness. Over a vast time interval this ground ice layer (or ice sheet) has been failing to a variable extent and in a number of ways depending on different volcano characteristics.

As a result it is suggested that Martian volcanoes can be classified or assigned an evolutionary status depending on how widespread their interaction is with the ground ice layer. Thus, for example, within the Tharsis region the volcanoes Olympus Mons and Arsia Mons can be regarded as two evolutionary end points. Volcanism in the former has completely built up through and destroyed the ice sheet over the source area but is at a very early stage in doing so at the latter.

This method could provide valuable information on the relative ages of Martian volcanoes where age dating by counting impact craters is probably of but minor value due to lava or sedimentary accumulation and impact crater burial.

References: [1] J. Helgason (1999) *Geology 27*, no. 3, 231-234. [2] Squyres et al. (1987) *Icarus, 70*, 385-408.

GEOLOGICAL MAP OF THE SKAFTAFELL REGION, SE-ICELAND: GLACIAL-INTERGLACIAL HISTORY 0-5 MA. J. Helgason, Ekra Geological Consulting, Thorsgata 24, IS-101 Reykjavik, Iceland, e-mail: jhelgason@simnet.is

The Skaftafell region, Southeast Iceland, boarders Vatnajökull glacier on the south side with vast sandur plains on the lowland front formed by jokulhlaups. A detailed map of Skaftafell's bedrock geology is presented that covers Skaftafell, Skaftafellsheiði, Hafrafell and Svínafell, mountain cliffs that are separated by outlet glaciers and valleys.

The Skaftafell region of Southeast Iceland offers highly variable lithology due to volcanism extending over numerous glacial and interglacial periods during the last 5 Ma. Over 90 stratigraphic sections were studied and on basis of lithology, paleomagnetic signature (over 1000 cores from 248 units), and age dating [1], the stratigraphic history of the area was determined with emphasis on glacial-interglacial transitions and landscape evolution.

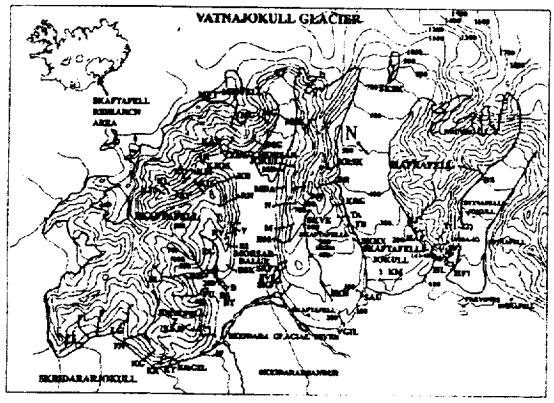

Skaftafell region showing location of investigated stratigraphic profiles. Width of image approxmately 25 km.

Lavas and sediments were deposited during interglacial periods. During glacials, subglacial volcanism produced a succession of lithologic units ranging up dip from: pillow lavas and lobes - pillow block breccia - isolated pillows - hyaloclastite breccia - primary hyaloclastite - reworked hyaloclastite (on top and flanks).

The stratigraphic succession is compiled into two master sections for the Skaftafellsfjöll (2.8 km) and Hafrafell (1.9 km). The Skaftafellsfjöll section is dividable into 25 stratigraphic formations with 12 interglacial and 11 glacial periods. The Hafrafell was divided into 36 formations with 11 interglacial and 10 glacial periods. Correlation of the two master sections with K-Ar age dating, paleomagnetic signature and lithologic characteristics demonstrates a minimum of 16 glacial stages for this region during the last 5 M yr.

A clear evolution in landscape is observed from a low relief lava terrain toward a land deeply incised with valleys by glaciers (negative landforms) and subglacial volcanically formed ridges (positve landforms). Thus, local relief changed from approximately 15 m to over 2000 m in the last 5 M yr.

References: [1] Helgason J. and Duncan R. A. (2000), work in preparation.

GROUND ICE IN ICELAND: POSSIBLE ANALOGS FOR EQUATORIAL MARS. J. Helgason, Ekra Geological Consulting, Thorsgata 24, IS-101 Reykjavik, Iceland, e-mail: jhelgason@simnet.is.

Ground ice preservation in nonglaciated regions on Earth is normally terminated annually outside permafrost terrains. In Iceland old ice has been found under at least three different contitions that may serve as potential Martian analogs or lead the way where to look for ground ice on Mars. Three reconnaissance cases of ancient ground ice in Iceland are briefly reported.

A: Basaltic Scoria/Ice (ice residence: >64 yr). The main event of the AD 1875 volcanic eruption in Askja was first observed on January 3rd that year. The spattering lava material agglutinated to form a 1-2 m thick layer on snow that had fallen earlier that winter. In 1939 [1] a roughly 2 m thick compact snow was photographed under the solidified lava material from 1875 (see below).

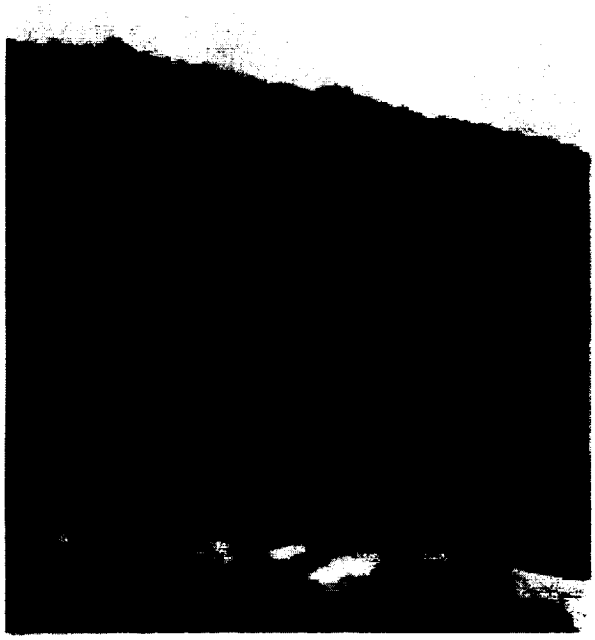

Photo by Vigfús Sigurgeirsson, 1939 in [1].

No intervening material is recorded between the ice and the overlying chilled lava material. Thoroddsen [2] visited this area on July 25th, 1884 and made the following note (transl. from Icel., JH): "It is odd to see in places layers of glacier or snow in between ancient lava flows in the cliffs. When the lavas flowed, centuries ago, they flowed over snow and were unable to completely melt it and now the snow is seen as layers of rock in the cliffs because they are at such a high elevation above sea level that the ice can never be thoroughly melted by the sun". Collapse structures where the ice has melted are commonly seen in the AD 1875 basalt lava flow.

B: Moraine/Ice (ice residence: >100 yr?). In the Grímsvötn jokulhlaup of October and November 1996 the meltwater erosion exposed buried ice banking up against the Sandgígur terminal moraines. The age of the Sandgígur is dated at about 2200 year BP. The moraine material on top of the ice was approximately 4 m thick and the exposed ice wall was also about 4 m high [3]. The contact between ice and moraine was made up of fine grained material. The ice differs from normal glacier ice in being a mixture of sand and ice. A few large ice blocks of this kind were found on the sandur plain below in between the large ice blocks that broke off the Skeidarárjökull glacier suggesting a somewhat large source than observed the in situ exposure. While the age of this ice is unconfirmed it was found in situ on the upward side of the Sandgígur terminal moraine, that are located 5 km south of the present ice margin.

C: Ash deposit/Ice (ice residence: >600 yr?). A less well documented case is that of the rhyolite ash deposit from the Öræfajökull 1362 AD volcanic eruption [4]. In two places on the south side of Öræfajökull volcano, i.e. above Hvanndalur in Svínafell at an elevation of approximately 800-1000 m, and on Bleikafjall at approximately 800-900 m, ice has been seen under the 1362 AD ash deposit. The primary nature of the ash deposit in these locations remains to be confirmed.

High vertical heatflow and atmospheric temperature/humidity conditions in Iceland appear to have but minor impact on ground ice stability. Failure of the bedrock "roof" causing rapid interaction with ground water and/or slow sublimation of the lower ice layer surface, are suggested as important factors affecting stability of ground ice in Iceland.

References: [1] Ólafur Jónsson (1962), In: *Dyngjufjöll og Askja*, with an english summary, Bókaforlag Odds Björnssonar, pp. 96. [2] Þorvaldur Thoroddsen (1958), *Ferðabók*, vol. 1, Oddi, Reykjavík, 2nd ed., pp. 391. [3] Hálfdán Björnsson (pers. comm.) Kvísker in Öræfi, SE-Iceland, [4] Sigurður Björnsson (pers. comm.) Kvísker in Öræfi, SE-Iceland.

ON THE PRESENT MARTIAN WATER-ICE RESERVOIR IN EQUATORIAL MARS. J. Helgason, Ekra Geological Consulting, Thorsgata 24, IS-101 Reykjavik, Iceland, e-mail: jhelgason@simnet.is

Three assumptions relating to the Martian hydrological budget are widely accepted, i.e. a) rampart crater formation involved melting of a ground ice layer to produce fluidized ejecta pattern [e.g. 1], b) "onset diameter" of rampart craters decreases toward polar regions [e.g. 2], and c) equatorial regimes on Mars are devoid of ground ice due to sublimation [3].

This idea, i.e. of a lack of ground ice in the Martian equatorial regimes is challenged. Thus, if rampart crater formation involved melting of a ground ice layer and this layer has subsequently been removed we are left with the inevitable corollary that break down of the ground ice layer should have produced a particular landscape. This landscape should have formed in response to melting of a variably thick ground ice layer. The variable thickness would have led to some areas subsiding more than others and thus a particular surface pattern should have emerged. However, such a pattern is not observed in vast areas with a high concentration of rampart craters. On the contrary, widespread occurrence of rampart craters set in "unaffected" regions suggests that substantial fossil ground ice still resides at depth in between the rampart craters in equatorial Mars.

The observation that large onset diameters tend to cluster in equatorial Mars may suggest that the ground ice layer is thicker there than at higher latitudes.

Support for massive ground ice in present equatorial Mars comes from a morphological study of the volcano triplets: Arsia, Pavonis and Ascraeus Mons, where it is postulated, on basis of morphological features, that substantial jokulhlaups are shaping the landscape in response to subglacial volcanism [4].

References: [1] Carr, M.H. et al. (1977) *JGR, 82*, 4055-4065. [2] Kuzmin, R.O. (1980) *Dokl. ANSSSP, 252*, 1445-1448. [3] Squyres, S.W. et al. (1992), in *MARS* Ed. H.H. Kieffer et al., UA press, 523-554. [4] Helgason, J.(1999) *Geology, 27*, no. 3, 231-234.

Viking Orbiter image (643A78) of Ascraeus Mons with erosional features, i.e. valleys, circular vent structures and erosively formed grabens that may have formed in response to subglacially induced jokulhlaups.

TOPOGRAPHY AND STRATIGRAPHY OF THE POLAR LAYERED DEPOSITS ON MARS. K. E. Herkenhoff and R. L. Kirk, U. S. Geological Survey (Astrogeology Team, 2255 N. Gemini Dr., Flagstaff, AZ 86001; kherkenhoff@usgs.gov).

Introduction: The martian polar layered deposits (PLD) are probably the best source of information about the recent climate history of Mars [1-8], but their origin and the mechanisms of accumulation are still a mystery [9]. The polar layers are sedimentary deposits that most planetary scientists believe are composed of water ice and varying amounts of wind-blown dust [3-5], but their composition is poorly constrained [10]. Because climate changes are likely recorded as variations in composition or deposition/erosion rates between layers, the detailed stratigraphy of the PLD is of great interest. Layer thicknesses of ~10 to 50 m were observed in Viking Orbiter images of the north PLD by Blasius *et al.* [11], and recent Mars Orbiter Camera (MOC) images resolve layers with similar or lesser thicknesses [12]. In order to accurately determine the thickness of layers and interpret PLD stratigraphy, the topography of exposures must be known. Here we describe preliminary results of a study to evaluate the topography and stratigraphy of the PLD using photoclinometry on MOC images.

Approach: In MOC image AB106705, taken during southern springtime when the surface was covered by seasonal CO_2 frost, numerous layers are visible due to their terraced topography (Fig. 1, top). The knobs and pits also visible in the image may be degraded impact craters, perhaps secondaries of the ~20-km crater McMurdo at 84.5° S., 359° W [8]. Assuming that the seasonal frost has the same albedo throughout the part of the image shown in Figure 1 (top), the topography was quantified using a two-dimensional photoclinometric technique. This image was taken in a highly oblique viewing geometry (emission angle 62°). It was therefore necessary to resample the image from the square pixels on the ground (as obtained by the MOC scanner) to square pixels in a plane perpendicular to the viewing direction as assumed by the two-dimensional photoclinometry algorithm of Kirk [13], which was developed for framing-camera imagery. The derived topographic model was then resampled to square pixels on the ground before analysis. Parameters required for the photoclinometric analysis are (1) the brightness contribution of atmospheric haze, which was estimated from measurements of the brightness of nearby shadows, (2) the brightness normalization of the surface, adjusted to make the recovered terrain nearly level, and (3) the scattering law, which was taken as purely Lambertian. The combined result of errors in these estimates is an overall uncertainty in the scaling of the recovered topography of a few tens of percent. Little or no clear evidence was seen of local albedo variations that would introduce artifacts within the topographic model.

Stratigraphy: MOC images of the south PLD show evidence for layering on the same scale as observed in the north PLD. Selected profiles across the image are shown in Figure 1 (bottom). The terraces in the profiles indicate that the layers are ~10 m thick, somewhat thinner than the north PLD layers on average. Some of the layers crop out as ridges rather than horizontal terraces, as also seen in the north PLD [14]. Both the terraces and ridges are evidence for variations in resistance to erosion within or between layers. As in the north PLD, it is difficult to determine the causes of these variations in resistance [14]. Assuming that the composition of the layers is laterally homogenous, differences in layer expression on either side of the depression in Fig. 1 suggest that morphology is controlled by erosional processes as well as physical or compositional differences such as dust/ice ratio. For example, regional-scale slopes in the polar regions will receive varying amounts of insolation, perhaps strongly affecting erosion of volatile-rich sediments. As more MOC images of both polar regions during summer are taken and released, we will attempt to correlate topographic slopes with albedo variations in order to distinguish among possible hypotheses for PLD formation and evolution. An update on this work will be given at the conference.

References: [1] Murray, B. C., (1972). *Icarus* **17**, 328-345. [2] Cutts, J. A., *et al.* (1976). *Science* **194**, 1329-1337. [3] Cutts, J. A., *et al.* (1979). *J. Geophys. Res.* **84**, 2975-2994. [4] Squyres, S. W. (1979). *Icarus* **40**, 244-261. [5] Toon, O. B., *et al.* (1980). *Icarus* **44**, 552-607. [6] Carr, M. H. (1982). *Icarus* **50**, 129-139. [7] Howard, A. D., *et al.* (1982). *Icarus* **50**, 161-215. [8] Plaut, J. J., *et al.* (1988). *Icarus* **76**, 357-377. [9] Thomas, P., *et al.* (1992). In *Mars*, University of Arizona Press, Tucson, pp. 767-795. [10] Malin, M. C. (1986). *Geophys. Res. Lett.* **13**, 444-447. [11] Blasius, K. R., *et al.* (1982). *Icarus* **50**, 140-160. [12] Edgett, K. S. and M. C. Malin (2000). *Lunar Planet. Sci.* **XXXI**, abstract #1068. [13] Kirk, R. L. (1987) Ph.D. thesis, California Institute of Technology Division of Geological and Planetary Sciences. [14] Malin, M. C. and K. S. Edgett (2000). *Lunar Planet. Sci.* **XXXI**, abstract #1055.

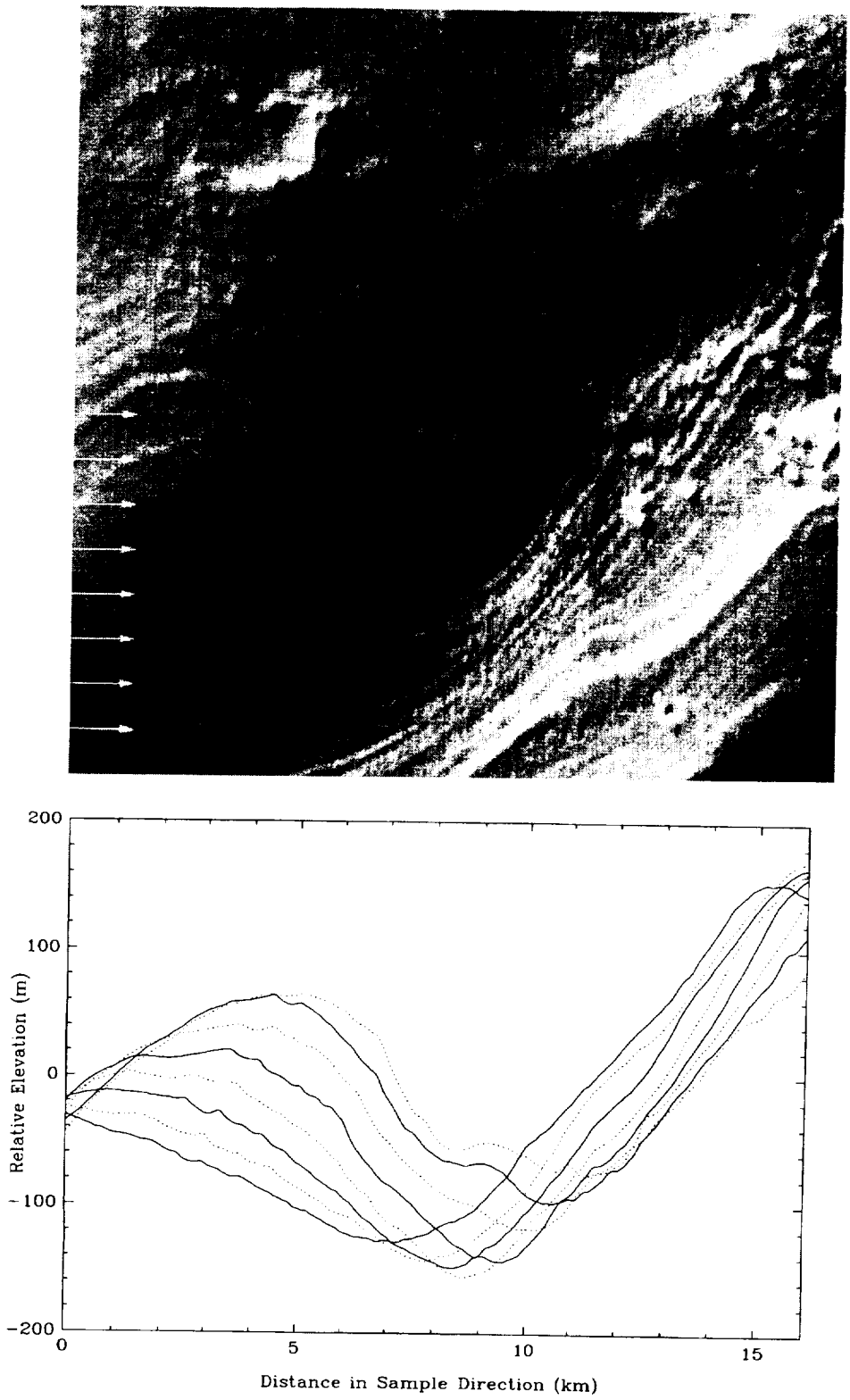

Figure 1. (Top) Central part of MOC image AB106705 of the south polar layered deposits at 84.7°S, 10.6°W (near the residual ice cap) during southern spring. Illumination from upper left, image is ~16 km across, resolution 33 m/pixel. Locations of profiles shown in plot at bottom indicated by arrows. (Bottom) Topographic profiles across entire width of image at 1, 2, ... 8 km from bottom. Vertical exaggeration 28X.

ACCUMULATION PROCESS AT MARS NORTH ICE CAP. Keiji Higuchi, (Nagoya City Science Museum, Nagoya, Japan).

1. Introduction: Mass balance of ice cap depends on accumulation and ablation processes. Accumulation process at the Mars North Ice cap can be speculated on the basis of informations on accumulation process in the inland area of the Antacrtic Ice Sheet of the Earth. Higuchi (1974) proposed three accumulation processes in such area, namely, (1) directsublimation of water vapour on the surface, as frost crystals, (2) snowfall on the surface, through formation of ice crystals in the Atmosphere, as snow crystals, and (3) sublimation of water vapour on drifting snow crystalsnear the surface. Relating to the processes of (1)and (2), Higuchi (1969) emphasized the effect of radiative cooling of ice crystals on their formation and growth processes.

On the other hands, Isono et al. (1957) studied growth process of ice crystals in carbon dioxide gas and other gases, by laboratory experiments. Kobayashi (1958) studied on the habit of snow crystals produced at low pressure in the chamber. Komabayashi (1970) studies shape instability of crystals of ice, carbon dioxide, and ammonia grow in cold chamber, theoretically and experimentally. Watanabe (1974) and Takeda(1975) made experimental studies on formation of crystals of ice and carbon dioxide at low temperature and low pressure.

On the basis of the results obtained by the studies as mentioned
above, accumulation process at the Mars North Ice cap is considered.

2. Formation of crystals of ice and carbon dioxide: In general case of snowfalls on the Earth, latent beat of sublimation of water vapour on the surface of ice crystals are transferred by heat conduction of surrounding air. But, as shown by Higuchi(1969), latent heat are transferred also by radiative cooling of ice crystals, and so ice crystal can grow under lower supersaturation of water vapour than the case without radiative cooling. In the case of carbon dioxide atmosphere of the Mars, such a effect is much more predominant than atmosphere of the Earth, since diffusion process of water vapour through the gas is much more rapid because of low pressure of atmosphere.

On the other hand, we can expect that radiative cooling of dust particles in the Marsian atmosphere will contribute to mucleation of crystals of ice and carbon dioxide on them, especially during the Polar night.

In conclusion, it can be said that formation of ice and carbon
dioxide in the atmosphere and surface of Mars North Ice Cap would occur
even under condition of extremely low content of water vapour in the
atmosphere.

3. Shapes of crystals of ice and carbon dioxide: According to the experimental results by Kobayashi(1958), Komabayashi (1970), Watanabe (1974) and Takada (1975), in the case of ice and carbon dioxide formed in Marsian atmosphere and at the surface of North Ice Cap, their shapes are not such complicated one as dendritic type of snow crystals on earth, but can be considered as simple type as solid column, similar to column type of snow crystals in the atmosphere of the Earth.

It is difficult to estimate particle size of crystals of ice and carbon dixide covering the surface of Mars North Ice cap, but their size could be in the order of micron to millimeter, since colour of its surface is white as seen in the observational results.

QUATERNARY ICE SHEET THICKNESS, JÖKULHLAUPS AND RAPID DEPRESSURIZATION OF PILLOW BASALTS A. Höskuldsson[1], M.R. Carroll[2] and RSJ Sparks[3]. 1)South Iceland Institute of Natural History, Strandvegur 50, 900 Iceland. 2)Dipt. di Scienze della Terra, Via Gentile III da Varano, Universita' di Camerino, 62032 Camerino, Italy. 3)University of Bristol, Wills Memorial Bld. Queensroad, BS1-8RJ, Bristol UK.

Introduction: In this presentation we report results from analysis of pillow basalt formations in Kverkfjöll, NE-Iceland. Pillow basalt formations are commonly found in Iceland. These formations record to eruption under glacial conditions, with most examples being related to the last glaciation. These formations are well preserved and pristine glass can be found on the pillow rims in all cases. The sharp division of pillows and hyaloclastites that is observed in many sub glacial volcanic formations is thought to reflect pressure conditions surrounding the vent at time of the eruption.

Morphological studies of pillows, viscosity calculation and analogue experiments suggest that pillows size spectrum is primarily controlled by eruption rate and viscosity [1]. Existence of extensive lava flows on the sea floor has, on the other hand, been explained by very high eruption rate [2].

Vesicular glassy rims observed on pillow margin a result from quenching of the magma when it comes in contact with water.

Confining pressure influences degassing of the magma and degassing is further limited by the actual amount of volatiles in the magma prior to eruption. At low pressures the most abundant volatile in magma is H_2O. Glass from quenched pillow rims can thus be useful to determine the pressure under which the magma was extruded.

The Mount Virkisfell pillows

The outer crust of the pillows consists of well-formed basaltic glass with thickness ranging from 7 cm to 0.1 cm. On average the glassy rims of Virkisfell are 1.5±0.5 cm thick.

Radial prismatic cooling joints are prominent from the outer rim of each pillow towards its center. The joints do not penetrate into the vesiculated cores of the pillows. However, in pillows lakking a vesiculated core the joints reached the pillow center .

Concentric bubble layers, 5-10 cm thick, are best developed along the sides and top half of the pillows. Between the bubble layers there is a 1 to 7 cm thick bubble-free zone. Vesicular cores showed a maximum size of 170 cm long and 60 cm thick in a pillow that measured 200 cm long and 114 cm high.

Zone of accumulated plagioclase crystals were observed in about 93% of the pillows, typically in the lower half of the pillows. Thickness of the accumulation layer varies, but it is most commonly about 16 cm.

Spaces between the pillows were partially filled with fragments of glassy rim from adjoining pillows and by silty sediments.

Shape and size distribution of pillow lobes

The pillows are most frequently ellipsoidal (46%) to spherical in shape (31%). About 16% of the pillows had sagged tip and only 7% of pillows in the pile are flat sheets. The pillows are slightly flattened, that is the V-axis is in general smaller than is the H-axis. In average the H-axis of the Virkisfell pillows is 1.13±0.85 m and the average V-axis is 0.72±0.41 m. Frequency histogram for the V/H axis ratio of the pillows shows the median value to be 0.75. This reflects the flattened nature of the pillow lobes. The average size spectrum of the pillows elsewhere in Kverkfjöll ranges from H-axis of 1.3-1.6 m and for V-axis 0.8-1.2 m. Measurements of H- and V-axis indicates that the pillows in Virkisfell are in general larger than those that have been previously described from southern Iceland where average H-axis is measured 0.64 m and average V-axis 0.39 m [3].

Vesiculation in the pillows

Vesiculation in the pillows is present from the rim to the core. The glassy sideromelan rim shows vesicularity of 10-20%. Through the crystallized portion of the pillow to the core, vesicular bands occur on regular intervals. The vesicular bands have porosity similar to that of the glassy rim (10-25 vol%). When reaching the core of the pillow vesicularity increases drastically. About 79% of pillows measured in Virkisfell contained a vesiculated core. Vesicularity of the cores was measured as low as 40% and as high as 60% with the average of 49±5%. The cores vary in size but most frequently V-axis is 0.15-0.20 m and the H-axis between 0.30-0.45 m. The shape of the cores is in general reflecting the shape of the pillows. Cores most commonly occur at the distance of some 0.25 m from the bottom of the pillows.

Vesicles

Vesicle shape varies between the banded vesicular zones and the cores. Vesicles in the cores are spherical in shape and in general larger than those vesicles observed in the vesicular banded zones. Vesicles in the banded zones are both spherical and elongated. The core vesicles are near spherical in shape. Vesicles where divided into two groups, single vesicles and

coalesced vesicles. Shape analysis of the vesicles shows that they are equidimensional. Histograms for the measured major axis versus the measured minor axis shows that for single vesicles the most common ratio is 1.0 and that for coalesced vesicles 1.1. The surroundings of the banded zone vesicles are crystallized, whereas, in the cores crystals are finer grained, needle shaped in a glassy matrix. The core vesicles regularity and hyalocrystaline walls indicate a sharp and short growing period.

FTIR measurements

The FTIR measurements were carried out to determine the amount of water in the glassy rim of Mount Virkisfell pillows and other pillow formations in the Kverkfjöll area. The glass making up the rim is fresh and unaltered. For the Virkisfell pillow margins the average wt% H_2O content is 0.89±0.03. Highest values were measured at Karlsrani with an average wt% H_2O of 1.04±0.03. Other pillow formations in the Kverkfjöll area range in wt% H_2O as follows, Vegaskarð 0.85±0.02, Lindarhryggur 0.92±0.02, Kreppuhryggur 0.96±0.03 and Karlshryggur 0.95±0.04.

Estimation of eruption pressures

Infrared measurements of glassy pillow rim material showed no CO_2 above the detection limit (<30 ppm) and so in the following discussion we assume the major volatile component was H_2O. Following this approach, we calculate the following pressures from the measured H_2O contents of glassy pillow rims with no CO_2 and with 30ppm CO_2: Virkisfell - 78±6 to 133±4 bars, Karlsrani 110±9 to 154±6 bars, Vegaskarð 70±5 to 128±3 bars, Lindarhryggur 84±5 to 138±3 bars, Kreppuhryggur 93±6 to 143±4 bars and Karlshryggur 90±8 to 141±5 bars. Note that all of these must be considered as maximum pressures because it is possible to have eruption and quenching of supersaturated melts.

Recalculating the environmental pressures during the Kverfjöll eruptions indicates that Virkisfell erupted under an ice sheet 863±67 to 1481±45 m thick. Other formations give estimated thickness ranging from 775 to 1714 meters. However, it shows that although the volcanic formations are close in space they must vary enough in time to allow for variations in icesheet thickness.

Magma degassing and jökulhlaup

The sudden increase in porosity towards the core of the pillows suggests that some environmental factor changed drastically during the eruption of Virkisfell and the other pillow ridge formations investigated. Porosity increases have not been observed in the pillow formations at MOR [4]. Since pressure and crystallization principally control magma degassing, one of these must change in sub-glacial Icelandic environment. We can exclude crystallization since it occurs both in Iceland and in MOR. Pressure in MOR environment is stable and only changes slightly during eruption by upward accumulations. However, in Iceland, draining of melt water from above an erupting vent can change water pressure drastically. Jökulhlaup are common feature in Iceland and do occur when water trapped by glacier escapes from the eruptive vent [5] [6]. Observations of the eruption of Gjalp in 1996 at Vatnajökull Iceland do support the idea that a sudden decrease in water pressure above an erupting vent or cooling magma body can restart an eruption. In Gjalp it was observed that during the Jökulhlaup volcanic explosions reoccurred, this was about 3 weeks after the eruption ended. This suggests that magma stored within the volcanoclastic pile was remobilize due to pressure decrease above the vent. Magma at such a shallow depth has surely reached saturation with regards to water and thus is highly sensitive to all external pressure changes.

The Virkisfell magma had about 0.89±0.03 wt% H_2O at time of quenching. We can estimate the amount of water released during depressurization from the initial present estimate of 78 to 133 bars. Average porosity of the pillows cores is about 49±5%, taking account of the porosity in the pillow rims (about 20%) the net increase is about 29%. This represents about 29 to 44 bar depressurization or a drop in the water table of 290 to 440 m.

References:

[1] Fridleifsson et al. (1982) JVGR 13 103-117. [2] Bryan W.B. (1991) Oceanus Winter 34 42-50 [3] Walker G.P.L. (1992) Bull. Volc. 54 459-474 [4] Ballard R.D. & Moore J.G. (1977) Springer 114 p [5] Björnsson H. (1988) Soc. Sci. Isl. 45 [6] Hoskuldsson A. & Sparks R.S.J. (1997) Bull. Volc. 59 219-230.

AN ICE FLOW MODEL OF THE NORTH POLAR MARTIAN ICE CAP. C.S. Hvidberg, University of Copenhagen, Department of Geophysics, Juliane Maries Vej 30, DK-2100 Copenhagen, Denmark. Email: ch@gfy.ku.dk.

Introduction: The north polar ice cap on Mars has been mapped with the Mars Orbiter Laser Altimeter (MOLA) [1]. The surface of the ice cap rises about 2800 m above the surrounding surface. The appearance of the ice cap surface is dominated by an irregular spiral structure around two smooth centres. A large valley, Chasma Boreale, separates the two centres into a large elliptically shaped part which is centred at the pole, and a smaller part with a lengthy shape. The spiral structure appears as a results of a pattern of pronounced troughs and scarps at the surface. The steep, equator-facing scarps are dark due to a high dust concentration on the surface, while the more plane, pole-facing (or horizontal) terraces are light. The scarps have been related to a pattern of accumulation and ablation over the surface, with ablation along the dark, equator-facing scarps and accumulation along the light more plane terraces [2,3]. Assuming that the ice flows, a model was proposed, which explains the spiral structure as a result of the accumulation and ablation pattern over the ice cap, and qualitatively relates the scarps and the troughs to ice flow [3].

In this work, the ice flow in the northern cap is modelled. The flow model includes longitudinal stresses, and consider the effects from the ice temperature, which may be widely different from surface to bottom.

The ice flow model: On Earth, the ice sheets flow under their weight as a result of gravity. Accumulation in the central parts is accompanied by ablation in the marginal areas. On Mars, the gravity is smaller, the ice is colder and probably stiffer, and the accumulation and ablation is poorly constrained. If the ice cap is shrinking today, it might be stagnant. The geometry of the northern Martian ice cap is considered, and the deformation of the ice mass as a result of gravity is modelled by an ice flow model.

The ice flow model is axi-symmetrical, and models the ice flow along a line from the centre to the margin with a typical topography from MOLA data, i.e. with scarps and terraces becoming more pronounced as the margin is approached. The model assumes that the ice density is as water ice, and that the constitutive equation is given by the commonly applied flow law for water ice, Glens flow law (see Paterson, 1994). The ice thickness related to the area covered by the ice cap, is used to estimate the flow parameters. The model considers all stresses and include the effect from the temperature distribution through the ice, and calculates the ice flow. If the ice cap is close to steady state, the ice velocities along the surface are balanced by surface accumulation and ablation. Assuming steady state, particle trajectories are derived from the ice flow pattern.

Results: The resulting ice flow pattern is in agreement with the suggested flow pattern by Fisher (1993). The ice moves generally in the direction from the centre towards the margin. The longitudinal stresses are large enough to drag the lowest part of the ice past the pronounced scarps at the surface, even when the surface is north-facing. The scarps affect the ice flow down to the bottom. The ice velocities are highly enhanced in the vicinity of the scarps. If the ice cap is close to stea dy state this flow pattern must be accompanied by enhanced accumulation and ablation associated with the scarps.

References.

[1] Zuber, M. and others (1998). *Science*, 282, 2053-2060. [2] Howard, A.D. and others (1982). *Icarus*, 50, 161-215. [3] Fisher, D.A. (1993). *Icarus*, 105, 501-511.

SPRING AND SUMMER CHANGES AT THE SOUTH POLE AS SEEN BY THE MARS ORBITER CAMERA. A.P. Ingersoll[1], B.C. Murray[1], S. Byrne[1], E. De Jong[2], G.E. Danielson[2], K.E. Herkenhoff[3], H.H. Kieffer[3] and L.A. Soderblom[3]. [1]Division of Geological and Planetary Sciences, Caltech, 1200 E. California Blvd., Pasadena, CA 91125, US. [2]Jet Propulsion Laboratory, [3]United States Geologic Survey. Correspondence Email: api@gps.caltech.edu

Introduction: The Mars Orbiter Camera (MOC) on the Mars Global Surveyor (MGS) spacecraft has been able to follow individual features as the CO_2 frost disappears and exposes the material underneath. Because the orbit of MGS is inclined at an angle of 93 degrees relative to the equator, the spacecraft gets especially good coverage of the ring at 87 degrees latitude. The following is a list of phenomena that have been seen during the spring and summer at the South Pole.

(1) Circular depressions, described by Thomas et al. [1], which are ~ 10 meters deep and 100's of meters in diameter. They are found only within the residual polar cap, the part that survives the summer. The high areas between the depressions are flat-topped mesas whose sides are concave circular arcs. In some places the depressions form patterns that exhibit north-south symmetry, suggesting some control by sunlight.

(2) Dark layers that are exposed on the walls of the mesas. Each layer is at most a few meters thick. The dark layers might accumulate during climatic episodes of high atmospheric dust content, or they might accumulate during the annual cycling of dusty CO_2.

(3) Albedo differences that develop during the summer within the residual cap. These include subtle darkening of the floors of the depressions relative to the mesas and occasional major darkening of the floors, especially near the edge of the cap. The floors and mesas form a distinct stratum, suggesting they represent a distinct compositional boundary. For instance the floors may be water and the mesas may be CO_2.

(4) Small dark features that appear in spring on the seasonal frost outside the residual cap. Some of the features have parallel tails that are clearly shaped by the wind. Others are more symmetric, like dark snowflakes, with multiple branching arms. After the CO_2 frost has disappeared the arms are seen as troughs and the centers as topographic lows.

(5) Polygons whose sides are dark troughs. Those that are outside the residual cap seem to disappear when the frost disappears. The polygons and the dark snowflake-like structures may be related, and suggest that CO_2 frost may form cohesive slabs as described by Kieffer et al. [2].

(6) Irregular depressions outside the residual cap. They look like degraded versions of the circular depressions inside the residual cap, and may be a remnant of the cap's changing location.

(7) Areas of burial and exhumation of circular depressions. Thomas et al. give an example with a sharp boundary: On one side the depressions are buried and on the other side they are exposed. In other cases there are rounded troughs up to 1 kilometer wide, which are dark in summer and appear to have eroded down below the floor of the circular depressions.

References: [1] Thomas P.C. et al., (2000), Nature, 404, 161-164. [2] Kieffer H.H. et al., (2000), J. Geophys. Res., in press.

COMPARATIVE ANALYSIS OF THE MARTIAN ICE CAPS TOPOGRAPHY. RESULTS FROM THE MARS ORBITER LASER ALTIMETER (MOLA) INVESTIGATION. Anton B. Ivanov, Duane O. Muhleman, *California Institute of Technology, Pasadena, CA, 91125, USA, anton@gps.caltech.edu.*

Introduction

The evolution and origin of the residual ice caps and the layered deposits are poorly understood. The layered deposits are thought to be a record of the climatic variations on Mars, which are possibly due to variations in the planet's orbit. Just like the core samples from the Antarctic, they can help us to look in to the past climate of Mars. We have developed a time dependent ice sublimation model [1] to reproduce the observed shape of the North Polar Ice Cap. Results of the model were compared to the MOLA topographic profiles. We attempted to constrain the time scale of the formation of the current ice caps, having sublimation as the only process that modulates the shape of the ice caps. Spiraling troughs in the polar layered deposits are a long-standing mystery. Their formation has not been yet explained. We attempted to analyze trough shapes and their time scales with the sublimation model. The model can reproduce the shape of the troughs very well. Sublimation models can not fully explain the process of the trough formation. However, the model can help to bound the time scales for trough formation. We argued in [1] that sublimation is a very important process for the evolution of the ice caps and its time scales are shorter than that of the ice flow.

In this work we will present comparison of the sublimation model results for the North and South Polar Ice caps and analysis of the trough shapes for both poles.

South Polar Ice Cap: flow and sublimation

On Earth, the sublimation and evaporation of the ice caps is relatively unimportant compared to the flow of ice, ultimately to the oceans. Ice flow and deformation on Mars is considerably less important, since the Martian ice is very cold, mostly less than 200K. Viscous flow models (e.g. [3]), which take into account H_2O ice rheology at these low temperatures, can reach a reasonable agreement with the topography data. Troughs and chasms can not be explained by viscous flow. Sublimation and wind erosion are the two most significant mechanisms for their formation. Nevertheless, the time scales for the two processes - flow and ablation - are sufficiently difficult to estimate with the information about the ice caps we have now. We are prudent that both processes along with the wind erosion are important, but possibly acting on different time scales. The flow rate of the ice cap is largely dependent on the rheology of ice. While it is generally accepted, that the Northern Polar Layered Deposits (NPLD) are composed of water ice and dust, there were no consensus on the composition of the South Polar Layered deposits (SPLD).

Topography cross sections through the centers of both ice caps along 0°-180° longitude are shown at Fig. 1. It is apparent, that central parts of the ice caps are quite similar in size, at least cuts through this particular longitude. Nye et. al. suggested [2], based on rheological properties of CO_2 ice, that it is not possible to construct ice CO_2 cap this big and hence composition of the SPLD is possibly similar in composition to its northern counterpart.

We have applied the sublimation model [1] to the SPLD with albedo 0.65 which is close to the albedo of the observed residual CO_2 ice cap and accounting for the difference in isolation. The results can be seen in Fig. 2. The model fits the slopes of the southern ice cap fairly well. The number of cycles (130) required to fit this slope of SPLD edge is the same as required for the same longitude cut at the NPLD. We have found that setting albedo to 0.55 (same as for NPLD) would erase the ice cap rapidly. Due to hot summers in the south, evaporation rates increase exponentially and water evaporates quickly. It is known from observations that water ice is not exposed on the surface of the SPLD. The ice in the layered deposits should be covered by a layer of dust that can protect it from rapid evaporation during the summer.

Troughs

For our analysis we used MOLA topography grid compiled from passes completed during Science Phasing Orbit and first six month of the mapping orbit (resolution 0.75km/pixel). 194 profiles were manually measured across the troughs. Profiles were extracted from the grid to measure slope and height of north and south walls. Each trough was approximated as a V-shape. It is a good first order approximation, even though many troughs have exhibited complex shapes with a lot of curvature. This dataset of trough shapes allowed compilation of some simple statistics on wall slopes and depths. As expected, the south facing wall (or north wall) is generally higher than the north facing slope (or south wall) and has a larger slope, because it receives more sunlight and hence sublimates more material. The variance of the compiled statistics is high, which reflects a large variety of slope characteristics. Figure 3 illustrates the two most common trough profiles. Although it is very hard to define an "average" trough, an example shown with characteristics closest to the average parameters of the compiled statistics. Processes that form troughs differ in magnitude, depending on location of the trough within the ice cap. For example, troughs that are located on the edges of the cap are more likely to be eroded by winds. Troughs that are located inside the the ice cap were possibly shaped by sublimation and deposition of the material as well as wind erosion. We will also present results of comparison of the observed trough characteristics with the output of the sublimation model. Initial results indicate that troughs shapes simulated by this model correspond well to the observed shapes. The analysis was performed for the North Polar Terrain and we plan to complete it for the South Polar Terrains.

TOPOGRAPHY OF THE MARTIAN POLAR ICE CAPS

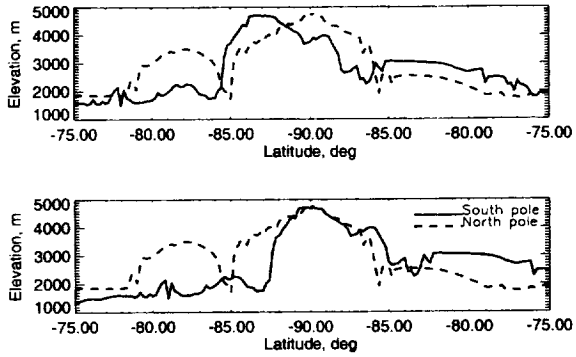

Figure 1: Comparison of north and south ice caps topography. South Pole profiles is the solid black, North Pole profile is the dashed line. The upper panel shows relative offset ($\approx$ 3 deg.) of the south polar cap topography maximum from the real pole. On the lower panel, topography of the South polar ice cap is shifted 3° towards the true pole to emphasize similar sizes of the ice caps. The slopes on the edges of the ice caps are very similar. Vertical exaggeration about 100:1

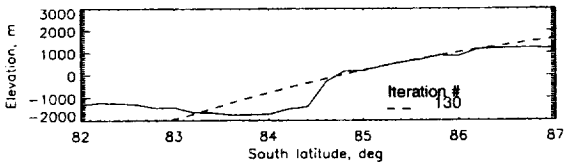

Figure 2: Application of the sublimation model to the southern ice cap. Black solid line is the MOLA data across the cap and dashed red line is the sublimation model results. Note that MOLA topography data was shifted 3.5 km down.

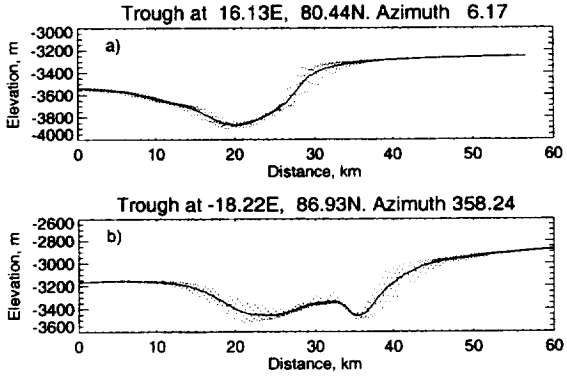

Figure 3: 2 most common trough profiles in the North Polar Layered Terrain. Vertical exaggeration 1:15

Conclusions and future work

Results of the sublimation model suggest that the Northern Polar Ice cap is probably still evolving due to sublimation and accumulation of ice on its surface. South Polar Layer deposits are preserved under a protective layered of dust in the current obliquity cycle. However, overall shape of the SPLD is consistent with the sublimation model. Changes in eccentricity and obliquity in the past may change the duration of north and south summers, so the Southern Ice Cap is sublimating and northern ice cap is stagnant under a protective layer of dust. This might be a clue to development of the layered terrains.

We have suggested that the time scale for the evolution of the current shape bounded by 10-100 million years. We favor lower bound of this estimate. The time scale for trough formation was found to be bounded by 1 and 16 millions of years. This time scale may be even shorter because we did not account for the wind erosion in our model. All the orbital variations are of order of 100s of thousands of years with a long wavelength component of 1-2 million years. Orbital variations lead to significant changes in the climate of Mars and possibly responsible for the formation of the layered terrains. We will include these variations in our model to carry out more reasonable estimates for the time scales of evolution for the Martian Polar Ice Caps and better understand formation of the layered terrains.

References

[1] IVANOV, A., AND MUHLEMAN, D. The the role of sublimation for the formation of the northern ice cap: Results from the mars orbiter laser altimeter. *Icarus 144*, 2 (2000), 436--448.

[2] NYE, J. F., DURHAM, W. B., SCHENK, P. M., AND MOORE, J. M. The instability of a south polar ice cap on mars composed of carbon dioxide. *Icarus 144*, 2 (2000), 456--462.

[3] ZUBER, M. T., LIM, L., AND ZWALLY, J. The role of viscous flow in the morphology of the martian north polar cap. In *First International Conference on Mars Polar Science and Exploration*. LPI contribution No. 953, Lunar and Planetary Institute, Houston, 1998, pp. 45--46.

OBSERVATIONS OF THE POLAR NIGHT CLOUDS ON MARS WITH THE MARS ORBITER LASER ALTIMETER (MOLA). Anton B. Ivanov, Duane O. Muhleman, *California Institute of Technology, Pasadena, CA, 91125, USA, anton@gps.caltech.edu.*

Introduction

Condensation of CO_2 at the winter poles is a very important process in the current climate of Mars. Almost 25% of the Martian atmosphere is recycled through the polar ice caps every year. The condensed form of CO_2 have never been observed or quantified in any significant detail. The Mars Orbiter Laser Altimeter (MOLA) is a very sensitive instrument and was able to detect faint returns coming from the clouds, forming over the polar regions when they were shrouded in winter darkness. The clouds are probably composed of CO_2 ice, which formed in very cold polar winter temperatures. CO_2 ice clouds were first suggested by Gierasch and Goody [3]. A recent review by Forget [1] discusses recent advances in modeling CO_2 condensation rates during the polar night. A direct observation of CO_2 clouds was made by the Mariner 6 and 7 infrared spectrometers ([4]); three bright limb crossings yielded spectra with a spike at 4.26 μm which was attributed to reflection in the strong ν_3 band from solid CO_2 at $\approx$ 25 km altitude. However, the range of occurrence of CO_2 clouds was highly uncertain. The Viking Infrared Thermal Mapper (IRTM) instruments found areas in the winter polar regions with anomalously low brightness temperatures at 20-μm wavelength, some below 135K ([5]). The location and brightness temperatures of these areas sometimes varied on the scales of days, suggesting complex physical processes.

In this presentation we will discuss continuing observations of the polar night clouds during the second North Polar Winter with the MOLA instrument. We will describe seasonal, spatial and elevation distributions of the polar clouds and cloud opacities in the North and South Polar regions of Mars. We will also present some correlations between MOLA cloud heights and MGS Thermal Emission Spectrometer (TES) brightness temperature observations.

Observations

Figure 1 illustrates occurrence of the clouds as a function season on Mars. The number of cloud returns is binned in 1° of L_s for both Science Phasing Oribts (SPO) and Mapping observation periods. The number of returns during the Science Phasing Oribt was multiplied by 6, to account for a less dense coverage compared to the Mapping orbits. SPO orbits had slightly preferential conditions for cloud detection (lower altitude and higher laser output). The most extensive cloud formations were observed over the Northern Ice Cap in the end of the northern winter (L_s = 300° – 360°). Mars Global Surveyor has entered its second Martian year operation, so mapping data overlaps with the SPO data, starting at L_s = 300°. From the start of the mapping observations (L_s = 103°) to the end of the southern winter, MOLA detected extensive cloud formations in the South Polar region, especially over the South Polar Layered deposits. Practically, no clouds have been observed in the south polar region after L_s = 150°. Clouds reemerged over the North Polar region around L_s = 195°. They exhibit same structure and reflective properties as clouds, observed in the end of the northern winter. Observed cloud patterns are remarkably similar from year to year. Note, that cloud densities drop significantly right after the start of the dust storm season (L_s = 220° – 245°). The atmosphere warmed up due to the presence of dust lifted by the storms and higher temperatures prevent forming CO_2 clouds.

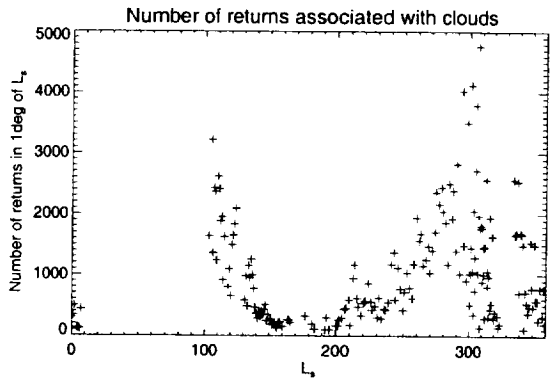

Figure 1: Number of cloud returns during SPO (L_s = 300° – 7°) and Mapping orbits (L_s = 103° – 326°). Mapping orbits have coverage 6 times denser than SPO orbits, so the number of cloud returns taken during SPO was multiplied by 6. Extensive cloud formations are observed near the north polar region during the end of northern winter (L_s = 300° – 360°). Clouds disappear as soon as northern spring sets in. In the time of mapping campaign, south polar clouds decay during the end of the southern winter. Clouds reappear over the North pole after L_s = 195°.

By the differences in reflective properties and spatial occurrence, we were able to classify two types of clouds : polar clouds forming poleward of 80° and clouds that formed only in the southern hemisphere just off the pole the latitudinal range from 70°S to 80°S. We will describe a comparison of the backscattering coefficient measured for Martian clouds with values for some Earth clouds distributions.

CO_2 snowfall

Simultaneous observations during the Science Phasing Orbit by MGS TES and MOLA instruments0 enabled us to address the question of the low brightness temperature zones observed by both TES and Viking IRTM (Infrared Thermal Mapper) instruments. MOLA cloud detections helped us to distinguish

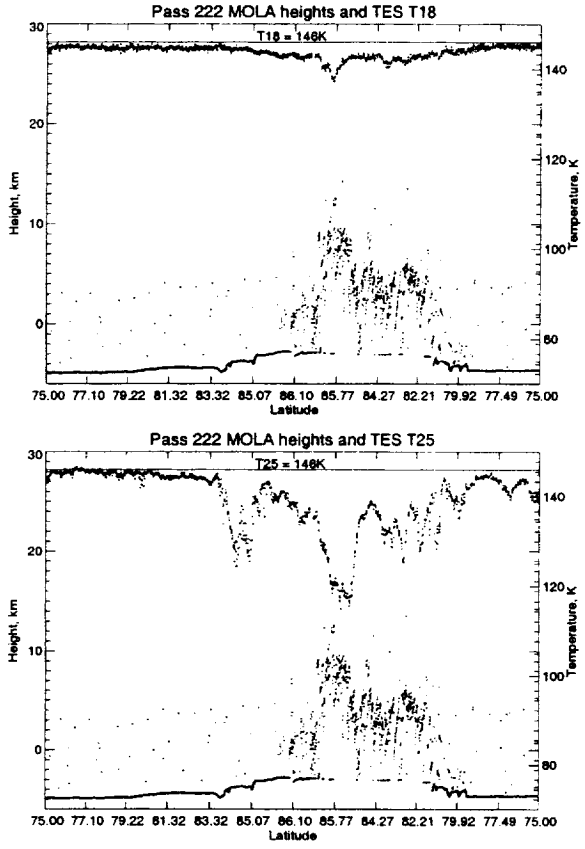

Figure 2: Comparison of the TES brightness temperature data with the MOLA cloud observations. Data shown are for track 222, north of 75°N. MOLA cloud observations are shown by colored dots in the bottom part of the graphs. Brightness temperatures are shown in the upper part of both graphs. Temperature minimum at 86°N correlates well with the extensive cloud formation.

between the contributions of the CO_2 snowfall and condensing CO_2 on the ground. Comparison of the TES and the MOLA data in tracks 222 (Figure 2) and 226 suggests that T25 temperatures are possibly due to the grain size effects of snow at the ground and the atmosphere is transparent at this wavelength. Snow grains might have just fallen from the atmosphere or formed on the ground. T18 channel also observes some of the grain size effect, but the extremely low temperatures are due to atmospheric effects. Minimum brightness temperatures in both T18 and T25 occur in the same places in both tracks and are possibly observed in the atmosphere when the ground is completely obscured by the condensing ice particles. MOLA and TES simultaneous observations suggest that large grains of CO_2 form in the atmosphere and fall out, or in other words, CO_2 snowfall. It has been suggested before [2] as an explanation for the low brightness temperatures the Viking IRTM data. We should note, however that observed low brightness temperatures still can be interpreted as a grain size effect. However, the correlation of MOLA cloud observations and TES brightness temperature measurements significantly weakens that hypothesis.

We have presented comparison of the data taken during the Science Phasing Orbits. We are starting to analyze data obtained by the Thermal Emission Spectrometer and Radio Science investigations for the first month of the Mapping operations and present initial results at the conference.

References

[1] FORGET, F. Mars co_2 ice polar caps. In *Solar System Ices*, B. Schmitt and et al., Eds. Kluwer Academic Publishers, 1998, pp. 477--507.

[2] FORGET, F., HOURDIN, F., AND TALAGRAND, O. co_2 snowfall on mars: Simulation with a general circulation model. *Icarus 131*, 2 (1998), 302--316.

[3] GIERASCH, P. J., AND GOODY, R. A study of the thermal and dynamical state of the mars atmosphere. *Planetary Space Science 16* (1968), 615--646.

[4] HERR, K., AND PIMENTAL, G. Evidence for solid carbon dioxide in the upper atmosphere of mars. *Science 167* (1970), 47--49.

[5] KIEFFER, H. H., CHASE, C. S. J., MINER, E. D., D.PALLUCONI, F., G. MUENCH, G., NEUGEBAUER, G., AND MARTIN, T. Z. Infrared thermal mapping of the martian surface and atmosphere; first results. *Science 193*, 4255 (1976), 780--786.

SUBGLACIAL AND SUBMARINE VOLCANISM IN ICELAND. S. P. Jakobsson, Icelandic Inst. of Natural History, P. O. Box 5320, 125 Reykjavik, Iceland

Introduction: Iceland is the largest landmass exposed along the Mid-Ocean Ridge System. It has been constructed over the past 16 Ma by basaltic to silicic volcanic activity occurring at the Mid-Atlantic Ridge, and is topographically elevated because of the abundant igneous material produced in association with the Iceland hot spot, the center of which is thought to be located beneath Vatnajokull glacier [1]. The axial rift zones which run through Iceland from southwest to northeast are in direct continuation of the crestal zones of the Mid Atlantic Ridge and are among the most active volcanic zones on Earth.

Subglacial Volcanism: Volcanic accumulations of hyaloclastites which are deposits formed by the intrusion of lava beneath water or ice and the consequent shattering into small angular vitric particles, combined with pillow lavas, irregular intrusions and occasionally subaerial lavas, are widely exposed in the volcanic zones of Iceland. These rocks mainly formed subglacially during the Upper Pleistocene but also during Recent times. The origin of the hyaloclastite volcanoes was for a long time a matter of controversy [2] and these volcanoes are still imperfectly known.

The distribution of Upper Pleistocene and Recent eruption units whose essential constituent is hyaloclastite, is shown in Fig. 1. Most of of these units belong to the Moberg Formation [3] formed during the Upper Pleistocene (0,01 - 0,78 Ma). They are predominantly of subglacial origin. Tuffs and tuff breccias predominate along with pillow lavas. Moraines and fluvioglacial deposits are often intercalated with the hyaloclastites. Intra- and interglacial lavas are also an important constituent. Subglacial eruptions within the ice caps of Vatnajökull and Myrdalsjökull have continued up to the present [4].

The hyaloclastite units shown in Fig. 1 cover an area of about 10.600 km2. Hyaloclastites hidden by present ice caps may bring the total area to some 15.000 km2. Basalts are estimated to be • 90 % of the volume, probably < 5 % are intermediate rocks and • 5 % silicic rocks. These eruption units can be divided into three morphological classes, hyaloclastite mounds and ridges, tuyas (flat topped and steep sided volcanoes that erupted into a glacial lake thawed by the volcano), and extensive flows of hyaloclastites combined with columnar basalt.

Distinction is made between three main phases in the generation of a subglacial volcano, e. g. pillow lava, hyaloclastite and subaerial lava.

A pile of undegassed pillow lava forms if the hydrostatic pressure exceeds the gas pressure of the magma. Pillow lavas are often found at the base of hyaloclastite mounds, ridges and tuyas [5]. The thickness of basal basaltic pillow lava piles often exceeds 60-80 meters and a 300 m thick section has been reported. Pillow lavas may also form lenses or pods at a higher level in the volcanoes.

It has been suggested that at a water depth less than approximately 100-150 m, basaltic phreatic explosions produce hydroclastites. It appears feasible to subdivide the hyaloclastites of the Icelandic ridges and tuyas, genetically into two main types. A substantial part of the base of the submarine Surtsey tuya is poorly bedded, unsorted, hydroclastite, which probably was quenched and rapidly accumulated below the seawater level without penetrating the surface [6]. Only 1-2 % of the volume of extruded material in the 1996 Gjalp eruption fell as air-fall tephra, the bulk piled up below the ice [4]. The coarse-grained, often massive core of many of the larger tuyas and ridges may have formed in this way.

At shallow water depths (approximately 20-30 m in the submarine Surtsey eruption, the phreatic eruptions start to penetrate the water level and bedded hyaloclastite (tephra) is deposited by air-fall or base-surge on ice or land, as e. g. in the Surtsey and Gjalp eruptions. In many cases part of the tephra is deposited in ponded water or by running water at or close to the volcano during the eruption. These hyaloclastites are generally more fine-grained than the lower, more massive part described above. Pillows never occur. Examples of this type of hyaloclastites are ubiquitous in Iceland.

Subaerial lavas cap the hyaloclastites section of the tuyas and possibly about 10-15 % of the Icelandic hyaloclastite ridges. These lavas are comparable to other subaerial lavas, sheet lavas are most common but massive, simple flows also occur. The lavas grade into foreset breccias, and sometimes into gently dipping, degassed pillow lava.

Subglacial hyaloclastite ridges, mounds and tuyas are distributed throughout the volcanic zones of Iceland. The number of exposed units may easily exceed 1000-1200 [2]. A recent study (unpublished) in the northern part of the Western Volcanic Zone has identified 83 generally large subglacial volcanoes, of which 59 are hyaloclastite ridges or mounds and 24 are tuyas. The most common lithofacies is poorly bedded tuff breccia, often with pods and lenses of pillow lava and finely bedded tuff.

The area between Vatnajökull and Myrdalsjökull in the Eastern Volcanic Zone is dominated by hyaloclastite ridges, no tuyas are found in the area [7]. The ridges are generally much longer than in the Western Volcanic Zone and may reach a length of 45 km. They commonly

have a present relief of 300-400 m.

Submarine volcanism: A minor part of the hyaloclastite volcanoes in Iceland have formed in marine environments. The best examples are found in the archipelago of Vestmannaeyjar, southwest of the tip of the Reykjanes Peninsula and offshore the Northern Volcanic Zone. A few the hyaloclastite volcanoes in the coastal regions of Iceland may also have formed in a submarine environment. According to the present terminology, most of the abovementioned islands are hyaloclastite ridges, a few are tuyas. As far as can be seen these islands are built up in the same way as the subglacail volcanoes, however, they are generally much more eroded due to marine abrasion.

The best known Icelandic example of a submarine hyaloclastite volcano is the island of Surtsey, which was constructed from the sea floor (depth 130 m) by phreatic submarine and effusive subaerial volcanic activity during 1963-1967, on the Vestmannaeyjar shelf 30 km off the south coast of Iceland [8]. When the eruption ceased the volume of Surtsey was ~ 0.80 km3, of which 0.12 km3 was above sea-level. The island had then reached a maximum height of 174 m and area of 2.7 km2. The island tuya consists of bedded alkali basalt hyaloclastite deposited by phreatic eruptions during 1963 -1964; lava flows of 1964 -1967, that produce foreset breccias where they enter the sea; coastal sediments formed by marine abrasion; aeolian sand formed by wind erosion of tephra, mainly deposited on the flanks of the tephra cones [6].

Marine abrasion has caused rapid cliff recession, and longshore currents have deposited a sand-gravel spit on the north shore. Lava units, particularly thin pahoehoe sheets, have been heavily abraded. Subaerial lava is currently dissappearing at • 0.1 km2 per year. However, the palagonite tuff, formed by hydrothermal activity, is most resistant to marine erosion. The area of Surtsey has shrunk from its original 2.7 km2 to 1.48 km2. Experiments with models of the decrease indicate, however, that Surtsey will last for a long time. Perhaps the final remnant of Surtsey before complete destruction will be a palagonite tuff crag similar to several of the other islands in the Vestmannaeyjar archipelago.

Consolidation and alteration. The bulk of the hyaloclastites in Iceland are consolidated and altered. Volcanic glass is thermodynamically unstable and basaltic glass alters easily to palagonite, which is a complex substance and variable in composition. Alteration primarily occurs under two different types of conditions, in short-lived, mild, hydrothermal systems and at weathering conditions. In Surtsey, hydrothermal activity, consolidation of the tephra, have been monitored closely since 1967 [6,9]. A hydrothermal system was developed due to intrusive activity within the tephra cones in late 1966. Surface temperature measurements in the hydrothemal area showed nearly constant heatflow until 1973 when temperatures started to decline. Temperatures in a drill hole in the eastern margin of the hydrothermal area indicate that the system has been cooling at a rate of • 1° C per year since 1980. Hydrothermal activity caused rapid alteration of tephra producing the first visible palagonite tuff in 1969. By estimate 65 % of the tephra pile was converted to palagonite tuff in 1976. Since then the visible area of palagonite tuff has gradually increased due to erosion of loose tephra on the surface.

References: [1] Saemundsson, K. (1986) *In: The geology of North America, Vol. M. Geol. Soc. Amer,* p. 69-86. [2] Chapman, M. et al. (2000) *In: From the Deep Oceans to Deep Space: Environmental Effects on Volcanic Eruptions. Plenum Press (In press).* [3] Kjartansson G. (1960) *In: On the geology and geophysics of Iceland. Internat. Geol. Congr. 21. Session. Guide to excursion No. A2,* p. 21-28. [4] Gudmundsson, M. T. et al. (1997) *Nature 389,* 954-957. [5] Jones J. G. (1970) *J. Geol. 78,* 127-140. [6] Jakobsson, S. P. & Moore J. G. (1982) *Surtsey Res. Progr. Rep. 9,* 76-93. [7] Vilmundardóttir, E. G. & Snorrason S. P. (1997) *Skaftárveita. Berggrunnur vid Langasjó.(In Icelandic).Orkustofnun OS-97067,* 24 p. [8] Thorarinsson, S. (1967) *Surtsey.The new island in the North Atlantic. Viking Press,* 115 p. [9] Jakobsson, S. P. (1978) *Bull. Geol. Soc. Denmark 27* , 91-105. [10] Johannesson, H. & Saemundsson K. (1998) *Geological map of Iceland. Bedrock geology. 1:500.000, Icel. Inst. Natural Hist.*

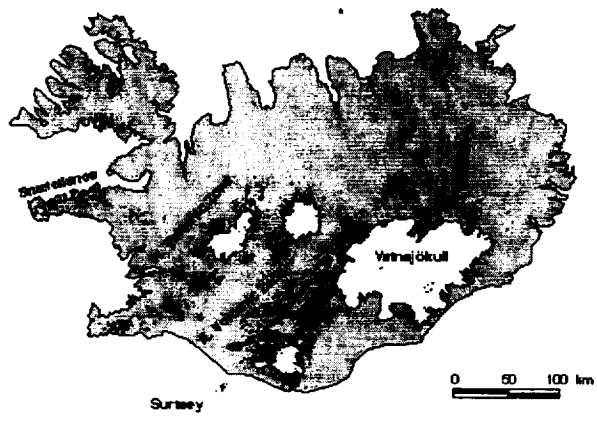

Fig. 1. Distribution of Upper Pleistocene (<0,78 Ma) and Recent hyaloclastites and associated lithofacies in Iceland. Modified after [10].

THE 1999 SEASONAL RECESSION OF MARS' SOUTH POLAR CAP: MOC OBSERVATIONS. P. B. James[1], B. A. Cantor[1], M. C. Malin[2], and S. Davis[2]. Dept. Physics and Astronomy, University of Toledo, Toledo, OH 43606, [2] Malin Space Science Systems, San Diego, CA

The seasonal recession of the Martian South Polar cap has been observed for many years by ground-based astronomers and by spacecraft. The Viking regression in 1977 appeared to be slower than the average of ground based observations but was very similar to the especially good 1971 data set acquired by the International Planetary Patrol. Examination of all of these data sets suggests interannual variability, but no rigorous correlation with other variable phenomena on Mars, such as dust storms, has been possible. The Wide Angle (WA) cameras of the Mars Orbiter Camera (MOC) on the Mars Global Surveyor Spacecraft (MGS) have almost continuously mapped Mars since the start of the Mapping Mission in April 1999. Because the MGS orbit is inclined by about 3° to the poles, images of the polar regions are acquired every two hours. Therefore MOC WA images of the entire south polar cap at low emission angles have been obtained almost every (terrestrial) day during the late winter to late summer cap recession. These data greatly augment the previous coverage of Viking [1], which was less complete in both space and time, and of MOC during MGS aerobraking in 1997 [2], which was limited and provided low resolution.

Accurate topographical data from the Mars Orbiter Laser Altimeter (MOLA) experiment [3] have greatly facilitated interpretation of the numerous irregularities in the cap recession. Correlations are established both with absolute elevation, frost generally favoring lower areas, and slopes, with frost favoring south facing inclines. The regression curve for the south polar cap in 1999 is similar to the "historical average" and faster than that of 1997; the current MOC observations are very similar to the 1997 aerobraking observations. The images have been used to study the behavior of frost albedo in the cap; the new data confirm that the frost in the anomalous, early darkening regions in the cap has color (red/violet albedo) more characteristic of frost than of unfrosted terrains.

This work was supported by a Mars Mission Data Analysis Grant from the Mars Exploration Directorate.

[1] P.B. James et al. (1979), JGR 84, 2889-2922.
[2] P.B. James et al. (2000), Icarus 144, 410-418,
[3] D.E. Smith et al. (1999), Science 284, 1495-1503.

THERMOPHYSICAL PROPERTY MEASUREMENTS OF ALASKAN LOESS AS AN ANALOG FOR THE MARTIAN POLAR LAYERED TERRAIN. J. B. Johnson[1] and R. D. Lorenz[2], [1]US Army Cold Regions Research and Engineering Laboratory (P. O. Box 35170, Ft. Wainwright, AK 99709; jjohnson@crrel.usace.army.mil), [2]Lunar and Planetary Lab., University of Arizona (1629 E. University Blvd., Tucson, AZ, 85721; rlorenz@lpl.arizona.edu).

Introduction: The polar layered terrain (PLT) may contain the best evidence for periodic climate changes on Mars. The PLT consists of a sequence of layered eolean deposits thought to be cemented by volatiles. The PLT also contains regions of erosion scarps with slopes of 20-25° [1]. The thickness of the layers, the amount of volatiles contained in them and scarp slope vary with wind regimes, soil properties, and global climate changes [2]. Estimates of ice sublimation on Mars, under current conditions, indicate an ice loss of about 10 cm/yr in the layered deposits [3]; precluding the existence of an ice rich PLT without the existence of an insulating crust to inhibit sublimation [4]. The formation process of an insulation crust may include the desiccation of mineral rich ice from the PLT leaving behind lag deposits and bonded soil grains that form an ice-free low thermal inertia surface crust [5]. Interest in learning more about the character of the PLT and climate change on Mars is motivated by the desire to understand the processes relating to seasonal and long-term cycling of volatiles and to determine the thermal, physical, and mechanical properties of the PLT. Accordingly, quantitative information on analog materials, like Alaskan loess, will be useful in interpreting in-situ measurements on Mars.

Permafrost Tunnel and Field Loess: Our in-situ measurements of thermal conductivity, density, and shear strength for desiccated loess were conducted at the US Army Cold Regions Research and Engineering Laboratory's Permafrost Tunnel. The tunnel was bored into the side of a loess hill located north of Fairbanks, Alaska, and is maintained at ambient temperatures of between –2 °C and –5°C to preserve the periglacial features. The cold dry air circulated in the tunnel during winter sublimates the ice in the frozen soil, producing a layer of desiccated soil up to 10 cm thick on the tunnel walls and ceiling over the last 35 years. The formation process and structure of the desiccated soil may be similar to the Mars polar layered soils providing a convenient terrestrial analog to estimate the expected thermal conductivity, density and strength of Mars soils.

Measurements of thermal conductivity, density, and shear strength were also made in-situ on Permafrost Tunnel dust, and samples from the Chena River Spur Road and Birch Hill to determine the spatial variation of loess properties in a limited geographical region.

Soil Analysis: The loess deposits originate from sandbars along the Tanana River. Loess grain size, composition, and density appear to be affected by the distance that soil grains were carried from the source material. The Chena Spur Road loess, located 5 km from the Tanana River, has a higher density and is coarser grained than either the Permafrost Tunnel or Birch Hill loess; it consists of quartz, muscovite, and heavier dark minerals. The Permafrost Tunnel loess, located 24 km from the Tanana, and Birch Hill loess, located 10 km from the Tanana, have a similar grain size distribution. The grain size distribution by mass is 95% of the material is in grains smaller than 100 microns, 50% is smaller than 20 microns, and 10% is smaller than 8 microns [6].

The Permafrost desiccated loess has a low density as a result of the high ice content of permafrost (50% to 80% by volume) (S2, S3, and S4, Table I). The mineral composition of the Permafrost Tunnel and Birch Hill loess consists of muscovite and dark heavy minerals, but little quartz.

Table I. Properties of Alaskan loess.

Sample description	Bulk density (kg/m^3)	Moisture % of dry weight	Shear strength (kPa)	Thermal conductivity (W/m-K)
Permafrost Tunnel				
S1	1000	5.7	20-30	0.18
S2	700	11.4	3-4	0.07
S3	970	4.5	4-5	0.1
S4	620	11	1-8	0.13
S5- Dust	755	6.3	<0.5	0.08
Chena Spur Road				
S6	1350	2.5	11-32	0.8
S7	1360	4.8	12-30	0.73
Birch Hill- S8	1160	1.6	n/a	0.15

The shear strength of the loess samples, measured using a Geonor H-60 vane tester, indicates the degree of cohesive bonding since the samples were taken from an unsupported vertical face, indicating that internal friction is negligible. Thermal conductivity was measured using the transient line-source technique [7].

Results and Discussion: Shear strength measurements indicate that all samples, except the dust pile were bonded (Table I). The strength of Birch Hill loess was not measured, but is similar to the strength of the Chena Spur Road loess.

The specific mechanism of cohesion for the desiccated loess (S2, S3, and S4, Table I) is not known, but is probably a combination of bonding between soil grains by water soluble minerals, electrostatic attraction of unbonded grains and a reinforcing effect from roots. Observation of the disaggregation of loess clods,

under a microscope, indicates that the primary strength originates from bonded soil grains. When a sample is saturated with water it loses strength, indicating the presence of water soluble mineral grain bonds. Disaggregated, grains cling to each other and to the remaining clod via static charge. Roots appear to be a minor source of soil strength.

Laboratory filamentary sublimate residues made by sublimating dirty ice may be bonded by ionic forces [5], rather than purely electrostatic – consistent with our findings above. If the Martian PLT were deposited as dry dust and ice frost, without encountering a liquid phase, a sublimation cementation mechanism might not operate. Hence, electrostatic forces would play a bigger role.

The angle of repose for disaggregated samples of all loess samples was around 35°, which is the slope that an unsupported loess pile can maintain. In the presence of vibrations or wind, the stable slope angle for a pile will be less than its angle of repose.

The primary heat path of an unbonded dry granular material is through the air from grain to grain. Hence, thermal conductivity is relatively unaffected by material composition, but is controlled by grain size, material porosity, and atmospheric pressure [8]. When a granular material is bonded, or wet, a direct heat path exists through the solid bond or the water connecting adjacent grains, as well as through the air. As the degree of bonding or wetness increases, the amount of heat conducted through the bond or water contact also increases, in comparison to the heat flow through the air. As a result, the mineral composition of the grains becomes an important factor in determining thermal conductivity, in addition to grain size and porosity [9]. The Birch Hill, Chena Spur Road, and Permafrost Tunnel cut face (S1) loesses are well bonded which means that a good heat flow path exists through grain contact bonds so that material composition influences thermal conductivity. Consequently, the relatively high thermal conductivity of Chena Spur Road loess may occur because it has a lower porosity, larger grain size and higher percentage of quartz, as compared to the Birch Hill or S1 loesses. Quartz has a thermal conductivity of around 7.7 W/m-K compared to 2.0 W/m-K for most other soil minerals [9].

The bulk density of the desiccated loess in the Permafrost Tunnel ranged from 620 to 1000 kg/m^3 and the thermal conductivity varied between 0.07 and 0.18 W/m-K (S1, S2, S3, and S4, Table I). The difference in thermal conductivity between bonded desiccated loess (S2, S3, S4) and unbonded loess (S5) was extremely modest and is due to the high porosity of the material and indicates that most heat flow is transferred from grain to grain through the air [10].

Application to Mars: The process of formation and the physical and thermal properties of the Permafrost Tunnel loess appears to be very similar to the PLT. The Permafrost Tunnel loess consists of ice rich eolean deposits with a layer of low density, bonded ice-free loess at the surface of the tunnel wall. The ice free layer of bonded material has retarded the rate of sublimation of ice to 10 cm in 35 years, a depth that would probably be attained in one to six years without an insulating layer. We calculated sublimation rates of between 6 and 30 cm/yr for ice exposed to Permafrost Tunnel thermal conditions using a mass flux formulation [11]. This provides support for the hypothesis that an insulating, low-density layer at the surface of the PLT may significantly reduce the rate of sublimation from layered deposits.

Further evidence of the applicability of relating the Permafrost Tunnel desiccated Loess with the PLT is that the thermal inertia of the desiccated loess is similar to measured values of PLT thermal inertia, $(\rho c_p k)^{0.5}$. To calculate the thermal inertia we use the density, ρ, of desiccated loess (800 kg/m^3), the specific heat, c_p, of representative rock materials at a Mars temperature of 200 K (650 J/kg/K) [12], and the thermal conductivity, k, of desiccated loess corrected to the Mars atmosphere (.025 W/m-K) [13]. The calculated thermal inertia is 114 J/m^2/s$^{0.5}$/K, which falls within the range of derived values for the PLT of 75-125 J/m^2/s$^{0.5}$/K [14].

If PLT soils are similar to desiccated loess, with an angle of repose of about 35°, the 20-25° erosion scarp slopes may represent the stable slope angle of unconsolidated soil under current wind conditions. Even modest bonding of the PLT might support much steeper slopes than those observed within the PLT, as is observed in Alaskan loess deposits.

We note that if the PLT has as low a density and a similar cohesion as the Alaskan desiccated loess, for depths of more than a few tens of centimeters, a Mars lander's legs will sink deep into the PLT ground. Similarly, an impact penetrometer will penetrate many meters deep.

References: [1] Herkenhoff K. and Murray, B. (1990) JGR, 95, 14511-14529. [2] Carr, M. H. (1982) Icarus, 50, 129-139. [3] Hofstadter, M. D. and Murray, B. C. (1990) Icarus, 84, 352-361. [4] Paige, D. A. (1990) Nature, 356, 43-45. [5] Storrs, A. D., Fanale, F. F. P., Saunders, R. S., and Stephens, J. B. (1988) Icarus, 76, 493-512. [6] Sellman, P. V. (1967) CRREL Technical Report 199, Hanover, New Hampshire. [7] Sturm, M. and Johnson, J. B. (1992) JGR, 97(B2), 2129-2139. [8] Wechsler, A. E., Glaser, P. E., and Fountain, J. A. (1972) Progr. Astronaut. Aeronaut., 28, 215-241. [9] Farouki, O. T. (1981) CRREL Monograph 81-1. [10] Woodside, W. and Messmer, J. M. (1961) J. Appl. Phys., 32, 9, 1688-1706. [11] Giddings, J. C. and LaChapelle, E (1962) JGR, 67, 2377-2383. [12] Winter, D. F. and Saari, J. M. (1968) Boeing Sci. Res. Lab. Doc. D1-82-0725, Geo-astrophysics Lab. [13] Presley, M. and Christensen, P. (1997), JGR, 102, 6551-6566. [14] Vasavada, A. et al. (Submitted) JGR.

STABILITY OF WATER ICE BENEATH POROUS DUST LAYERS OF THE MARTIAN SOUTH POLAR TERRAIN.

H.U. Keller[1], Yu.V. Skorov[1,2], W.J. Markiewicz[1] and A.T. Basilevsky[1,3]. [1]Max-Planck-Institut für Aeronomie, Max-Planck-Str. 2, 37191 Katlenburg-Lindau, keller@linmpi.mpg.de, [2]Dept. of Planetary Physics, Keldysh Inst.of Applied Mathematics, Miusskaya Sq.4, 125047 Moscow, [3] Vernadsky Institute, Russian Academy of Science, Kosygin St. 19, 117975 Moscow, CIS.

Introduction: The analysis of the Viking IRTM data show that the surface layers of the Mars south polar layered deposits have very low thermal inertia between 75 and 125 J m^{-2} $s^{-1/2}$ K^{-1} [1]. This is consistent with the assumption that the surface is covered by a porous layer of fine dust. [2] determined a slightly higher value based on a thermal model similar to that of [3]. In this model the heat transfer equation is used to estimate the thickness of the layer that protects the ground ice from seasonal and diurnal temperature variations. The physical properties of the layer are unimportant as long as it has a low thermal inertia and conductivity and keeps the temperature at the ice boundary low enough to prevent sublimation. A thickness between 20 and 4 cm was estimated. This result can be considered to be an upper limit.

We assume the surface to be covered by a porous dust layer and consider the gas diffusion through it, from the ground ice and from the atmosphere. Then the depth of the layer is determined by the mass flux balance of subliming and condensing water and not by the temperature condition.

The dust particles in the atmosphere are of the order 1 μm. On the surface we can expect larger grains (up to sand size). Therefore assuming an average pore size of 10 μm, a volume porosity of 0.5, a heat capacity of 1300 J kg^{-1} K^{-1} leads to a thermal inertia of ~ 80 J m^{-2} $s^{-1/2}$ K^{-1}. With these parameters a dust layer of only 5 mm thickness is found to establish the flux balance at the ice-dust interface during spring season in the southern hemisphere at high latitudes (where Mars Polar Lander arrived). Figure 1 shows the diurnal temperature variation at the ice-dust surface. The maximum of 205 K well exceeds the sublimation temperature of water ice at 198 K [2] under the atmospheric conditions. The corresponding vapour flux during the last day is shown in Fig. 2 together with the flux condensing from the atmosphere.

The calculations show that the sub-surface ice on Mars can be thermodynamically and dynamically stable even if it is protected by a porous dust layer of only a few millimetres in thickness.

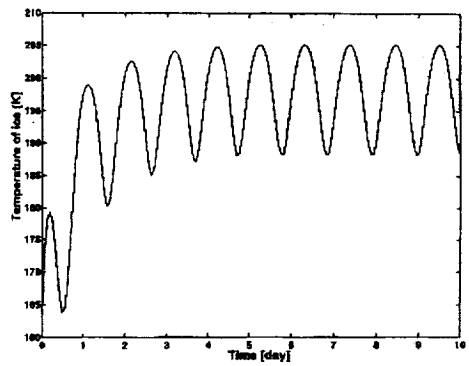

Figure 1: Diurnal temperature variations at the ice-dust boundary. The thickness of the dust layer is 5 mm and the equilibrium temperature of ice sublimation is 198 K. Under these conditions the net flux of vapour is zero and the ground ice level is constant.

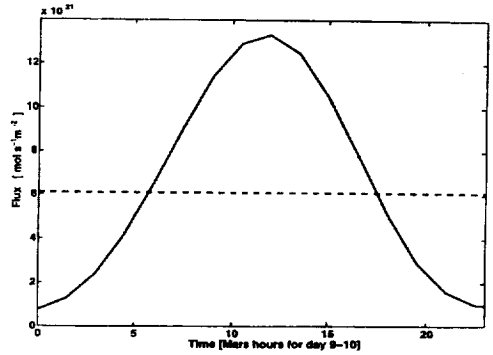

Figure 2: Sublimation flux corresponding to the temperature of the ice surface presented in Figure 1 (solid curve) and the condensation flux at the upper (dust) surface from the atmosphere (dotted curve) for the last day of the simulation.

References: [1] Vasada A.R. and Herkenhoff K.E. (1999) *Fifth Conference on Mars, Abstract #6086, LPI Contributions 972, Houston.*

[2] Paige D.A. and Keegan K.D. (1994) *J. Geophys. Res.*, 99, 25993-26013.

[3] Kieffer H.H. et al. (1977) *J. Geophys. Res.*, 82, 4249-4291.

COMPARISON OF SOME PARTS OF THE SOUTHERN "ETCH-PITTED" AND NORTHERN FRETTED TERRAINS ON MARS. A. Kereszturi, Department of Physical Geography, Eötvös Loránd University, H-1083 Budapest, Ludovika tér 2., Hungary (kru@iris.geobio.elte.hu).

Introduction: The purpose of this work was a morphological comparison of two types of eroded surface on Mars. These are the etch-pitted eroded parts of the southern layered terrains [1] and the northern fretted terrains sculpted by fretted channels. There are some similarity of them: 1. both depressions are relatively young, may be the result of active precesses, 2. the formerly flat surface was eroded away, 3. the morphology of the depressions is somewhat similar, 4. ice is probably near to the surface at both places [2]. Based on the up-to-date results the fretted terrains are formed by ice creeping [3] and the etch-pitted terrains by wind erosion [4]. The subsurface ice may played a role at both places in the generation of the depressions.

Working method: The surveyed terrains are for etch-pitted 1. between 72°-80°S, 60°-100°W, 2. between 70°-76°S, 350°-20°W and a somewhat similar appearance part of the fretted terrains 3. between 34°-42°N, 324°-336°W. Based on the Viking images [5] morphological comparison and simple morphometric measurements were happened. The measurements were made for two diameters for the etch-pitted depressions and for the length and width of the channel-like depressions. To compare shape and morphology, sketches were made for the three regions. Because of the images limited resolution and quality only the clearly visible, greater than 1 km depressions were represented.

Results: There are no great differences in the dimensions between the two types of depressions but there are far more longer depressions (channels) on the surveyed fretted terrain. On Figure 1. the widths and lengths are indicated in km for several depressions (note the different scale of the two axes). On Figure 2. are three sketshes for the depressions excluded the undisturbed craters. (A and B for etch-pitted and C for fretted terrains.) The illustrations are mercator projected so length is variable in the pictures as indicated by two lengths scales on each picture. The coordinates of the corners and the north pole's direction are indicated too. From C to A the terrains are more and more eroded as it is visible in the number of the opened depressions. On Figure 3. are some examples for the features (E for etch-pitted, F for fretted). The similarities are follows: 1. the depression's walls are sometimes sinuousing, 2. some channel-like depressions are on the etch-pitted terrain too, which are runnung into greater depressions. The differences are the follows: 1. there are more elongated depressions on the fretted terrain suggesting longitudinal sediment transport, 2. craters are favourable places for the erosion on the fretted terrain, 3. the layers on the etch-pitted terrain are thick enough to cover the craters below, 4. on the etch-pitted terrain the formation of the depressions take place at isolated places, but later they can grow into each other, 5. on the fretted terrain the bottom of the depressions are more often smooth, suggesting greater sedimentary infill.

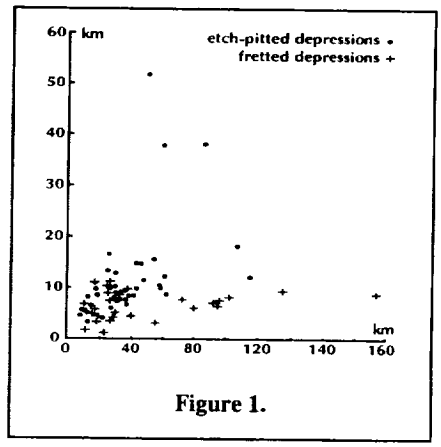

Figure 1.

It is not the conclusion of this work to suggest similar origin for the etch-pitted and fretted depressions. But it is interesting to compare them because this may show up some similar properties of the surfaces or erosion processes. It is useful because new theories shows that the state of the subsurface ice varied in greater scale in the past of than previously thought [6,7] (polar basal melting, climatic oscillations because of the lack of a stabilizing great moon [8] etc.). Future work will related to the comparison of smaller depressions on these and other obviously eroded parts of the surface of Mars, possibly included the recent discovered pits on the south polar cap by the MGS.

References: [1] The surface of Mars, Carr M. H. (1981), Yale University Press. [2] L. A. Rossbacher, S. Judson: (1981) Icarus 45/39. [3] Sharp R. P. (1973), JGR, 78/4073. [4] M. C. Malin, K. S. Edgett (1999) LPSCXXX, #1028. [5] Planetary Data System, Imaging Node. [6] N. Mangold, P. Allemand, J. P. Peulvast (2000) LPSCXXXI. #1131. [7] R. W. Zurek (1998) LPSCXXIX. #6028. [8] A. V. Pathare, D. A. Paige (2000) LPSCXXXI. #1571.

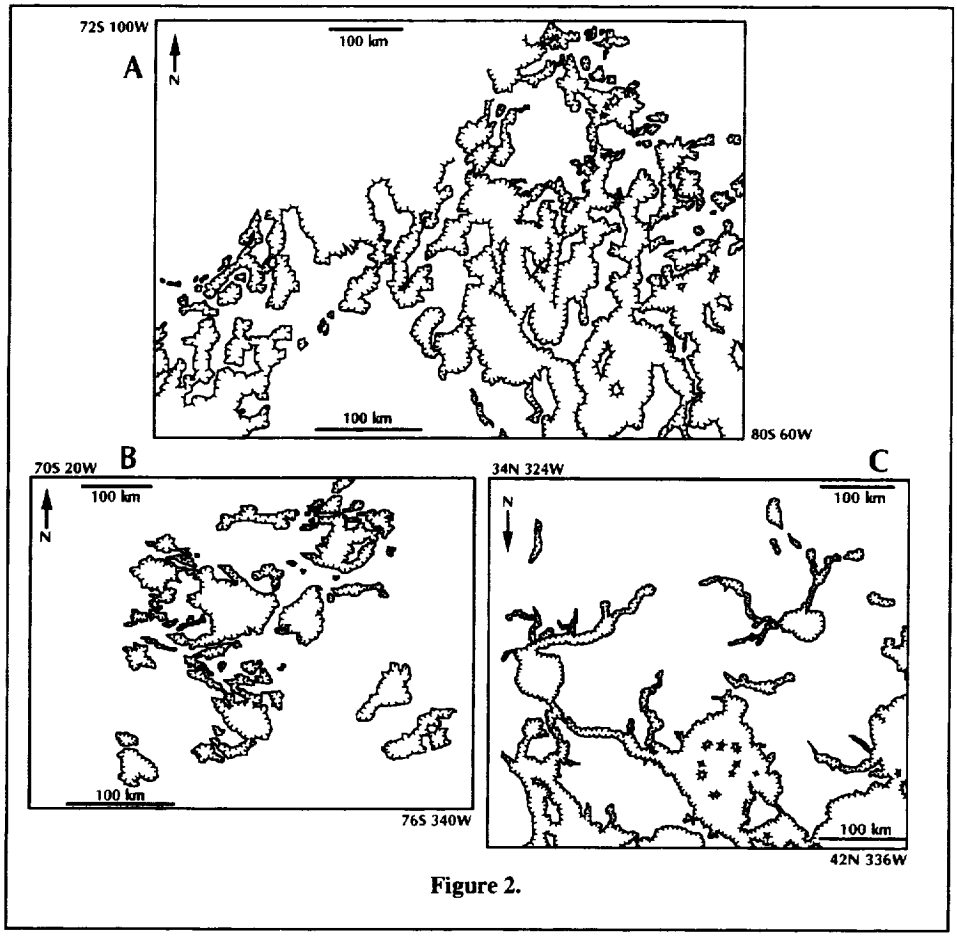

Figure 2.

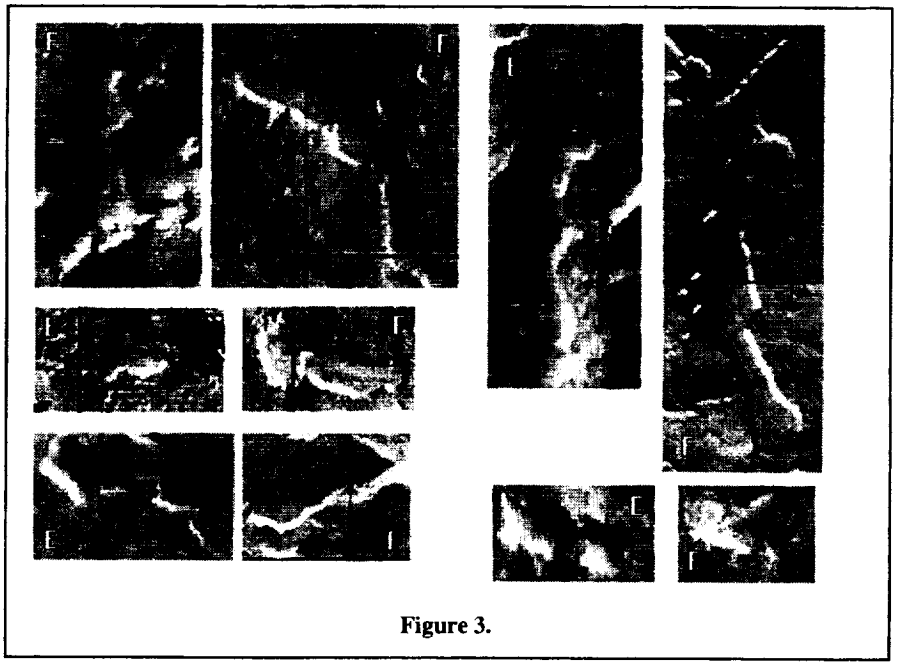

Figure 3.

ANNUAL PUNCTUATED CO_2 SLAB-ICE AND JETS ON MARS. H. H. Kieffer, U.S. Geological Survey, 2255 N. Gemini Dr., Flagstaff, AZ 86001

Thermal Emission Spectrometer (TES) observations indicate that some areas of Mars' seasonal south cap, informally called the "Cryptic" region, are composed of CO2 ice of indeterminately large grain size [1,2]. The low albedo of this material indicates that a large fraction of the solar flux is being absorbed in or beneath this slab. The surface reflection and transmission of a plane-parallel slab of pure CO2 were calculated using the complex index of refraction [3]. A CO2 ice slab is virtually transparent to solar radiation (72% of solar energy incident at 60 degrees off-vertical will reach the bottom of a 1 m thick layer) whereas thermal emission effectively comes from about 8 mm depth. The upper cm or so is in net radiative loss and will anneal any initial porosity or cavities that form in this region.

The winter condensation of CO2 probably includes atmospheric dust in roughly its average mass fraction in the atmosphere, about 3.E-4. This dust has little effect on thermal spectral fluence in the slab. Dust will modify the depth of penetration of sunlight, but does not influence the basic aspects of the model as long the solar penetration is greater than thermal flux attenuation length. Embedded dust grains will absorb solar flux and form individual small gas pockets. If the CO2 deposit is impermeable, the grain will rest on a microscopic gas layer of subliming gas, and "burrow" downward. Because of the net flux loss environment, the hole will probably seal in at the top, yielding a sealed finite vertical columnar hole that travels downward with the grain. When the grain reaches the bottom of the impermeable layer, it will be ejected downward. This self-cleaning, self-annealing process will tend to reduce the amount of dust in the ice through the spring. Because the net solar flux is greater toward the top of the slab, the uppermost particles will move most rapidly, resulting in concentration of dust as a descending "curtain" in the slab, leaving clean ice above.

Porosity will generally be sealed in a region that grows downward from the surface. Thus, the gas formed by springtime sublimation generally cannot diffuse upward through the CO2 deposit. Localize gas escape pathways thru the slab must develop; those large enough to carry adequate warm gas from the sub-slab layer to remain open will grow into vertical columnar vents. It is difficult to predict the spacing of such vents, but they collectively must carry the total sublimation gas flux of about 10 kg/m^2/day.

The sub-slab lateral gas velocity will depend upon the geometry of the flow; the average velocity must initially decreases away from the vent. Because the thermal inertia of the Cryptic region is low [4], it is likely that the surface material is loose, and that channelized flow will develop by scouring, beginning near the vents and radiating outward. Although velocities on the order of ten m/s are required to initiate transport of fine material by saltation [5,6], injection of dust released from the CO2 into the lateral flow may initiate motion and scouring at lower velocities; 2 mm/s vertical velocity is adequate to maintain atmospheric dust in suspension. Also, the initial gas flow is likely to be diffuse flow through the soil (versus stream flow above the soil in classic saltation), and small soil grains may begin to move well before saltation threshold velocities. Dark radially converging dendritic patterns are visible in MOC images of some portions of the spring polar cap [7]; these have been termed "black spiders" by the MOC team [8]. In this model, these patterns represent channels formed by sub-slab channelized flow of the sublimation gas toward the vents. Increasingly large particles could become entrained closer to the vent.

The velocity in the vents will be approximately .005 X^2 m/s, where X is the ratio of vent separation to vent diameter. For example, for vents 1 m in diameter spaced by 100 m, the gas velocity would be ~50 m/s. When the jets exhaust into the atmosphere and velocities decrease, the coarser entrained material will fall out in the prevailing downwind direction; in this model, the oriented dark fans seen in the MOC images are caused by this process.

This is an exotic model that agrees with observations thus far. It predicts that the dark fans will be oriented into the prevailing wind, that they are seasonal and will disappear with, or shortly after, the CO2 is gone, and that the "black spiders" will be found only in the Cryptic region.

References:

[1] Kieffer et al., Jour. Geophys. Res. in press, 2000
[2] Titus et al., manuscript in preparation, 2000
[3] G. Hansen, Jour. Geophys. Res. 102, 21,569-21,587, 1997
[4] D.A. Paige and K.D. Keegan, Jour. Geophys. Res. 99, 25,993-26,013, 1995

AN OVERVIEW OF TES POLAR OBSERVATIONS TO DATE. H.H. Kieffer, T. Titus, K. Mullins, *Geological Survey, Flagstaff, AZ 86001, USA*, P.R. Christensen, *Geology Department, Arizona State University, Tempe, AZ 85287, USA.*

The Thermal Emission Spectrometer (TES) has made observations of the Martian polar regions over the last three years. These observations are a combination of low resolutions scans (aerobraking observations of the south pole) and high resolution "noodles" (aerobraking observations of the north pole and all mapping phase observations). This review summarizes important results to date [1,2], which include:

- Both polar caps are mostly dark ice (not frost) prior to exposure to solar insolation.
- The asymmetric recession of the south polar cap is dominated by albedo variations, especially the Cryptic region, which remains a dark slab of CO_2 throughout its sublimation.
- Seasonal cap appearance is largely determined by frost grain size. The geographic patterns repeat each year.
- Cold spots observed during the northern winter are a spectral-emissivity effect mainly due to surface accumulation of fine-grained frost or snow; their kinetic temperatures are not exceptional.
- Cold spots are concentrated near topographic features, eg. craters, chasma, and slopes of the perennial cap.
- Mapping data has constrained the characteristic time scales of cold spot formation and dissipation during the polar night; both are a few days.

References: [1] Kieffer et al., Jour. Geophys. Res., in press, 2000. [2] Titus et al., manuscript in preparation.

POSSIBLE MELT-WATER LAKES BENEATH PLANUM AUSTRALE, MARS: PREDICTIONS BASED ON PRESENT AND PAST POLAR DEPOSITS. E. J. Kolb[1] and K. L. Tanaka[2], [1, 2]U. .S. Geological Survey, 2255 N. Gemini Dr., Flagstaff, AZ 86001.

Introduction: We have synthesized (1) MOLA elevation data, (2) geologic mapping observations, and (3) estimates for load-induced lithospheric sagging to derive isopach maps of the south polar layer deposits (SPLD) of Mars. Isopach maps of SPLD composed of CO_2 clathrate were used to calculate the present extent and thickness of potential basal melting and to consider the implications of a young, pre-eroded SPLD.

Isopach maps of the SPLD: Geomorphological features and controls in conjunction with MOLA derived digital elevation models of areas adjacent to the SPLD were studied to determine SPLD basal surface elevations. Calculated basal elevation values were binned into 30° arc regions and interpolated into a SPLD basal surface map. We calculated SPLD volumes using the isopach surface modified to account for load-induced sagging determined by Airy-type isostatic compensation of the Martian lithosphere. The amount of sagging depends on SPLD density; we examined the effects of water ice (1000 kg m^{-3}), CO_2 clathrate (1120 kg m^{-3} [1]), and an ice/dust aggregate (2000 kg m^{-3} [2]).

Volume estimate inaccuracies include the MOLA data gap interpolation from 86 to 90°S and south polar lithospheric flexural strength, including strain hardening that may have developed over SPLD history [3-4]. The latter effects may substantially reduce the actual depth of lithospheric depression and thickness of material. Thus we consider end-member cases where load depression varies from zero to the maximum estimate.

Basal melting predictions: Isopach map maximum thicknesses of the current SPLD's approach ~4.3 km. Therefore, we did not consider water- or CO_2-ice compositions for SPLD because of the great thicknesses required for load-induced basal melting of a water-ice SPLD and the inability for substantial thicknesses of solid CO_2 to develop under present conditions [5]. However, partial basal melting of the SPLD can be consistent with a composition of CO_2 clathrate.

Integrating CO_2-clathrate melting-point pressure-temperature values of ~8.4 MPa and 284 K [6] given martian polar conditions indicate that melting should occur where clathrate thicknesses exceed two kilometers [6]. Based on this value, we generated maps illustrating potential clathrate melt regions below the SPLD (Fig. 1). The thickest region of potential melting is centered at the present pole. A relatively thin, 320-m-thick melt layer occurs near 180°W, 87°S if maxiumum lithospheric sagging took place (Fig. 1a). Basal melting of a larger, hypothetical SPLD was investigated by adding 1 km to the thickness of the isopach map of Fig. 1. The resulting basal melt region extends across most of the current cap area and has a calculated maximum melt depth of ~3.6 km (Fig 2).

Implications for the SPLD: Cross sections of a CO_2 clathrate SPLD (Fig. 3) show potential lake depths. In Fig 3a., where the melt thickness is ~2.4 km, a highly unstable situation would exist. Foundering of the overlying SPLD's and perhaps period, relatively recent catastrophic drainage of the basal lakes would be expected. Evidence of such events, however, are not observed. The same processes should occur for thicker SPLD (Fig 2). To maintain stability, containment by a greater layered deposit extent is required. Remnant drainage features of a larger SPLD could include the esker-like sinuous ridges adjacent to the SPLD.

The region of less melt thickness should be more stable (see Fig. 3b). The SPLD surface above this potential melt region is characterized by a smooth, gently sloping topography unseen elsewhere on the SPLD. SPLD surfaces north of this region contain many semi-circular escarpments (not to be confused with the apparently wind-eroded trough features) that appear lobate in map view. The smooth SPLD area may represent an area of accumulation above the melt region, while the lobate features may be caused by compressive flow of the SPLD outside of the melt region. We also note that layering is generally absent in the SPLD in Viking images of this region.

We suggest that near the present pole, the SPLD probably is largely made up of water ice and dust, preventing an excessively deep sub-ice lake to form. Near the smooth SPLD area, the SPLD could be made up mainly of CO_2 clathrate and contain a basal lake. MOC images may prove helpful in determining whether or not the SPLD has been deformed in this area

Long-term evolution of the polar deposits and possible basal melting: MOLA data for the pitted material of Cavi Angusti and the adjacent plains surface of the Dorsa Argentea Formation (DAF) [7] show that the pit floors lie at elevations somewhat below the surrounding plains. Thus pitted material either fills a basin lying below the DAF or the relatively thick pitted material load has caused local lithospheric sagging. Within the cavi are NNE-trending channel-like features similar in size and shape to the SPLD spiral troughs. Many of the SPLD troughs parallel this trend and where several terminate at the SPLD margin, channel features of Cavi Angusti emerge. The SPLD trough and cavi channel parallelism suggests either that cavi morphology in part controls SPLD trough formation or that both SPLD and cavi material have undergone similar erosional processes.

Viking images reveal several small sinuous ridges on the Cavi Angusti plateaus. These ridges are similar to those overlying the DAF, which have been interpreted as possible eskers [8]. Eskers in turn may be an indicator of basal melting [9]. Given the dating by [10], the pitted materials was deposited after emplacement of the DAF. If the cavi sinuous ridges are genetically and temporally related

to the DAF sinuous ridges, they may help in the further interpretation of the origin and relationships of the DAF and pitted materials and the former presence of sub-ice lakes.

South polar deposition may record significant global climatic events. One scenario consistent with present data and worthy of further study may have resulted from a temporary, denser, warmer climate in response outflow channel activity [11]. The progression might include (1) initial CO_2 clathrate-rich deposition, (2) basal melting of the initial polar deposit and emplacement of the DAF, (3) pitting of the initial deposit, (4) emplacement of a partly clathrate-rich SPLD, and (5) local deformation of the SPLD above zones of basal melt water.

References: [1] von Stackelberg M. and Muller H. R. (1954) *Z. Electrochem, 58*, 25-39. [2] Smith D. E. et al. (1999) *Science, 284*, 1495-1503. [3] Plaut, J. J. et al. (1988) *Icarus, 75*, 357-377. [4] McGovern P. J. et al. (2000) *31st LPSC*, Abst. #1792. [5] Dobrovolskis A. and Ingersoll A.P. (1975) *Icarus, 26*, 353-357.[6] Kargel J. S. and Ross R. G. (1998) *Solar System Ices*, 33-62. [7] Tanaka K. L. and Scott D. H. (1986) *U.S. Geol. Surv. Misc. Inv. Series Map I-1802C*. [8] Howard, A. D. (1981) *NASA Tech. Memo 84211*, 304-307. [9] Head J. W. (2000) *LPSC XXXI*, #1121. [10] Plaut J. J. et al. (1988) *Icarus, 75*, 357-377. [11] Baker, V. R. et al. (1991) *Nature, 352*, 589-594.

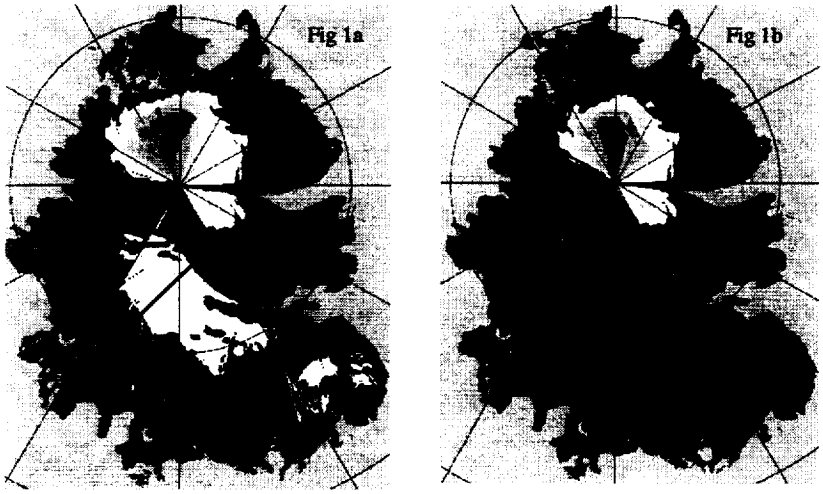

Figure 1. Isopach maps of the south polar layered deposits. The blue areas represent potential sub-SPLD lakes produced by basal melting of a CO_2-clathrate SPLD. Melt regions shown for (a) maximum estimated lithospheric depression and (b) no lithosheric depression.

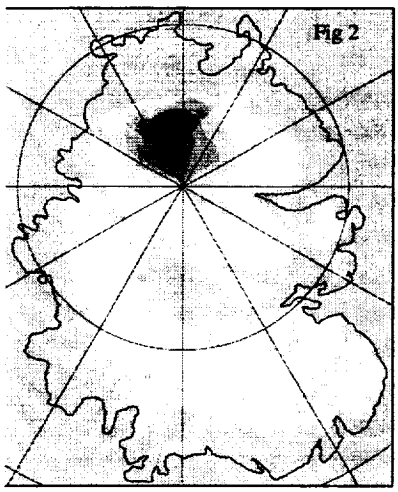

Figure 2.- Basal melt depths (blue tones) beneath a hypothetical deposit 1 km thicker. than the present SPLD (black outline). Maximum thickness ~3.6 km.

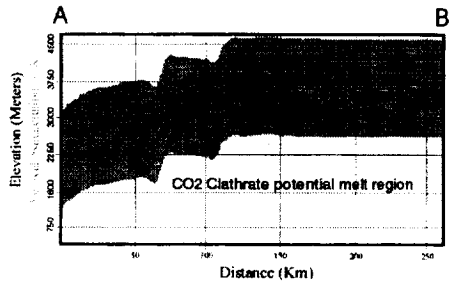

Figure 3a. Cross section A-B from Fig 1a of a CO_2-clathrate SPLD. The depth of basal melting locally exceeds 2 km. This scenario would be highly unstable.

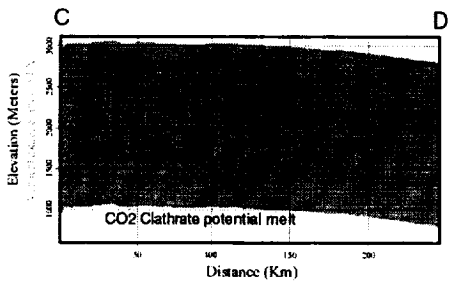

Figure 3b. Cross section C-D from Fig 1a of a CO_2-clathrate SPLD The maximum potential lake depth s is ~320 meters.

THE APPLICATION OF PENETRATORS TO CHARACTERIZE PHYSICAL PROPERTIES OF EXTRATERRESTRIAL ICE SURFACES. Norbert I. Kömle and Günter Kargl Institut für Weltraumforschung, Österreichische Akademie der Wissenschaften, Elisabethstrasse 20, A-8010 Graz, Austria.

Penetrators as tools for exploring extraterrestrial solid surfaces have been developed for a couple of space missions to Mars, the Moon, comets, and the icy satellites of the giant planets. They are particularly useful to characterize the strength properties and the layering of planetary near-surface layers. Being currently engaged with the development of an instrumented 'anchoring harpoon' for the lander of ESA's comet mission *Rosetta*, we propose similar devices for application aboard future Mars lander missions.

In particular we report on results of a considerable number of laboratory experiments performed both at our lab in Graz and in cooperation with the *Institute for Extraterrestrial Physics* in Garching/Germany. Test shots into various analog materials (porous water and carbondioxide ices, cohesionless granular materials like sand, and cohesive materials like foamed glasses) demonstrated that it is possible to extract valuable information on the variation of material strength along the penetration path of a 'projectile' in the target, if one measures the deceleration history with an integrated shock accelerometer. 'Dynamic Penetromety' measurements of this type have the advantage that they need little additional mass and power and sometimes (like in the case of the *Rosetta Lander*) are actually a spin off of the requirement to fix the spacecraft at the surface. Despite of the need for a high sampling rate (50 - 100 kHz) in order to obtain a reasonable depth resolution, the total data volume of such measurements is rather modest, because a typical penetration event takes only a few milliseconds time.

For Mars research (especially for the exploration of Mars polar deposits) the methods described may prove as very useful, because they are robust, easy to do, and - due to their low mass and power requirements - several mini-probes equipped with accelerometers could investigate the layering at different places within one larger mission.

BACTERIAL PRESENCE IN LAYERED ROCK VARNISH-POSSIBLE MARS ANALOG? D. Krinsley[1] and B. G. Rusk[2], Department of Geological Sciences, 1272 University of Oregon, Eugene, OR 97403-1272, [1]KRINSLEY@OREGON.UOREGON.EDU, [2]BRUSK@DARKWING.UOREGON.EDU.

Rock varnish from locations in Death Valley, California; Peru; Antarctica; and Hawaii reveal nanometer scale layering (<1nm to about 75nm) when studied with transmission electron microscopy (TEM). Parallel layers of clay minerals containing evidence of presumed bacteria were present in all samples. Samples range in age from a few thousand years to perhaps a million years. Diagenesis is relatively limited, as chemical composition is variable, both from top to bottom and along layers in these varnish samples. Also, occasional exotic minerals occur randomly in most varnish sections, and vary in size and hardness, again suggesting relative lack of diagenetic alteration.

Bacteria in rock varnish have been documented by the presence of living bacteria on the surface of varnish collected in the field [1], [2], and bacterial cultures obtained from powdered varnish [3]. Indirect evidence suggesting the presence of bacteria in varnish includes observations of varnish cross sections that are the proper size and shape for bacteria [5], and apparently are impregnated with Mn and Fe oxides [2], [4], [5]; measurements of varnish pH which are unsuitable for physical and chemical oxidation of manganese [1]; finding of Mn/Fe accretions in soils, caves, springs, lakes, ore deposits, and oceans due to microorganisms [6]; and finally, the presence of what appear to be bacterial stromatolites in rock varnish. All samples contain what are likely bacterial waste products. The abundance of this material suggests the presence of bacteria in large numbers.

Evidence for the bacterial origin of the structures in the four samples includes: shape (mostly cigar shaped with some rounded forms); average diameters and lengths about the same as living bacteria; bacteria like objects grouped in clusters; presumed bacterial fruiting bodies; internal structural organization within presumed bacterial walls; coatings of Fe and Mn oxides on presumed cell walls in a number of bacteria-like objects; possible broken cell walls with presumed granular waste structures inside and outside of these walls (see fig. 2); bacteria that have penetrated clay mineral layers, feathering and destroying portions of their structures. Clay lattice layers do not appear in the last feature. Where bacteria have not penetrated clay mineral layers, layering is usually regular and lattice layers may be present.

Only a few shapes that could be complete Mn/Fe bacterial casts were present (Fig. 1), but many more fragments of cell-wall casts were observed (Fig. 2). Many of the full casts came from the Antarctic varnish. The excellent fossilization at this site may be due to combinations of cold and aridity. Other organisms have been fossilized in Antarctica by rock coatings of amorphous silica [7]. These electron-opaque shapes and internal structures are similar to bacteria found in other geomicrobiological contexts.

Figure 1. TEM image of possible bacterial remains. Arrow indicates complete bacterium. Other fragmentary remains are imaged as well. Sample is from Kaho'olawe, Hawaii

Although they are a bit small for normal bacteria, they might be submicron buds and hyphae of budding bacteria [8,9,10,11,12,13,14,15,16], or nanobacteria, [17,18] The small size may also be a result of a size reduction caused by dessication. Energy dispersive X-ray analyses of the largest forms show six fold to twenty fold enrichment of Mn, compared to adjacent varnish. Manganese precipitation by bacteria can occur intra- and extracellularly [17]. Bacillus can create casts of manganese around its cell walls [18], as can budding bacteria. In addition to oxidized Mn, divalent manganese can also bind to bacteria [19].

Granular textures are quite common. Granular areas have oval and elongate shapes that conform with adjacent clay layers. These granular textures are similar to iron coatings on clays [20] and biogenic manganese precipitates [12,21,13,18]. Although ambiguous because of the mixture of crystalline and amorphous material, electron diffraction patterns on these granular particles show a hexagonal net of spot reflections. This would be

consistent with the birnessite mineralogy found in infrared studies [22]. It is likely that these granular forms are the remains of bacterial casts, or perhaps bacterial waste products, as suggested by J. G. Retallack (pers. comm. 1995).

Figure 2. TEM image of Nanolayer-parallel bacterium fragment with Fe/Mn enrichment especially along cell walls. Granular structures partially outline the bacterium. Sample is from Antartica

Slightly smaller than the granular forms are oval-shaped clusters of nanometer-scale dots. In many cases, the dots are organized into shapes resembling granular forms. These dot clusters could be transition forms between granular textures and nanometer scale unit cells of Mn/Fe oxides between clay monolayers.

Assuming that some water is necessary for the presence of bacteria, why do they occur in the Death Valley California desert, an extremely dry area? When the desert cools at night and the dewpoint is reached, some moisture is available and penetrates into irregularities in varnish crusts. With the advent of daytime, the temperature rises, water within the varnish may evaporate, setting up stresses in the upper layers of varnish, that may become contorted and cracked. The process continues, day after day, thus supplying water and crust openings for bacterial growth and penetration. Organisms may then be covered with airborne deposits of clays. Presumably, the accumulation of clay protects these objects from dessication and radiation.

Finally, it should be noted that bacteria are found in many types of rocks [see 5], including varnish. It has been suggested that varnish occurs on Mars [7]; even if it does not, crusts are commonly present. If these crusts are built up layer by layer at the nanometer level [4], Martian organisms may well be preserved within layers. The only caveat here is that crusts and surface coatings might provide insufficient protection from radiation due to the thin Martian atmosphere. However, it is possible that microscopic fossils are preserved if the crusts and coatings are sufficiently ancient. Since crusts appear to be common on Mars, and surface coatings have been indicated for rocks examined by Sojurner [23,24]], any site with suggestions of crust or rock coating would be ideal for sampling. This would greatly simplify any organic search strategy for Mars.

References:

[1]Dorn, R. and Oberlander, R. (1980) Am. Geog. Ann. Meeting Abstr. 207 [2]Krinsley, D. and Dorn, R. (1991) Calif. Geol. 44, 107-115. [3] Nagy, B. et al. [1991] Sediment. 38, 1153-1171. [4] [Krinsley, D. (1998) Sediment. 45, 711-725. [5] Westall, F. (1999) J. Geophys.. Res.104, E7, 16,437-16,451. [6] Dorn, R. et al. (1992) Chem. Geol. 99, 289-298. [7] Friedmann, E.I., (1982) Science 215, 1045-1053. [8]Chukhrov, F.V. and Gorshkov, A.I. (L981) Chemie Erde 40,
207-216. [9] Dubinina, G.A. (1980)In: Geology and Geochemistry of Manganese. Vol. III. eds:. I.M. Varentsoov & G. Grasselly, 305-326. [10] Giovanoli, R. (1980) Chimia 34, 308-310. [11] Hirsh, P. (1974) Ann. Rev. Microbiol. 28, 391-444. [12] Kuznetsov, S.I. (1970) In: The Microflora of Lakes and its Geochemical Activity. ed: C.H. Oppenheimer, 365-407. [13] Perfil'ev et al. (1965) Applied Capillary Microscopy. The Role of Microorganisms in the Formation of Iron-Manganese Deposits. Consultants Bureau, New York. [14] Tyler, P.A. and Marshall, K.C. (1967) Arhiv. Fur Mikrobiologie 56, 344-353. [15] Wolfe, R.S. (1964) Principles and Applications in Aquatic Biology. ed: H. Heukelekian & N.C. Dondero, Wiley & Sons, NY, 82-97. [16] Folk, R.L. (1993) J. Sed. Petr. 63, 990-999. [17] Folk, R.L. (1994) Geographie physique et Quaternaire 48, 233-246. [18] Nealson , K.H. and Tebo, B. (1980) Limits of Life eds: C. Ponnamperuma & L. Margulis, D. Reidel, Dordrecht, 173-182. [19] Vojak, P.W.L. (L984) Microbios. 41, 39-47. [20] Emerson, S. (1982) Geochim. Cosmochim.Scta 46, 1073-1079. [21] Robert, M. and Terce, M. (1989) Effects of Geols and Coatings on Clay Mineral Properties. Springer, Berlin, 57-71. [22]Mulder, E.G. (1972) Revue d'ecologie et de biologie du sol 9, 321-348. [23] Stoker, C. (l998a) J. Geophys. Res. 103, 18557-28575. [24] Stocker, C. (1998b) in first Conf. On Mars Polar Sci. and Exploration. LPI Contr. 953, LPI, Houston.

CO_2 CLATHRATE HYDRATES ON MARS. W.F.Kuhs and A.Klapproth, MKI Universität Göttingen Goldschmidtstr.1, 37077 Göttingen, Germany. E-mail: kuhs@silly.uni-mki.gwdg.de

A report on laboratory work will be given which has established the formation conditions of CO_2 clathrate hydrates, their (meta)stability and their physico-chemical properties under Martian conditions. Specifically, the stability limits in p-T space will be presented, quantitative information on the formation and decomposition kinetics as well as numbers for important physical and microstructural quantities (stoichiometry, density, compressibility, thermal conductivity, porosity, specific surface, spectroscopic properties for remote sensing) will be given. From our laboratory experiments (physico-chemical work, diffraction, spectroscopy, electron microscopy and computer simulations) we conclude that CO_2 clathrate hydrates are stable under Martian polar surface and sub-surface (regolith) conditions and we give some suggestions for a detection of CO_2 clathrate hydrate in the presence of CO_2 and water ice. The slow formation and decomposition kinetics found to be on a timescale of many hours to days mean that local p-T conditions averaged over the diurnal cycles are relevant for clathrate hydrate stability on Mars. Finally, we discuss the possible role of CO_2 clathrate hydrate at present and in the history of Mars.

CHARACTERISTICS OF HYALOCLASTITE RIDGES UNDER WESTERN VATNAJÖKULL.
K.A.Langley[1], M.T. Gudmundsson[1] and H.Björnsson[1], [1] Science Institute, University of Iceland, Hofsvallagata 53, 107 Iceland.

The interaction between volcanoes and ice can result in the creation of very distinctive landforms, including tuyas, hyaloclastite ridges and extensive hyaloclastite beds and columnar jointed flows. Such features have been observed in many places around the world although most abundantly in Iceland, the Canadian Cordillera and Antarctica.

Iceland affords one the most accessible and perhaps one of the most interesting locations to study these phenomena. Not only does it proffer numerous examples of each, but also the occurrence of present day subglacial and submarine volcanism offers the opportunity to witness and study the processes associated with the formation of these products in situ.

Vatnajökull, Europe's largest ice cap, straddles an active section of the neovolcanic zone; the expression of the current plate boundary as it passes through the island. An extensive radio echo sounding survey, conducted by the Science Institute of the University of Iceland, has been carried out across the ice cap. The data has been used to construct ice surface and bedrock topography maps as well as to describe the subglacial geology and define the ice and water drainage basins of Vatnajökull [1], [2], [3], [4],

The aim of the present work was to study the characteristics of the hyaloclastite ridges beneath the glacier using the radio echo data. Two types of ridge have been determined. The smaller shorter units termed simple ridges are thought to correspond to single eruption units. The larger scale morphological units, referred to here as composite ridges, may include several of the simple ridges and are thought to have been formed during a number of eruptions along single or parallel fissures. In attempt to validate this, a pseudo survey was conducted over an ice-free area of similar morphology and known petrology. It was determined that the simple ridges do indeed correspond to individual eruption units although, it is unlikely that all the units can be identified from the radio echo data alone.

Of special interest were the width length ratios of the ridges. A particularly useful comparison was that of the width length ratios of other hyaloclastite ridges in the now ice-free section of the Eastern Volcanic Zone (Jakobsson, pers. com.). This indicated that the subglacial composite ridges are on average approximately the same lengths as the ice-free ridges but in general much wider. This difference could be due to the different erosional and depositional regimes one might expect to find in the two environments. For example, it is evident that deposition of glaciofluvial sediments and subaerial lavas in the ice-free areas have filled in valleys and covered the bases of many ridges. The width of these ridges will be underestimated. Conversely, in a subglacial environment such as that under Vatnajökull, glacial and fluvial erosion are more likely to dominate, especially with regards to the jökulhlaups and the surging behaviour of many of the outlets. Where this erosion has caused the overdeepening of valleys, the width of the ridges will be overestimated. The length of the ridges correspond to the length of the fissures along which they were erupted and thus reveal information on the tectonics involved.

References:

[1] Björnsson, H. 1982. *Nordic Hydrology* 213-232, [2] Björnsson, H. 1986. *Annals of Glaciology.* 8, 11-18. [3] Björnsson, H. 1988. *Hydrology of Ice Caps in Volcanic Regions*. Soc. Sci. Isl. Rit 45, Reykjavik, 139 pp., [4] Björnsson, H and P. Einarsson 1990. *Jökull* 40, 147-168

MARTIAN CHANNELS AND THEIR GEOMORPHOLOGIC DEVELOPMENT AS REVEALED BY MOLA. J.K.Lanz, R.Hebenstreit, R.Jaumann, *German Aerospace Institut (DLR), Rutherfordstrasse 2, 12489 Berlin, Germany.*

One of the most striking features of Mars are enormous channels and channel systems that shape its surface. Outflow channels more than 2000 km long and several 100 km wide reveal a vast amount of erosional landforms resembling terrestrial flood features. Runoff channels with dendritic networks and fretted channels with features resembling terrestrial rock glaciers show the variety of processes that shaped the landscape. Newly released MOLA tracks give a detailed insight in the development of the shape of cross sections along those Martian channels. We have studied numerous such cross sections (sometimes more than 100 per channel!) looking for the processes involved in the evolution of the channels.

The MOLA data also allowed the generation of longitudinal profiles, by extracting the deepest points of all cross sections as given by the MOLA tracks.

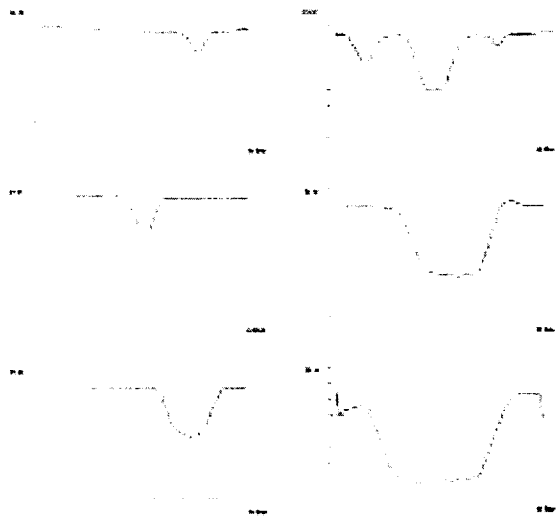

fig.1: Sample cross sections of Nirgal Vallis (top left: channel head, bottom right: end of the channel)

Cross sections of **runoff channels** (e.g. Nirgal Vallis) showed a striking similarity with terrestrial channel networks that were formed by sapping. They are U-shaped in the upper parts of the channels and box-shaped in the lower parts. They generally increase in width and depth downstream but often stagnate over long distances. No inner channels were found, possibly because of the limited vertical resolution of the MOLA tracks.

The longitudinal profile of Nirgal Vallis shows a continuous downstream slope as one would expect from a channel formed by sapping as well as by surface runoff. These observations currently are compared with MOLA tracks of the more dendritic type of runoff channels hoping to find similarities or differences that might reveal more about the evolution of those channels and the processes involved.

Outflow channels show a more irregular developement. Up to now we have concentrated our studies on clearly defined channels such as Shalbatana or Kasei Vallis in the circum Chryse region. Cross sections of Shalbatana Vallis for example (see fig.2) reveal a discontinuity in width and depth. Depth decreases dowstream by more than 1500 m while width changes irregularly.

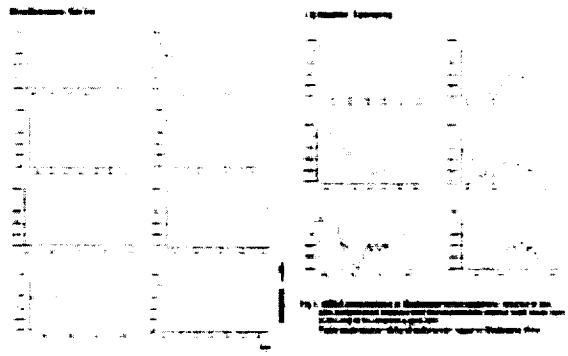

fig.2: Shalbatana Vallis cross sections

The decrease in depth is not gradual. About 100 km from the channel head (chaotic terrain) there is a sharp change in depth from 3500 m to 2500 m. The longitudinal profile of Shalbatana Vallis shows that on the first 100 km the channel floor ascends by 1000 m (see fig.3). The gradient of the surrounding terrain decreases gradually towards Chryse Planitia.

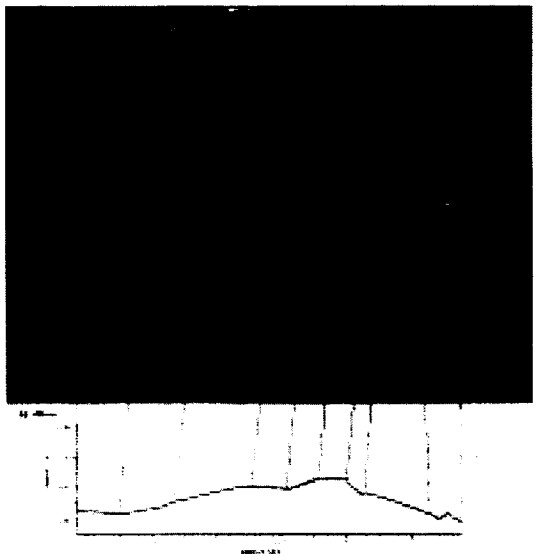

fig.3: Longitudinal profile of Shalbatana Vallis; note the strong ascend by 1000 m on the first 100 km

Tectonic processes therefore do not seem to be responsible for the discontinuity in the longitudinal profile. Emptying of the reservoir below the chaotic terrain and a resulting collaps of the whole structure might have led to the observed discontinuity. It is also imaginable that water (covered with ice?) filled the depression until it reached the appropriate level, eventually flowing out towards Chryse Planitia following the given gradient and eroding Shalbatana Vallis.

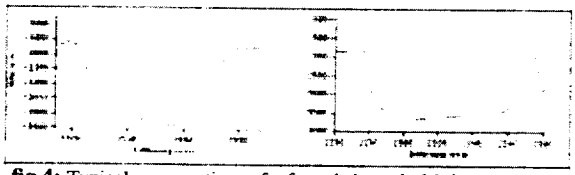

fig.4: Typical cross sections of a fretted channel; debris aprons can be seen to merge at the channel floor (left)

Fretted channels revealed a rather unique appearance dominated by box-shaped valleys with long debris aprons at the bases of most of the steep slopes which not allways could be recognized on high resolution imagery. Opposing debris aprons could often be seen to merge at the channel floor which leads to the characteristic shape of the MOLA profiles (see fig.4).

A longitudinal profile along a fretted channel (38°N, 342°W) showed many irregularities without any continuity in the slope direction.

As more MOC images are released we will try to include those in the interpretation. Up to now high resolution imagery for the channels are still sparse (one MOC-image for Shalbatana Vallis, two MOC-images for Nirgal Vallis, none for the fretted channels so far worked on) and the answers they reveal are rather limited. High resolution stereo data, as those which will be taken by the european Mars Express Mission in 2003, will contribute greatly to the interpretation of the processes involved in the evolution of the martian channels.

References:

[2]Carr M.H. (1981) The Surface of Mars, 232p.

[1]Leopold L.B. et al. (1992) Fluvial Processes in Geomorphology, 522p.

A TEMPERATURE, SCARP AND ICE FLOW MODEL OF THE NORTHERN REMNANT ICE CAP ON MARS. J. Larsen.[1], [1]Department of Geophysics. University of Copenhagen (Juliane Maries Vej 30, DK-2100 Copenhagen Ø. janus@gfy.ku.dk)

Introduction : Climate history from several hundreds of thousand years has been recorded in the terrestrial ice sheets. Drilling deep ice cores though the ice sheets and analyzing the ice and the impurities has assessed this climate history. The visible stratification that is seen the troughs in the polar deposits on mars, indicate that the climate history of mars has been recorded in the Martian ice cap as it is the case for the terrestrial ice sheets. If the polar caps on Mars accumulate under present climate the accumulation rates are very low [1] and even under high obliquity climates the accumulation rates are much lower than for the terrestrial ice sheets. Lower accumulation rates yield thinner yearly layers and consequently more years are presents in an e.g. 3 km thick ice cap. Several millions year of Martian climate history could present in the 3–4 km thick [4] Martian ice caps.

The model : The first step when one wants to assess climate history from an ice cap is to constrain the dynamics of the ice cap because the dynamics determines the stratigraphy of the ice. Assuming that the north polar cap on mars consists of dirty water ice a simple 2D ice flow model has been set up.

The strain-stress relation for ice is highly dependent on the temperature. The temperature distribution in the ice has been modeled by solving the heat flow equation, including changes in insolation caused by the variation of obliquity and eccentricity.

The very characteristic spiral pattern of trough/scarps that overlay the northern polar cap must be included in the ice flow model in order to obtain an estimate of the ice cap dynamics. This has been done by parameterizing the mass balance according the accublation ideas original proposed by Howard [3] and further developed by Fisher [2]. Terrestrial ice sheets have one large accumulation zone covering the upper parts of the ice and one smaller ablation zoned near the ice edge. On Mars the dark steep (5-10 degrees) equator facing slope of the scarps ablate and the less steep (1-2 degrees) or pole ward facing slopes accumulate, thereby dividing the ice cap into alternating zones of ablation and accumulation, which has been named accublation by Fisher [2].

Results and discussion : The temperature model shows that the warm thermal wave for high obliquity periods propagate trough the ice and reaches the base of the ice cap approximately half an obliquity cycle later. This means that when the surface is cold due to little insolation during low obliquity, the basal layers are relatively warm, increasing the ice flow. One could imagine an ice cap that under low obliquity expands because it flattens out due to the ice flow and because the ice cap accumulate in the cold climate. Under high obliquity the ice is close to stagnant because the cold thermal wave has reached the basal layers. The surface ablates due to high insolation, and consequently the ice cap shrinks.

The ice flow model shows that when the mass balance is parameterized according to the ablation theory and a scarp is initiated near the ice edge, it propagates across the cap without any forcing. Because the ice flow does not depend only on the surface slope, but also on the total ice thickness the scarps propagate up to a certain point on the ice where they close up due to the ice flow. This could explain why the upper parts of the ice are scarp free.

In the flow model the scarps has to be initiated near the ice edge, and even though scarps in the model can grow from a small perturbation of the surface, the model cannot explain why the scarp are largest near the ice edge. An oscillating ice cap as described above could explain this. When the ice cap at its maximum extension begins to ablate, small undulations on the surface will grow larger as they propagate toward the pole. The last scarp is made up by the ice edge itself, which withdraws as the ice cap shrinks. The scarps grow larger towards to pole until the point where the ice flow becomes larger (because the ice is thickens toward the pole) than the ablation. From this point the scarps will become smaller and smaller toward the pole until they disappear. A present obliquty the part of the ice cap where the scarp grows taller toward the pole has ablated away.

The flow model does not take the longitudinal stresses into account, which is not realistic, when dealing with the large (compared to the ice thickness) scarps. The model therefore fails to reproduce a realistic stratigraphy. Christine Schøtt Hvidberg, University of Copenhagen has developed a glacial flow model of the martian polar caps that takes the longitudinal stresses into account.

References: [1] Farmer, C.B., D.W. Davies, and D.D. LaPorte, (1976), Science, 194, 1339-1341.[2] Fisher, D.A., (1993), Icarus, 105, 501-511.[3] Howard, A.D., (1978), Icarus, 34, 581-599.[4] Zuber, M.T., *et al.*, (1998), Science, 282, 2053-2060.

COLD-BASED GLACIATIONS ON MARS: LANDSCAPES OF GLACIAL SELECTIVE LINEAR EROSION ON DEVON ISLAND, NUNAVUT, ARCTIC CANADA, AS A POSSIBLE ANALOG. Pascal Lee[1], [1]NASA Ames Research Center, Moffett Field, CA 94035-1000, USA, pclee@mail.arc.nasa.gov.

Introduction:

The apparent selective nature of erosion on Mars is discussed in light of observations of landscapes of glacial selective linear erosion observed on Devon Island, Arctic Canada, and at other high-latitude sites on Earth. Emphasis is placed here on the creation of so-called landscapes of little or no glacial erosion following the disappearance of former dominantly cold-based ice covers. Possible implications for Mars are explored.

Selective linear erosion on Mars:

A remarkable characteristic of much of the record of erosion revealed on Mars by Mariner 9, Viking and MGS imaging is the selective distribution of martian "fluvial" features, both on local and regional scales [1]. The puzzling element is the contrast between terrains that have seemingly undergone "fluvial" dissection in a wetter past on the planet and their juxtaposition to vast tracks of upland terrains on which there is generally no evidence for any fluvial erosion at all. Fluvial features being generally sparser at high latitudes on Mars than at lower ones, the contrast noted above becomes even more conspicuous as one approaches the current polar regions of Mars.

The selective distribution of martian valley forms is important because it is commonly invoked as an argument for favoring the release of underground water as the likely fluvial erosional agent for the formation of many valleys on Mars, over precipitation followed by surface runoff which would be expected to have led to more widespread, less selective fluvial erosion. Also, glacial hypotheses invoked to explain martian surface features are often given reticent acceptance if at all because widely-recognized glacial signatures such as moraines are apparently rare on Mars. However, the Earth experiences forms of glaciation in which dominantly cold-based ice covers rather than wet-based ones prevail, and landscapes of "glacial selective linear erosion" and of "little or no glacial erosion" can result once the ice covers have disappeared.

We report here on a suite of observations of landscapes of glacial selective linear erosion made at and near Haughton Crater on Devon Island in the Canadian High Arctic where Mars analog field studies are currently in progress under the auspices of the NASA Haughton-Mars Project (HMP) [2,3]. Glacial selective linear erosion on Devon Island has produced landscapes and specific geologic features, including valley forms and adjacent landscapes of little or no glacial erosion, that are morphologically and contextually similar to possible counterparts observed on Mars, including terrains at high latitudes and in circumpolar areas. Possible analog features will be examined and the possibility of cold-based glaciation on Mars will be discussed.

Landscape of glacial selective linear erosion on Devon Island:

The landscape of Devon Island, like that of many islands of the Candian Arctic Archipelago, is in effect a textbook example of one of *glacial selective linear erosion* [4,5,6]. Such a landscape is characterized by localized, deep, and often sinuous troughs, separated by vast tracks of plateau surfaces presenting only a relatively sparse distribution of discrete networks of meltwater channels and otherwise little modification. It is generally thought that such landscapes develop beneath ice sheets, with the troughs marking former ice streams and the intervening plateaux marking areas of slowly moving or cold-based ice [e.g., 7]. Positive feedbacks between subglacial topography, ice thickness and velocity, basal temperature and erosion rates are often invoked to explain trough location and formation. The geologic features typifying glacial selective linear erosion on Devon Island are examined below:

Glacial meltwater channel networks. The glacial meltwater channel networks of Devon Island have been considered previously and were discussed as possible analogs for small valley networks on Mars [5,6]. In the context of selective linear erosion, those reported on Devon Island likely reflect the preferential erosion of ice-marginal and/or subglacial bedrock in areas where streams of glacial meltwater would converge and flow. Surrounding areas may remain protected by a static ice cover and hence experience contrastingly little erosion.

*Glacial trough valleys.*The larger scale trough valleys of Devon Island form a network of deeply incised, often winding, U-shaped and V-shaped "canyons" gouging the surrounding plateau, in many places down to the crystalline basement underlying the

island's top sequence of Paleozoic carbonate-dominated sediments. The troughs concentrate along the coastal areas of Devon, thereby revealing their probable origin as outlet glacial troughs carved at the periphery of a broader regional ice cover that rested on Devon Island during at least the Last Glacial Maximum [5]. The troughs are morphologically reminiscent in planform and scale to some of the V-shaped troughs valleys of Ius Chasma in western Valles Marineris [1]. That even the V-shaped winding trough valleys of Devon Island are fundamentally glacial in nature is supported by the combined observation of: a) the systematic transition of the larger troughs to more classic U-shaped forms and fjords downstream, b) the common lack of any apparent deep-seated structural control in the distribution of the troughs, c) the observation that the troughs currently emerging from underneath the edge of the receding ice cap in the eastern part of Devon Island are still partially filled with ice displaying streaming flow lines and, in the summer at least, often torrential subglacial meltwater streams, d) the ubiquitous presence of preglacial forms such as tors along the rim of the troughs, and e) the frequent absence of any significant feeder stream and the negligible role of sapping.

Landscapes of little or no glacial erosion.. Surrounding uplands spared from glacial and meltwater erosion (protected by the cold-based ice cover) may display remarkably little evidence of any former glacial occupation. Vast intervening areas of the Devon Island plateau present such landscapes of little or no glacial erosion (Figure 1).

Figure 1. Von Braun Planitia, Devon Island. A view of inter-valley upland terrains showing a lack of obvious evidence of former glacial occupation (NASA HMP).

Periglacial features and process at Haughton and on Devon Island have also yielded possible analogs to landforms observed at high latitudes on Mars [3]. They also offer possible insights into the environmental evolution of Mars at high latitudes and may help guide the search for near-surface H2O as a resource for human exploration.

Conclusion: The possibility dominantly of cold-based glaciations on Mars will be discussed.

Acknowledgements: This research was carried out under the auspices of the NASA Haughton-Mars Project and is supported by NASA, the National Research Council (NRC), the Geological Survey of Canada, the Nunavut Research Institute (NRI), the Polar Continental Shelf Project (PCSP) of Canada, the National Geographic Society, and the Mars Society. Thanks are also due to all other members and sponsors of the HMP.

References: [1] Lee, P. 2000. *LPSC XXXI.* [2] Lee, P. (1997) *LPI Contrib. 916*, 50. [3] Lee, P. et al. (1998) *LPSC XXIX*, 1973-1974. [4] Dyke, A. S. (1999) *Quaternary Sci. Rev.*, 18, 393-420. [5] Lee, P. et al. (1999) *LPSC XXX*. [6] Lee, P. and J. W. Rice, Jr. (1999) *Fifth Mars Conference*. [7] Benn, D. I., and D. J. A. Evans (1998) *Glaciers and Glaciation*, Arnold, London.

LUMINESCENCE DATING OF MARTIAN POLAR DEPOSITS: CONCEPTS AND PRELIMINARY MEASUREMENTS USING MARTIAN SOIL ANALOGS. K. Lepper[1], C. K. Kuhns[2], S. W. S. McKeever[3] and D. W. G. Sears[4]; [1]Environmental Science Program / Department of Physics, lepper@okstate.edu; [2]Department of Chemical Engineering; [3]Department of Physics, u1759aa@okstate.edu. [1,2,3]Mailing address: Department of Physics, 145 Physical Sciences Bldg., Oklahoma State University, Stillwater, OK 74078; [4]Cosmochemistry Group, Dept. of Chemistry and Biochemistry, University of Arkansas, Fayetteville, AR 72701. dsears@comp.uark.edu.

Introduction: Martian polar deposits have the potential to reveal a wealth of information about the evolution of Mars' climate and surface environment. However, as pointed out by Clifford et al. in the summary of the *First International Conference on Mars Polar Science and Exploration* [1], "The single greatest obstacle to unlocking and interpreting the geologic and climatic record preserved at the [martian] poles is the need for absolute dating." At that same conference Lepper and McKeever [2] proposed development of luminescence dating as a remote *in-situ* technique for absolute dating of silicate mineral grains incorporated in polar deposits. Clifford et al. [1] have also acknowledged that luminescence dating is more practical from cost, engineering, and logistical perspectives than other isotope-based methods proposed for *in-situ* dating on Mars.

We report here the results of ongoing experiments with terrestrial analogs of martian surface materials to establish a broad fundamental knowledge base from which robust dating procedures for robotic missions may be developed. This broad knowledge base will also be critical in determining the engineering requirements of remote *in-situ* luminescence dating equipment intended for use on Mars.

Background:

Geologic Clocks and Luminescence Properties. A successful geologic clock is based on three fundamental concepts; (i) the existence of a measurable property that changes (ii) at a stable, predicable rate over an appropriate time scale and (iii) has a means of distinguishing intervals. When evaluating the luminescence properties of sediments the above concepts translate into; (i) the luminescence signal should increase with absorbed radiation dose, (ii) the signal should be stable under natural and experimental conditions, and (iii) the signal should be depleted ("zeroed") while the mineral grains are transported.

General Principles of Luminescence Dating. Over geologic time, ionizing radiation from the decay of naturally occurring radioisotopes and from cosmic rays liberates charge carriers (electrons and holes) within silicate mineral grains. The charge carriers can subsequently become localized at crystal defects leading to accumulation of a "trapped" electron population. Recombination of the charge carriers results in photon emission, i.e. luminescence. The intensity of luminescence produced is proportional to the number of trapped charges, and thereby the time elapsed since deposition of the mineral grains. Experimentally, thermal or optical stimulation can be employed to liberate trapped charge and thus produce thermoluminescence (TL) or optically stimulated luminescence (OSL), respectively. The response of the luminescence signal to ionizing radiation and the local ionizing radiation dose rate of the deposit must also be determined.

The event dated by luminescence techniques is the last exposure of the sediment grains to sunlight (i.e. a luminescence age is effectively a depositional age). Solar radiation, particularly UV radiation, optically stimulates and removes pre-existing trapped charge accumulated prior to burial and efficiently resets the luminescence clock. Eolian sediments are generally well dispersed when transported, so their exposure to solar radiation is high, making them prime candidates for accurate luminescence dating [3]. Because a luminescence date is a depositional age and eolian sediments are optimal, the technique is uniquely suited to address questions of chronostratigraphy and climate evolution as recorded in the polar deposits on Mars.

Historical perspective on luminescence dating. Luminescence dating is a well-established terrestrial absolute dating technique that has been applied to terrestrial geologic research for over 20 years and even longer in archeological research [4]. Recent advances in equipment design [5] and experimental techniques [6,7] have made it possible to preform fundamental luminescence dating measurement from less than 1 mg of sediment [8]. The success of these advances paves the way for the automation and miniaturization that will be required for robotic dating experiments on Mars.

Investigations of the Luminescence Properties of the Mars Soil Simulant JSC Mars-1: We have previously reported our preliminary characterization of the fundamental luminescence properties of the JSC Mars-1 soil simulant [9]. The results indicated that the **bulk** sample has a wide dynamic radiation dose response range, with no unusual or prohibitive signal instabilities, and is susceptible to solar resetting. These three properties form a stable base for future investigation of the material's utility for luminescence dating.

However, objections to JSC Mars-1 have been raised [10]. First, the grain size distribution of eolian surface sediments on Mars, **as inferred** from Viking Lander data and Pathfinder airborne particulate data, is domi-

nated by grains that are less than 10 microns in diameter (fine silt and clay fractions) [10]. The dominant grain size fraction in JSC Mars-1 is, however, medium sand (250-450 microns) [11]. The second principle objection to JSC Mars-1 is based on differences in composition [10]. From available geochemical data for martian soils, JSC Mars-1 appears to be deficient in sulfur and chlorine and enhanced in plagioclase feldspar [12]. Allen has repeatedly addressed these concerns and maintains that, "JSC Mars-1...is a reasonable approximation for martian mineralogy, chemistry, grain-size distribution, and magnetic properties in as far as we actually know those parameters for the planet [10]."

Despite the objections, JSC Mars-1 remains a valid and widely recognized Mars soil simulant. However, to address the objections to the simulant in the context of our own research we have characterized the luminescence signal response (TL and OSL) to applied radiation and the luminescence signal stability for various grain-size fractions isolated from JSC Mars-1. We found that all grain size fractions analyzed exhibit signal growth with applied radiation. We have also undertaken the production of aggregate sediment particles using clay and silt fractions from JSC Mars-1 cemented by calcium sulfate and sodium chloride. The fundamental luminescence properties of these simulant aggregates will also be characterized and the results discussed in this presentation.

Potential *in situ* OSL dating platforms: We envision the development of DS2-like "chrono-probes" or a deck-mounted luminescence dating module suitable for deployment by lander or rover on the surface of Mars. The essential elements of either system would include a sample collection device, a sample chamber, an optical stimulation source (IR laser or green LEDs with filters and lenses), a light sensor (photodiode) and an irradiation source (e.g. a low level Sr-90 beta source). Many of these components have already been engineered in the soil water detection experiment aboard the DS2 Mars microprobes and in the MECA microscopy station on the Mars Polar Lander (Table 1).

Also needed is a mechanism for determining the background radiation dose rate in the sample location. To do this we propose the use of a OSL dosimeter probe such as carbon-doped sapphire [13] or silica glass doped with rare earth elements [14]. After exposure of the OSL dosimeter in the martian soil for a suitable period, the signal can be read via stimulation with the same light source used for dating measurements. This type of dosimeter can be calibrated prior to launch and maintain its calibration integrity during transit.

Table 1. Components required for an *in-situ* luminescence dating experiment compared to components engineered for experiments on previous missions.

Required for a Luminescence Dating Exp.	Available in **DS2** - Water Detection Exp.	Available in **MECA** microscopy station*
sample collection	soil auger	robotic arm*
sample chamber	single sample cup	Multi-sample turntable
optical source	IR laser	LEDs
light sensor	photodiode	CCD camera
irradiation source	none	none

*aboard Mars Polar Lander

Summary: Luminescence dating is uniquely suited to assist in the task of deciphering the depositional history, chronostratigraphy, and climate evolution recorded in the martian polar deposits. We discuss in this presentation the requirements for an *in-situ* robotic luminescence dating module and the results of preliminary laboratory tests on martian soil analogs. The results point toward the realistic potential for the development of luminescence dating as a valuable tool for absolute dating of the eolian sediments incorporated in the martian polar deposits.

References:

[1] Clifford S.M. et al. (2000) *Icarus,* in press. [2] Lepper K. and McKeever S.W.S. (1998) LPI Contibution No. 953. [3] Berger G.W. (1990) *J. Geophys. Res,* 95(B8), 12375-12397. [4] Aitken M.J. (1985) Thermoluminescence Dating. [5] Bøtter-Jensen L. and Duller G. (1992) *Nucl. Tracks and Radiat. Meas,* 20(4), 549-553. [6] Duller G. (1994) *Quat. Sci. Rev,* 13, 149 156. [7] Duller G. (1995) *Radiat. Meas,* 24(3): 217-226. [8] Lepper K. et al. (in review) *J. Geophys. Res.* [9] Lepper K. and McKeever S.W.S. (2000) *Icarus.* in press. [10] Hargraves R.B. et al., with reply by Allen (1999) *EOS,* 80(15), 168-169 [11] Allen C. et al. (1998) *EOS,* 79(34), 404. [12] Morris R. *Pers. comm.* [13] Bøtter-Jensen L. and McKeever S.W.S. (1996) *Radiation Protection Dosimetry,* 65, 273-280. [14] Justus, B. et al. (1997) *Radiation Protection Dosimetry,* 74, 151-154.

COMPACT ACOUSTIC INSTRUMENTATION FOR STUDYING IN-SITU THE MARTIAN POLAR CO_2 CYCLE. R. D. Lorenz, Lunar and Planetary Lab, University of Arizona, Tucson, AZ 85721 (rlorenz@lpl.arizona.edu)

Introduction

Compact and robust instrumentation can monitor the temperature, pressure and gross composition of the near-surface martian atmosphere. This could place important constraints on the CO_2 condensation process (frost vs snow), as well as meteorology at large. Accommodation on a penetrator or hard lander allows delivery in a low-cost or piggyback mission. Measurements proposed include, speed of sound and windspeed and direction via acoustic measurements, total pressure and temperature via conventional means and possibly CO_2 partial pressure measurement by tunable diode laser. Interleaved battery-powered landers are suggested as an alternative to the technical challenges of long-lifetime landers in polar winter.

Speed of Sound Measurement

Measurement of the speed of sound was proposed as early as 1966 [1] as a diagnostic of composition in the Martian atmosphere. The technique shows promise for the in-situ investigation of the atmospheres of the outer planets [2], and a speed of sound sensor is flying to Saturn's satellite Titan on board the Huygens probe [3]. Furthermore, an acoustic resonance sensor is being flown to measure windspeed (0-40 ms-1) and direction (to 3°) as part of the environmental sensors package [4] on the British Beagle 2 lander on the ESA Mars Express mission.

The speed of sound in an ideal gas depends on the relative molecular mass and ratio of specific heats of the gas mixture. Argon and Carbon Dioxide are near-end-members for these quantities (M_{Ar}=40, M_{N2}=28, M_{CO2}=44 ; γ_{Ar}=1.667, γ_{N2}=1.4, γ_{CO2}=1.3). If the CO_2 in Mars' seasonal caps forms by direct condensation onto the surface as frost, then the local near-surface atmosphere will become compositionally enriched in the 'trace' gases N_2 (present in the global atmosphere at 2.7%) and Ar (1.6%). This enrichment decreases the relative molecular mass, and increases the ratio of specific heats : both factors would tend to increase the speed of sound.

As an example, at 150K, the 'regular' atmosphere has a speed of sound of about 193 m/s, while if the CO_2 were depleted by half, the speed of sound would rise (roughly) to 196 m/s. It should be straightforward to measure the speed of sound to 1 part in 1000, if temperature effects on the instrument are well-calibrated.

If CO_2 condenses instead as snow [5], and settles from high altitudes, the atmosphere should be much more well-mixed, and no such depletion should be observed.

Performing speed of sound measurements in four directions allows the wind direction and speed to be determined in three dimensions - three sensors in a plane allow the azimuth and speed to be measured.

Thus a speed of sound measurement could form a valuable comprehensive element of a landed meteorology package. Although the high-sensitivity acoustic array detectors as might be required for a sodar are sensitive to alignment considerations, a simple short pathlength speed of sound sensor need only individual sensing elements which can be extremely robust. Pathlengths for the acoustic measurement need only be a few centimeters, so no deployable elements are required – the sensors can be hard-mounted onto the lander.

Absorption Measurement

The absorption of near-IR by CO_2 makes its abundance easy to measure. In principle a simple absorption cell with a stable source would be able to detect the CO_2 partial pressure. A tunable diode laser [6] source may make long-term calibration more robust since the absorption band itself can be accurately measured against a continuum. Note that a long pathlength may not be necessary for the large partial pressures of CO_2, so a mirrored Herriot cell and the associated optical alignment may not be necessary.

Knowing temperature and total pressure facilitates interpretation of the absorption spectrum, but the spectrum alone may yield important constraints on these parameters as well as the CO_2 number density.

Total Pressure

A robust pressure sensor [7] using silicon micromachined technology was developed for the DS-2 mission, but had to be discarded for packaging considerations.

It might be interesting to combine this 'conventional' measurement with an ion mobility pressure [8] meas-

urement, which is also sensitive to gas composition. This sensor, using the radioactive source from a smoke detector, is also compact and robust.

Temperature

It is difficult to accurately measure the temperature of a tenuous gas - in particular because the radiative balance of the sensor, rather than the thermodynamic temperature of the gas, can dominate the sensor temperature. However, careful radiative design and sensor mounting will allow simple thermocouples or RTDs to make useful measurements

Combining Measurements

Any of the sensors described above would produce useful information if an adequate time-series of measurements were made (notably pressure measurements). The synergy between the various sensors is powerful : if composition is known from the combination of total pressure and CO_2 partial pressure, then the speed of sound measurement becomes a good gas thermometer, and with separate surface temperature measurement allows excellent constraints on the heat budget of the surface.

The combination of sensors allows the unambiguous resolution of the various environmental parameters. Since each is quite simple and inexpensive, their combination in a single package is advocated. This also allows scientifically for 'graceful degradation', in that useful measurements can still be made if one or more sensors fail, at impact for example.

Instrument Platforms

All of the sensors described above should survive landing decelerations of tens of thousands of g. They can thus be emplaced on small landers without requiring airbags or parachutes. Such landers of mass ~1-2kg can be manufactured cheaply and delivered several at a time as secondary payloads.

Ideally, long-term sensing would be performed by each platform, to study seasonal change. This may challenge available battery performance, especially at low polar temperatures and given the impact survivability constraints. On the other hand, if suitable orbital communications infrastructure exists, the mission could last many weeks. The main power consumer on DS-2 was the soil analysis experiment and the radio. Without the energy cost of soil heating, and expected improvement in communications power performance, a DS-2 energy budget applied to the measurements described here could last many weeks.

The alternative, radioisotope power, is probably difficult to accept politically. If battery-powered landers are made small and cheap enough, however, they might be delivered in salvos, such that measurements from one salvo overlap with measurements from another. In other words, it may be easier to build and deliver many short-lived landers than to meet the challenges of long lifetime.

Conclusions

Several flight-ready sensing techniques, all of which have mass requirements of only a few grams each, can be combined to study the CO2 condensation/sublimation cycle. They are robust enough to be accommodated on landers or penetrators like DS-2 without deplyable decelerators like parachutes, making them amenable to low-cost delivery in large numbers. Overlapping short-lived missions may prove more cost-effective for this application than the (power) challenges of landers with long lifetimes through the polar winter.

References

[1] Hanel, R. A. and Strange, M. G. *Journal of the Acoustical Society of America*, 40, 896-905, 1966 [2] Lorenz, R. D., *Planetary and Space Science*, 47, 67-77, 1999. [3] Zarnecki,J.C., et al pp. 177-195 in Wilson, A. (ed) 'Huygens : Science, Payload and Mission', *ESA Special Publication SP-1177*, August 1997 [4] Towner, M. C. et al., *LPSC XXXI*, CD ROM Proceedings paper 1028, 2000 [5] Forget, F. et al., *J. Geophys. Res.*, 100, 21,219-21,234, 1995 [6] May, R. and Webseter, C., *J. Quant. Spectrosc. Radiat. Transfer*, 49, 335-347, 1993 [7] Reynolds, W. C. et al. *ASME, DSC*, 66 401-406, 1998 [8] Buehler M. G. et al, *J. Vac. Sci. Technol.* A 14(3), 1281-1287, 1996

ENTROPY PRODUCTION AND THE MARTIAN CLIMATE. R. D. Lorenz[1], [1]Lunar and Planetary Lab, University of Arizona, Tucson, AZ 85721 (rlorenz@lpl.arizona.edu)

Summary

The latitudinal heat flow, and hence both the variation in temperature across Mars' surface and the strength of winds and the CO_2 frost cycle, can be successfully predicted by assuming the flow maximizes the production of entropy [1]. This simple principle also applies to the Earth [2] and Titan [1], and requires minimal prior knowledge to predict the climate state. The principle predicts higher heat flow than does conventional pressure-scaling : this has important implications for low- and high-latitude temperatures on Mars in the past and future.

Background: Entropy Production by Latitudinal Heat Flow

In 1-D zonal energy balance climate models [3,4,5] the flow of heat from warm to cold regions is usually parameterized by a heat diffusion term, such that the heat transport is proportional to the latitudinal temperature gradient. This approach - which essentially bundles sensible and latent heat transport in the atmosphere with sensible heat in the ocean into a single parameter D yields quite good agreement with annually-averaged, and seasonally-varying, terrestrial conditions with D chosen arbitrarily (~0.65 $Wm^{-2}K^{-1}$) . Typically, D is scaled with pressure or density [6,7], or occasionally with pressure plus the reciprocal of the rotation rate and other parameters [8], when applied to other epochs or planets.

In a remarkable paper, Paltridge [2] pointed out that if the entropy production associated with latitudinal heat flow on Earth is maximized as a function of D, the resultant D_{MEP} is in fact the same value as is found empirically to agree with the present temperature distribution. In other words, the motion of the atmosphere and ocean appear to conspire so as to maximize the production of entropy.

This discovery, although substantiated by other studies, has remained controversial. Objections have included 1) the woolly notion of what is being maximized (e.g. Lorenz [9] and Lin [10] have noted that the terrestrial climate appears to maximize 'available potential energy') and 2) the fact that the principle specifies the climate state in apparent disregard [11] of 'controlling' parameters such as surface pressure.

More recently, however, Ohmura and Ozuma [12] showed that the *vertical* temperature profile of the earth's troposphere also appears consistent with a convective heat flux profile that maximizes entropy production. Furthermore, Lorenz et al. [1] showed that both present Mars and Titan have annually-averaged climates consistent with D values that are not predicted by pressure or other physical scaling, but are predicted by the principle of maximum entropy production. Not only does this finding suggest the principle may have considerable predictive value for other planets and epochs, but it makes the terrestrial situation appear far from coincidental.

One challenge is that while the principle appears to predict the climate state, it sheds no light on the actual processes involved.

Application to Mars

On Mars, the expected sensible heat flow in the thin atmosphere is small: pressure scaling suggests D~0.001-0.01 (e.g.[13]), and some models have successfully ignored this transport altogether [14]. In fact, much latitudinal heat transport is by latent heat associated with the pressure cycle and deposition and sublimation of CO2 frost at high latitudes. Previous models have implicitly invoked this heat flow, while rarely explicitly accounting for it. James and North [6] do quantify the latent heat transport and find the resultant effective D of order 0.1-1 $Wm^{-2}K^{-1}$.

Yet almost magically, without considering Mars' radius, rotation rate or surface pressure (beyond the effects of pressure on the greenhouse effect) the maximum entropy production principle predicts D~0.5 $Wm^{-2}K^{-1}$. {The heat flow F between low latitudes at temperature T_0 and high latitudes at T_1 is given by $F=D(T_0-T_1)$, and the entropy production maximized is $(F/T_1-F/T_0)$}. Within a factor of two a simple 'blackbody' energy balance works [1], although more generally a simple greenhouse/antigreenhouse model [15] can be applied.

What are the implications of this number? Ignoring terms of order unity, $D\sim\rho C_p Hv/R$, with H the scale height ~ 10km, C_p is specific heat capacity of ~1000 $Jkg^{-1}K$-1, and ρ is surface atmospheric density of 0.02 kgm^{-3}, suggests for D=0.5 $Wm^{-2}K^{-1}$ that typical windspeeds v~10 m/s – consistent with Viking measurements [16]. Also, with a temperature difference of

~50K, this implies a heat transport of ~25 Wm^{-2} or ~10^9 J/m^2 over half a Martian year, or the latent heat of about 1m thickness of CO_2 frost, as observed [17].

If we accept the remarkable success of this principle in predicting latitudinal temperature contrasts and the strength of the circulation, we can apply it to Mars with other atmospheres, taking only the global radiative properties into account.

Application to Mars Paleoclimate

An important immediate result of the implied circulation is that even in a thicker atmosphere, the equator-to-pole temperature contrasts would be significant. Thus models that consider only globally-averaged conditions will overpredict the amount of greenhouse warming required to reach the water melting point on th warmest parts of the surface (conventionally, and at present, the equator, although during periods of high obliquity, high latitudes in fact receive higher annually-averaged insolation, and would be more favorable to liquid water and life.) For example, using a simple greenhouse model [15] infrared optical depth τ=5.3 is required to bring global average surface temperatures up to 273K, the melting point of water. However, for low-latitude regions to have habitable annual-average conditions requires only τ=3.7. Since τ scales typically as a power of CO_2 pressure less than 1, this corresponds to a factor of ~2 reduction in required atmospheric pressure.

However, since the atmospheric pressure of the whole planet is controlled by the vapor pressure at the coldest point [7,18], the existence of substantial temperature contrasts has profound implications for the evolution of Mars' global climate conditions. Specifically, even if the atmosphere were thick and the average planetary temperature were higher, the poles would still be relatively cold (which makes it difficult for the atmosphere to stay thick).

The heat flow (or specifically, D) scales somewhat with total insolation, such that under a faint early sun, transport is weaker. For the Earth, this has the effect of decoupling somewhat the warm equatorial regions from the cold icecaps, and inhibits runaway glaciation [19,20] – although the planet cools as a whole by ice-albedo feedback, the equatorial regions remain warm. For Mars, the effect may be the opposite, in that the poles cannot be warmed enough to sustain a significant CO_2 atmosphere and hence seasonally-averaged habitable conditions. This question will be the subject of a future study.

Conclusions

A principle of Maximum Entropy Production (MEP) appears to be successful in predicting the climate state of Earth, Mars and Titan. It has important, and perhaps surprising, implications for models of Mars' paleoclimate and may become an important tool in the study of planetary climate.

References. [1] Lorenz, R. D., Lunine, J. I. and McKay, C. P., submitted (2000) [2] Paltridge, G. W., *Q. J. Roy. Met. Soc.* 101, 475-484 (1975) [3] Sellers, W. D. , *J. Appl. Met.* 8, 392-400 (1969) [4] Caldeira, K. and Kasting, J. F., Nature, 359, 226-228 (1992) [5] North, G. R., R. F. Calahan and J. A. Coakley, *Rev. Geophys. and Space Phys.*, 19, 91-121 (1981) [6] James, P. B. and G. North, *J. Geophys. Res.* 87, 10271-10283 (1982) [7] Gierasch, P. J. and Toon, O. B., *J. Atmos. Sciences*, 30, 1502-1508 (1973) [8] Williams, D. and Kasting, J. F. *Icarus*, 129, 254-267 (1997) [9] Lorenz, E. N. (no relation!) 86-92 in *Dynamics of Climate*, R. L. Pfeffer (ed), Pergamon Press (1960). [10] Lin, C. A., *Geophys. Res. Lett.* 9, 716-718 (1982) [11] Rodgers, C. D. *Q. J. Roy. Met. Soc.*,102, 455-457 (1976) [12] Ohmura H. and Ozuma A. *J. Climate*, 10, 441-445 (1997) [13] Hoffert, M. I., A. J. Callegari, C. T. Hsieh and W. Ziegler, *Icarus*, 47, 112-129 (1981) [14] Wood, S. E. and Paige, D. A. *Icarus* 99, 1-14, (1992) [15] McKay, C. P., Lorenz, R. D. and Lunine, J. I., *Icarus*, 137, 56-61 (1999) [16] Lorenz, *J. Spacecraft & Rockets*, 33, 754-756 (1996) [17] Forget, F. in B. Schmitt et al. (eds) *Solar System Ices*, 477-507, Kluwer (1998) [18] Leighton R. and Murray, B. *Science*, 153, 136-144 (1966) [19] Endal, A. S. and Schatten, K. H. J. *Geophys. Res.*, 87, 7295-7302 (1982) [20] Gerard, J-C, Delcourt, D. and Francois, L. M., *Q. J. Roy. Met. Soc.* 116, 1123-1132 (1990)

MICROBIOLOGY AND GEOCHEMISTRY OF ANTARCTIC PALEOSOLS. W. C. Mahaney[1], D. Malloch[2], R.G.V. Hancock[3], I.B. Campbell[4], and D. Sheppard[5]--[1]Geomorphology and Pedology Laboratory, York University, Atkinson College, 4700 Keele St., North York, Ontario, Canada, M3J 1P3; bmahaney@yorku.ca, [2]Department of Botany, University of Toronto, Toronto, Ontario, Canada, MALLOCH@Botany.UToronto.ca, [3]Department of Chemistry and Chemical Engineering, Royal Military College, Kingston, Ontario, Canada, K7K 7B4, Hancock-R@rmc.ca, [4]Land and Soil Consultancy Services, 23 View Mount, Stoke, N.Z., Campbell.lsc@xtra.co.nz, [5]Geochemical Solutions, P.O. Box 33224, Petone, N.Z., dsheppard@xtra.co.nz.

Samples of ancient soils from horizons in paleosols from the Quartermain Mountains (Aztec and New Mountain areas of the Antarctic Dry Valleys) were analyzed for their chemical composition and microbiology to determine the accumulation and movement of salts and other soluble constituents. The salt concentrations are of special interest because they are considered to be a function of age, derived in part from nearby oceanic and high altitude atmospheric sources. The geochemistry of ancient Miocene-age paleosols in these areas is the direct result of the deposition and weathering of till, derived principally from dolerite and sandstone source rock, in association with airborne-influxed salts.

Paleosols nearer the coast have greater contents of Cl, and farther inland near the Inland Ice Sheet, nitrogen tends to increase on a relative basis. The accumulation and vertical distribution of salts and other soluble chemical elements indicate relative amounts of movement in the profile over long periods of time, to the order of several million years. Iron, both in total concentration and in the form of various extracts, indicates it can be used as a geochronometer to assess the buildup of goethite plus hematite over time in the paleosols. Trends for ferrihydrite, a partially soluble Fe-hydroxide, shows limited profile translocation that might be related to the movement of salt.

Six of the eight selected subsamples from paleosol horizons in three soil profiles contained nil concentrations of bacteria and fungi. However, two horizons at depths of between 3 to 8 cm. yielded several colonies of the fungi *Beauveria bassiana* and *Penicillium* spp., indicating some input of organic carbon. *Beauveria bassiana* is often reported in association with insects and is used commercially for the biological control of some insect pests. *Penicillium* species are commonly isolated from Arctic, temperate and tropical soils and are known to utilize a wide variety of organic carbon and nitrogen compounds.

THE GEOMORPHIC EXPRESSION OF NORTH VERSUS SOUTH POLAR LAYERED OUTCROPS ON MARS AT METER TO DECAMETER SCALES. M. C. Malin and K. S. Edgett, Malin Space Science Systems, P. O. Box 910148, San Diego, CA 92191-0148, USA.

Synopsis: Mars Orbiter Camera (MOC) images acquired by the Mars Global Surveyor (MGS) since 1997 show that the layered outcrops and general geomorphic character of the two martian polar regions are radically different. These differences occur at scales of hundreds to thousands of meters, and are likely to indicate differences in depositional, erosional, and climate history between the two poles over long periods of time (perhaps millions of years).

Observations: MGS began orbiting Mars in September 1997. As of April 2000, hundreds of MOC images cover portions of the north and south polar residual caps and surrounding layered terrain at scales ranging from 1.4 to 15 m/pixel under illumination and seasonal conditions that include winter, spring, and summer in the south and spring, summer, and autumn in the north. These images reveal major differences in the morphology of the two residual cap surfaces and neighboring polar layered terrain.

Residual Caps. The two residual polar caps differ geomorphically from each other as well as from the rest of the martian surface. Initial observations were summarized by *Thomas et al.* [1]. What is most striking is the "swiss cheese"-like morphology of much of the south residual cap (Fig. 1a). No surfaces elsewhere on Mars have this pattern of circular depressions and sags among arcuate-scarped mesas. The north residual cap, in contrast, is largely flat at the hectometer scale but exhibits abundant decameter-scale pits (Fig. 1b)—these pits have not been seen on the south residual cap. The "swiss cheese" terrain in the south is a long-term geologic feature, not an expression of seasonal wintertime frost. In summer, this terrain has been observed in a state of defrosting such that the arcuate scarps (Fig. 2)—some of them exhibiting alternating light- and dark-toned layers (Fig. 3)—are dark relative to their winter/spring appearance.

Dark Lanes. Like everything else about the two polar caps, the dark "lanes" that occur in each residual cap differ between the poles. In the north, the equator-ward slopes exhibit banding and ridge-and-trough morphologies indicating layers of material of differing thickness, albedo, and resistance to erosion; while the poleward slopes are usually mantled and show no evidence of layering (Fig. 4a). Dark lanes in the south polar region show a semi-symmetric pattern of somewhat stair-stepped and folded/wrinkled layers on either side of a trough; these typically bound a rugged, medial ridge (Fig. 4b).

Polar Layered Terrain. The layered units that surround each residual polar cap (and which are more extensive in the southern hemisphere) also exhibit different geomorphic expressions between the north and south poles [2]. Though there are exceptions, in general the layers in the north tend to be expressed in the walls of the 'dark lanes' as a sequence of ridges and depressions while southern layers tend to have a stair-stepped or cliff-bench topography (Fig. 5). Layered outcrops in both hemispheres exhibit considerable evidence for a diversity of physical properties, for example layers that are expressed as ridges must consist of material that is more resistant to erosion than those expressed as depressions. When exposed at the surface in planimetric form, some layers in the south polar region develop spidery networks of closed gully-like depressions that are confined to that specific layer (Fig. 6a); others have a smooth-textured surface (*e.g.*, bright mesas in Fig. 6b); still others are rugged or rough at meter scales (Fig. 6c). Low albedo dunes superposed upon layered units in both hemispheres (Fig. 6d) indicate that the layers form a hard substrate across which sand can be transported via saltation—this observation might indicate that the upper surfaces of the polar layered units are not mantled by thick dust as has been interpreted on the basis of thermal inertia mapping [3].

Conclusions. MGS MOC images are giving us a new perspective on the geomorphology and geologic history of Mars. The observations presented here lead to two basic conclusions:

(1) The polar layered units include individual layers that have properties that differ from other layers. This means that individual layers probably record changes in materials deposited and processes that have operated over geologic time scales.

(2) The polar layered materials both on and off the residual caps are different in the north relative to the south, and different as well from other parts of Mars. The two polar regions have likely been quite different from each other—in terms of climate and materials deposited—for a very long time.

References. [1] Thomas P. C. *et al.* (2000) *Nature, 404,* 161–164. [2] Malin M. C. and Edgett K. S. (2000) *LPS XXXI,* #1055. [3] Paige D. A. and K. D. Keegan (1994) *JGR, 99,* 25993–26013.

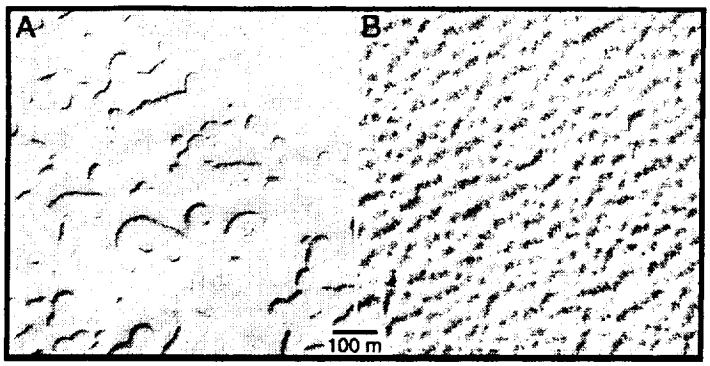

Figure 1

Figure 3

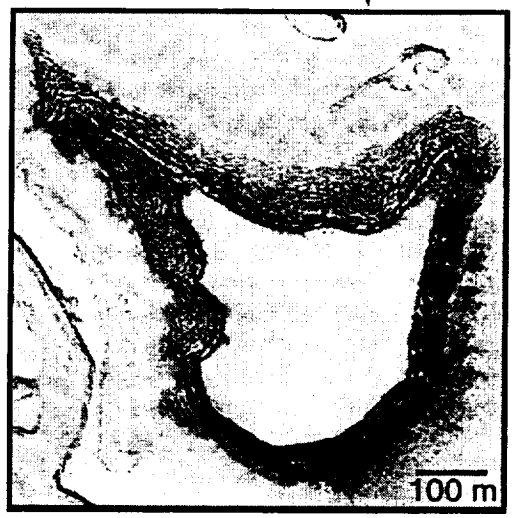

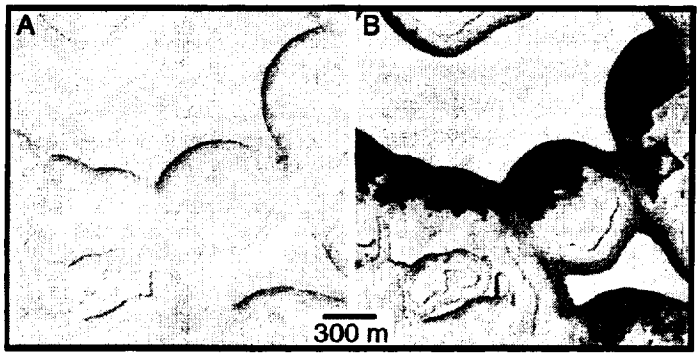

Figure 2

Figure 4

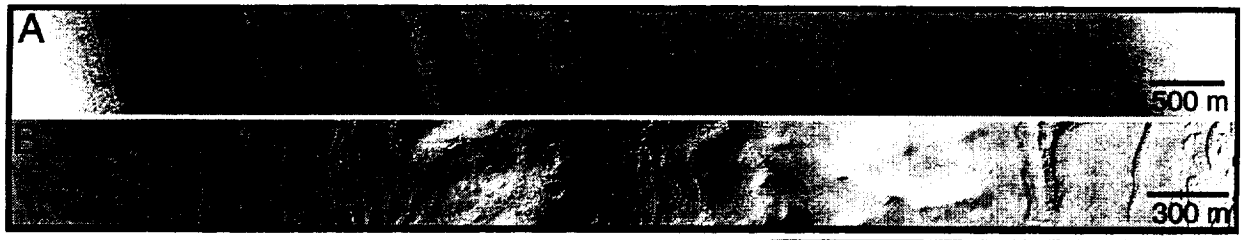

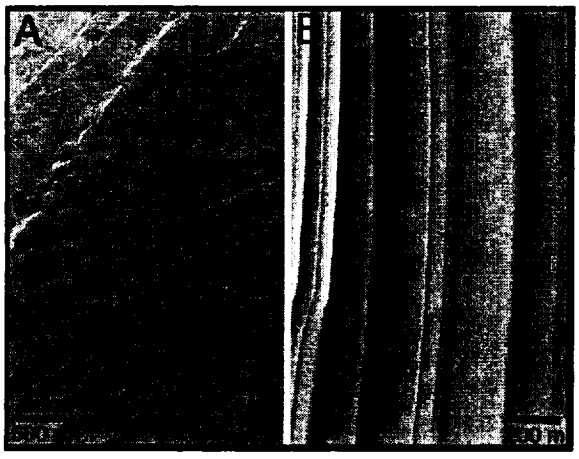

Figure 5

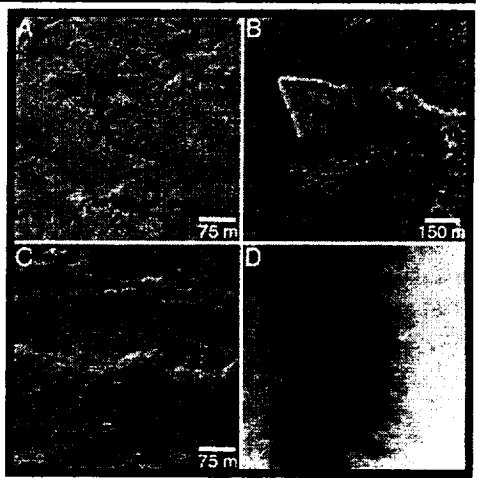

Figure 6

All illuminated from upper left. **Figure 1:** Typical surface morphology of south (A) and north (B) residual caps; (A) M09-05133; 87.1°S, 95.4°W. (B) CAL-00433; 86.9°N, 207.5°W. **Figure 2:** Defrosting south residual cap (A) at Ls 254° (M10-00093) and (B) Ls 320° (M13-01121); 86.5°S, 344.7°W. **Figure 3:** Banded slopes on mesa in south residual cap at Ls 306°, M12-02295; 87.0°S, 341.2°W. **Figure 4:** Dark lane crossings in (A) north polar cap, M00-02072; 86.0°N, 258.4°W and (B) south polar cap, M08-05817; 86.8°S, 350.8°W. **Figure 5:** Typical layer expressions (A) stair-stepped in south, M13-00253; 87.0°S, 187.7°W and (B) ridged-and-troughed in the north, SP2-52406; 86.3°N, 199.2°W. **Figure 6:** South polar layered unit surfaces in planview; (A) gullied surface, M12-00228; 77.9°S, 193.0°W; (B) smooth, mesa-forming units (light-toned), M09-06148; 79.6°S, 298.3°W; (C) typical rugged polar surface, M12-00563, 86.7°S, 264.9°N; (D) eolian dunes traveling across layered terrain surface, M12-00230; 76.7°S, 195.4°W.

THE MARS SURVEYOR 1998 LANDING ZONE: SEARCHING FOR MARS POLAR LANDER IN HIGH RESOLUTION MOC IMAGES. M. C. Malin and K. S. Edgett, Malin Space Science Systems, P. O. Box 910148, San Diego CA 92191-0148, USA.

Between mid-December 1999 and early February 2000, forty images (~400 MBytes) were acquired of the area believed to be the location where the ill-fated Mars Polar Lander is believed to have crashed, uniquely covering 667 km^2 and, additionally, covering most of this area stereoscopically. These images cover most of the landing ellipses identified as encompassing the most probable crash site (Figure 1). No evidence of the lander or of the lander delivery system (parachute or aeroshell) was seen. A geomorphic sketch map was created at a scale of 10 m/pixel (Figure 2). Eleven characteristic morphologies (+ one "other") and three qualitative assessments of topographic roughness were plotted on a base map compiled from the MOC images. By these criteria, 36% of the surface is considered smooth, 26% intermediate and 33% rough (5% was not classified owing to uncertainty in application of the qualitative criteria, *e.g.*, are sand dunes rough or smooth?). To quantitatively assess the topographic roughness, a topographic profile in a characteristically rough area was constructed by point stereophotogrammetry. These data were then calibrated against a nearby Mars Orbiter Laser Altimeter (MOLA) topographic profile to produce a controlled MOC topographic profile (Figure 3). Slopes were measured over distances ranging from 10 to 150 m, with slopes measured over long distances typically shallower than those measured over short distances. In the most topographically rugged region within the landing zone (*e.g.*, on the slopes of the depression along the western margin of the landing zone uncertainty ellipses), no more than 12% of the surface has slopes in excess of 10° when sampled at scales of 10-40 m/pixel; about 4% of the surface has slopes greater than 15°. Sampling over longer distances yielded lower slope values. Indeed, much of the landing zone is substantially smoother. Figure 4 shows the frequency of occurrence of a given slope angle as a function of slope angle for the same three metrics as described above. The overlap between the adjacent sample metric (red circles) and the other, larger sampling window computations (blue squares and green diamonds), shows that these measurements reasonably sample the range in slopes. Figure 5 shows close-up examples of some stereo pairs, illustrating the steepest and most rugged relief in the vicinity of the landing site. The polar landing site was less hazardous than many areas on Mars, but not without hazards. It is unlikely that the lander failed owing to geology.

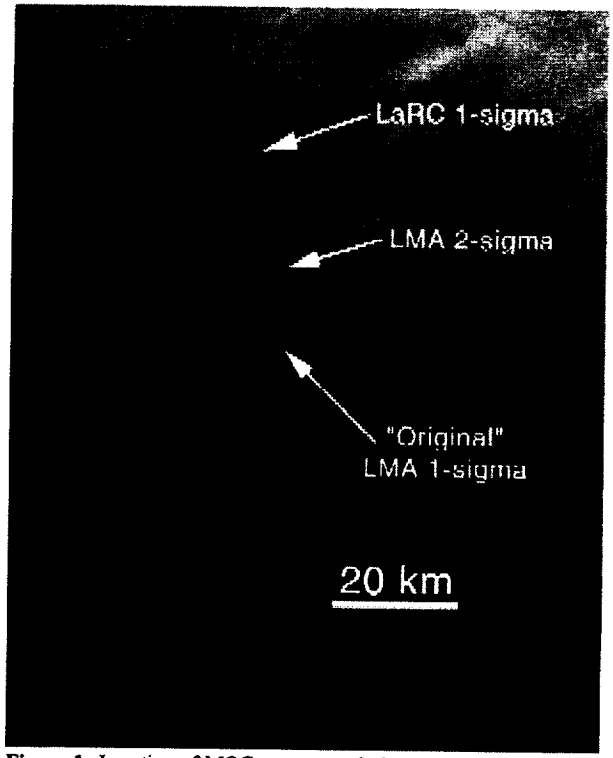

Figure 1: Location of MOC narrow angle image coverage as determined by simulataneous wide angle imaging, superimposed on a two-frame Viking Orbiter image mosaic registered to the targeting inertial coordinate system.

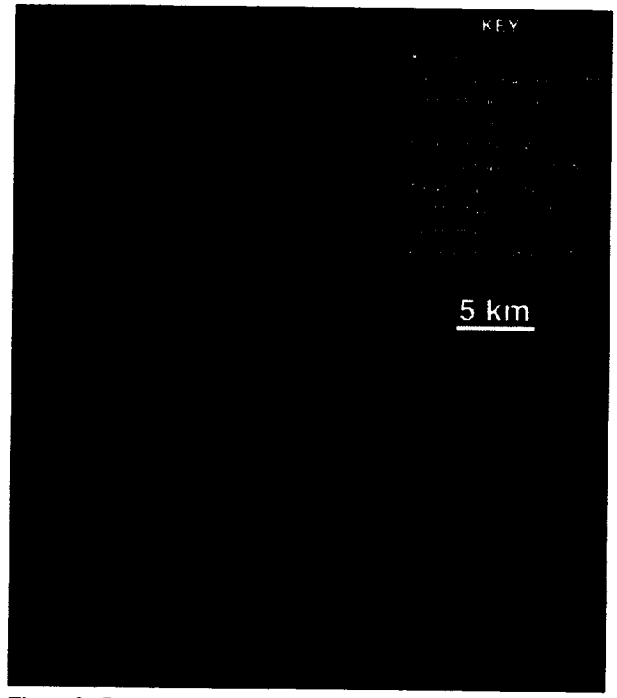

Figure 2: Geomorphic Map of MOC Images of MPL landing zone.

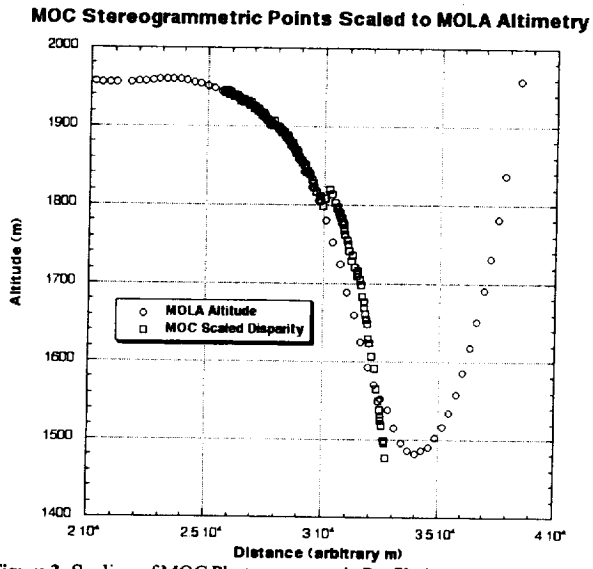

Figure 3: Scaling of MOC Photogrammetric Profile (squares) to MOLA Laser Altimetry Profile (circles).

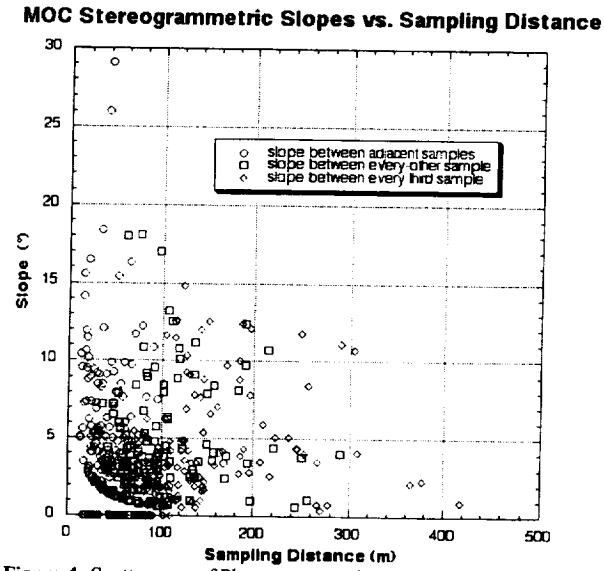

Figure 4: Scattergram of Photogrammetric Slope as function of Sampling Distance.

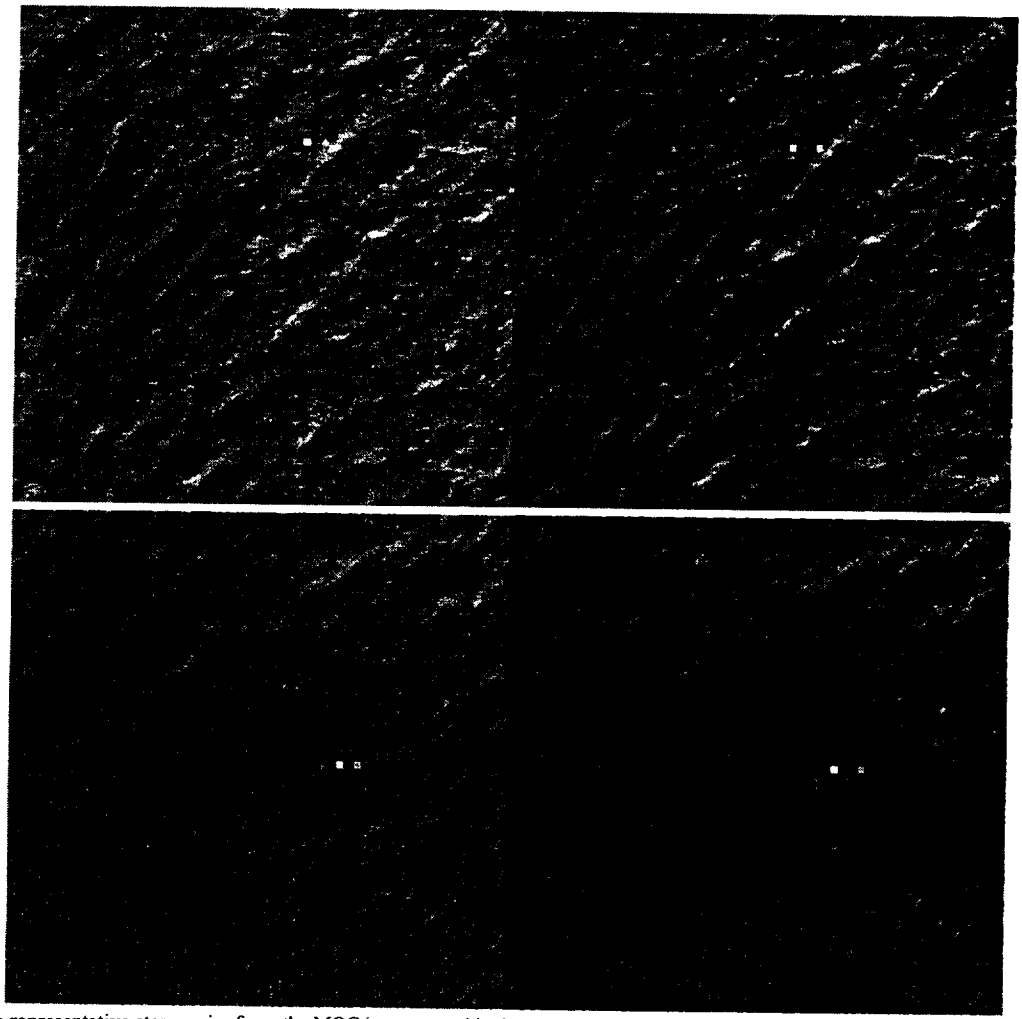

Figure 5: Two representative stereopairs from the MOC images used in determining the topographic profile. The two small squares in each image are 10 m on a side, 40 m apart horizontally, and 10 m apart vertically. It can be seen by comparing the vertical relief of nearby features to these squares that the typical local relief in the area is less than 5 m.

CRATER DENSITY OF LOBATE DEBRIS APRONS AND FRETTED CHANNELS: PALEOCLIMATIC IMPLICATIONS. N. Mangold, Orsay-Terre, Equipe Planétologie, UMR 8616, CNRS et Université Paris-Sud, Bat. 509, 91405 ORSAY Cedex, France, mangold@geol.u-psud.fr.

Lobate debris aprons and fretted channels show convex shapes and lineated features usually explained by the viscous creep of an ice-rock mixture [1,2]. This interpretation is consistent with the stability of ice at few meters deep in the ground at latitudes nearby 40° [2]. Very few craters have been identified on Viking images of lobate debris aprons, so these features have been mapped as upper Amazonian deposits [1]. However no ages have been determined statistically. We examine hereafter the morphology and distribution of craters over lobate debris aprons using new high-resolution MOC images.

Many craters of several tens or hundred meters of diameter are observed on the surface of lobate debris aprons. However most of them do not show a typical shape. We can distinguish between fresh craters, with a classical circular shape, and degraded craters (Fig. 1). Degradation can be attributed to three processes:

(a) Relaxation. The floor of the crater is filled by a central peak or central bulge that sometimes completely fill the depression (Fig. 1A top left). This may be due to the effect of ice creep after impact.

(b) Deformation. The crater is not circular but elliptical (Fig. 1B) or over-thrusted by some flows (Fig. 1C). The deformation is due to the ice creep. Deformed craters are often affected by the process of relaxation.

(c) Surface degradation (Fig. 1D, 1E). The crater is degraded by some surface process possibly related to sublimation. Indeed fractures created during the impact can accelerate the process of thermokarst that may be active on the whole surface of the debris aprons [see abstract in this volume by Mangold et al. "Thermokarstic degradation of lobate debris aprons"]. Such degradation can also affect relaxed or deformed craters.

None of the three kind of degradation is an homogeneous process. For example, deformed craters, like such on figure 1B, is observed when the deformation is localized on discontinuity, analogous to "shear-zone" in terrestrial rocks, but the bulk deformation of the debris aprons is homogenous in other and does not deform small craters strongly. In that case we can not supposed that little degraded craters are younger than strongly degraded craters. If no gradient of degradation is possible, fresh undegraded craters can all the same be considered as younger than degraded craters. We then count fresh undegraded craters separately from the degraded. Pits possibly corresponding to very degraded craters or "ghost" craters have not been taken in account. Figure 2 summarizes the counting over 5 MOC images of 5 different lobate debris aprons in order to obtain a significantly large surface of 345 km^2, even the age of each one of the debris aprons may not be exactly the same. The result is compared in the same graphic to the chronology proposed by Hartmann et al.[3] taking in account new models of cratering rates.

We note that the total population of craters does not follow a classical slope, i.e. the ages given by the small craters are younger than the ages given by the large craters. The explanation can be given in two ways. First the resolution of the images used is around 5m/pix, so 50 meters large craters are at the limit of the resolution. The second point, and probably the most important, is that the degradation is stronger for small craters than large craters. For example, figure 1E shows two craters of 400 m large. A 50 m large crater would no more be identifiable with such an important degradation. Furthermore, the wavelength of the topographic heterogeneities observed at the surface of the debris aprons is of the order of 50 m. This implies that there is a great number of small craters that are no more identifiable. The age given by the largest craters, about 100 My, is then the minimal age for the formation of lobate debris aprons. On other hand, less than 20% craters can be considered as fresh craters. Assuming that fresh craters are always younger than degraded craters, the age of few million years given by the fresh craters can be interpreted in two ways:

(1) If there was episodic climate changes during the last 100 My, this age can correspond to the last episode of degradation during such climate change;

(2) If we assume that the climate did not change drastically over the last 100 My, this age means that the different processes of degradation occurred continuously during this period and only need some million years to have visible effects on craters.

The second point seems to be more realistic especially because there is a continuity between fresh craters and degraded craters. For example, the rims of the crater at the right bottom of the figure 1A show the beginning of a degradation. Very few craters may be considered as completely fresh. This study then concludes that the crater population over lobate debris aprons is very diversified because of the different kind of existing degradation. The exact age of these features can only be minimized to about 100 Ma. This age means that these features were active at least 100 My ago and deformation probably continued more recently.

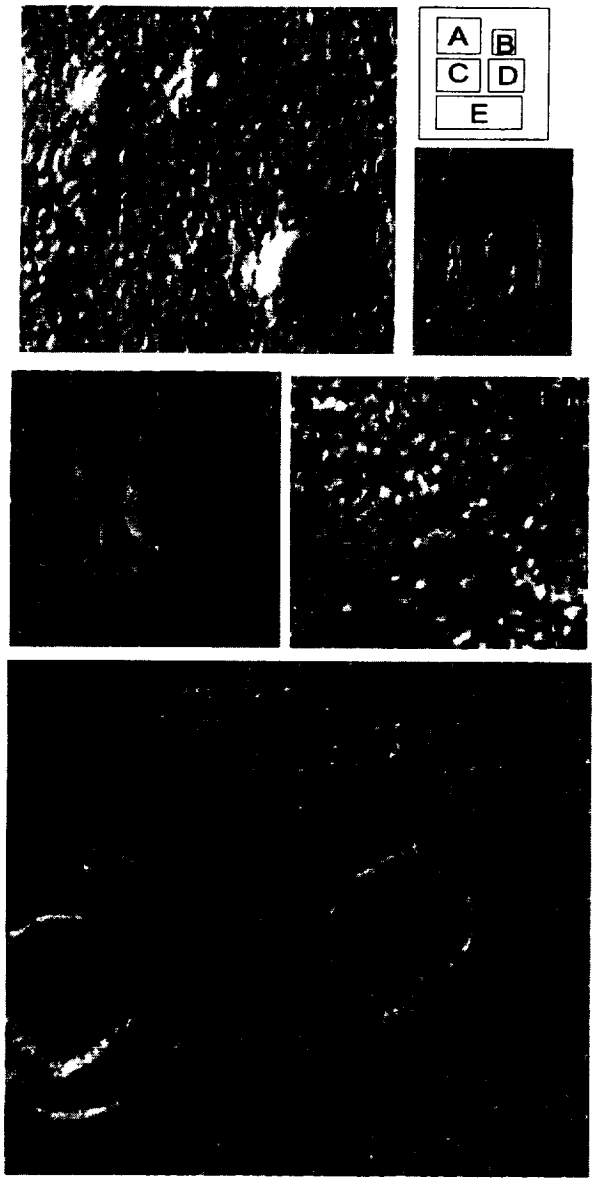

Fig. 1: Comparison of different degraded craters on lobate debris aprons. A: MOC51907 (coord.: 41.9N, 326.3W). Fresh crater (lower right) and small craters at different stage of relaxation (upper left). B. MOC53604 (coord.: 38.8N, 336.5W). Crater deformed in the direction of lineations. C. MOC46305 (coord.: 40.4N, 340.3W). Crater degraded and partially buried by deformation. D. MOC20504 (coord.: 40.2N, 337.8W). Small degraded crater. E. MOC50006 (coord.: 41.2N, 334.8W). Large degraded craters.

Fig. 2: Crater count of 5 debris aprons (taken from MOC images 20504, 44605, 46305, 48204 and 53604). Absolute ages are taken from Hartmann et al. [3].

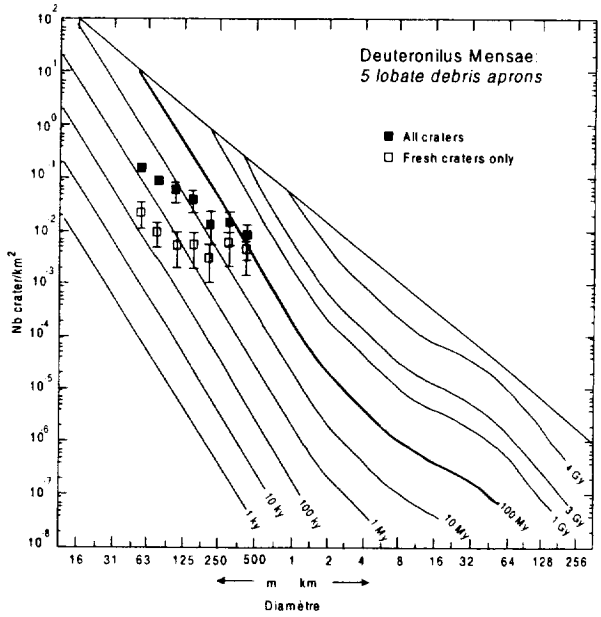

References: [1] Squyres S. W. (1989) *Icarus*, 79, 229-288. [2] Carr M. H. (1996) *Water on Mars*, Oxford Univ. Press. [3] Hartmann W. K. et al. (2000) LPSC 31th conference.

GIANT PALEO-ESKERS OF MAURITANIA: ANALOGS FOR MARTIAN ESKER-LIKE LANDFORMS.

N. Mangold[1], [1]Orsay-Terre, Equipe Planétologie, UMR 8616, CNRS et Université Paris-Sud, Bat. 509, 91405 ORSAY Cedex, France, mangold@geol.u-psud.fr.

Introduction: Several regions of the southern Martian hemisphere display sinuous braided ridges sometimes interpreted as eskers because of their similarities with terrestrial eskers [1,2]. This hypothesis has important climatic implications because eskers are related to water flows under ice sheets. Possible recent glaciations are postulated according the nature of these landforms [2]. However the esker hypothesis remains controversial. Some other explanations have been proposed like dikes or wrinkle ridges [3,4]. Recently, new MOLA data measured the height and width of the most elevated of these ridges. These data seem to confirm the esker hypothesis [5,6]. Their width and height are nevertheless at the upper limit of terrestrial eskers. The giant paleo-eskers described in this study are in the order of magnitude of Martian esker-like features in a dry Saharian environment.

Description of Mauritanian paleoeskers: The region called Adrar is located in the middle of Mauritania West of the Saharian desert. It consists on a slowly dipping plateau dissected by scarps of several hundred meters high. It is composed mostly by sandstones sometimes interrupted by carbonates with stromatolite levels formed under shallow water [7]. These units are from 600 to 440 million years old. Two units are distinct from the others because they show many features usually observed in glacial environment: "roches moutonnées", groove marks, conglomerate diamictite levels, polygons [8]. These units formed during the late Precambrian and late Ordovician glaciations, respectively 560 and 440 My ago [9]. At that time, Africa was shifted by plate tectonics at the position of the south Pole. The surface of the plateau, at the summit of the stratigraphic column, corresponds to the paleosurface of the late Ordovician. Two landforms called Zerga mountain and Herrour mountain are located at the surface of this plateau. Both landforms have about 50 km long, 1 km wide and a small sinuousity. Deynoux [8] proposed that these features were giant paleo-eskers because of this sinuosity but also because of their coarse sandstone composition with isolated pebbles and their association with the glacial paleosurface and related sedimentary figures. Their conservation at the present surface may be due to a difference in the erosion. Indeed the weak fine sandstone of the overlying layer was probably quickly eroded in comparison to the hard coarse grain sandstone of the paleo-eskers. The interpretation that these features are eskers related to some water flows under a large ice sheet is now widely accepted [9].

Compared topography of Mauritanian eskers and postulated Martian eskers: Mountain Zerga is a very impressive features because it lies over a very flat plain (Fig. 1). Its width is never smaller than 1 km reaching 1.5 km in several places, and its height varies around 100 to 150 m. This elevation is a minimum because erosion has removed the upper part of the paleo-esker. The maximum height of Zerga of 150 m then represents a potential height for the esker before erosion. On the other hand, MOLA data of esker-like features in the southern hemisphere of Mars give a range of several km wide (2-4 km) and elevation of 50 m to 120 above surrounding plains [5]. These values are in the same range than the sizes of the Mauritanian giant paleo-eskers.

Conclusion: This comparison may confirm that Martian sinuous ridges are eskers formed in a glaciation context. The comparison of Mauritanian giant megaeskers is an interesting complement to the observation of eskers in Canada because they are affected by aeolian erosion like Martian eskers are.

References: [1] Howard A., *NASA TM-84211*, 286, 1981; [2] Kargel and Strom, *Geology*, 20, 1992; [3] Tanaka and Scott, *Geologic Map of the polar regions of Mars*, 1987; [4] Ruff and Greeley, LPSC XXI, 1047-1048; [5] Head J. W., LPSC XXXI [6] Hiesinger H. and Head J. W., LPSC XXXI [7] R. Trompette, *Ph. D. Thesis*, 1969; [8] Deynoux M., *Ph. D. Thesis*, 1980; [9] Diemer E. et al., *La géologie de la Mauritanie*, 1991.

Fig. 1: View from the top of the Zerga mountain (giant paleoesker), 120 m above the surrounding plains.

SLOPE ANALYSIS OF SCARPS IN DEUTERONILUS MENSAE FROM MOLA DATA AND VIKING D.E.M.: EVIDENCE FOR LANDSLIDES CONTROLLED BY GROUND ICE. N. Mangold[1], D. Baratoux[2] and V. Frey[1], [1]Orsay-Terre, Equipe Planétologie, UMR 8616, CNRS et Université Paris-Sud, Bat. 509, 91405 ORSAY Cedex, France, mangold@geol.u-psud.fr, [2]Lab. Sciences de la Terre, UMR 8515, CNRS UCB Lyon1, 69622 VILLEURBANNE Cedex, France.

Goal of the study: The surface of Mars is affected by a large variety of features related to ice like lobate debris aprons, softened craters or fretted channels [1]. Many of these features are observed in the region of Deuteronilus Mensae where kilometer high scarps separate northern plains from southern highlands. The formation of lobate debris aprons at the foot of these scarps involves processes due to ice creep and mass wasting [2,3]. The measurements of the volume of these debris aprons from new MOLA data (Mars Observer Laser Altimeter) conclude that only huge landslides can produce such volumes [4]. The goal of this study is to test this result by the measurements of the slopes of scarps using both MOLA data and Digital Elevation Model (D.E.M.) calculated from Viking images. It also point out that the combination between MOLA data and Viking D.E.M. is very useful to measure steep slopes.

Scarp #	*Profile*	*Height (m)*	***Steepest Slope Angle (°)***
A	205	807	**25**
B	205	1045	**19**
B	445	1194	**22**
C	353	573	**11**
D	353	514	**10**
D	390	368	**9**
D	445	461	**13**
E	390	492	**12**
F	390	1025	**24**
G	390	775	**15**
G	445	840	**16**
H	390	684	**16**
H	445	715	**19**

Tab. 1 : Steepest slope angles calculated for 8 scarps (A-H) crossed by profiles 205, 353, 390 and 445. Corresponding difference in elevation is indicated for each slope.

Scarp slopes using MOLA data: About 20 MOLA profiles from the Aerobraking and Science Phasing orbits cross the region of Deuteronilus Mensae (38°-48°N, 326°-342°W). Given the relative position of the scarp with respect to the MOLA track, we deduce the angle of the steepest slope. The slopes are calculated on the upper part of each scarp, from the scarp rim to the first significant inflexion point on the slope, in order to avoid any debris aprons in the measurement. These extreme points are always separated by at least 4 MOLA shots. Table 1 summarizes values calculated for different scarps crossed by profiles 205, 353, 390 and 445. All values are lower or equal to 25°. For a given scarp, there is a good agreement between calculated slopes along different profiles. Profiles 353, 390 and 445 cross scarp D and calculated slope angles range between 9° and 13°. Profiles 390 and 445 also cross two other scarps (G and H), and measured slope angles range between 15-16° and 16-19°, respectively. Identically, scarp B, which is crossed by profiles 205 and 445, is characterized by a slope angle of 19-22°. Thus, for each studied scarp, the calculated slope angles using different MOLA profiles cluster within a 4°-range.

Scarp slopes using Viking DEM: The new method to process D.E.M. from Viking images, presented in a companion paper [5], has been applied to available images in the Deuteronilus Mensae area (Fig. 1). The expected vertical precision is about 50 m and horizontal resolution about 100m for three couples of images. This method is a good complement to MOLA data. Indeed slopes computed from D.E.M. can be measured over the whole length of selected scarps while MOLA data only give specific values on selected 2D tracks. Furthermore, even the vertical resolution of MOLA is less than 1 m, each shot is separated by 300 m or more horizontally. The D.E.M. is helpful to measure slopes when scarps are crossed by few MOLA points because its horizontal resolution is better.

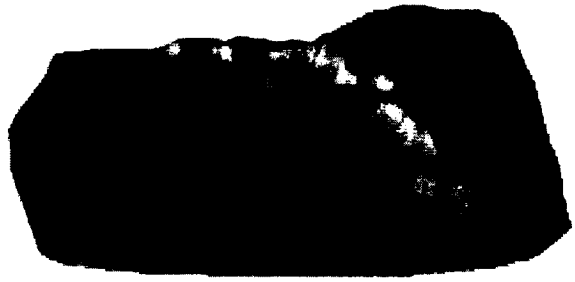

Fig. 1 : 3D simulation of the D.E.M. derived from Viking images 529a05 and 675b62 (Coord. 41N, 342W). Vertical exaggeration: 10x. View angle: 40°.

Results and geomorphic consequences: The results of the slope angles calculated from the Viking D.E.M. and those measured using MOLA in table 1 are in good agreement. The slopes of the upper part of all scarps are always lower than 25° and mostly between 15 and 20°. These values are very low in comparison to terrestrial values of scarps usually above 30°. This value of 30° corresponds approximately to the angle of internal friction of all classical rocks [6]. However frozen ground follows a behavior different from usual rocks. Values as low as 12° [7] or 19° [8] are reported from experimental tests on ice-rich frozen ground. The measurement of low slopes on Mars suggests that the material of these scarps corresponds to an ice-rich permafrost. This assumption is consistent with the hypothesis of landslides at the origin of lobate debris aprons [3,4]. Indeed, the slope of 20° is too low to produce the fall of isolated rocks removed from the scarp. Lobate debris aprons may then formed only with processes involving landslides in an ice-rich permafrost.

References: [1] Carr M. H. (1996) *Water on Mars*, Oxford Univ. Press. [2] Squyres S. W. (1978) *Icarus*, 34, 600-613. [3] Lucchita B. K. (1984) *J. Geophys. Res.*, 89, supp. B409-B418. [4] Mangold *et al.* (2000), LPSC 31th ,. [5] D. Baratoux, et al. (2000) this volume. [6] *e.g.* Jaeger and Cook (1979) Fundamentals of rock mechanics. [7] Parameswaran V. R. et Jones S. J. (1981), *J. Glaciology*, 27, 95. [8] Chamberlain E. et al. (1972), Géotechnique 22, 3, 469-483.

THERMOKARSTIC DEGRADATION OF LOBATE DEBRIS APRONS AND FRETTED CHANNELS. N. Mangold, F. Costard and J.-P. Peulvast, Orsay-Terre, Equipe Planétologie, UMR 8616, CNRS et Université Paris-Sud, Bat. 509, 91405 ORSAY Cedex, France, mangold@geol.u-psud.fr.

Introduction: Lobate debris aprons are landforms observed in the mid-latitudes regions of Mars at the foot of kilometer high scarps [1]. Because of their lobate front and convex shape they have been interpreted as the result of the viscous deformation of an ice-rock mixture [2]. Recent analyses of MOLA data confirm these previous conclusions [3]. Fretted channels correspond to lineated valley fills interpreted in the same way by viscous deformation of ground ice but guided by the shape of the valley [2]. New MOC high resolution images of the surface of both lobate debris aprons and fretted channels show mysterious network of knobs and highly dissected units. This study proposes to explain these landforms by a thermokarstic degradation due to the sublimation of ground ice.

Observations: A close look to the surface of lobate debris aprons show complex landforms at the scale of several hundred meters (Fig. 1 and 2). Three morphologic units can be distinguished: (1) Flat unit with several pits and troughs; (2) Partially dissected unit with many knobs and buttes; (3) Completely dissected units with few knobs. Figure 2 only presents units 2 and 3. The unit 3 is always at elevation lower than the unit 1 (sketch of figure 1). This difference is of the same order of magnitude than the width of knobs on unit 2, several tens of meters. On other hand, knobs are never more elevated than the surface of unit 1. These observations confirm the assumption that these units corresponds to three different stages of dissection. In agreement with this assumption, there is a difference of roughness between unit 1 and 3 showing that the dissected unit 3 has different surface characteristics than unit 1. Furthermore, unit 3 on figure 2 is not completely dissected because several "coffee grains" shaped knobs are present. These small knobs are less elevated than nearby knobs of unit 2 and show a central depression. They can be considered as collapsed knobs at the transition between unit 2 and 3. However, such knobs may not be present everywhere at the transition between these two units. We also observe on both figure 1 and 2 several preferential lineations in the direction of the dissected units. This is especially the case on figure 2 where the network of knobs is distributed in an orthogonal pattern. These directions may come from the flow of the icy debris apron but they seem to have an influence in the dissection process. Finally figure 3 summarizes in a schematic 3D representation the different units. It clearly proposes that unit 3 is at the end of a process of dissection. This process generates firstly pits and troughs usually following main directions inside unit 1. In unit 2 these pits become coalescent and create a network of knobs. Collapsed knobs are at the transition between the knobby unit 2 and the rough final surface of unit 3.

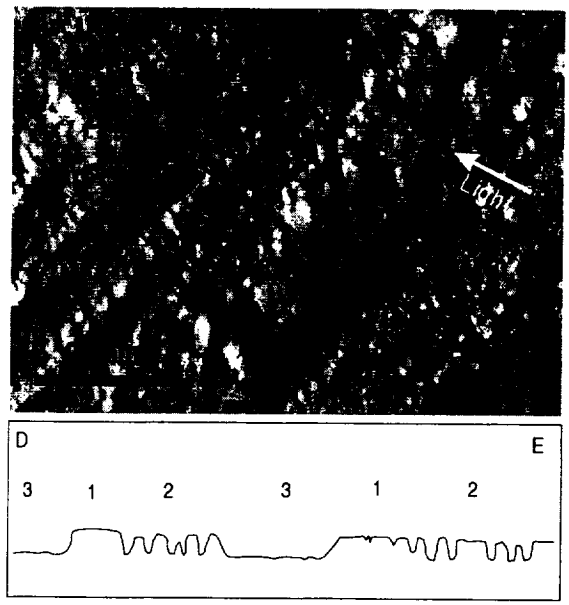

Fig. 1: Close look to MOC image #fha1072 (Coord. 45N, 322W) corresponding to the surface of a lobate debris apron. The sketch represents an interpretative unscaled topographic cross-section through the different units detailed in text.

Interpretation: All these observations can be explained by the single process of sublimation of ground ice. Indeed lobate debris aprons and fretted channels contain an ice-rich material that explains their convex shape and lineated structures. At the latitude at which they are observed of 35 to 50°, ice is not stable at surface [4]. A thickness of ground of 10 to 30 meters may be affected by sublimation at these latitudes over durations of several hundred million years [4]. This process may explain most of the landforms observed. Usually, thermokarst formed by sublimation develops following a random organization that is not observed here. However, the organization observed in this case corresponds to the orthogonal pattern of fracturation and lineation due to the flow. Such pattern is usually observed in terrestrial pure ice glaciers. The longitudinal trend of fractures is due to the downward flow and lateral fracturation is observed orthogonal to the flow. Thus, these fractures produce heterogeneities in the subsurface accelerating the process.

Fig. 2: MOC image #52106 (Coord. 40.5N, 306W). Surface of a lobate debris apron highly affected by knobby unit 2. The sketch B represents "coffee grains shaped knobs" that may correspond to a transitional stage between unit 2 and 3.

Indeed, fractures give a surface of contact between ground ice and atmosphere. The sublimation is then more active than in the porosity of the ground where the size of voids limit the sublimation rate. While ice sublimates, rocks are no more cemented and fall inside the fractures. Then fractures become larger and larger until the isolation of knobs (Fig. 4b). The transition between second and third stage may be explained by the conjugate role of sublimation and relaxation of ground ice inside knobs (Fig. 4c). The final dissected unit (Fig. 4d) presents a roughness different to that of unit 1 because of the boulders and debris produced by such process.

Finally, the thermokarstic dissection of the surface of lobate debris aprons by sublimation of ground ice explain all characteristics of the described landforms like the main directions of dissection or the difference of roughness.

References: [1] Carr M. H. (1996) *Water on Mars*, Oxford Univ. Press. [2] Squyres S. W. (1978) *Icarus*, 34, 600-613. [3] Mangold *et al.* (2000) LPSC 31*th* [4] Fanale, J. R. *et al.* (1986) *Icarus*, 67, 1-18.

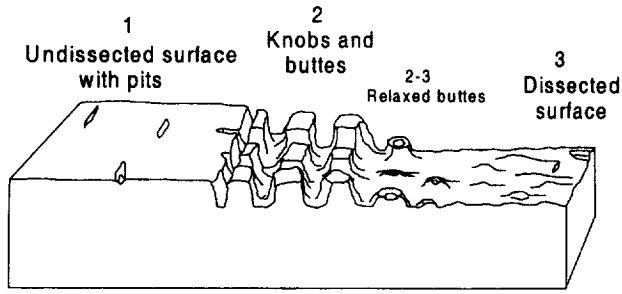

Fig. 3: Synthetic 3D sketch of the different units observed on debris aprons.

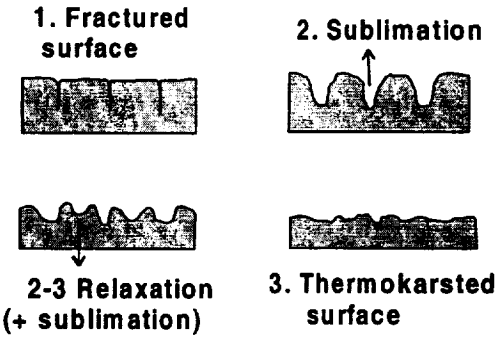

Fig. 4: Evolution of the surface of lobate debris aprons and fretted channels by sublimation of ice facilitated by large fracture network due to ground ice deformation.

THERMOKARSTIC DEGRADATION OF THE MARTIAN SURFACE. N. Mangold[1], F. Costard[1] and J.-P. Peulvast[1], [1]Orsay-Terre, Equipe Planétologie, UMR 8616, CNRS et Université Paris-Sud, Bat. 509, 91405 ORSAY Cedex, France, mangold@geol.u-psud.fr.

Introduction: Thermokarst on Mars has been widely described at the scale of Viking images [1,2]. It usually consists on large pits and troughs of several hundred meters deep attributed to the collapse of rocky material after the sublimation or melting of ground ice. The MOC images observed and interpreted in this study may provide evidence for a new kind of thermokarst features on Mars at the scale of several tens of meters.

Observation and interpretation: Figures 1 and 2 show MOC high resolution images of the surface of dissected terrains in the mid latitudes of the southern hemisphere. These terrains can be described as composed by three main units: (1) "Undissected" unit with few pits and troughs; (2) Partially dissected unit with many knobs and buttes, chaotic terrains; (3) Completely dissected units with few knobs. These kind of features may correspond to a process that dissects unit 1 in unit 3 with an intermediate unit 2 as summarized on figure 3. The thickness of the dissected unit may be about 20-30 m. This kind of dissected terrain is equivalent to the dissected terrain of lobate debris aprons and fretted channels [3, see companion paper "Thermokarst on lobate debris aprons and fretted channels" by Mangold *et al.* in this volume]. This means that we can explain the formation of these landforms by the sublimation of ground ice. All small fractures or units with large porosity are submitted to a high rate of sublimation in comparison to units with small porosity and devoid of fractures. The difference with the surface of lobate debris aprons [3] is that the distribution of knobs in chaotic terrains of unit 2 is mainly random. This is clearly explained by the fact that fractures due to deformation has an orthogonal pattern that does not exist on other terrains. However, the same kind of mechanism may exist: the right bottom of figure 1 shows that fractures can initiate and develop in coalescent pits. Even the origin of these fractures is not examined here, this process may explain the formation of pits and chaotic terrains. Unit 3 corresponding to the last stage of dissection shows usually a very rough texture that is consistent with a terrain rich in boulders and rocks that is supposed to exist after sublimation.

Distribution in latitude: This kind of dissected terrains has been observed in many regions of the whole planet [4]. This distribution is clearly depending on the latitude (Fig. 4). Such distribution is completely in agreement with the process of thermokarst due to sublimation. Indeed, ice is supposed to be completely stable in the porosity of the surface poleward of 50° [5]. This stability is deduced from the frost point of ice, 198 K at the current Martian pressure of 6 hPa. In the latitudes from 35 to 50°, ice is stable at several tens of meters in the ground and completely unstable in the equatorial regions. In the mid-latitudes of 35 to 50° ice progressively sublimates to the atmosphere. The duration of the process may be several million years to several billion years depending on porosity and pore size. The latitudes of the pictures where dissected terrain are observed correspond exactly to the range of latitudes where ice is present in subsurface but may progressively sublimate due to an annual average temperature higher than frost point. This correlation is the main agreement in favor to the explanation of thermokarst formed by sublimation of ground ice.

Climatic implications: The process of sublimation expected by thermodynamic properties is confirmed by the observation of these thermokarstic landforms. The next step in the understanding of this process is to focus on the age of the dissected units and the duration of this process in order to establish when this process began. It has an important implication on the climate evolution and stability because the climatic conditions need to be about the same as those of the present time.

References: [1] Carr M. H. (1996) *Water on Mars*, Oxford Univ. Press. [2] Costard and Kargel, Icarus, 114, 93-112, 1995, [3] Mangold et al., this volume. [4] Mustard J. and Cooper (2000) LPSC 31*th* [5] Fanale, J. R. *et al.* (1986) *Icarus*, 67, 1-18.

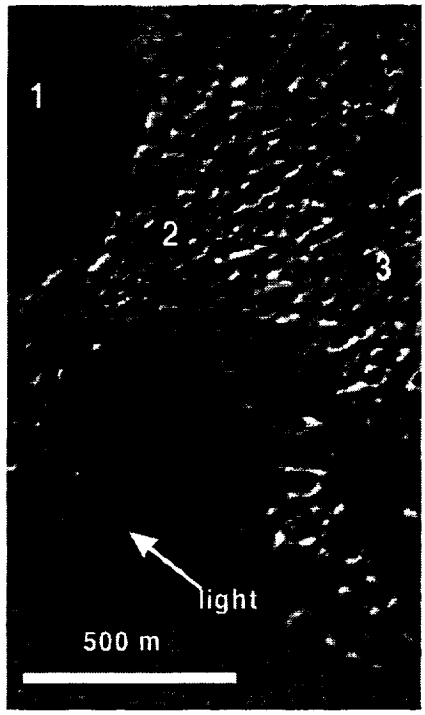

Fig. 1: MOC image #fha00982 (Coord. 40.5S, 240W). Dissection of a plain into chaotic terrains.

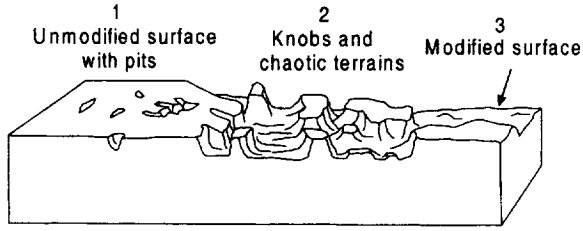

Fig. 3: Synthetic interpretation of morphologic units observed in dissected units.

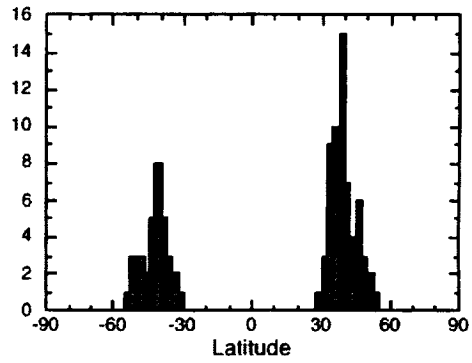

Fig. 4: Distribution in latitude of MOC images showing dissected terrains [from 4].

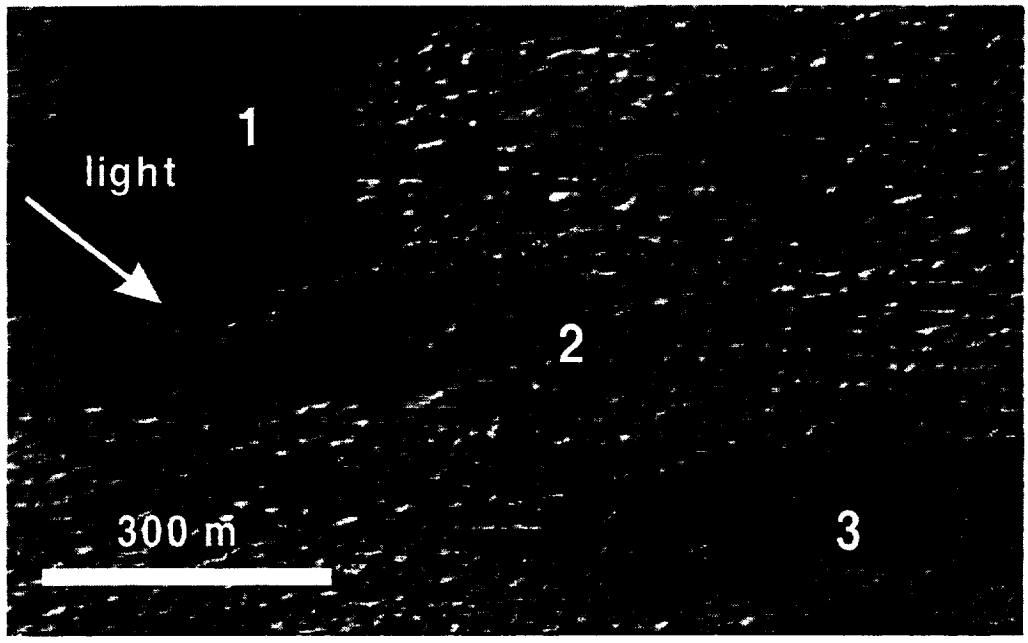

Fig. 2: MOC image #fha01450 (43.6S, 239.6W).

EFFECT OF SURFACE ROUGHNESS ON ICE DISTRIBUTION IN THE SOUTH SUBPOLAR REGION OF MARS. W. J. Markiewicz[1], K. J. Kossacki[1,2], H. U. Keller[1], [1]*Max-Planck-Institute for Aeronomy, Max-Planck-Str.2, D-37191 Katlenburg-Lindau, Germany,* [2]*Institute of Geophysics of Warsaw University, Pasteura 7, 02-093 Warsaw, Poland, (markiewicz@linmi.mpg.de).*

Abstract. We investigate the influence of a shallow trench on the local temperature distribution and the ice content in the Martian regolith. The model used in this paper is an extension of that presented in [2] which was used to analyze heat diffusion and to calculate the temperature distribution in the vicinity of a small surface trench. In addition, our model now includes water vapour diffusion through the pores of the ground regolith, water adsorbtion on the mineral grains and time evolution of the water ice in the regolith. Our simulations predict an accumulation of sub-surface ice close to the colder wall of the trench, as well as below its bottom. This is due to different exposure of trench surfaces to the solar and scattered radiation. We also expect changes of average surface albedo due to the diurnal frost formation.

Introduction. It is commonly expected, that some amount of water ice should be stored in the Martian regolith. One dimensional models of heat transport in soil suggest that ground ice could be stable at depths that depend on latitude. According to the work by [3] dealing with heat conduction and diffusion of vapour, ice may be stable at latitude as low as 45 degrees. These authors consider only latitudes lower than 60°, but extrapolation of their results for latitude 76S (the latitude of the Mars Polar Lander landing site) suggests the presence of ice at a depth of only few centimeters. A simple thermal model of the south subpolar region presented by [4] shows temperature low enough at depth larger than 20cm. This model however, yields only temperature profiles versus depth and latitude, but not the ice content. Detailed simulations of the ice content in the Martian regolith, including vapour exchange with the atmosphere were presented by [3] and [1]. The regolith part of their model, however, is only 1D and assumes a flat surface. This leads to significant inaccuracy since the presence of surface features will result in local and possibly regional changes of soil temperature.

In the present work we analyze the influence of a shallow trench on a local distribution of temperature and ice content. Our model is an improvement over that presented in [2] which was initially developed in preparation for the Mars Polar Lander mission. Our results can also describe the evolution of natural surface features. One example are the cracks visible in the image of Malea Planum in the southern region of Mars, taken by the Mars Global Surveyor (MGS) Mars Orbiter Camera (MOC) (MGS MOC Release No. MOC2-189, 15 November 1999). This image was taken after spring retreat of the polar cap when ice is still present in cracks enhancing their visibility.

The present model includes the following elements omitted in the previous work: 1) water vapour diffusion in the pores of the ground regolith, 2) water adsorbtion on the mineral grains composing the regolith, 3)time evolution of water ice in the regolith. The model includes thermal diffusivity dependence on local amount of water ice. The grains of dust are assumed spherical, but flattened at their contact areas. When ice forms, it is assumed that it covers all surfaces uniformly. Thus, geometrical considerations allow us to find the instantaneous value of the time dependent Hertz factor. The corresponding thermal diffusivity is calculated assuming that the pores can be modelled in the usual way by bundles of long channels of constant cross-section.

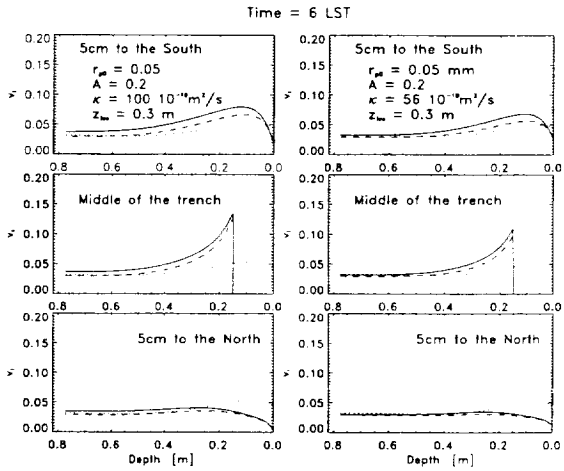

Figure 1: The ice volume fraction versus depth with $\kappa_0 = 56\,10^{-10}\,\mathrm{m^2 s^{-1}}$ (right) and $\kappa_0 = 100\,10^{-10}\,\mathrm{m^2 s^{-1}}$ (left). Results are presented for three places: 5 cm from the north edge of the trench (upper panels), in the middle of the trench bottom (middle) and at 5cm distance from the south upper edge (bottom). The curves are drawn for 6:00 LST. The ice distribution obtained in the 1D case without a trench is shown as dotted line. See text and legend.

Results. Fig.1 shows morning profiles of ice volume fraction below the trench and at its sides. For comparison we added also the profiles resulting from modelling without a trench. The difference is clearly visible. The soil at the colder southern side of the trench and below its bottom is significantly enriched in ice. The ice volume is only weakly dependent on the assumed thermal diffusivity.

To the south of the trench the ice volume fraction has a maximum at a depth somewhat dependent on κ_0. A significant night time increase of ice is also predicted for the surface of the soil. This can lead to an increase of the average surface albedo. A corresponding decrease of ice is observed near the north wall of the trench. The implied nighttime redistribution of the subsurface ice is farther illustrated in Fig.2 with four snapshots of the diurnal variation of the ice volume fraction. These results were obtained with $\kappa_0 = 100 \times 10^{-10}\mathrm{m^2 sec^{-1}}$. During the day almost all of the near surface ice is sublimated away or adsorbed except for some ice formation on the left (north) wall in the morning period. During the night, however

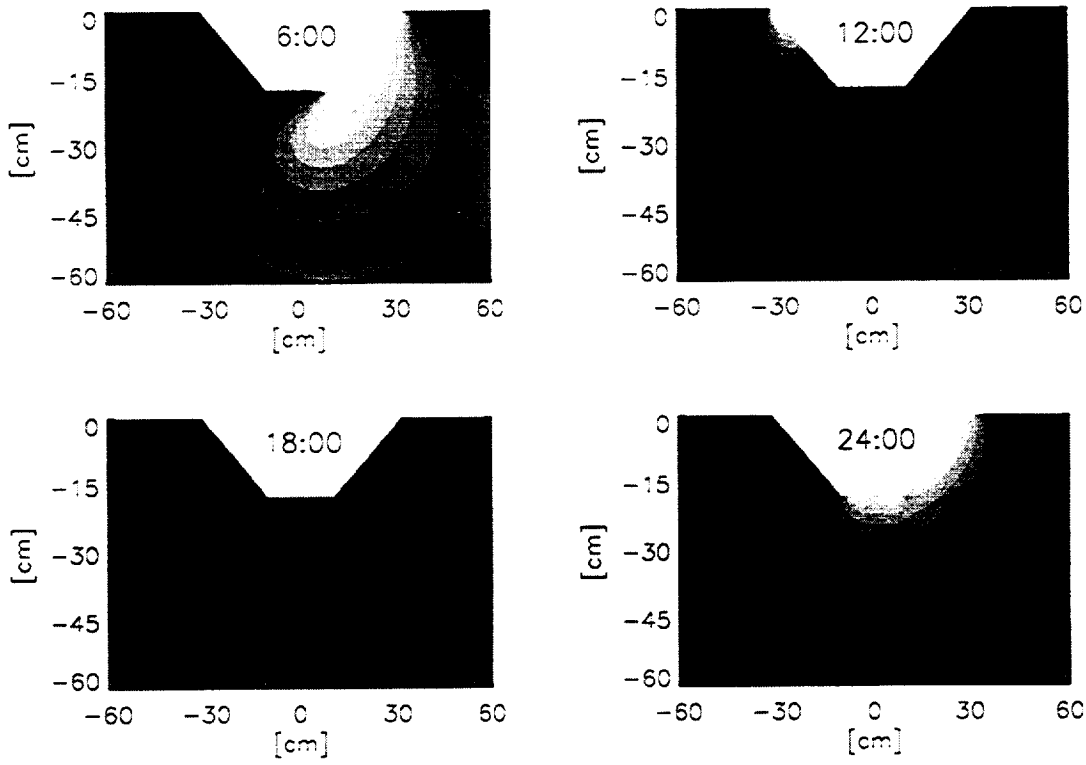

Figure 2: Ice in the regolith at four times of day. Contours of volume fraction filled by ice are plotted against the spatial dimensions. The contours are separated by 1% with black corresponding to 0% and white to 10%. North is to the left and the trench lies East-West. $\kappa_0 = 100 \times 10^{-10} \mathrm{m}^2 \mathrm{sec}^{-1}$.

the volume fraction of ice increases to nearly 10% at the bottom and right (south) side of the trench.

Discussion. In this work we consider the influence of a shallow trench on a local temperature field and the corresponding distribution of ice in subpolar Martian soil. We find that the different geometries and hence exposures of the surfaces relative to the solar and scattered radiation lead to nighttime accumulation of ice close to the bottom and colder wall of the trench. The time scale of this process is several hours. During the day almost all of the near surface ice is sublimated away or adsorbed. This means that the act of digging a trench, as was planned to be done during the Mars Polar Lander operations, significantly alters the presumed sub-surface structure of the permafrost. On the other hand, the volume of ice condensed in the trench at night reflects thermal diffusivity of the regolith, and could be used to deduce its value. Our simulations with a trench result in significant increase of ice content near the surface at night and in the morning. This may have important consequences for observations of polar regions with orbiter cameras that do not resolve such small scale surface roughness. Morning observations may suggest a larger albedo due to partial surface coverage by ice.

This work was intended as support of search for subsurface water ice with the Mars Polar Lander. We also wanted to understand how digging in the Martian soil disturbs its thermal state and hence changes the morphology of the permafrost. Martian regolith contains natural cracks and trenches. Therefore, our results can also increase the understanding of their diurnal and seasonal cycles. We analyze in detail a relatively shallow trench, but the presented model may also be applied to study seasonal evolution of larger surface structures.

References [1] Jakosky B. M., A. P. Zent and R. W. Zurek 1997 The Mars water cycle: determining the role of exchange with the regolith. *Icarus*, **130**, 87-95. [2] Kossacki K. J., W. J. Markiewicz and H. U. Keller 2000 Small scale trench in the martian soil: conditions for condensation of atmospheric volatiles, *Icarus, in press*. [3] Mellon M. T. and B. M. Jakosky 1993 Geographic variations in the thermal and diffusive stability of ground ice on Mars. *Journal of Geophysical Research E*, **98**, 3345-3364. [4] Paige D. A. and K. D. Keegan 1994 Thermal and albedo mapping of the polar regions of Mars using Viking thermal mapper observations: 2 South polar region. *Journal of Geophysical Research*, **99**, 25993-26013.

RETURN TO THE POLES OF MARS. D.J. McCleese, Mars Surveyor Office, Jet Propulsion Laboratory, 4800 Oak Grove Drive, Pasadena, CA 91109 (daniel.j.mccleese@jpl.nasa.gov).

Introduction: The loss of the Mars Polar Lander (MPL) raises the question of when NASA might attempt a return mission to the Polar Regions? This paper describes future opportunities for recovering the science lost with MPL.

Mars Surveyor Planning: Investigations of life, climate and resources – linked by the common theme of "follow the water" – have recently been reconfirmed as the overarching goals for the Mars Surveyor Program. It was within the context of these goals that the MPL mission was given high priority by NASA in 1995 and eventually launched in 1998. However, since the decision was made to puirsue MPL, NASA has shifted the focus of the Mars Surveyor Program toward the goal of bringing samples of Mars to Earth.

The technical challenges and financial demands of sample return have had the unintended impact of reducing the breadth of research in the Mars Surveyor Program. This reduction in program breadth has raised the issue of whether polar science would soon be given a priority sufficient to recover the science lost with MPL.

Recovery of Polar Science: The loss of both Mars Surveyor '98 missions has motivated a reconsideration by NASA, by the science community, and by JPL of the feasibility of a return of samples early in this decade. Further, the concomitant compromise in other research, particularly that which must be conducted at the planet, is under review. Flexibility in program planning is very likely be emphasized by NASA in future program plans.

Access to Polar Layered Terrain: Small landers, referred to as Scouts, may be enabling for investigations of the Polar Regions. Landers of less than 100 Kg launch mass and utilizing entry, descent and landing technologies derived from Mars Pathfinder are being currently under study. Scouts may be a robust landing system that might permit numerous sites to be visited planet-wide at a relatively low cost. Much of the science that was to have been accomplished by MPL could be addressed with just one Scout lander. Perhaps these vehicles will provide a means of assuring a balanced program of research at the surface of Mars.

HIGH ENERGY NEUTRON DETECTOR FOR MARS SURVEYOR ORBITER 2001: LOOKING FOR WATER ICE. I.G.Mitrofanov, N.F.Sanko, A.S.Kozyrev et al.

The main scientific objectives of Russian High Energy Neutron Detector HEND are to measure the Albedo of high-energy neutrons from the surface of Mars. HEND will work in integration with US Gamma-Ray Spectrometer and Neutron Spectrometer to provide the map of nuclear lines and neutron albedo.

HEND has three ^{3}He-based counters of neutrons for energy ranges 0.01 – 1.0 eV, 1.0 – 1000.0 eV and 1.0 – 1000.0 keV with thin, medium and thick moderators, receptively. For the highest energy range of 1.0 – 10.0 MeV HEND has one Stilben-based scintillating detector with active anti-coincidence shielding around it. These detectors will provide the data to build the maps for neutrons at different energy ranges.

With the increase of hydrogen content in the surface layer, the termalization path of high-energy neutrons is shortened, and the ratio between original high-energy neutrons and thermal neutrons decreases. The mapping measurements of this water-sensitive signature are the important objective of neutrons measurements. The resulting map of hydrogen aboundence will be created taking into account the local day-to-night temperature variations, the lattitude and the season variations.

POLAR LAYERED DEPOSITS: PRELIMINARY STRATIGRAPHIC ASSESSMENT FROM MGS OBSERVATIONS. B.C. Murray[1], S. Byrne[1], G.E. Danielson[2], K.E. Herkenhoff[3], L.A. Soderblom[3] and M.T. Zuber[4]. [1]Division of Geological and Planetary Sciences, Caltech, 1200 E. California Blvd., Pasadena, CA 91125, US. [2]Jet Propulsion Laboratory, [3]United States Geologic Survey [4]Massachusetts Institute of Technology. Correspondence Email: bcm@caltech.edu

Introduction: Global and hemispheric climatic, volcanic and impact events that modulated the formation of the Martian polar layered deposits can be revealed by detailed stratigraphic analyses of well-exposed sequences of those layers. Complete three-dimensional MOLA topography of the north and south polar deposits is now available, and very abundant MOC imagery that is well calibrated is becoming available. This paper presents an assessment of the polar stratigraphic potential based on observations from MGS mapping cycles through M7.

Stratigraphic Correlations: The early MOC and MOLA coverage in the south reaffirms the earlier impression that the layered deposits there are quasi-horizontal. Generally a single layer crops out over a large area, with exposed stratigraphic sections visible primarily at equatorward-facing scarps or within depressions, like in Figure 1. (Part of frame AB109503 at 74 S, 213 W. Illumination from lower right, north to bottom.) There a 700-meter thick sequence of about 35 layers is well exposed. Individual layers average about 20 meters thick with some as thin as 10 meters. The layers are visible because of intrinsic differences between adjacent layers in albedo, outcrop slope, and outcrop texture; see also Malin and Edgett[1] and Herkenhoff and Kirk[2]. Similarly detailed layering, for example, is evident in Figure 2 (MGS MSSS Release No. MOC2-148, 19 July 1999. Parts of frames M00-01754, 02100, 02072. North to top). As discussed by Edgett and Malin [3] marker horizons can be correlated over a 100 Kms along strike within the same trough (approximately 86 N, 258-282 W, near the edge of the northern residual cap). Thus at least regional-scale correlations are apparent. Examination of many images makes us optimistic that a detailed hemispheric stratigraphic column can be compiled for the south and perhaps the north. Thus it should be possible to test hypotheses of layered deposit formation, as well as to constrain portions of Martian global history.

Rich Record of Environmental Change: In addition, the detailed variations in apparent albedo, in outcrop slope, and in along-strike texture (all of which make the layering visible in imagery) must all result from variations in intrinsic lithologic properties of the individual layers. Such attributes in turn reflect changing depositional conditions from layer to layer. Thus the polar layered deposits probably record a richer variation of depositional attributes, and thus Martian environmental fluctuations, than anticipated in previous theories of origin.

References: [1] Malin M.C. and Edgett K.S. (2000), LPSC XXXI, Abstract 1055. [2] Herkenhoff K.E and Kirk R.C. (2000), this conference. [3] Edgett K.S. and Malin M.C. (2000), LPSC XXXI, Abstract 1068.

Figure 1.

Figure 2.

DIFFERENTIAL SCANNING CALORIMETRY AND EVOLVED GAS ANALYSIS AT MARS AMBIENT CONDITIONS USING THE THERMAL EVOLVED GAS ANALYSER (TEGA). D. S. Musselwhite[1], W. V. Boynton[1], D. W. Ming[2], G. Quadlander[1], K. E. Kerry[1], R. C. Bode[1], S. H. Bailey[1], M. G. Ward[1], A. V. Pathare[3], R. D. Lorenz[1], D. A. Kring[1], H.V. Lauer[2], Jr. and R. V. Morris[2]. [1]Lunar and Planetary Laboratory, University of Arizona, Tucson, Arizona 85721 (donm@lpl.arizona.edu), [2]NASA Johnson Space Center, Mail Code SN2, Houston, Texas 77058, [3]Dept. of Earth and Space Science, University of California, Los Angeles, California 90024

Introduction: Differential Scanning Calorimetry (DSC) combined with evolved gas analysis (EGA) is a well developed technique for the analysis of a wide variety of sample types with broad application in material and soil sciences [1]. However, the use of the technique for samples under conditions of pressure and temperature as found on other planets is one of current development and cutting edge research [2,3]. The Thermal Evolved Gas Analyzer (TEGA), which was designed, built and tested at the University of Arizona's Lunar and Planetary Lab (LPL), utilizes DSC/EGA [4]. TEGA, which was sent to Mars on the ill-fated Mars Polar Lander, was to be the first application of DSC/EGA on the surface of Mars as well as the first direct measurement of the volatile-bearing mineralogy in martian soil.

Experiments: We are conducting DSC/EGA experiments at Mars ambient temperature and pressure using the TEGA engineering qualification model (TEGA-EQM). The TEGA-EQM is a high fidelity simulator of the TEGA flight model (TEGA-FM) that was sent to Mars. The TEGA-EQM is being tested in an environmental chamber capable of reproducing Mars ambient conditions of temperature and pressure. The TEGA-EQM has overall the same design of ovens, manifold plumbing, and EGA (TEGA utilizes a tunable diode laser (TDL) for EGA) and reproduces the gas flow and gas flow geometry of the TEGA-FM. The experiments conducted at LPL are complimentary to experiments done at NASA's JSC and ARC. The tests run at LPL better reproduce the total operating conditions of the TEGA on Mars. The experiments conducted at JSC and Ames utilize conventional lab-bench DSC (but adjusted for lower temperature and pressure operating conditions) and, therefore, they can turn around many more experimental runs than the TEGA-EQM at LPL.

A series of geologic samples have been run in the TEGA-EQM. The analysed materials run include: calcite, lepidocrocite, pyrolusite, hydromagnesite, and free water ice. In addition, Mars soil analogues have been run as unknowns. The results of one such experiment are presented here. These illustrate both our ability to accurately determine the mineralogy of martian soil with the TEGA and some of the differences between DSC/EGA run under normal laboratory conditions and those run under Mars ambient conditions.

To identify a sample run in TEGA (on Mars or as an unknown on the TEGA-EQM) the following approach is taken: 1) run unknown sample on TEGA-EQM using procedures planned for Mars; 2) identify onset and peak temperatures in DSC and EGA; 3) assign preliminary composition and mineralogy; 4) run candidate mixtures in Perkin-Elmer DSC at JSC; 5) run best-guess candidate sample in the TEGA-EQM; 6) refine best guess based on results; 7) repeat steps 4, 5 and 6 as necessary.

Discussion: Figure 1 shows the DSC and TDL trace for a representative Mars analogue unknown which was provided to the TEGA Team by R. V. Morris. The Team did not know the actual chemistry or mineralogy of the unknown sample during the procedure described above. The sample was run with a flow rate of 0.4 sccm yielding an oven pressure of 100 mbar N_2 (unlike a standard DSC, the flow rate and

Figure 1. Unknown Sample

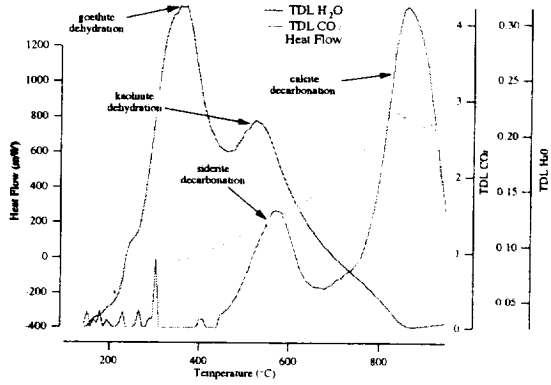

oven pressure are coupled in the TEGA). The sample was heated at 20 °C/min. Two major H_2O releases and two decarbonation events are clearly evident in the TDL data (Fig. 1). The best guess sample composition was formulated by comparing the data for the unknown sample to the large library of low pressure DSC/EGA traces produced at JSC[3]. The data for the best guess sample (Fig. 2), which was run with the same gas flow and temperature ramp rates as the unknown, match the volatile release events for the unknown sample rather well. The mineral composition for the unknown and best guess samples are listed in Table 1. A 1:1 phyllosilicate, similar to kaolinite, was identified as a mineral component of the unknown sample. The sample supplier (Morris) was unaware of the presence of this phase before our analysis. The

identification of the phase was subsequently confirmed by x-ray analysis. The main difference between the unknown and best guess sample composition is that the best guess sample contains palagonite, which is not present in the unknown sample. The volatile-bearing phases of the unknown were revealed at the end of the 1st best guess run so no iterations of steps 4, 5 and 6 described above were performed. Our second guess was, therefore, our final determination. The palagonite was included in the best guess in order to account for the low temperature shoulder (<100°C) in the water release data of the unknown sample. It did not, in fact, reproduce the water-release shoulder well in the TEGA-EQM run and would have been eliminated in the second iterative step.

Figure 2: Best Guess Sample

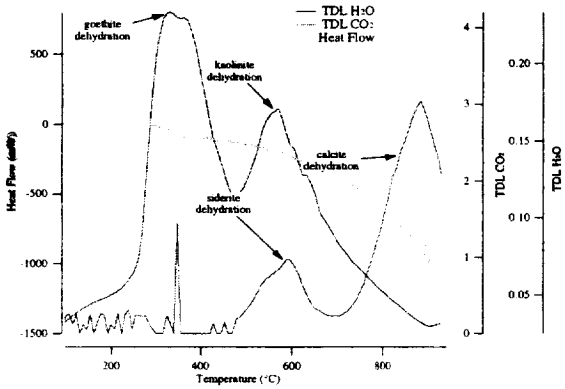

Temperatures of features in the TDL data for the unknown and the best guess are shown in Table 2 along with assigned causes of the features. Also listed are onset and peak temperatures from 1 atm DSC/EGA studies. Comparison of the onset temperatures of the outgassing events in the unknown and best guess samples with literature values for samples run at standard pressure illustrates the effect of the lower pressure. The onset temperature for the dehydration of goethite occurs 10 to 20°C lower for the 100 mbar runs compared with 1atm runs and the dehydration of kaolinite occurs 40°C lower. Temperature of onset for the siderite decarbonation occurs 20 to 50°C lower for the 100 mbar runs compared with 1 atm runs and calcite decarbonation occurs 110 to 235 °C lower.

Unknown #2 [a]		First best-guess candidate composition		Second (and final) composition	
12.1%	siderite	8%	siderite [b]	10%	siderite
44.1%	calcite	38%	CaCO3 (reagent) [c]	47%	CaCO3
[redacted]		6%	kaolinite (poorly crystalline) [d]	8%	kaolinite
29.1%	goethite (poorly crystaline)	28%	goethite (synthetic) [e]	35%	goethite
2.3%	quartz	20%	palagonite [f]		

[a] not known to be present until DSC results from TEGA suggested its presence (later confirmed by XRD)

Sample designation, source

[a] British Chemical Standard, Limonitic iron ore BCS No. 301/1 (mineral percentages calculated from chemical data)
[b] Ward's Scientific
[c] Fischer Scientific
[d] Georgia (Clay Minerals Society Reference Clay KGa-2)
[e] [5]
[f] Pau Haleau (Hawaii cinder cone) [6]

Comparing the TDL data between Figures 1 and 2 we see interesting similarities and differences in detail. The relative peak heights of the 1st water release between the two samples is *exactly* what it should be given the (slight) differences in the percentage of goethite between the unknown and best guess samples. Also, the relative peak heights of the 1st and 2nd water releases for the unknown are very close to the relative proportion of water contained in the goethite and kaolinite in the unknown; however, the relative peak heights of the 2nd water release between the unknown and the best guess samples are out of proportion with respect to to their relative kaolinite contents; i.e.,. the second water release in the best guess sample is 2.5 times larger than it "should" be given the proportion of kaolinite relative to goethite in the sample. Thus, an additional high-temperature release of water has occurred in the best guess sample compared with the unknown sample. This is probably due to a difference in composition and or structure of the kaolinite in the best guess sample compared with that of the 1:1 phyllosilicate in the unknown sample. The presence of palagonite in the best guess sample may also have had an effect. The relative heights of the CO_2 release peaks both within and between the samples is fully consistent with the amount of the two carbonate types in each sample.

event	T (°C) unknown	T(°C) best guess	assigned cause	T (°C) 1 atm data [7]
Onset of 1st H_2O peak	200	211	goethite dehydration	220 - 400
1st H_2O peak	354	331		
Onset of 2nd H_2O peak	468	469	kaolinite dehydration	510
2nd H_2O peak	527	569		600
Onset of 1st CO_2 peak	451	480	siderite decarbonation	500
1st CO_2 peak	572	587		585
Onset of 2nd CO_2 peak	685	705	calcite decarbonation	830 - 920
2nd CO_2 peak	863	889		830 - 940

The enthalpy of decarbonation of the calcite can be seen in the DSC traces for the unknown and best guess samples (Figs. 1 and 2) starting just above 700°C. This corresponds with the CO_2 release seen in the TDL data.

This test of the TEGA-EQM illustrates the outstanding capabilities that a TEGA-like instrument will have on a Mars surface mission (such as the Mars Polar Lander) for detecting and identifying volatile-bearing phases.

References: [1]Hoehne et al.(1996) *Differential Scanning Calorimetry*, Springer, Berlin. [2] Golden et al. (1999) *LPSC XXX*. [3] Lauer et al. (2000) *LPSC XXXI* [4] Boynton et al. (2000) *JGR* (submitted) [5] Morris, R.V. etal, (1985) *JGR*, **90**: 3126-3144. [6] Morris etal. (2000) *JGR* (in press) [7] Blazek (1973) *Thermal Analysis* Van Nostrand Reinhold, London

IS POLAR CLATHRATE STORAGE FRACTIONATION OF THE MARTIAN ATMOSPHERE THE CAUSE OF THE NAKHLITE KR TO XE RATIO? Musselwhite, D.S., Swindle, T.D. and Lunine, J.I. Lunar and Planetary Laboratory, University of Arizona, Tucson, Az 85721. donm@lpl.arizona.edu

Abstract: Nakhlites, martian meteorites representing cumulate magmatic rocks, contain evidence of atmosphere from the time of their ejection from Mars. We postulate that the martian atmosphere at that time had a lower Kr/Xe ratio compared with the modern atmosphere due to the release of these and other gases from polar clathrate possibly during a period of high (~60°) obliquity.

Introduction: Noble gases are good tracers of the volatile history of a planet. Noble gases in meteorites from Mars reveal interesting details of that planet's volatile history. Figure 1 shows a plot of $^{129}Xe/^{132}Xe$ ratio *versus* Kr/Xe ratio for all martian meteorite types identified so far [1-3]. The shergottites and nakhlites each define distinct mixing arrays. Both have a low $^{129}Xe/^{132}Xe$ ratio end member which looks like Chassigny (martian mantle value). The high $^{129}Xe/^{132}Xe$ end member for the shergottites looks like EETA79001 Lithology C (thought to be trapped martian atmosphere). The nakhlites plus ALH84001 have a lower Kr/Xe ratio for the high $^{129}Xe/^{132}Xe$ end member than do the shergottites. The shergottites are thought to have obtained their atmospheric noble gas signature by shock emplacement during the impact that ejected them. The nakhlites and shergottites were ejected in separate events: 10 to 12 Ma and < 1 to 3 Ma, respectively [4,5].

Figure 1

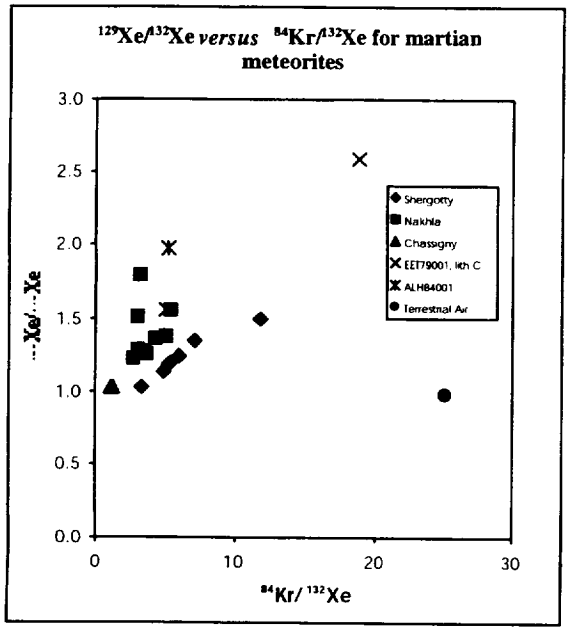

Previous models for low Kr/Xe in nakhlites: Several models have been put forward to explain the lower Kr/Xe ratio in the nakhlites: implantation of martian atmosphere which had been fractionated due to differences in water solubility [6]; shock implantation of atmospheric noble gases which were fractionated by differential adsorbtion on clays and other minerals in the rock [7]; assimilation of adsorption fractionated noble gases by the nakhlite parent magma [8]; or, the nakhlites are sampling a second mantle reservoir distinct from Chassigny - a mantle source with high $^{129}Xe/^{132}Xe$ and Kr/Xe ratio lower than atmospheric is predicted from early outgassing models [9,10]. There are problems with each of these models.

Clathrate release/impact trapping model: We wonder if, as with the shergottites, the high $^{129}Xe/^{132}Xe$ end member in the nakhlites might also be unfractionated atmosphere trapped in the meteorite by the impact which caused their ejection from Mars. The atmosphere at the time of the ejection of the nakhlites could have had a lower Kr/Xe ratio than the present-day atmosphere if it was affected by gases released from clathrate in the polar caps due to changes in polar heat balance during a high obliquity excursion [11].

CO_2 clathrate hydrate may be abundant at the martian polar caps [12]. Jakosky, et al. [13] explore the implications of obliquity variations for changes in the atmospheric pressure over time. As Mars approaches a high obliquity state, sublimation of clathrate hydrate releases CO_2 into the martian atmosphere. They have estimated that as much as 200 mbar of CO_2 hydrate could be present in the present-day polar caps. While obliquity varies between 10 to 40° on a 10^5 year timescale, obliquity excursions up to 60° occur on a 10^7 year timescale. It is these larger excursions that can produce significant sublimation of the polar caps. Work by [14] shows that both Kr and Xe are significantly sequestered into CO_2 clathrate hydrate. Depending on the model temperature of formation, and assuming a 200 mbar CO_2 equivalent of clathrate, the amount of Xe in the polar caps is from 50 to 10^4 times that in the present atmosphere and the amount of Kr in the polar caps is from 2 to over 100 times that in the present atmosphere. So not only are the polar caps potentially much larger reservoirs of the heavy rare gases than the atmosphere, the Kr/Xe ratio in the polar clathrate is significantly lower than the present-day martian atmosphere.

Clathrates could exist at other locations on Mars especially in the regolith In fact, these other clathrate reservoirs are potentially quite a bit more abundant than those in the polar caps [15]. However, it is not clear whether the possible mechanisms of formation of these regolith clathrates would allow for trapping of atmospheric noble gases. Further, the potential regolith clathrate reservoirs would of necessity be sealed off from the atmosphere by overlying water ice and would not feel the effects of obliquity excursions. For these reasons we consider only polar clathrates as potential sources for atmospheric noble gases. The regolith clathrate reservoirs are thought to have been released by catastrophic periodic outflow events [16] due to internal heating processes. Such a release would cause thickening and therefore warming of the atmosphere which, in turn, would cause sublimation of the polar caps. The release of regolith volatiles thus provides a possible alternative to high obliquity as the cause of polar cap

sublimation. It is interesting to note that there is new evidence for young (~10 Ma) outflow channels [17].

We can calculate the amount of clathrate from the polar caps needed to sublimate to give the nakhlite Kr/Xe ratio for a given temperature of formation model of [14]. Depending on the model temperature of formation, the fraction of the atmosphere composed of gases released from clathrate hydrate at the time of nakhlite ejection is from 0.6% (or about 0.04 mbar of CO_2) considering the highest temperature (200K) of clathrate formation to 60% (or about 8 mbar of CO_2) considering the lowest temperature (150K) of clathrate formation. These amounts of clathrate-derived volatiles are clearly a small fraction of the total possible volume of clathrate at the poles (200 mbar of CO_2). These results suggest that only a modest amount of the polar cap volatiles reside in the atmosphere at any given time during their exchange between the poles that occurs during the obliquity swings.

The issue of where the various noble gas components reside in the nakhlites is not resolved [8,18]. The siting of noble gases in the meteorites is crucial to testing between the different models of formation of the lower Kr/Xe ratio for the high $^{129}Xe/^{132}Xe$ ratio end member in the nakhlites. Siting in similar materials (impact melt) between shergottites and nakhlites would favor the impact emplacement models (including the polar clathrate release of noble gases model).

Possible role of Xe isotopic fractionation from clathrate sequestering: Due to the large mass range of xenon (the mass # varies from 124 to 136 for the stable isotopes of Xe), mass fractionation of the isotopes should also occur during partitioning between the atmosphere and clathrate. The clathrate structure would be expected to show a slight preference for the heavier nuclides. And thus we should see depletion of heavy isotopes in the atmosphere today compared with the bulk atmosphere-surface-polar cap invenory. We are presently developing a quantitative thermodynamic model to assess the significance of this possible source of isotopic fractionation. The results of this could serve as a check on the clathrate release / impact trapping model. There should be a difference in the Xe isotopic fractionation of the trapped gases between the shergottites and the nakhlites. Less depletion of the heavier isotopes of Xe should be seen in the nakhlites in comparison to the shergottites. Indeed, the $^{136}Xe/^{132}Xe$ ratio is slightly higher in the in low temperature release steps from ALH84001 [7].

Implications for future missions: In the interest of advancing our understanding of the history of martian volatiles and the evolution of the martian climate over time, the existence and extent of clathrates at the poles needs to be determined. Clathrates are likely not stable at the surface of the polar caps or layered terrains, but they are stable very near the surface. Therefore an *in situ* determination (rather than by remote sensing) of the existence of clathrate will have to be made. How can we identify clathrate in the polar caps? Simply measuring the ratio of water to CO_2 will not work, as any formation of clathrate would necessarily be accompanied by formation of either water ice or CO_2 ice depending on which species was in excess. With some luck, simple trenching below the surface of the layered terrain surface could expose clathrate at a modest depth (meter) but the exposed clathrate would quickly become unstable. DSC/EGA such as employed with the TEGA on the Mars Polar Lander [19,20], could identify clathrate from the combination of the onset temperature of reversion of clathrate to CO_2 and H_2O ice in the DSC and the release of CO_2 vapor. However, the clathrate has to remain stable while being delivered to any analytical device. Clathrate is likely stable below about 10 meters or so in the caps themselves, necessitating the use of a substantial drilling rig in order to sample it.

References: [1] Ott, U. (1988) *GCA***52**, 1937-1948; [2] Swindle, T.D. et al.(1986) *GCA* **50**, 1001-1015; [3] Swindle, T.D. et al.(1995) *GCA* **59**, 793-801; [4] Warren, P.H. (1994) *Icarus* **111**, 338-363 [5] Eugster, O. (1997) *GCA* **61**, 2749-2757; [6] Drake, M.J. et al. (1994) *Meteoritics* **29**, 854-859 [7] Gilmour, J.D. et al (1998) *GCA* **62**, 2555-2571 [8] Gilmour, J.D. et al (1999) *EPSL* **166**, 139-147; [9] Swindle, T.D. and Jones, J.H. [10] Musselwhite D.S. and Drake, M.J. (2000) *Icarus* (in press) [11] Jakosky, B.M. et al (1993) *Icarus* **102**, 286-297;[12] Miller, S.L. and Smythe, W.D.(1970) *Science 170,* 531-533. [13] Jakosky, B.M. et al. (1995) *JGR* **100**, 1579-1584 [14] Musselwhite D.S. and Lunine J.I. (1995) *JGR 100,* 23,301-23,306. [15] Kargel, J.S. and Lunine, J.I. (1995) in *Solar System Ices* , 97-117; [16] Baker, V.R. et al. (1991) *Nature* **353**, 589-594; [17] Baker, V.R., personal communication; [18] Swindle, T.D. et al. (2000) *Meteoritics* **35**, 107-115; [19] Boynton, W.V. et al. (2000) *JGR* in press; [20] Musselwhite, D.S. et al (2000) (this volume).

EVIDENCE FOR A SURGING ICE-SHEET IN ELYSIUM PLANITIA, MARS. J. Nussbaumer[1], R. Jaumann[1], and E. Hauber[1], [1]DLR Institute for Space Sensor Technology and Planetary Exploration, Rutherfordstr. 2, D-12489 Berlin, Germany; juergen.nussbaumer@dlr.de.

Introduction: High resolution Viking images (orbit 724A, 14m/pixel) show evidence for ancient glaciation in parts of southeastern Elysium Planitia. While previous authors have mapped the materials as thin lacustrine and fluvial deposits [1], we present evidence for erosional and depositional processes associated with glacial environments. The previous ice sheet formed hummocky goundmoraines, eskers, and possibly pingos.

Geomorphology: Detailed geomorphological mapping of high resolution Viking Orbiter images reveals several features which can be attributed to glacial and periglacial processes in the southeastern part of Elysium Planitia (Fig. 1).

Ground moraines. The presence of a former ice sheet is indicated by hummocky terrain resembling terrestrial ground moraines. A sharp contact marks the boundary between the ice sheet and an adjacent yardang field.

Eskers. The ground moraine is locally overlain by mostly curvilinear features. They are interpreted as eskers, sinuous ridges of glacifluvial sand or gravel

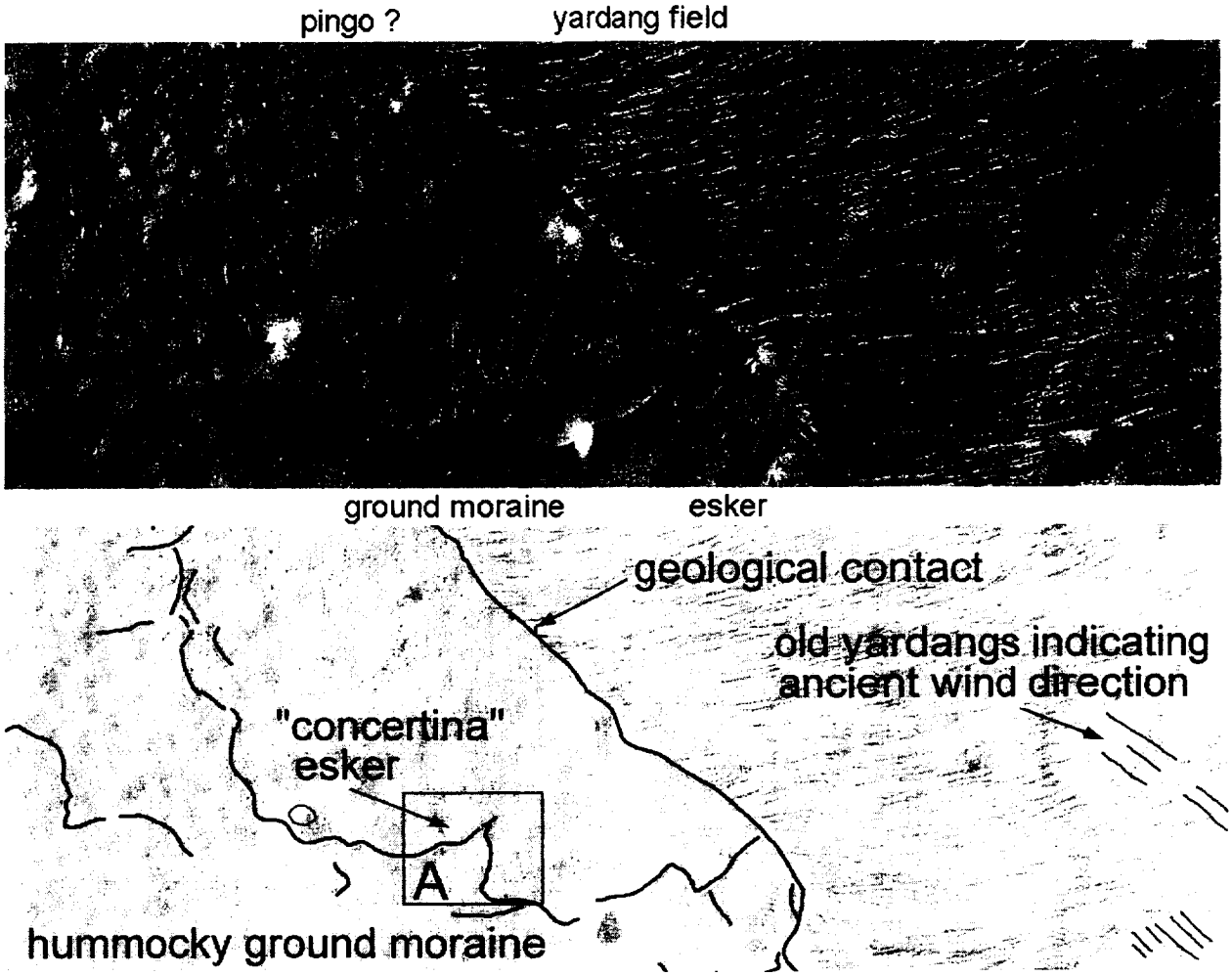

Figure 1: Image mosaic of Viking orbit 724A (14m/pixel; image width 60km, North is up, center at 207°W, -3°S) and geomorphological sketch map. Hummocky groundmoraines, eskers, and possibly pingos are evidence for former glaciation. The outlined box A marks the location of eskers deformed into a zigzag pattern typical for terrestrial *concertina eskers* (compare with box A' in Fig. 2).

formed as infillings of ice-walled rivers [2,3]. Locally, the sinuous pattern of the eskers (as seen in plan view) is changed into a jagged or zig-zag path. On Iceland, previously sinuous eskers have been shortened and crumpled into such a zigzag pattern by the advancing glacier snout (Fig. 2) [4,5]. These so-called *concertina eskers* are associated with *surging glaciers*, characterized by periodic changes in flow velocities over various timescales [6]. It is important to note that the surges are NOT triggered by climatic oscillations, but by oscillations in the internal workings of the glacier [7]. Therefore, although it is tempting to ascribe the former existence of a possible surging glacier on Mars to previous climatic changes, this assumption is not supported by terrestrial analogy.

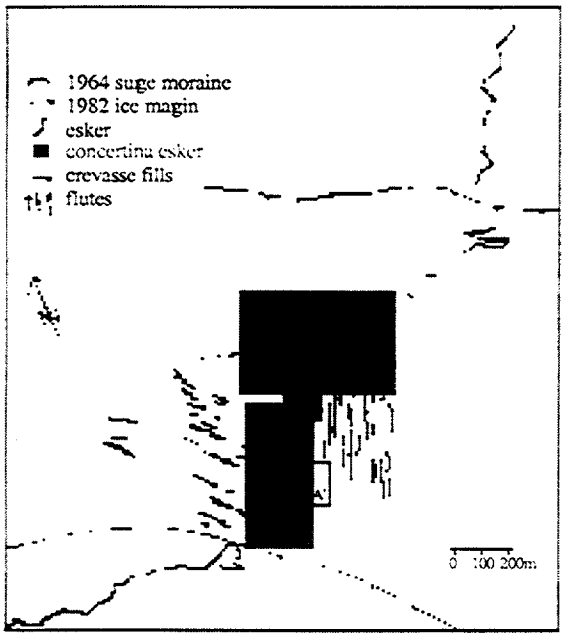

Figure 2: Sketch map of concertina eskers associated with the Bruarjökull glacier in Iceland. Eskers are deformed by the advance of the glacier snout. Note the similarity of the feature in the outlined box A' with the esker in box A of Fig. 1 (modified from [5]).

Pingos. Several circular hills are distributed on the ground moraine, partly characterized by depressions on their top. They are interpreted as pingos, ice-cored hills formed in periglacial environments on Earth by the intrusion and subsequent freezing of pressurized water or by the growth of ice lenses [2,3].

Boulder trains. Boulder trains are widespread on the ground moraine (Fig. 3). While they also occur in the lee of obstacles in large floods or downslope from outcrops on steep slopes, they can also be associated with glacial deposits [8]. There, they indicate the direction of ice movement during the last stage of glaciation [9].

Conclusions: Several landforms in southestaren Elysium Planitia suggest previous local or regional glaciation. The relatively young age (Amazonian, see [1]) and the geographic location near the equator bears important paleoclimatic implications. Further investigations (especially more detailed age determinations by crater counting and high resolution imagery by the *Mars Observer Camera* or future instruments) are required to confirm or reject the possibility of near equator glaciation in the comparably recent past of Mars.

References: [1] Scott, D.H. and Chapman, M.G. (1995) USGS Map I-2397. [2] Washburn, A.L. (1973) *Periglacial Processes and Environments*, Edward Arnold, London. [3] French, H.M. (1976) *The Periglacial Environment*, Longman, London. [4] Sharp, M. J. (1985) *Quaternary Research, 24*, 268-284. [5] Knudsen, O. (1995) *Quaternary Science Reviews, 14*, 487-493. [6] Benn, D.I. and Evans, D.J.A. (1998) *Glaciers and Glaciation*, John Wiley, New York. [7] Meier, M. F. and Post, A. S. (1969) *Canadian Journal of Earth Sciences, 6*, 807-819. [8] Lucchitta, B.K. (1998) *LPS XXIX*, 1287-1288. [9] Sugden, D.E., Glasser, N.F., and Clapperton, C.M. (1992) *Geografiska Annaler, 74A*, 253-264.

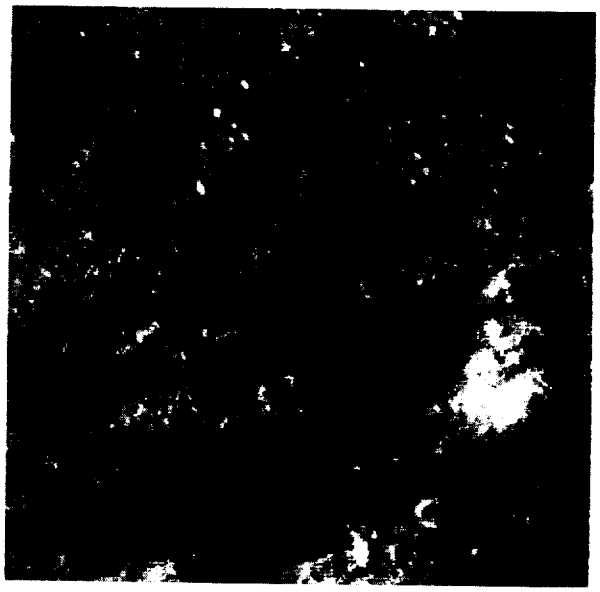

Figure 3: Boulder trains possibly related to a pulse of erosion at the end of the last glacial cycle when the ice was thin [9]. They also indicate ice movement from SE towards NW (topographic data from the *Mars Observer Laser Altimeter* show that topographic gradient is towards NW; Viking orbit 724A, width of image 10 km, North is up).

Possibilities of using MARSES instrument for long-term monitoring and subsurface studies in arctic and arid lands.

Y. R. Ozorovich[1] ,V. M.Linkin[1] ,W.D.Smythe[2] , B. Zoubkov[1], F. Babkin[1]

[1]Space Research Institute,Russian Academy of Sciences, 84/32 Profsoyuznaya st.,Moscow, 117810,Russia
Tel:7-095-333-3177;Fax:7-095-333-2177;e-mail: yozorovi@iki.rssi.ru.
[2] JPL/NASA,4800 Oak Grove Drive,Pasadena,CA 91109,USA; e-mail: wsmyth@spluvs.jpl.nasa.gov.

Introduction:

The MARSES is the sounding instrument developed of searching for groundwater, water-ice or permafrost layers existing in some depth under the visible surface in the dry lands of Mars. One of the more important challenges facing natural resource managers today is how to identify, measure and monitoring the cumulative impacts of land use decisions across space and time. The secondary task is to measure the soil properties of Martian subsurface, which includes porosity, electrical resistance of the liquid phase, thermal conductivity, temperature dependence. A main task of the MARSES monitoring system is to examine changes in the subsurface properties of local areas regolith on the Martian surface on the base of the database of various soil slices in terrestrial conditions.

Comparative investigation of Martian and Terrestrial frozen rocks

The main goal of the MARSES monitoring experiment, based on the MARSES instrument is a comparative investigation of Martian and Earth's cryolithozone (possible investigation of subsurface relics of martian life), drylands soil slices, and the interpretation of geophysical data of subsurface soil structure [5], including :

- theoretical development of comparative models of subsurface frozen dryland structure for typical rocks which formed martian cryolithozone in the mixture of poligonites and montmorillonites;
- development of the software package for detailed analysis of subsurface martian structure - porosity, electrical resistance of liquid phase, thermal conductivity, temperature dependence, which are in agreement with the interpretation of data obtained in the field testing and laboratory supporting measurements;
- possibility to study subsurface frozen water component using TEM instruments and induced polarization (IP) device in several areas which are close to martian conditions: Antarctic, Iceland, Hawaii (volcanic area), arid lands;
- improvements of hardware and software on the base of field studies results in order to use in the Earth conditions, including environmental and geophysical application, and future space experiments on the Martian surface.

Preliminary results of field studies in the Arctic area and at Sir Bani Yas Island.

Results of the field season in the Arctic area revealed the existence of strong surface layer with high induced polarization (IP) effect. On the basis of gained results we have formulated the complex program of frozen soil structures sounding during future field expedition in the Arctic area. Various instruments are proposed to be employed including TEM and DC techniques. The first field measurements on Sir Bani Yas Island (UAE) revealed the existence of thermodynamic balance between phase conditions of subsurface water, fresh and salted.

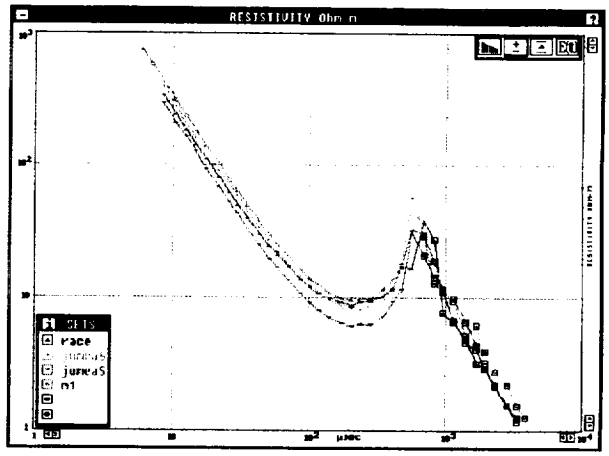

Figure 1 shows measurements on Sir Bani Yas Island, UAE

Controlling of this balance is an urgent task for operative monitoring subsurface system in drylands area in variuos regions of the world for long-term monitoring nature subsurface ecosystem.

Building of geographical slice using different instruments allows to obtain correct parameters for MARSES TEM in order to employ it in frozen soils sounding on the surface of Mars and for many applications for long-term monitoring and subsurface studies in the Earth's conditions.

References:

[1] Clifford S.M. (1993) *JGR, 98,* 10973–11016. [2] Toulmin P.,*et al,* (1977) *JGR,82,*4624-4634 [3] Fanale F.P. (1986) *Icarus, 67,*1-18.[4] Kuzmin R.O.,*et al,*(1988) *LPS Conf.XIX Abstracts,657-658* [5]Ozorovich Y.R.,*et al,*(1988) Tentative of e/m sounding (low-frequency) sounding cryolithozone of Mars, Preprint IKI, No.1477 [6]Ozorovich Y.R., *et al,*(1988) Microwave remote sensing of martian subsurface parameters, Preprint IKI,No.1531. [7] Ozorovich Y.R., *et al,* (1999) Mars Electromagnetic Sounding Experiment - MARSES, Proceedings of LPSC, March 15-19,1999.

AFTER THE MARS POLAR LANDER: WHERE TO NEXT? D. A. Paige, Dept. of Earth and Space Sciences, UCLA, Los angeles, CA 90095. dap@thesun.ess.ucla.edu.

Introduction: The recent loss of the Mars Polar Lander (MPL) mission represents a serious setback to Mars science and exploration. Targeted to land on the Martian south polar layered deposits at 76° S latitude and 195° W longitude, it would have been the first mission to study the geology, atmospheric environment and volatiles at a high-latitude landing site. Since the conception of the MPL mission, a Mars exploration strategy has emerged which focuses on Climate, Resources and Life, with the behavior and history of water as the unifying theme. A successful MPL mission would have made significant contributions towards these goals, particularly in understanding the distribution and behavior of near-surface water, and the nature and climate history of the south polar layered deposits. Unfortunately, due to concerns regarding the design of the MPL spacecraft, the rarity of direct trajectories that enable high-latitude landings, and funding, an exact reflight of MPL is not feasible within the present planning horizon. However, there remains significant interest in recapturing the scientific goals of the MPL mission. The following is a discussion of scientific and strategic issues relevant to planning the next polar lander mission, and beyond.

Volatiles and Atmospheric Measurements: MPL included the most sophisticated package of meteorology and volatile-sensing instruments ever flown. Its deployment at a high-latitude landing site during the late spring season would have provided the first opportunity to characterize global-scale weather patterns in the southern hemisphere, as well as measurements of the abundance of water ice and adsorbed water and carbon-dioxide in the soil, and water vapor in the overlying atmosphere. These would have been combined with orbital atmospheric sounding and general circulation models to provide a much better picture of the behavior and distribution of water on Mars. In-situ measurements like those intended by MPL are the only means of obtaining this type of information, and should definitely be repeated in future polar lander missions.

MGS Results: In 1995, when the concept for the MPL mission was originated, our understanding of Mars was based almost exclusively on then Viking and Mariner 9 datasets. Since that time, the Mars Global Surveyor (MGS) orbiter has provided significant new datasets which are revolutionizing our understanding of the planet. The MGS results in the north and south polar regions that have been published to date have been particularly exciting. MOLA topographic maps show that both polar caps have approximately 3 km of total relief; and have shapes that are consistent with those expected for large ice sheets. The MOLA data also suggest that both caps may have been significantly larger at some point in their past history [1]. The north polar cap lies in a regional topographic depression which may have once held an ancient ocean. The south polar deposits lie on a regional topographic high[2] , and show distinct evidence for glacial flow [1]. Both polar regions show evidence for the outflow of liquid water into surrounding depressions [2]. In the south, the flow of water can be traced into the Argyre basin, and then across the equator into the northern lowlands [3]. The high-resolution MOC images of the north and south polar caps show a diverse array of fresh surface textures on the residual caps and associated layered deposits which suggest that the polar regions are not presently being "mantled" by dust and ice as thought previously, but instead are being actively modified by processes that have as yet, been not defined [4,5]. In total, the MGS data suggest that the Martian polar regions we see today are the product of a complex climatological and hydrological history which may be intimately connected to the climatological and hydrological history of the planet as a whole.

Polar Landing Sites: MPL was the first Mars mission whose scientific strategy was driven by the desire to obtain detailed measurements at a pre-chosen landing site. Because of their extensive geographic extent, and the expected uniformity in their morphological characteristics, the south polar layered deposits represented an excellent target for the first polar lander mission. The north residual cap is another good example of a large, relatively homogeneous target. However, as we study the Martian polar regions in greater detail, it is becoming clear that to sample the true diversity of polar terrains, and to reconstruct the geologic and climatologic history they may contain, many more landings will eventually be required. In many cases, a precision landing with an error ellipse of less than 5 km would be required to enable detailed examination of specific features of great scientific interest, i.e. an exposure of layers or a suspected ancient outflow channel or esker deposit.

The Desirability of Landing Robustness and Mobility: One of the key new pieces of information that the MGS MOC images have provided, is that

polar terrains that appear to be smooth and homogeneous at 1000m scales, are definitely not smooth and homogeneous on 10 m scales. Figure 1 shows examples of high-resolution textures in the north and south polar regions revealed by MOC.

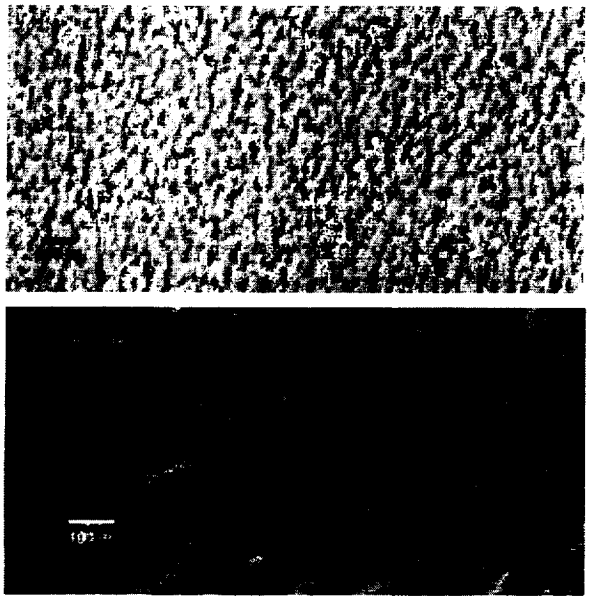

Figure 1. MGS MOC images of surface textures at the Martian north residual water ice cap (top), and south polar layered deposits (bottom). [6]

The implications of this new information are two-fold. First, a robust landing system will be required to ensure safe landings on most polar terrains. Second, a mobile traverse of on the order of 200m should be sufficient to sample the fine-scale diversity of most polar terrains.

Instrumentation: The MPL MVACS payload developed a number of new experimental approaches and technologies that were successfully demonstrated in testing. The use of a dexterous, multi-jointed robotic arm to obtain surface and subsurface soil and ice samples within a wide workspace appears to be a very flexible approach that can be adapted to a wide range of future mission scenarios. The use of Tunable Diode Laser Spectrometers (TDL) to measure the concentration of water vapor and carbon dioxide gas in the Martian atmosphere, and in evolved gases from heated soil and ice samples is a powerful and robust approach. Improvements in TDL technology in future mission should enable detailed *in-situ* characterizations of the isotopic composition of Martian water and carbon-dioxide. The use of a focusable camera mounted on the robotic arm that can obtain close-up images of the surface and samples is also a very powerful technique that can be extended to true microscopic resolution on future payloads.

Future polar lander payloads should also include newly-developed instruments which could take advantage of the sample acquisition and analysis capabilities of the MVACS payload in a complimentary manner. For example, the addition of an organics detection experiment could significantly extend the search for near-surface organics begun by the Viking landers during the 1970's to environments that could have a greater potential for the preservation of organics.

Conclusions: While the near-term prospects for recovering the scientific objectives of the MPL mission are uncertain, it is clear that an integrated scientific strategy to study Mars' climate, resources and life must include detailed study of the polar regions at multiple landing sites. The MGS results indicate that both the north and south polar regions contain a number of sites of high-scientific interest, and that with foreseeable improvements in our capabilities for robust, precisely-targeted landers, these sites should be accessible to the next generation of Mars landers. The scientific strategy advocated here is basically an extension of that originally employed for MPL. It starts with the selection of a specific landing site of high-scientific interest, followed by the design of a flexible integrated payload package that is capable of characterizing its environmental conditions, the abundance and behavior of its volatiles, and the fine-scale composition and geology of its deposits at and below the surface. While the return of samples from polar sites may result in significant additional science return, we are presently very far from a situation where sample return is *required* to make further scientific progress. Furthermore, because of the significant expense and risks associated with sample return, the non-zero probably of "negative progress" (i.e. mission failure) should be a significant factor in the decision making process. When viewed from a larger perspective, the opportunities and challenges facing future polar lander missions have a great deal in common with all Mars missions.

References: [1] Head, J. W. (2000) *LPS XXXI.* [2] Smith, D. et al. (2000) *LPS XXXI.* [3] Parker, T. J., Clifford S. M. and Banerdt, W. B. (2000) *LPS XXXI* [4] Malin, M. C. and Edgett, K. S. (2000) *LPS XXXI.* [5] Thomas etal. (2000) *LPS XXXI.* [6] MSSS Website (http://www.msss.com)

A BRIEF SUMMARY OF THE GEOMORPHIC EVIDENCE FOR AN ACTIVE SURFACE HYDROLOGIC CYCLE IN MARS' PAST. T. J. Parker, Jet Propulsion Laboratory, California Institute of Technology, 4800 Oak Grove Dr., Pasadena, CA 91109 (timothy.j.parker@jpl.nasa.gov,).

Origin and Maintenance of Martian Basins:

Because Mars is just over half the Earth's diameter (about 6800km), it does not exhibit global tectonism on a scale comparable to Earth and Venus. But because it is still a large body compared to Mercury and the moon, it has had an atmosphere and climate over the history of the solar system. This is why Mars has been able to retain surfaces produced both through volcanic and climatic processes that are intermediate in age between volcanic surfaces on the moon and Mercury and both types of surfaces on Venus and Earth. For the purposes of this discussion, this has important implications about the origins and evolution of topographic depressions that potentially may have contained lakes.

Tectonism is probably the most important process on Earth for producing closed depressions on the continents, and is clearly responsible for maintenance of the ocean basins through geologic time. This is probably also true for depressions in the highland terrains and lowland plains of Venus. On Mars, however, tectonism appears limited to relatively small amounts of regional extension, compression, and vertical motion largely due to crustal loading of the two major volcanic provinces - Tharsis and Elysium

Impact craters and large impact basins (including all or parts of the northern plains) are clearly more important sites for potential lake basins on Mars, though they were likely more important on Earth, and Venus as well, during the period of heavy meteorite bombardment throughout the solar system prior to 3.5Ga. Comparisons of the relative importance of other formative processes on Mars with those on Earth are less obvious, and some may be quite speculative, since our understanding of the early Martian environment is still rather limited.

Sedimentary Basins?:

The primary sources of influx into the northern plains are the circum-Chryse outflow channels, which include the largest channel systems on Mars, and several modest-size outflow channels and valley networks west and south of the Elysium volcanic complex. In addition, many valley networks terminate at the boundary between the southern highlands and northern plains, though the basin continues its gentle, regional gradient far beyond the mouths of these networks. This may suggest a common base level for these channels, or reworking of their distal reaches by a later highstand. The Chryse channels alone are large enough to have produced several large lakes, even a sea or ocean, within the northern plains over a very short span of time.

In the southern highlands, several basins on the order of several tens to a few hundred kilometers across, and parts of Valles Marineris have been found to contain remnants of former alluvial or lacustrine sedimentary deposits. Many of these basins were simply in the path of short-term catastrophic floods, and thus may not have contained lakes for very long. The thick Valles Marineris layered deposits occupy deep tectonic and collapse depressions in the Martian crust, and appear to have been fed by groundwater rather than overland flow. The deposits are on the order of kilometers thick and appear finely laminated (in high-resolution Viking Orbiter images), and so probably indicate the presence of lakes for long periods of time.

Many highland basins contain peculiar, hummocky deposits that have been interpreted as the eroded remnants of lake sediments. The largest highland basins, Argyre Planitia (800km interior diameter) and Hellas Planitia (1500km interior diameter) appear to contain massive accumulations of layered sediments that are now being exposed by eolian deflation. Those in Argyre may be on the order of hundreds of meters or more thick, whereas those in Hellas appear to have been as much as a few kilometers thick.

Channels as Sources for Ponded Water on Mars:

Outflow channels and valley networks on Mars are generally described as having originated from underground sources, by the catastrophic failure of a subterranean aquifer or by groundwater sapping, respectively. The best known outflow channels can, in fact, be traced back to a collapsed terrain source. Many valley networks have theater-like headward terminations which suggest flow of groundwater atop a permeability boundary at depth, similar to sapping valleys in the Colorado Plateau. Nirgal Vallis is an often-cited example of this type of network.

However, a number of outflow channels and valley networks do not exhibit subterranean sources. Two of the largest of these, Mawrth Vallis and Ma'adim Vallis, are problematic. Mawrth Vallis may indeed have had an underground source that has subsequently been buried by ejecta from the crater Trouvelot (at 26°N lat., 13° lon.). Ma'adim Vallis may not

be a true outflow channel at all, as it exhibits many characteristics of large valley networks - such as numerous tributaries. If it is a "valley network" rather than an outflow channel, then it may be the largest on Mars - requiring an impressive groundwater system to carve it through sapping alone.

A number of relatively small-scale outflow channels and "stem" valley networks in the cratered uplands terminate headward at the surface, usually within moderate-size inter-crater plains regions (a few tens of thousands of square kilometers in area) that must have contained shallow lakes. In some cases, these lakes may have been fed by other channels further upslope, themselves fed through groundwater sapping or atmospheric precipitation, or both.

E.G., Mangala Valles:

Mangala Valles is a large outflow channel (about 850km long) in the eastern Memnonia region of Mars. The channel heads within a graben in Memnonia Fossae at 18.5°S latitude, 149.5° longitude. Mangala Valles is separated from Arsia Mons-derived volcanic plains by one of these ridges (from about 9°S to 20°S latitude, 147° longitude). The lower reaches of Mangala Valles begin where the channel crosses the remnant of another, less prominent northeast trending ridge at 9.5°S latitude, 151.5° longitude. South of this ridge the channel is a broad, relatively shallow system as much as 75km or more wide cut into a smooth plains surface. North of this ridge, Mangala Valles bifurcates into two large, incised channels, Mangala Valles to the north and Labou Vallis to the northwest. Northern Mangala Valles is a complex system of separate anastomosing channels ranging from less than 10km to more than 40km in width. Labou Vallis is a much less complicated single channel, ranging from about 5km to 40km wide.

An alternative interpretation to the graben source of Mangala Valles suggests that this plains uniis comprised of sediments deposited in a temporary lake which formed upstream from the northeast-trending ridge for two reasons. (I) Headward erosion escarpments within the Hchp unit (from about 10°S to about 16.5°S latitude on the east side of Mangala) are reminiscent of knick-point or cataract development in a rapidly drained lake. Current scours upstream from craters at 10.5°S latitude, 151° longitude and at 15°S latitude, 148.5° longitude, and others also suggest flow of water over the Hchp surface, rather than derived from the subsurface at the edge of the unit. (II) Spillways from the Hchp unit north across the heavily cratered terrain appear to have developed in at least two places prior to breaching of the ridge.

In this proposed flood scenario, then, the "true" source of the Mangala flood is the obstructing ridge at 9.5°S latitude, 151.5° longitude, which acted as a natural earthen dam that failed catastrophically. This explains why the most intense scouring and bifurcation of the system occur in this vicinity and downstream, where the flood's erosive capability was greatest. To the south (headward direction), this scouring became progressively less intense as the lake drained. The apparent source of the channel, the graben in Memnonia Fossae, therefore represents the point at which the lake level had dropped so that scouring of the bed, and subsequently the flood, ceased.

Where did the lake come from? The smooth plains surface extends from 9.5°S to almost 40°S latitude in the western hemisphere geologic map (Scott and Tanaka, 1986). I have identified a narrow sinuous channel, over 500km long and up to 1km wide, that appears to have originated in the vicinity of the terminus of Arsia Mons-derived volcanics to the east. This channel begins near 35°S latitude, 141° longitude, flowed initially southwestward for about 300km, then turned north within the Hpl_3 unit, eventually fading at about 34°S latitude, 147° longitude. It becomes visible again at 31°S latitude, 149.5° longitude, and "flows" an additional 50km or so northward. The plains between these two reaches comprise an area of approximately 40,000km^2, and may consist, in part, of lake sediments. A third reach can just be detected at 38.5°S latitude, 150.5° longitude, flowing north approximately 100km to 27°S latitude, 152° longitude, where it finally fades into the plains. The total length of this channel appears to be greater than 1500km. I would place the southern limit of the proposed lake at or near this latitude. The area of this lake would have been on the order of 60,000km^2. Assuming an average depth of 10-100m yields a total volume of 600-6000km^3, a rather modest volume for a Martian flood channel.

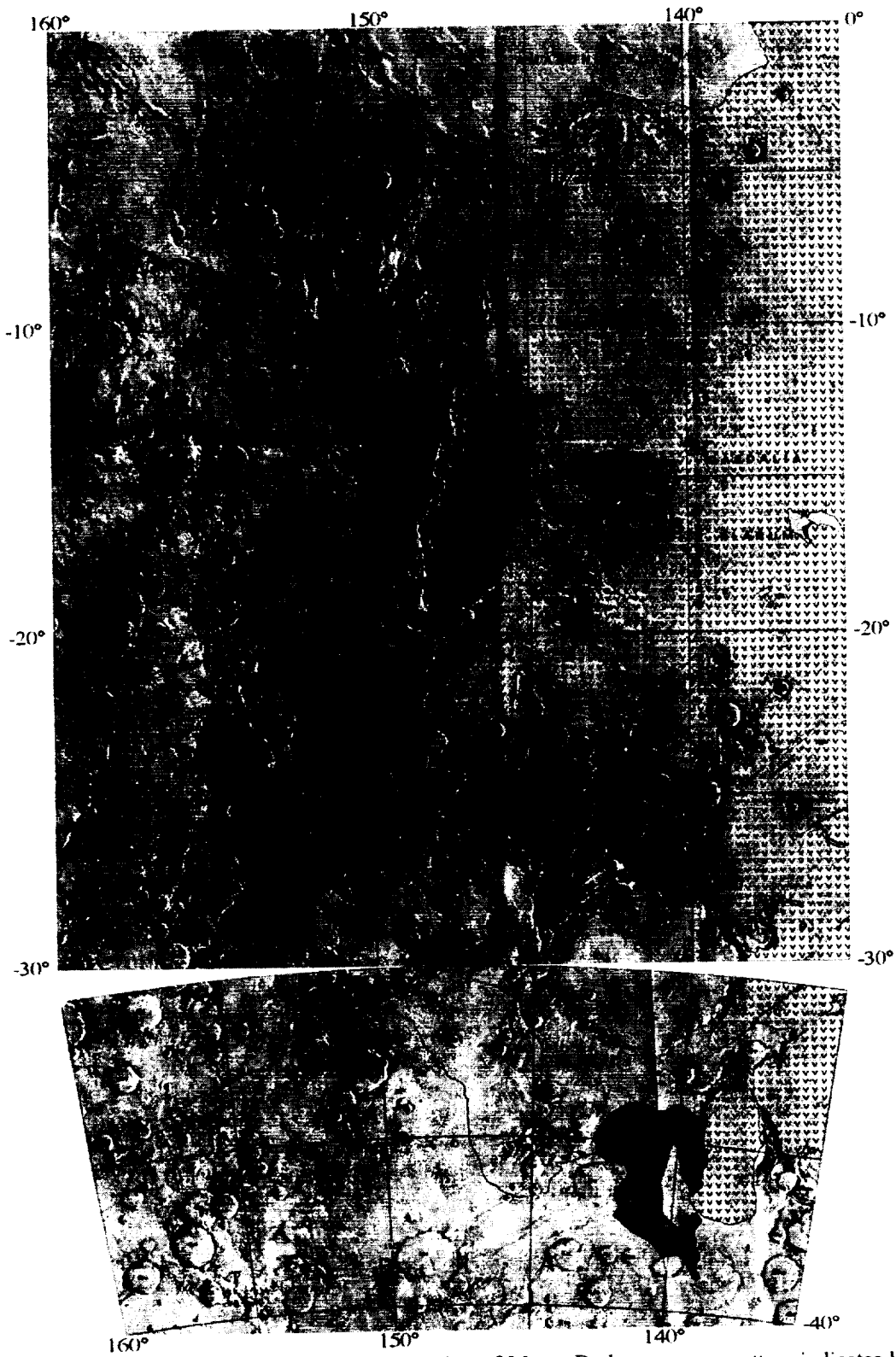

Figure 1: Shaded relief map of the Mangala Valles region of Mars. Dark gray wave pattern indicates locations of proposed source lakes. "V" pattern indicates extent of Arsia Mons Volcanic plains. Small, sinuous "source" channel is indicated by a thin black line connecting the southernmost lake with Mangala Valles.

ORBITAL VARIATIONS OF THE RHEOLOGY AND SUBLIMATION OF THE MARTIAN POLAR LAYERED DEPOSITS: GLACIOLOGICAL IMPLICATIONS. Asmin V. Pathare and David. A. Paige, UCLA (Earth and Space Sciences, 595 Young Drive East, Geology Rm. # 3806, Los Angeles, CA 90095-1567; avp@ucla.edu)

Introduction: Martian obliquity deviates aperiodically from its current Earth-like value of 25°, often surpassing 45° within the last 20 Myr [1]. We calculate the effects of the corresponding variations in insolation upon first the rheology and then the sublimation of the Polar Layered Deposits (PLD). We then consider the glaciological implications of this simultaneous increase in flow and ablation rates.

Rheology: Our model of present-day PLD flow rates improves upon prior work [2] by inputting driving stresses derived from Mars Orbiter Laser Altimeter (MOLA) data [3] and incorporating recent laboratory-measured rheological constants for both grain boundary sliding (GBS) and basal dislocation creep [4]. Although the direct effect of dust is to inhibit flow, its presence in the PLD increases density, lowers thermal conductivity [5], and precludes dynamic recrystallization [2], resulting in greater driving stresses, higher subsurface temperatures, and smaller ice grain sizes, respectively, all of which enhance GBS flow. We find that current flow velocities at the center of the north polar cap can exceed 3 cm/yr, which is fast enough to provide the rapid resurfacing implied by the extremely young north PLD surface age of < 100 Kyr [6].

To extend our flow model to other obliquities, we use a 1-D radiative-convective model to calculate annual average surface temperature (T_{AV}) as a function of obliquity (θ). We then input the orbital history over the last 20 Myr [1], and the corresponding $T_{AV}(\theta)$, into a 1-D subsurface conduction model to calculate basal PLD temperatures since 20 Ma. Assuming constant driving stress, we find as expected that total integrated flow in the north greatly increases during all recent excursions to high obliquity. Whether such flow also occurred in the south depends on the persistence of the south polar cap's yearlong CO_2 frost cover, which presently keeps T_{AV} at 148 K, thereby precluding the flow of any underlying H_2O ice. We show that if the south polar cap maintains this CO_2 frost cover up to θ = 35°, then enhanced flow caused by high obliquity epochs would have last occurred in the south 9 Ma, which is remarkably consistent with the south PLD surface age of 14 ± 7 Ma [6].

Sublimation: Our 1-D radiative-convective model of high-obliquity PLD loss rates improves upon prior work [7] in three main respects: a quasi-random Voigt model is employed to more accurately assess the water vapor greenhouse heating initiated by increased sublimation; the effects of atmospheric dust are incorporated; and idealized sublimation into a dry atmosphere is not assumed. We subject several representative PLD surfaces (described by albedo *a*, thermal inertia *ti*, latitude *lat*, and surface slope α) to the full range of orbital variations (involving obliquity θ, eccentricity *e*, argument of perihelion ω).

We find that for average north PLD surface conditions (*a*=0.35, *ti*=600 J/m^2/s$^{1/2}$/K, *lat*=85°N, α=0°), maximum sublimation rates for a pure ice deposit vary from mm/yr for present-day conditions (θ=25°, e=0.09, ω=251°) to m/yr at high obliquity (θ=45°, e=0)-- a three order of magnitude increase. However, the PLD probably contain some dust, which should form a lag deposit that inhibits further sublimation [7,2]. We will consider the evolution of such a lag deposit as a function of obliquity. Ablation may also be enhanced from the steep troughs in the north PLD; hence we will also consider the effects of surface slope on sublimation for various orbital configurations.

Implications: The origin of the layering characteristic of the PLD is commonly ascribed to orbitally-dependent variations in the relative deposition rates of the ice and dust presumed to comprise these layers [7]. We propose an alternative "Milankovitch" model involving a glaciological origin for the layers of the PLD. We will show that even for constant (i.e., obliquity-invariant) ice/dust relative accumulation ratio, layering can still result from the increased flow and ablation brought about by orbitally-induced changes in the rheology and sublimation of the PLD.

References: [1] Touma J. and Wisdom J. (1993) *Science, 259,* 1294–1297. [2] Hofstadter M.D. and Murray B.C. (1990) *Icarus, 84,* 352-361. [3] Zwally H.J. and Saba J.L. (1999) *5th Intl Mars Conf.* [4] Durham W.B. et al. (1997) *JGR, 102,* 16293-16302. [5] Clifford S.M. (1993) *JGR, 98,* 10973-11016. [6] Herkenoff K.E. and Plaut J.J. (2000) *Icarus, 144,* 243-253. [7] Toon O.B. et al. (1980) *Icarus, 44,* 552-607.

FIELD INVESTIGATIONS OF ICELANDIC JÖKULHLAUPS AS AN ANALOG TO FLOODS ON MARS. James W. Rice Jr. (1), Andrew J. Russell (2), Fiona S. Tweed (3), Óskar Knudsen (4), Matthew J. Roberts (2 & 3), Philip M. Marren (2), Richard I. Waller, E. Lucy Rushmer (3), Helen Fay (2), and Timothy D. Harris (5), (1) Lunar and Planetary Laboratory, University of Arizona, PO Box 210092, Tucson, AZ 85721-0092, USA (jrice@lpl.arizona.edu); (2) School of Earth Sciences & Geography, Keele University, Keele, Staffordshire, ST5 5BGl; (3) Division of Geography, Staffordshire University, College Road, Stoke-on-Trent, ST4 2DE; (4) Klettur Consulting Engineers, Bíldshöfda 12, IS 112 Reykjavík, Iceland; (5) Department of Earth & Environmental Sciences, University of Greenwich, Medway University Campus, Chatham Maritime, Kent, ME4 4TD.

Jökulhlaups are believed to play a dominant role in the evolution of proglacial outwash plains in many parts of the world and strongly influence the morphology and dynamics of glacier margins. Improved understanding of the characteristics and geomorphic effectiveness of such high magnitude events is invaluable for understanding former ice sheet dynamics, processes and rates of deglaciation and predicting the environmental impacts of future events. Although the characteristics and immediate geomorphic impact of storage-release events such as the November 1996 jökulhlaup at Skeidarársandur have been investigated, few studies have focussed on the impact of volcanically-generated jökulhlaups released directly into the proglacial zone. Spectacular jökulhlaup induced fracturing and sediment fills within Skeidarájökull illustrate the importance of jökulhlaups as a mechanism of sediment entrainment into glaciers and ice sheets.

Seismic activity within the Katla volcanic system underneath the Myrdalsjökull ice cap during late July 17th and early July 18th 1999 was accompanied by the development of a 1.5 km diameter, 50 m deep depression in the accumulation area of Sólheimajökull. At the same time a jökulhlaup was released from the snout of Sólheimajökull, destroying power lines, splashing over a bridge on Iceland's main road and transporting ice blocks 8 km into the sea. The jökulhlaup at Sólheimajökull in July provides a superb opportunity to examine the immediate impact of a sudden magmatically-triggered event on a glacier and sandur which are thought not to have experienced an event of this size since 1357 AD.

This paper aims to: (1) to describe flood flow conditions (2) identify the immediate impact of the jökulhlaup on the glacier and (3) identify the immediate impact of the jökulhlaup on the 1 km wide, 8 km long area flanking the Jökulsá á Sólheimasandi between the glacier and the sea. Field data collection was carried out on the day of the flood and in the following three weeks.

Flood wash limits and river channel cross-sections were surveyed using an EDM allowing the calculation of peak flood discharge. Within flood sedimentary structures, surface grain-sizes and ice block grounding structures were measured.

The jökulhlaup burst from the glacier at a number of locations ranging from supraglacial fracture outlets up to 2 km from the glacier snout to marginal conduit outlets up to 4 km up glacier of the snout. Jökulhlaup flows exited the glacier snout via two main conduits. Supraglacial jökulhlaup outlets consisted of multiple up-glacier dipping fractures at a variety of angles. Grey silt sands were deposited within the fractures and across the glacier surface forming a distinctive patch. Marginal outlets on the western margin of the glacier supplied boulders up to 5 m in diameter with flows subsequently entraining even larger boulders up to 10 m in diameter from older ice-marginal sediments. Lateral outflow resulted in the temporary storage of jökulhlaup water within former ice-dammed lake basins. Sedimentation within these basins consists of deposition of sands and silts with a series of ripple-marks occasionally sliced through by iceberg keel marks. Localised deltaic deposition occurred where outflow entered these temporary storage locations. At the glacier snout flows from the western outlet were estimated to have a peak discharge of between 4000 and 6000 m^3s^{-1} allowing the transport of boulders up to 11m in diameter. The new outwash fan deposited in front of the western outlet ranges in thickness from 6 m proximally to less than 1 m distally. Deposition of ice blocks, boulders and finer-grained matrix occurred simultaneously resulting in

the post flood development of kettle holes and large-scale obstacle marks. Sedimentary structures indicate flows were hyperconcentrated probably during the rising stage of the flood. The eastern outlets at the glacier snout had a much lower discharge of approximately 1000 m^3s^{-1}. Sediment from the main eastern conduit consisted of better-sorted, finer-grained deposits containing fewer ice blocks.

The overall geomorphic impact of this flood was confined to a main proglacial channel incised into older jökulhlaup deposits. Large amounts of sediment are thought to have been transferred directly from the glacier to the sea, although zones of localised deposition occur in front of the western outlet and within the ice-marginal lake basins. The sedimentary characteristics of this event will be compared with those recorded within the newly exposed sedimentary record of Sólheimasandur.

Although the characteristics and immediate geomorphic impact of storage-release events, few studies have focused on the impact of volcanically generated jökulhlaups released directly into the proglacial zone. Spectacular jökulhlaup induced fracturing here at Sólheimajökull illustrate the importance of jökulhlaups as a mechanism of sediment entrainment into glaciers and ice sheets. This unexpected sudden flood had a significant impact on both glacier and proglacial zone, providing a sobering reminder of the ongoing potential at this site for sudden outbursts.

Martian Flood Landforms

The successful landing of Mars Pathfinder near the confluence of Ares and Tiu Valles on July 4, 1997, has prompted new interest in understanding the nature of the geomorphology of the outflow channels around the margins of the Chryse Basin. This portion of Chryse Planitia exhibits a very rich and complex history. The regional geomorphology displays a comprehensive collection of both erosional (streamlined islands, longitudinal grooving, fluvially modified impact craters and associated ejecta blankets, terraces) and depositional landforms (smooth channel deposits, deltas, and block fields).

The Mars Pathfinder landing site is replete with landforms and textures that indicate a rich complex fluvial history on both a regional and local scale. On a regional scale the geomorphology displays a comprehensive collection of both erosional and depositional landforms created by multiple catastrophic floods. Locally we have noted the existence of terraces, perched boulders, abundant imbricated clasts, shadow zones, pebble clusters, and percussion marks. All of this evidence provides strong credence to the hypothesis that catastrophic floods formed this landscape.

Surprisingly, the floors of the outflow channels are heavily cratered by small craters (< 100 m diameter). It is proposed here that some of these small craters may actually be kettle holes. Deposition and subsequent melting of stranded ice blocks, which were transported by the floods, forms kettle holes. Melting of the stranded and buried ice blocks leads to the development of a pitted outwash plain, similar to that formed by jokulhlaups in Iceland. A common and significant feature of many jokulhlaups is the transport of numerous large ice blocks into the proglacial meltwater system and outwash plains. Deposition and subsequent melting of these stranded debris rich ice blocks leads to the development of kettle holes and pitted outwash plains. The surface of Myrdalssandur, southern Iceland, is pockmarked with a large number of ring structures with rims up to 7 m high and over 40 m in diameter.

MESOSCALE SIMULATIONS OF MARTIAN POLAR CIRCULATION: II, NORTH POLAR WATER TRANSPORT. M. I. Richardson, and A. D. Toigo, Division of Geological and Planetary Sciences, MC 150-21, California Institute of Technology, Pasadena, CA 91125, mir@gps.caltech.edu, toigo@gps.caltech.edu

Exchange of water with the residual water ice cap at the northern pole is likely the primary mechanism controlling the water cycle and the global abundance of atmospheric water [1, 2]. The mechanics of this exchange lie in the mixing of water between the polar airmass immediately adjacent to the cap and the airmasses at lower latitudes. To date, the most detailed models of these transport processes have been undertaken with global three-dimensional models [2, 3]. However, such models are least valid in these regions due to the topology of their construction. For example in grid-point models, grid points evenly spaced in longitude become progressively more tightly packed in physical separation. This necessitates filtering of dynamical fields, which degrade and modify the circulation.

Mesoscale models represent an improved tool with which to investigate the polar circulation. They are designed to simulate limited domains and can be arbitrarily centred, in this case on the pole, eliminating topological problems common to global models. The only previous mesoscale study of northern polar water transport is described by [4], who examined aspects of cap edge water transport and localized water cold trapping. However, two-dimensional models, such as that used by [4], are inherently of limited utility for modeling transport due to their inability to treat the true three-dimensional complexity of atmospheric mixing processes (which are of crucial importance even in the global models).

We have adapted a fully three-dimensional mesoscale model to examine Martian polar water transport. The model and conversion are described by [5]. The model is based on the PSU/NCAR Mesoscale Model version 5 (MM5) and is fully adapted to Mars. The northern polar cap is represented by Mars Orbiter Laser Altimeter topography [6], and Viking Infrared Thermal Mapper albedo and thermal inertia as reprocessed by [7]. Water ice is prescribed to exist everywhere that the albedo is above a value of 0.4. Exchange of water between the surface and atmosphere is parameterized using the [8] surface flux scheme. Water transport in the atmosphere is implemented using the MM5 advection and diffusion schemes. Exchange of water between the vapour and ice phases in the atmosphere is implemented assuming instantaneous conversion at saturation to and from fixed ice particle sizes. More detailed microphysics may be implemented in the near future. Boundary and initial conditions for the simulations, including the spatial varying fields of atmospheric dust and water are derived from General Circulation Model (GCM) simulations with the Geophysical Fluid Dynamics Laboratory (GFDL) Mars GCM [9, 2, 10].

We will present results comparing the transport fluxes of water between the northern polar- and midlatitudes as simulated by the Mars MM5 and Mars GCM. We will describe the dominant modes of atmospheric transport, and comment on the implications for the water cycle control picture described by [2].

References: [1] Jakosky B. M. (1983) *Icarus, 55,* 19-39. [2] Richardson M. I. and Wilson R. J. (2000) this volume. [3] Houben H. H. et al. (1997) *JGR, 102,* 9069-9084. [4] Siili T. et al. (1999) *Bull. Am. Astron. Soc., 31,* 1147. [5] Toigo A. D. and Richardson M. I. (2000) this volume. [6] Smith D. E. et al. (1998) *Science, 279,* 1686-1692. [7] Vasavada A. R. et al. (2000) *JGR, 105,* 6961-6970. [8] Ingersoll A. P. (1970) *Icarus, 78,* 972-973. [9] Wilson R. J. and Hamilton K. (1996) *J. Atmos. Sci., 53,* 1290-1326. [10] Wilson R. J. et al. (2000) this volume.

CONTROL OF THE MARTIAN WATER CYCLE BY THE NORTHERN POLAR ICE CAP. M. I. Richardson[1] and R. J. Wilson[2], [1]Division of Geological and Planetary Sciences, MC 150-21, California Institute of Technology, Pasadena, CA 91125, mir@gps.caltech.edu, [2]Geophysical Fluid Dynamics Laboratory, Princeton, NJ 08542, rjw@gfdl.gov

Introduction: In order to undertake credible studies of the Martian climate at other epochs, one requirement is a mechanistic understanding of the processes controlling the water cycle. This need arises from the increasing role of atmospheric water ice and vapour as radiatively active species as global atmospheric water abundances increase. Further, a key motivation for modeling past climates is the need to understand temporal variations in the amounts, state, and locations of water. We have investigated the processes controlling the water cycle with the Geophysical Fluid Dynamics Laboratory (GFDL) Mars General Circulation Model (GCM) [1]. These simulations suggest that primary parameters controlling current global atmospheric water abundance are the albedo and thermal inertia of the northern residual water ice cap, which in turn will be controlled by the macro- and microphysical properties of the ice.

Model: The GFDL Mars GCM as used in this study simulates the circulation of the Martian atmosphere within a global domain with a horizontal resolution of 5° of latitude by 6° of longitude, and with 20 levels between the surface and roughly 85 km. The model includes dynamic and radiatively active dust, and a CO_2 cycle including the effects of seasonal CO_2 ice albedo. The water cycle includes a prescribed northern residual water ice cap between 80°N and the pole. Sublimation of vapour from the ice cap is parameterized using the Ingersoll [2] scheme, which treats turbulent and buoyant vapour transport. Within the atmosphere, vapour is transported by the model-resolved winds and by the same subgrid-scale diffusion as applied to temperature and momentum. The vapour can freeze in the atmosphere when saturation is reached in a given grid box. The resulting cloud ice is transported using the same treatment as vapour, save for the additional term associated with gravitational settling. Water ice can form on the surface as a result of ice precipitation or supersaturation of the lowest atmospheric level. When sufficient ice has settled, the albedo of the grid box is increased to 0.4 providing an albedo feedback mechanism. In some simulations we also employ a treatment of subsurface diffusion and adsorption of water. The two level scheme developed by Houben et al. [3] is used in these cases.

Summary of Results: A general pattern of behaviour emerges from all of our simulations of the water cycle. When the cycle has equilibrated, two pulses of vapour occur each year. The first, at roughly L_s=90° (northern summer solstice) is associated with sublimation from the northern residual ice cap. Vapour from this pulse is conveyed to the southern hemisphere, where it freezes and becomes incorporated in the southern seasonal cap. The second pulse of vapour occurs near southern summer solstice, when the seasonal cap sublimes. This vapour is more vigourously transported to the winter cap than during northern summer, resulting in a shorter-lived southern hemisphere vapour peak. This behaviour is consistent with observations from the Viking Mars Atmospheric Water Detector (MAWD) for northern summer, and roughly consistent with southern summer observations, although the data from that season are badly degraded by the occurrence of two global dust storms.

The modeled water cycle involves a significant "sloshing" of water between the seasonal ice caps. The amount of water involved in the sloshing (seasonal ice plus vapour) is roughly five times larger than the maximum globally integrated vapour content ($\sim 2 \times 10^{15}$g). The amount of vapour in the vapour phase at any moment depends on the competing rates of sublimation, transport, and condensation. The situation is more complicated if an adsorbing regolith is active, as some of the subliming water is trapped temporarily in the regolith. However, the activity or inactivity of the regolith does not significantly modify the mechanics of the water cycle. We find that the main effect of an active regolith is to modify the timing of vapour injection slightly and to slow the speed with which the model water cycle equilibrates. The latter effect results from the time needed to adjust the large amounts of water in the seasonal regolith reservoir to polar forcing. The former effect is illustrated by comparing southern summer vapour evolution with and without active regolith. With an inactive regolith, vapour sublimed from the seasonal cap appears immediately in the atmosphere as a rather larger pulse and is rapidly transported north. With an active regolith, some of the vapour is taken up as regolith adsorbate reducing the size of the pulse. As the vapour is transported northward, the reduction in vapour partial pressure releases adsorbed water from the regolith and the regolith adsorbed water inventory relaxes to the pre-seasonal cap release levels. The net effect of the regolith is simply to smooth out the vapour pulse.

Equilibration of the water cycle, while never fully complete due to inevitable net loss to the southern residual CO_2 ice cap, is accomplished in a rather straight forward manner. The mechanism is most easily understood by considering the annual cycle to consist of two parts, depending on whether the northern residual water ice cap is active (subliming) or not. During the "active" season (L_s=90°-130°), the rate of sublimation and hence the amount of vapour injected into the system depends on two factors: the cap temperature and the efficiency of off-cap transport. (As the

atmosphere is never fully saturated - except at low levels over the cap, where temperatures are strongly coupled to the cap surface temperature - the air temperatures are unimportant, except through coupling to transport.) Unless there is strong, secular accumulation of water in the regolith, only the southern residual cap can act as an annual average sink for water, which itself cannot accumulate more than ~10^{14}g of water annually due to the difficulty of conveying water efficiently to such a small portion of the Martian surface. Thus, almost all the water must return to the northern cap. The amount returning to the northern cap depends on the vigour of atmospheric mixing and on the gradient of vapour between the northern pole and the topics/mid-latitudes. The cycle works as a strong negative feedback system as there is - to first order - a separation of dependencies between outflow and inflow. For example, if too much vapour accumulates in the atmosphere, the return flow is enhanced, but the outflow remains nearly fixed. An important consequence is that if annual average cap temperatures increase (decrease), due to increased (decreased) obliquity, the global average vapour amount will increase (decrease) to some new stable level. This would not be the case if global vapour abundances were controlled by atmospheric saturation (as suggested by [4]) or by regolith buffering (as suggested by Houben et al. [3]). The controlling role of ice cap surface temperatures makes backward integration of the climate/water cycle problem (how did the water cycle differ in previous ages?) more tractable as errors in poorly understood regolith properties and atmospheric pressure and aerosol loading are de-emphasized (the latter are still important due to the effect on transport, but the transport dependency on air temperature predictions is far weaker than that of the water phase relationship).

Prerequisites for Paleo-Climate Studies: Significant work remains to be done before simulations of previous water cycle behaviour can be undertaken with any physical basis. Specific tasks remain validation of GCM water transport in the polar regions against models which better represent polar circulation (see [5]); validation of GCM global transport efficiencies against spacecraft data; incorporation of a radiative heating scheme which treats the increasingly important radiative impacts of water vapour and ice; incorporation of more realistic water ice microphysics and other cloud processes in order to assess changes in the role of clouds (see [6]); and, treatment of the processes controlling the injection of dust into the atmosphere. We are working on tasks 1, 3, and 4 at present. Task 5 likely will take longer to resolve, and will likely remain a model free parameter for some time. Task 2 will ultimately limit the utility of climate models and any attempt to quantitatively investigate climate and climate cycles coupled to polar processes and geology. Although MGS TES and instruments on Mars Express will aid in assessing the mixing behaviour of the atmosphere, significant progress requires multi-annual, three-dimensional mapping of temperature, dust, and water vapour from a regular, operational orbit of the kind promised by the PMIRR/MARCI combination on the Mars Climate Orbiter.

References: [1] Wilson R. J. and Hamilton K. (1996) *J. Atmos. Sci., 53,* 1290-1326. [2] Ingersoll A. P. (1970) *Icarus, 78,* 972-973. [3] Houben H. H. et al. (1997) *JGR, 102,* 9069-9084. [4] Davies, D. W. (1979) *JGR,* 84, 8335-8340. [5] Richardson M. I. and Toigo A. D., (2000) this volume. [6] Wilson R. J. et al. (2000) this volume.

MARS SECULAR OBLIQUITY DECREASE AND THE LAYERED TERRAIN. D. P. Rubincam. Geodynamics Branch, Code 921, Laboratory for Terrestrial Physics, NASA's Goddard Space Flight Center, Greenbelt, MD 20771. email:rubincam@denali.gsfc.nasa.gov.

Mars may have substantially decreased its average axial tilt over geologic time due to the waxing and waning of water ice caps through the phenomenon of climate friction (also called obliquity-oblateness feedback) [1]. Depending upon Mars' climate and internal structure, water caps of the order of 10^{17} - 10^{18} kg cycling with the obliquity oscillations could have either increased or decreased the average obliquity by possibly tens of degrees over the age of the solar system. Gravity and topography observations by the Mars Global Surveyor indicate that the south polar cap is mostly uncompensated, so that Mars may be largely rigid on the obliquity timescale. Further, Mars may be a water-rich planet, so that there is a large phase angle between insolation forcing and the size of the obliquity-driven water caps.

A stiff, water-rich planet implies an obliquity decrease over the eons. Such a decrease might account for the apparent youthfulness of the polar layered terrain. The idea is that fewer volatiles were available to be cycled into and out of the terrain at high mean obliquity, because of the eveness of insolation between equator and pole, and because of small insolation variations as the obliquity oscillated; so that the movement of volatiles and dust produced thin layers or perhaps no layers at all. As the average obliquity decreased, the insolation contrast between high and low latitiudes increased, plus the insolation variations over the obliquity cycle grew somewhat bigger, so that more volatiles and dust might have shuttled into and out of the polar regions, forming the observed thick layers late in Mars' history.

It may also be that the average tilt has decreased to the point where the climate friction mechanism is starving itself: more and more water has gotten locked up in the polar regions, making less available for cycling with the oscillations. And the layer-forming mechanism may be starving too: not only less water, but also at low average obliquity the atmospheric pressure is lower, so that dust storms become rarer, making less dust available to be deposited in the layers. The rate of water ice sublimation and the atmospheric pressure are both expected to drop sharply for obliquities only slightly lower than the present one. Hence there are qualitative reasons for believing that (a) the mean obliquity may be about as low as it can get, and (b) the mechanism for making the layers may turn off at low average obliquity, so that the layered terrain is a transient phenomenon. Thus the formation of the layered terrain may be intimately connected to a change in the mean axial tilt.

References [1] Rubincam D. P. (1999) *J. Geophys. Res. 104*, 30,765.

TOPOGRAPHY OF SMALL VOLCANOES AT THE MARGIN OF THE MARS NORTH POLAR CAP

S. E. H. Sakimoto[1], J. B. Garvin[2], M. Wong[1], and H. Wright[1,3]; [1](USRA at NASA's GSFC, Code 921, Greenbelt, MD 20771 USA; sakimoto@denali.gsfc.nasa.gov), [2](NASA's GSFC, Code 921, Greenbelt, MD 20771 USA; garvin@denali.gsfc.nasa.gov), [3] (USGS, Menlo Park, CA, 94025).

Introduction: Putative volcanic craterforms have been observed in the north polar region of Mars since Mariner 9. Hodges and Moore [1,2] described some of these features for the region they called the "Borealis Volcanic Field", and suggested that several were formed as a consequence of magma-ice or magma-water interactions. Mars Orbiter Laser Altimeter (MOLA) [1,2] topographic measurements confirm suggest that the features are unlikely to be of impact origin, and that there are many more of them present around the north polar cap than suspected from images alone. Analysis of one of the larger features—suggested by Hodges and Moore [3, 4] to represent a hydromagmatic explosion crater or maar—showed topographic characteristics more similar to a terrestrial small basaltic shield volcano [5, 6], possibly of recent origins. Recent work with the MOLA topography has also suggested that the possible volcanic extent of the Borealis Field is substantially larger in both number and range than previously mapped [5, 6, 7, 8]. Since the majority of these features are within 100 km of the present edge of the northern residual polar cap, and several extend into the Chasma Boreale cap re-entrant, they are some of the best Mars candidates for possible magma-water or magma-ice interactions. However, so far, these features have not displayed the expected average slope or other characteristics predicted for martian hydrovolcanic features, or even martian explosive volcanic features. Here, we show some of the range of feature types observed in the topography, along with their characteristic topographic measurements, and compare them to terrestrial and martian volcanic features.

MOLA Observations: Figure 1 shows a few of the volcanic features identified by Hodges and Moore [1, 2], as well as the many more revealed in the topography (and difficult if not impossible to see in the Viking Imagery). In Figure 1, the feature labeled "B1 MCC" is the cratered cone suggested on the basis of MOLA topography by Garvin et al., [5, 6] to be evidence of possible recent shield volcanism, rather than then maar or tuff cone suggested earlier [1,2]. The features in this Figure are all in the Vastitas Borealis Formation [8], and range from 1.5 to over 20 km in diameter, and from tens of meters to about a km in height. Average flank slopes range from ~1 to 7 degrees, and most of the features display a summit depression.

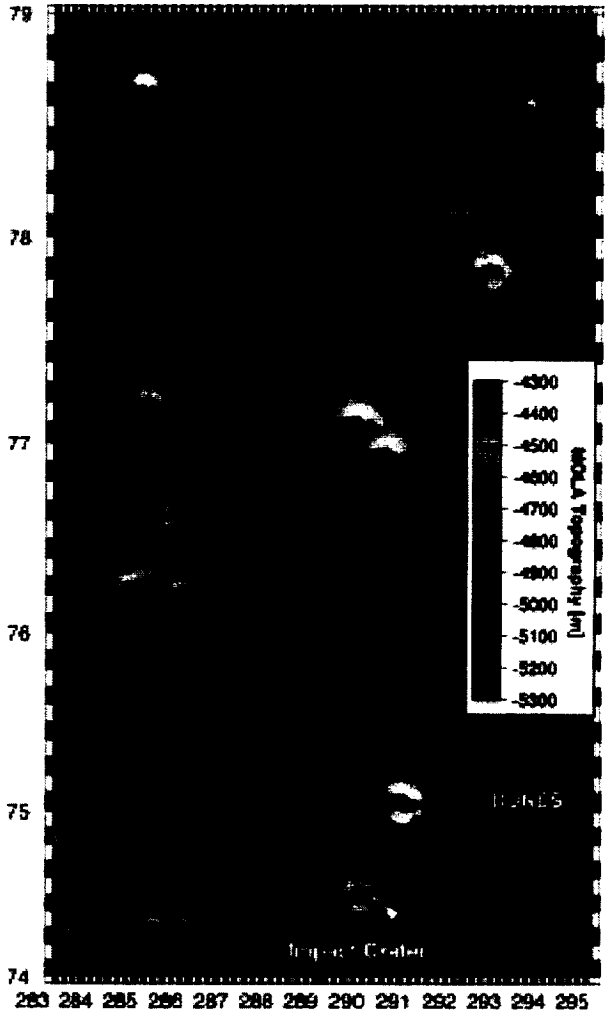

Figure 1. MOLA High-resolution digital elevation model of a portion of the Borealis Volcanic Field. Features marked B1, B2 were previously identified in Viking images as possible volcanic features [1,2]. Yellow arrows indicate many of the probable volcanic features apparent in the topography [5]. The pair indicated as "B15" is shown in profile in Figure 3. (For scale, grid is ~300 km top to bottom)

For all of the features so far examined closely in Figure 1, the slope break is gradual between the edifice and the surrounding plains, suggesting a lack of burial of the edifice base. Impact craters (one indicated at the bottom of figure 1) are noticeably lacking in comparison with the remainder of the Vastitas Borealis Formation.

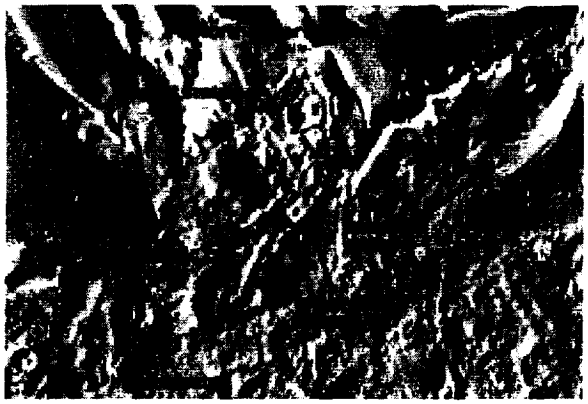

Figure 2. MOLA High-resolution digital elevation model (shown as shaded relief) of a portion of polar cap margin near the Olympia Planitia Dune Field.

Figure 2 shows another portion of the residual cap margin, this time outside the regions with previously mapped volcanics. Here, several cratered cones are apparent amongst several esker-like ridges similar to those suggested by Head [10] to be Eskers near the south polar cap. On the basis of their topographic morphology, we suggest that these cones are also volcanic [7], with flank slopes of a few degrees. To the West of these in the Olympia Planitia dune field, there are nearly a dozen more small cones and cratered cones partially buried by the dunes. It seems plausible that these may be of volcanic origins also.

Conclusions: We can now observe dozens of cones, cratered cones, and apparent breached or collapsed cones within 100 km of the Martian northern residual polar cap. Our topographic measurements suggest that these are very unlikely to be impact craters. With slopes ranging from 1–7 degrees, they are also less steep than predicted for explosive martian volcanic constructs (e.g. [9]), and do not display the characteristic slope breaks expected for table mountains or tuyas[11]. Summit craters for all examined so far have bases well above the surrounding terrain. Morphologically, they are similar, but not identical with the mid-latitude martian shield volcanoes cited as textbook examples of extrusive volcanism [4, 5, 6, 7 based on our current knowledge of eruption mechanics on Mars and the morphology of resulting edifices,], we suggest that that the majority of these features are extrusive basaltic edifices. Alternatively, and equally plausible, is the possibility that we are seeing the effects of water or ice on basaltic volcanism in ways we do not yet understand for Mars. Possibly slow extrusion into a northern ocean such as that suggested by [12], or some more subtle effect that perhaps modifies the resulting edifices but leaves them more similar to basaltic and martian mid-latitude extrusive shields than to terrestrial explosive eruptive products or predicted martian ones. We have undertaken preliminary models, but cannot yet explain the topography observed.

Acknowledgements. We thank G. Neumann for assistance with high-resolution grids and acknowledge the support of the MOLA science team . A portion of this work was performed under USRA contract NAS5-32484, and NASA Grant NAG5-8565.

References: [1] Smith D. E. et al. (1999) *Science 286*, 1495-1503. [2] Zuber M. et al. (1998) *Science 282*, 2053-2060. [3] Hodges C. A. and Moore H. J. (1979) *JGR, 84*, 8061-8074. [4] Hodges, C. A. and Moore H. J. (1994) *USGS Prof. Paper: 1534*. [5] Garvin, J.B. et al. (2000) *Icarus*, in press. [6] Garvin J. B. and Sakimoto S. E. H. (1999) *LPSC XXX*, CDROM, Abstract #1492, LPI [7] Sakimoto, S.E.H., et al., (2000), *LPSC XXXI*, CDROM, Abstract #1971, LPI. [8] Tanaka, K. L. and Scott, D. H. (1987) Geol. Map of the Polar Regions of Mars *USGS I1802c*. [9] Wilson, L. and J.W. Head III, 1994, *Rev. Geophys.*, 32, 221-263. [10] Head, J.W. III, (2000), *LPSC XXXI*, CDROM, Abstract #1119, LPI. [11] Wright, H.M., et al., (2000) *LPSC XXXI*, CDROM, Abstract #1894, LPI. [12] Head J. W. et al. (1999) *Science 286*, 2134-2137.

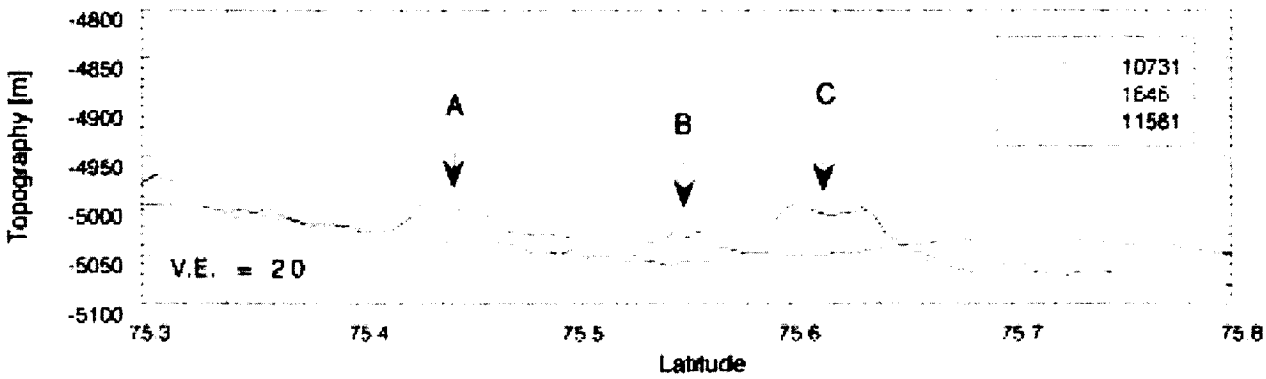

Figure 3. MOLA topographic profiles for several of the smallest cratered cones in the northern near-polar regions. Feature A has a diameter of 3.6 km, and a height of 45 m, Feature B has a diameter of 1.5 km, and a height of 20 m, Feature C has a diameter of 7.2 km, and a height of 65 m. MOLA pass numbers are indicated in the upper right. For scale, one degree of Latitiude is about 60 km. Vertical Exaggeration is 20.

THE FORMATION AND DETECTABILITY OF CO_2 CLATHRATE HYDRATE ON MARS. B. Schmitt, Laboratoire de Planétologie de Grenoble, UJF/CNRS, Bât. D de Physique, B.P. 53, 38041 Grenoble Cedex 9, France. E-mail: Bernard.Schmitt@obs.ujf-grenoble.fr

Introduction: CO_2 clathrate hydrate is suspected to be present near the surface of the south polar cap of Mars, and covered by seasonnal CO_2 frost during winter. After sublimation of this frost during summer times, it may be locally present at the surface where it may eventually decompose [see e.g. 1].

Clathrate Formation: Kinetic experiments have been performed on the formation of CO_2 clathrate by direct interaction of CO_2 gas with water ice grains at low temperature (195-213 K) [2]. We show the effects of several gas and solid phase parameters on clathrate hydrate formation rates: temperature, pressure difference with dissociation pressure, specific surface area and surface stability of water ice, ... The stability of the CO_2 clathrate and its decomposition kinetics have been also studied. Microphysical mechanisms for both formation and decomposition processes are proposed.

CO_2 clathrate on Mars. The conditions for CO_2 clathrate formation and stability in the atmosphere and at the surface of Mars are discussed and the formation rates are estimated from the extrapolation of our laboratory data to the relevant Mars conditions.

Clathrate IR spectrum: Laboratory data on the spectroscopic properties of CO_2 clathrate in the fundamental modes region (mid-infrared) are used to extrapolate its spectrum for the combination and overtone bands (near-infrared) [A laboratory spectrum will be possibly recorded in that range].

Detectability of CO_2 clathrate. Using the optical constants of water ice [3] and CO_2 ice [4], radiative transfer calculations [5] are performed to assess the detectability of CO_2 clathrate in reflectance spectra of Mars polar caps for different microphysical situations: 1) "pure" CO_2 clathrate; 2) mixed with CO_2 frost; 3) overlying water ice; 4) with a CO_2 frost layer on top; 5) thin water ice layer (from clathrate decomposition) overlying CO_2 clathrate. This study is performed at full spectral resolution (1 cm^{-1}) as well as at the resolution of the OMEGA spectro-imager (Mars Express mission).

References: [1] Kargel J. and Lunine J.I. (1998) *Solar System Ices,* Kluwer, 97-117. [2] Schmitt B. (1986) *Thesis, UJF-France,* 201-230. [3] Grundy W. and Schmitt B. (1998) *JGR E,* 103, 25809-25822. [4] Quirico E. and Schmitt B. (1997) *Icarus,* 127, 354-378. [5] Douté S. and Schmitt B. (1998) *JGR E,* 103, 31367-31390.

The jökulhlaup on Skeiðarársandur in November 1996: Event, discharge and sediment

Oddur Sigurðsson, Páll Jónsson, Árni Snorrason, Skúli Víkingsson, Ingibjörg Kaldal and Svanur Pálsson
National Energy Authority, Grensásvegi 9, Reykjavík

In the beginning of October 1996 a volcanic eruption within Vatnajökull ice cap melted approximately 3 km^3 of glacier ice. The melt water got trapped in a subglacial reservoir in the Grímsvötn caldera with water table at about 1500 m a.s.l. At about 9:30 pm on 4 November 1996 the ice barrier of the reservoir failed. At 7:20 am on 5 November a jökulhlaup broke explosively out 50 km down-glacier at eastern corner of the terminus of Skeiðarárjökull outlet glacier. This indicates a speed of about 5 km/h along the glacier bed. During the day the flood broke out successively farther to the west along the terminus which is at about 100 m a.s.l. At 15:40 pm flood liquid issued from almost the entire 20 km length of the terminus. The flood wave traveled 20-25 km to the coast at the speed of 8-10 km/h.

The two main channels of the jökulhlaup, Gígjukvísl and Skeiðará, had estimated peak discharge of 33,000 m^3/s and 23,000 m^3/s respectively. Fifteen hours after the break out at the terminus the combined peak discharge reached more than 50.000 m^3/s, the second largest river of the earth at that moment. The total area covered by the flood outside the glacier was about 750 km^2. The coastline advanced up to 800 m in front of the mouth of river Gígjukvísl. The area of the new land was measured to be about 7 km^2.

The Hydrological Service (HS) created a model to predict the progress of the small jökulhlaup in April 1996. The discharge of the flood was assumed to increase and decrease exponentially with time in accordance with the experience from earlier floods. The volume in the Grímsvötn caldera, the rate of growth and decrease of the jökulhlaup determine the progress of the flood. The Science Institute of the University of Iceland (SIUI) gave an estimate of the volume in the Grímsvötn caldera at the beginning of the jökulhlaup. The growth rate of the flood was calculated using the first three discharge measurements in Skeiðará, and the rate of decrease of the flood was estimated from experience from earlier floods. The prediction of the model made by HS agreed very well with discharge measurements made during the jökulhlaup, as well as predicting the discharge peak and its time of occurrence.

After the volcanic eruption started in Vatnajökull in the beginning of October 1996, HS decided to use the model described above to predict the progress of the expected great jökulhlaup. The HS made a new model based on how the volume of stored water in the Grímsvötn caldera changes with time accounting for both inflow and outflow of the Grímsvötn caldera. The plan was to use discharge measurements made at the beginning of the jökulhlaup and information from SIUI on the volume and inflow to the Grímsvötn caldera to calculate the growth rate of the expected jökulhlaup. To estimate the rate of decrease of the jökulhlaup, documentation of older large jökulhlaups from this century were used.

The model was used to predict possible scenarios of the progress of the expected jökulhlaup based on the hydrographs of four earlier jökulhlaups from the twentieth century. As soon as new information came from SIUI on the volume in the Grímsvötn cald-

era the new model was used to create scenarios of the expected jökulhlaup.

The catastrophic beginning of the jökulhlaup on Skeiðarársandur in November 1996 prohibited traditional measurements of the discharge during the event. During the jökulhlaup the discharge of the three major rivers on Skeiðarársandur was estimated during the first day of the flood, while it was still increasing, and on the second day when the flood was decreasing. The discharge was estimated independently by scientists from the HS and the Icelandic Public Roads Administration (IPRA). These independent estimations corresponded well with each other. The hydrographs of the three rivers were determined from these estimates, assuming that the discharge increases and decreases exponentially with time and by using additional information about the time of the peak discharge. The peak in Skeiðará was observed just before midnight and the peak in Núpsvötn was between 7 and 8 pm on November 5th. The jökulhlaup started with a huge flood wave in each of these rivers making it easy to schedule the beginning of the flood. According to HS, earlier jökulhlaups in Skeiðará show that assuming an exponential growth and decrease in the discharge, is a reasonable assumption, but the peak usually flattens out a little. This was taken into account by cutting 10% off the peak discharge, from each estimated hydrograph.

In the evening of the first day, the estimates were used as input to the new model. According to the model calculation, the peak discharge of the jökulhlaup was predicted to be about 45,000 m^3/s between 10 pm and 11 pm that evening. In the easternmost branch of the river Skeiðará the discharge kept increasing until 10:30 pm even though the growth was very slow from 7:30 pm. At the next visit at 00:30 am it was observed that the jökulhlaup was decreasing in agreement with the model forecast made by HS earlier that evening.

The total hydrograph of the jökulhlaup was estimated by adding the three individual hydrographs together. The curve of the total hydrograph is a little bit edged because of the mathematical methods used. The peak discharge of the flood according to this hydrograph is 52,000 m^3/s and the total flow volume that appeared on Skeiðarársandur is approximately 3.4 km^3 which correlates well with the volume estimated by the SIUI.

Conditions to take sediment samples from the flood were extremely difficult because of the size and the spreading of the jökulhlaup. Samples could only be taken from the surface at the riverbanks. Since sediment concentration increases with depth it can be assumed that measured concentration in the samples is about 1/5 to 1/2 of the real sediment concentration in the flood.

The sediment carried by the flood in the river Skeiðará alone is calculated to be about 60 million tons. The total sediment in the jökulhlaup from the Grímsvötn caldera is calculated to be about 180 million tons. In estimating the total sediment transport, only samples from Skeiðará were used, because of lack of samples from the other rivers.

These numbers which are greatly underestimated are much higher than numbers on sediment transport in jökulhlaups originating from the Grímsvötn caldera over the last 25 years. Those floods were much smaller and therefore sediment measurements were more accurate.

THERMAL CONTRAST AND SLOPE WINDS IN MARS' NORTHERN POLAR CAP EDGE REGION: 2-D SIMULATIONS. T. Siili[1], D. S. Bass[2] and H. Savijärvi[3], [1]Finnish Meteorological Institute, Geophysical Research, PO Box 503, FIN-00101 Helsinki, Finland, Tero.Siili@fmi.fi, [2]Southwest Research Institute, PO Drawer 28510, San Antonio, TX 78228-0510, USA, dsb@grouse.space.swri.edu, [3]Department of Meteorology, PO Box 4, FIN-00014 University of Helsinki, Finland, Hannu.Savijarvi@helsinki.fi.

Introduction: Orbital observations of the Martian polar cap and the atmosphere have shown the residual/permanent Northern polar cap to a) be composed primarily of water ice and hence during the spring and summer a major water vapor source [1], and b) lie considerably above its surroundings in the northern lowlands [2].

In previous works by the authors, brightening of the northern cap was documented in the visual and infrared Mariner 9 and Viking Orbiter observation after the retreat of the seasonal carbon dioxide cap at $L_s = 81°$. The association of this feature with seasonal variation of regional water transport have been investigated using both observational data sets [3-4] as well as 2-D modeling [5-6] of the cap edge regional/mesoscale circulation patterns.

Terrestrial observational and modeling experience as well as Martian simulation work [7-9] show that horizontal thermal contrasts generated, *e.g.*, between the ice-covered and ice-free regions on level or negligibly-sloped terrain drive sea-breeze like circulation patterns characterized by formation of daytime circulation cells with upwelling motion above the ice-free region and downwelling motion above the ice (Fig. 1). This circulation pattern may pick up sublimating water vapor in the near-surface layers and transport it across the ice edge towards the interior of the cap. The nocturnal – potentially reverse – circulation is weak in comparison.

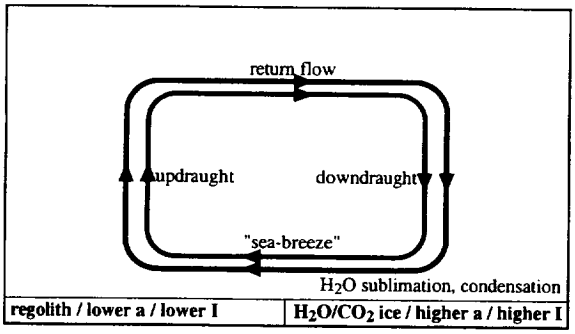

Fig. 1 Schematic of a cap edge region level-terrain surface thermal contrast circulation pattern as well as plausible subregions of H_2O sublimation (over water ice) and condensation (over H_2O and/or CO_2 ice).

Observations in, *e.g.*, Antarctic and Greenland as well as results of Mars simulations of fully or partially CO_2 ice-covered *slopes* in the Hellas and Argyre –like configurations point to significant contribution of slope-driven flows and complex interactions with the circulation patterns forced by the surface thermal contrasts. The slope flows tend to be directed downslope, concentrated in a shallow layer near the surface, and be diurnally fairly constant. During the seasonal cap retreat these flows may interact nonlinearly with the sublimation flow, resulting in, *e.g.*, downslope windstorm type phenomena [10] as well as influence the water vapor and dust transport features.

The goal of this work is to investigate the influence of some main features of the northern polar cap topography on the mesoscale circulations. We simulate the regional/mesoscale circulations and the associated water transport due to both the surface thermal contrasts generated by the regolith/water ice/CO_2 ice edges as well due to the ice cap sloping upwards towards its interior.

The model(s) used: The primary model used in this study is the Department of Meteorology/University of Helsinki 2-D Mars Mesoscale Circulation Model (MMCM) – a model based on a terrestrial 2-D mesoscale model [11]. The model represents a slice of the atmosphere of horizontal and vertical extents of up to 2000 km and 30 km, respectively (Fig. 2).

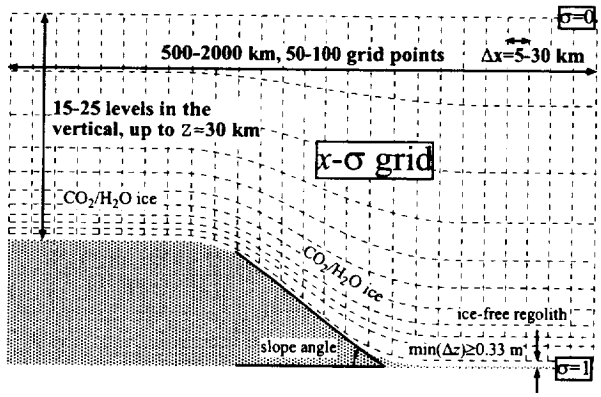

Fig. 2 Schematic of a the 2-D MMCM grid structure and description of the CO_2 and H_2O ice coverage variations.

The model has already been used to study a variety of Martian terrain-induced circulation phenomena, *e.g.*, slope winds [12], circulation driven by thermal contrasts caused by variations in surface albedo, soil thermal inertia [7], surface CO_2 [8] and H_2O [9] ice coverage as well as combinations of these effects [5-6, 10]. A one-dimensional (vertical) Boundary Layer Model (BLM) has been used in algorithm development [13-14] and independently to study, *e.g.*, the diurnal water vapor cycle at the Viking Lander 1 site [15] as well as the diurnal temperature cycle at the Mars Pathfinder

site [16].

The simulations: The model grid is perceived to be aligned along a longitude circle. The topography is semi-idealized and based on zonally averaged MOLA data in the chosen longitude region. Due to the 2-D approximation and the grid orientation, the simulated longitude regions are selected from areas outside the Chasma Boreale and its vicinity. The optical and thermal contrast caused by the regolith – water ice edge is described using albedo a and thermal inertia I differences. According to [17] the water ice thermal inertia is in the range of 600...1200 SI units and $a = 0.4...0.5$; $I = 900$ SI units and $a = 0.45$ have been used. The corresponding typical values for ice-free regolith are $I \approx 300$ SI units and $a = 0.25$. For CO_2 ice we have used $a = 0.7$; the CO_2 ice temperature is derived from the atmospheric surface pressure dependent CO_2 saturation temperature and is hence diurnally approximately constant.

We have investigated three major configurations: 1) the permanent cap and its slope still fully covered with CO_2 ice, but the adjacent regolith exposed of ice ($L_s = 70°$), 2) the seasonal cap retreated partly into the interior, exposing an annulus of water ice on the sloped cap edge before $L_s = 80°$, and 3) fully disappeared seasonal cap, *i.e.*, completely water ice covered slope (beyond $L_s = 81°$). In configurations 1-3 sensitivity to slope angle as well as in configurations 1 and 2 to the sublimation flow effects are investigated (the latter by means of the model's constant inflow lateral boundary condition). In the absence of relevant wind observations, we have attempted to constrain the simulations through comparison of the model's surface temperature predictions with orbital observations of IR surface brightness temperatures.

References:

[1] Jakosky, B. M. and Haberle, R. M. (1992) 969-1016 in Kieffer *et al.* (eds.) *Mars*, Univ. of Arizona Press, Tucson, AZ, USA. [2] Zuber, M. T. *et al.* (1998) *Science,* 282, 2053-2060. [3] Bass, D. S. *et. al.* (2000) *Icarus, 144,* 382-396; [4] Bass, D. S. and D. A. Paige (2000) *Icarus 144*, 397-409. [5] Siili, T. *et al.* (1999) In *The Fifth Int. Conf. on Mars*, Abstract 6089, LPI Contrib. No. 972 (CD-ROM). [6] Siili, T. *et al.* (2000). *Geophys. Res. Abstr.*, in print. [7] Siili, T. (1996) *J. Geophys. Res*, 101, 14957-14968. [8] Siili, T. *et al.* (1997) *Adv. Sp. Res*, 19, 1241-1244. [9] Siili, T. (1999) *Geophys. Res. Abstr.*, 1, 710. [10] Siili, T. *et al.* (1999) *Planet. Space Sci.*, 47, 951-970. [11] Alpert, P. *et al.* (1982) *Mon. Wea. Rev.*, 110, 994-1006. [12] Savijärvi, H. and Siili, T. (1993) *J. Atmos. Sci.*, 50, 77-88. [13] Savijärvi, H. (1991) *Contr. Atmos. Phys.*, 64, 103-112. [14] Savijärvi, H. (1991) *Contr. Atmos. Phys.*, 64, 219-229. [15] Savijärvi, H. (1995) *Icarus,* 117, 120-127. [16] Savijärvi, H. (1999) *Q. J. Royal. Met. Soc.*, 125, 483-493. [4] Paige, D. A. *et al.* (1994) *J. Geophys. Res.*, 12, 25959-25991.

AN OVERVIEW OF THE TOPOGRAPHY OF MARS FROM THE MARS ORBITER LASER ALTIMETER (MOLA). David E. Smith[1], and Maria T. Zuber[2,1]. [1]Laboratory for Terrestrial Physics, Code 920, NASA/Goddard Space Flight Center, Greenbelt, MD 20771 and [2]Department of Earth, Atmospheric and Planetary Sciences, 54-518, Massachusetts Institute of Technology, Cambridge, MA 02139; dsmith@tharsis.gsfc.nasa.gov.

Instrument and Mapping Attributes. The Mars Global Surveyor (MGS) [1] spacecraft has now completed more than half of its one-Mars-year mission to globally map Mars. During the MGS elliptical and circular orbit mapping phases, the Mars Orbiter Laser Altimeter (MOLA) [2, 3], an instrument on the MGS payload, has collected over 300-million precise elevation measurements. MOLA measures the range from the MGS spacecraft to the Martian surface and to atmospheric reflections. Range is converted to topography through knowledge of the MGS spacecraft orbit. Ranges from MOLA have resulted in a precise global topographic map of Mars (Fig. 1) [4, 5]. The instrument has also provided measurements of the width of the backscattered optical pulse and of the 1064-nm reflectivity of the Martian surface and atmosphere. The range resolution of the MOLA instrument is 37.5 cm [3] and the along-track resolution of MOLA ground shots is ~300 m; the across-track spacing depends on latitude and time in the mapping orbit. The best current topographic grid has a spatial resolution of ~1/16° and vertical accuracy of ~1 m [5].

Global Shape. The difference of ~20 km between the polar and equatorial radii of Mars observed by MOLA indicates that the largest contribution to Mars' shape is the planetary flattening (Table 1) [4]. The flattening is due mostly to the rotation of Mars but contains a small contribution (~5%) [6, 7] from the vast volcano-tectonic Tharsis province, situated near the equator (Fig. 1). Subtracting the gravitational potential or geoid [8] from radii measurements represents elevations in terms of topography and eliminates the contribution due to rotation, thus clarifying other long-wavelength components of the shape.

Geopotential topography on Mars has a 30-km dynamic range [4], the largest of the terrestrial planets. The large topographic excursions are due to ancient impact basins, large shield volcanoes, and the ability of the planet's rigid outer shell (lithosphere) to support significant stresses associated with surface and subsurface loads [5].

Major Features of Topography. The dominant features of surface topography are the south-to-north downward slope of 0.036°, the Tharsis province, and the Hellas basin [4]. The south-to-north slope is a consequence of the ~3-km offset between Mars' center of figure and center of mass along the polar axis [4, 9]. This global tilt is an ancient feature that controlled the transport of water and sediment throughout Martian history [4]. The flat northern lowlands constitute the largest sink for materials with gravity-dominated flow. MGS topography [4] and gravity [8] reveal the possibility for the surface [10] and subsurface [5] transport or water to high northern latitudes. The northern lowlands are the flattest large-scale surface in the solar system that has been measured by altimetry [3, 11]. The boundary of a geological contact [12] that encircles the lowlands represents a gravitational equipotential surface [13]. This observation, combined with the extraordinary flatness of the northern plains, has been interpreted as evidence that the northern hemisphere of Mars once contained a large standing body of water [13].

The Tharsis province, generally viewed prior to MGS as a single volcano-topographic rise, is now shown to consist of two broad rises (Fig. 1) [4]. The larger southern rise is superposed on heavily cratered highlands [5] as a quasi-circular feature that extends from ~220° E to ~300° E and from ~50° S to ~20° N. The southern rise spans about 10^7 km^2 in area, and contains the Tharsis Montes (Ascraeus, Pavonis and Arsia). The smaller northern rise, in contrast, covers approximately the same longitude band as the southern rise, but extends to ~60° N. It is dominated by the massive volcanic construct of Alba Patera (Fig. 1). The Olympus Mons edifice, thought before MGS to sit on the western flanks of the Tharsis rise, is now shown to be situated off Tharsis proper, but is likely genetically related to it.

The Hellas impact basin defines the deepest topography on Mars with its total relief of over 9 km. The basin is surrounded by a topographic annulus with thickness of up to 2 km above the surroundings that may be composed at least in part of Hellas ejecta. The Hellas annulus accounts for part of the elevation difference between the southern and northern hemispheres [4].

Polar Regions. MOLA altimetry has elucidated the nature and regional setting of the northern and southern polar layered terrains. In the north the region of high visible albedo corresponds well with the elevated polar deposits. The north polar deposits have an elevation of 3 km above the surrounding terrain, but the cap as a whole resides in a hemispheric-scale depression [4] such that the top of the northern cap lies 2 km below the average elevation of the equator. The southern polar cap has approximately the same relief as

the northern cap [5] but the zone of residual ice represents only about a third of the surface area of the layered deposits. The southern layered deposits are more asymmetrical in planform than their northern counterparts, though both are characterized by enigmatic spiral troughs that do not have a terrestrial counterpart.

The Mars '98 landing site (Fig. 2) lies in the (presumably) dust-covered polar deposits. Analysis of MOLA elevation data indicates that the landing zone is in generally smoother than "average Mars" [11]. However, the best post-landing reconstruction [JPL, Lockheed-Martin Astronautics, *pers. comm.*] indicates that the landing may have occurred at the margin of a regional depression with local slopes >10°. A comparison of point-to-point (~300-m) slopes derived from MOLA ranges to 100-m-scale backscattered pulse-widths shows a correspondence that indicates that 100-m-scale roughness in the landing zone is primarily due to slopes rather than to sub-footprint-scale variance (*e.g.* rocks) [J.B. Garvin, *pers. comm.*].

Clouds. The MOLA instrument routinely detects clouds over the winter polar cap [10, 14, 15]. Laser reflections from the atmosphere are obtained at altitudes from just above the surface to 15 km, but most are in the altitude range 5-10 km. A preponderance of cloud detections is made at the boundary of the ice caps and surrounding terrains. The cloud detections are all made in the dark, but the distribution may be biased by the MOLA observation geometry [14]. Sloping wavefronts are commonly observed at latitudes above ±70°, and imply the presence of propagating buoyancy waves. Atmospheric reflections are most likely composed of CO_2 ice, and indicate a near-surface lapse rate of 0.85°/km^{-1} that is set by the vapor pressure of dry ice [14].

References: [1.] Albee A. A. et al. (1998) *Science, 279,* 1671-1672. [2.] Zuber M. T. et al. (1992) *J. Geophys. Res., 97,* 7781-7797. [3.] Smith D.E. et al., (1998) *Science, 279,* 1686-1692. [4.] Smith D. E. et al. (1999) *Science, 284,* 1495-1503. [5.] Zuber M. T. et al. (2000) *Science, 287,* 1788-1793. [6.] Zuber M. T. and D. E. Smith (1997) *J. Geophys. Res., 102,* 28,673-28,685. [7.] Folkner W. M. et al. (1997) *Science, 278,* 1749-1752. [8.] Smith D. E. et al. (1999) Science, 286, 94-97. [9.] Smith, D. E. and M. T. Zuber (1996) *Science, 271,* 184-188. [10.] Zuber M. T. et al., (1998) *Science, 282,* 2053-2060. [11.] Aharonson O. et al. (1998) *Geophys. Res. Lett., 25,* 4413-4416. [12.] Parker T. J. et al. (1993) *J. geophys. Res., 98,* 11,061-11,078. [13.] Head J.W. et al. (1999) *Science, 286,* 2134-2137. [14.] Pettengill G. H. and P. G. Ford (2000) *Geophys. Res. Lett., 27,* 609-612. [15.] Neumann G.A. et al. (2000) *LPSC XXXI.*

Figure 1. Color-coded topography [5] superposed on shaded relief map of Mars from MOLA [2, 3]. Latitudes shown are between ±70°.

Figure 2. Three-dimensional view of the south polar layered terrains in the vicinity of the Mars '98 landing zone. V.E. = 20:1.

Table 1. Mars Geodetic Parameters from MOLA

Parameter	Value
Mean radius (m)	3389508 ± 3
Mean equatorial radius (m)	3396200 ± 160
North polar radius* (m)	3376189 ± 50
South polar radius* (m)	3382580 ± 50
Triaxial ellipsoid	
a (m)	3398627
b (m)	3393760
c (m)	3376200
1/flattening	169.8 ± 1.0
Directions of principal ellipsoid axes	
a	1.0° N, 72.4° E
b	0.0° N, 342.4° E
c	89.0° N, 252.4° E
Ellipsoid offset of COF from COM	
ΔX (m)	-233
ΔY (m)	-1428
ΔZ (m)	-2986
Elevation comparison with landers	
Viking 1 (m)	45
Viking 2 (m)	0
Pathfinder (m)	94

THE STRATEGY FOR POLAR EXPLORATION: PLANES, TRAINS, AND AUTOMOBILES

C. Stoker[1] and L. Lemke[2], ([1]M.S. 245-3, NASA Ames Research Center, Moffett Field, CA 94035, cstoker@mail.arc.nasa.gov); ([2]M.S. 244-14, NASA Ames Research Center, Moffett Field, CA 94035, llemke@mail.arc.nasa.gov)

Introduction-Exploration Objectives: The polar regions are both interesting and challenging to explore. The record of climate history and the behavior of Martian volatiles over time are thought to be contained in the polar terrains. Furthermore, the polar regions are probably the best environment to search for evidence of living organisms on Mars because they have both the presence of water ice and summertime temperatures at the surface that exceed the freezing point of water. In addition, melting at the base of the polar caps is predicted to occur which could result in a deep aquifer beneath the polar caps. Such an aquifer is potentially another habitat for life. Clearly, assessing the question of volaties, climate, and life in the polar regions would benefit from landed missions that can sample and interact with the surface. Mobility on the surface is also important for polar exploration due to the apparent wide diversity of terrains that occur on both local and regional scales.

Should We Bring Snowmobiles or All Terrain Vehicles? Possible polar surface exploration systems that incorporate mobility might include wheeled rovers, walkers, balloons which could touch down on the surface, airplanes that could land and take off, or ballistic hoppers. Choosing an appropriate mobility system requires sufficient knowledge of the surface properties to make intelligent design choices. The detailed structure of the surface at the scales which affect the design of lander or rover systems is unknown. Furthermore, the surface properties at scales of less than 1 m can't be characterized from orbit. Approximately 1/3 of the mass of the atmosphere is annually deposited and sublimated from the polar regions. This mass transport results in the highest erosion rates currently experienced on Mars and the terrains are therefor the youngest and most dynamically active. The dynamic behavior of the polar regions also make them especially challenging to explore, and possibly fundamentally different from other types of Martian terrain which have been characterized by previous landed missions High winds, high erosion rates, and sublimation degradation processes are expected to produce surfaces with a high degree of variability and small scale roughness. Surface bearing strength and mechanical properties are time varying and not characterized for any season. In fact, until a flawed engineering system was identified as the most probable cause, the surface environment of the landing site was a strong candidate to explain the failure of the Mars Polar lander mission. Greater characterization of the polar surface would allow a much improved basis for designing landing and mobility systems. Without such a characterization, any system design would be speculative and failure prone.

First Fly and Airplane: One approach to characterizing the polar terrain prior to designing a mission to land on and explore the surface is to first overfly it at close range with an airplane. Such aircraft missions have the advantage that they can be designed and tested on Earth with high reliability because the Martian atmosphere is much more uniform than the Martian surface, and its properties can be predicted with high confidence. Moreover, airplanes can be designed to fly at speeds much higher than the prevailing winds, thus allowing flight over long, preselected paths in a matter of a few hours or less.

The desirable capabilities of a Mars polar reconnaissance aircraft are as follows:

- Ability to fly at least one radial transect from the pole (90° North/South) through the layered terrain (70° North/South) so that the diversity of the polar terrain is represented in the acquired data set.
- Ability to fly close enough to the surface to allow imaging of surface features that represent potential hazards to surface landing and mobility systems at an appropriate scale (10-20 cm).

- Ability to determine the mechanical properties of the surface material at selected sites.

These capabilities would allow the collection of data that would permit the design of follow-on lander and rover missions with adequate confidence.

In addition to gathering information needed to design follow on missions, a polar aircraft mission could also be used to conduct scientific investigations that could not be conducted by any other means. One such investigation would be the electromagnetic sounding for a subsurface aquifer associated with melting at the base of the cap.

A set of functional requirements derived from these desired capabilities includes:

- A minimum flight path of 1200 km at an altitude of 1 km above the ground level during polar summer.
- Mass, volume, power, and data budgets for cameras, drop-sonde surface penetrators, and a subsurface electromagnetic sounder.
- The ability to relay all data off the aircraft before termination of flight.

A conceptual aircraft mission will be presented which is capable of accomplishing these objectives together with a summary of overall mission architecture characteristics and technical readiness.

ESTIMATION OF RADIATION PROTECTION BY A DENSE ATMOSPHERE AND MAGNETIC FIELD ON ANCIENT MARS.

W. Stumptner[1,2], H. Lammer[1] and N. Kömle[1], (1) Space Research Institute, Austrian Academy of Sciences, Elisabethstr. 20, A-8010 Graz, Austria, willibald.stumptner@oeaw.ac.at, (2) Institute for Geophysics, Astrophysics & Meteorology, Univ. Graz, Halbärthgasse 1, A-8010 Graz, Austria.

Mars today is a desert planet with minimal atmosphere, bombarded by intense UV and cosmic radiation. For life - as we know it it – the Red Planet would be a harsh environment, barely sufficient even for extremophile species. However, the Magnetometer/Electron Reflectometer experiment on board of Mars Global Surveyor has detected surface magnetic anomalies during its low aerobraking passes. These anomalies strongly indicate the existence of a strong ancient Martian magnetic field, which may have been of a magnitude up to that of Earth.

Combined with evidence for the presence of a denser, warmer and wetter atmosphere on early Mars - with the loss of atmospheric constituents to space reduced by the presence of a stronger magnetic field – the planet must have been much better protected from lethal radiation and small body impacts. We evaluate this protection and the atmospheric conditions during the first few hundred million years. As life on Earth might be as old as 3.8 Gyrs, similiar primitive life may have developed on Mars under the more favorable conditions outlined in this work.

Future missions e.g. Mars Netlander and Mars Express will provide us with critical information – both from orbit and on the ground – on the enigmatic Red Planet. They will determine the inner structure of Mars with seismometers, examine the surface material composition and look for predicted carbonate deposits, try to find areas with active hydrothermal vents, explore the edges of the polar caps and probe Martian soil for signs of life.

DETECTION OF SURFACE TEMPERATURE CHANGES FROM PASSIVE MICROWAVE DATA OVER ANTARCTIC ICE SHEET: A POSSIBLE APPLICATION ON MARS. S. Surdyk, Institute of Low Temperature Science (Hokkaido University, Kita-19, Nishi-8, Sapporo 060-0819, Japan); ssurdyk@pop.lowtem.hokudai.ac.jp

Introduction: According to [1], past telescopic observations had revealed that Mars possesses two polar caps that varie largely in size. Indeed, recent missions concluded that those polar caps undergo strong seasonal changes. Therefore the spatial and temporal survey of the temperature variation is an essential issue to understand more about the climate of Mars.

This paper presents a case of observation of temperature changes over Antarctica with passive microwave data. The present work suggests that the passive microwave data could be a valuable tool for the detection of surface temperature changes.

Why the passive microwave? For the observation of the Antarctic ice sheet, infrared images are now quite commonly used to draw map of the mean annual surface temperature, or monthly mean temperatures. However, daily time series observation from infrared images is more difficult to provide due to intermittent cloudy days, especially in winter. Unlike the infrared, the passive microwave data are quasi-independent of the atmosphere. And this advantage makes of the passive microwave a valuable observation tool, in the event of cloudy days or snowfalls. Like the infrared, the passive microwave brightness temperature, from its definition, is also a temperature indicator even though it is not a pure temperature signal, depending also on the surface properties.

In addition, the coarse resolution of the passive microwave data, often seen as a disadvantage, can be taken here as an advantage to establish with a reasonable number of pixels an image of the entire polar cap. This would induce at the same time saving of energy and a lower volume of data.

Nevertheless, considering the properties of the brightness temperature (variation in penetration depth, emissivity), it is clear that the passive microwave data will hardly provide accurate absolute temperatures but it can provide a very good estimate of the surface temperature variations as we will see hereafter.

Note as well, that at the difference of the infrared signal, if a drastic change of medium (ice/rock or water) occurs this will be so soon reflected on the microwave signal, since the microwave brightness temperature besides the medium temperature also depends on the medium characteristics.

Observation of a temperature change: In the case of the Antarctic and Greenland Ice sheet, the annual pattern of the brightness temperature at 37GHz is very similar to the one of the air temperature [2][3].

The figure 1 shows the annual pattern of air temperature at Dome C Automatic Weather Station (*74.50S, 123.00E, 3280m*) and for the same period the brightness temperature at 37GHz in vertical polarization. From figure 1, we can see that not only the seasonal trends are similar but also most the short time fluctuations are reflected on the brightness temperature. If we compare the amplitude of the short time fluctuations relatively to the amplitude of the seasonal signal, the fluctuations on the brightness temperature compared to those on the air temperature are much more attenuated. As well the seasonal signal is delayed by several days, whereas the short time fluctuations seems to be nearly synchronous This observation highlights that both seasonal signal and short time fluctuations depend on different mechanisms. It also clearly shows that the simple observation of the short time fluctuations will provide a pattern of the air temperature variations.

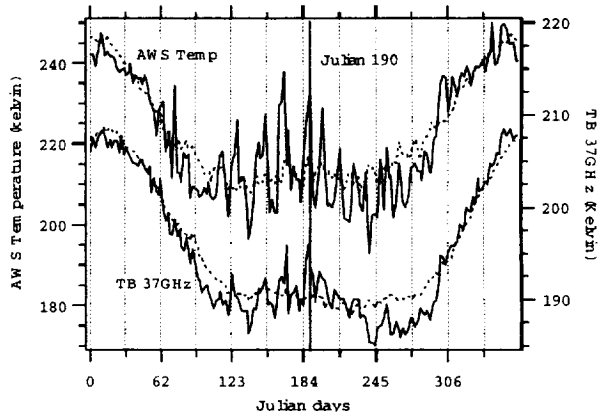

Fig. 1. Comparison of the air temperature at Dome C and the simultaneous brightness temperatures at 37GHz in 1982.

Now, if we remove the seasonal signal, from the brightness temperature, and observe then spatially how this remaining component is changing in space in the typical case of a winter warming, we can have an idea of for example the inclusion of the warm wave into the continent. Figure 2 displays the case of a warming observed at Dome C in 1982 on the Julian day 190. The figure shows actually the brightness temperature variation for the day where the maximum temperature

was observed, reference to figure 1. We can see clearly the inclusion of the warm wave on the continent following indeed the topography. The brightness temperature changes observed represents only a few days variation this emphasizes that the observation are really an effect of the surface temperature rather than a snow properties, which generally changes more slowly.

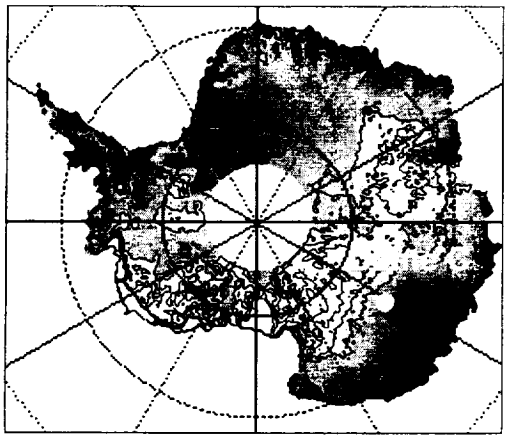

Fig.2. Observation of the inclusion of a warm wave in the direction of Dome C on Julian 190 of 1982; white color for negative variations, cooling, and black color for positive variations, warming.

References:

[1] Clifford S. M. and 53 coauthors. (1999) *Mars Polar Science special issue of Icarus.* [2] Sherjal, I., and M. Fily. (1994) *Ann. Glaciol., 20.* [3] Shuman, C.A., R.B. Alley, S. Anandakrishnan, and C.R. Stearns. (1995) *Remote Sens. Environ., 51, 245-252.*

Acknowledgements: The passive microwave data were provided by the National Snow and Ice data Center of Colorado (USA). The AWS data were provided by the Department of Meteorology of the University of Wisconsin, Madison.

MARTIAN NORTH POLAR WATER-ICE CLOUDS DURING THE VIKING ERA. L. K. Tamppari[1] and D. S. Bass[2], [1]Jet Propulsion Laboratory, M/S 264-538, 4800 Oak Grove Dr., Pasadena, CA 91109, USA, leslie.tamppari@jpl.nasa.gov, [2]Southwest Research Institute P.O. Drawer 28510, San Antonio, TX, 78228-0510, USA, dsb@swri.edu.

Introduction: The Viking Orbiters determined that the surface of Mars' northern residual cap consists of water ice. Observed atmospheric water vapor abundances in the equatorial regions have been related to seasonal exchange between reservoirs such as the polar caps, the regolith, e.g. [1] and between different phases in the atmosphere, e.g. [2]. Kahn [1990] modeled the physical characteristics of ice hazes seen in Viking Orbiter imaging limb data, hypothesizing that ice hazes provide a method for scavenging water vapor from the atmosphere and accumulating it into ice particles. Given that [1] found that these particles had sizes such that fallout times were of order one Martian sol, these water-ice hazes provided a method for returning more water to the regolith than that provided by adsorption alone. These hazes could also explain the rapid hemispheric decrease in atmospheric water in late northern summer as well as the increase during the following early spring. A similar comparison of water vapor abundance versus polar cap brightness has been done for the north polar region [3,4]. They have shown that water vapor decreases steadily between L_s = 100-150° while polar cap albedo increases during the same time frame. As a result, they suggested that late summer water-ice deposition onto the ice cap may be the cause of the cap brightening. This deposition could be due to adsorption directly onto the cap surface or to snowfall. Thus, an examination of north polar water-ice clouds could lend insight into the fate of the water vapor during this time period.

Method: Detection of water ice clouds in the polar regions using visible images has been difficult due to the inherent difficulties of distinguishing bright atmospheric condensates from surface ice features. In addition, water-ice hazes are typically thin and cannot, with visible data alone, be positively distinguised from dust hazes in the atmosphere, e.g., [5]. However, Tamppari *et al.* [2000] established a technique for detecting water ice clouds on Mars equaqtorward of ±60° μm [6]. This technique utilized the Viking Infrared Thermal Mapper (IRTM) data set and involved comparing brightness temperatures of the same surface location taken in both the 11 and 20 μm. In principle, this technique can be used with any thermal data set in which one channel senses the 11 μm water-ice absorption and the other does not. Essentially, during the daytime when the surface is warmer than the atmosphere, the brightness temperature in the 11 μm channel is reduced compared to the 20 μm channel when a water-ice cloud is present. This is due to the water-ice cloud absorbing surface radiation and re-radiating it at a lower temperature. This technique also depends upon properly modelling the brightness temperature of the surface, given spectrally dependent, non-unit surface emissivities [7].

In the north polar region of Mars over the regolith area surrounding the polar cap, this technique can be applied analogously as in the equatorial region [6], see Figure 1. However, over the polar cap itself, the signature would likely reverse, giving a warmer brightness temperature when a cloud is present by comparison to the very cold CO_2 cap temperature. In addition, the surface emissivities over the polar cap may be very different than over the soil.

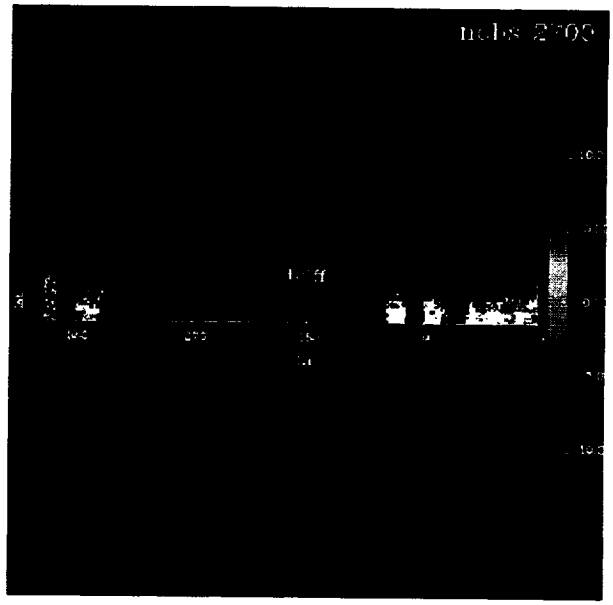

Figure 1. Shown here, in color, are water-ice clouds in the north polar cap region for L_s = 103.26-105.52°. West longitude is shown along the x-axis and latitude from 60-90°N is shown along the y-axis. Black indicates no data were present and white indicates where data were present, but no water-ice clouds were present. The cloud signature is shown in blues according to the temperature scale on the right. This signature is the result of differencing the 11 and 20 μm channel data after removing the surface spectral emissivity surface [6]. Darker blues imply a thicker or colder water-ice cloud.

We will show the water-ice cloud distribution poleward of 60°N, over the regolith. In a companion abstract [8], we relate these preliminary results to Viking Orbiter imaging data and water vapor abundance.

References: [1] Jakosky B. (1983) *JGR, 90,* 1151–1154. [2] Kahn R. (1990) *J. Geophys. Res., 95(B9),* 14677-14693. [3] Bass D. S. et. al. (2000) *Icarus, 144,* 382-396. [4] Bass D. S. and D. A. Paige (2000) *Icarus, 144,* 397-409. [2] Kahn R. (1984) *J. Geophys. Res., 89(A8),* 6671-6688. [6] Tamppari L. K. et. al. (2000)) *J. Geophys. Res., 105(E2),* 4087-4107. [7] Christensen P. R. (1998) *J. Geophys. Res., 103(E1),* 1733-1746. [8] Bass D. S. and L. K. Tamppari (2000), 2nd International Conference on Mars Polar Science and Exploration, Aug. 21-25.

REGIONAL GEOLOGIC HISTORY OF THE POLAR REGIONS OF MARS. K. L. Tanaka[1] and E. J. Kolb[1], [1]U.S. Geological Survey, 2255 N. Gemini Dr., Flagstaff, AZ 86001, ktanaka@usgs.gov.

Introduction: Geologic mapping and topical studies of the martian polar regions based on Mariner 9 and Viking data have identified major geologic units and structures and their formational sequence [e.g., 1-3]. However, several fundamental questions remain poorly answered, such as: (1) What has been the history of ice and dust deposits at the poles and their subsequent modification over geologic time? (2) Is their a signature of melting and discharge from any polar deposits? (3) Can long-term or sporadic climatic and geologic changes of global significance be detected in the polar geologic records? (4) How have volcanism, tectonism, and impacts been involved in the geologic evolution of the polar regions?

Here we discuss how these questions are currently being re-examined with Mars Global Surveyor data and new geologic mapping of the polar regions.

History of ice and dust deposition: The south polar layered deposits (SPLD) make up Planum Australe as well as isolated outcrops within surrounding craters and local depressions out to 60° S. [2]. The timing of initial SPLD deposition is poorly constrained; the unit overlies middle Hesperian units of the Dorsa Argentea Formation (DAF) and younger cavi material [2]. SPLD are Late Amazonian, and recent crater counts using Viking images of frosted surfaces suggest that the mean surface age is <10 Ma [4]. In comparison, the north polar layered deposits (NPLD) also make up a large plateau, Planum Boreum, and local outliers out to about 73°N. The high-standing, rounded topography of Olympia Planitia suggests that its dune field overlies a large patch of NPLD. In turn, NPLD rest on Late Hesperian/Early Amazonian materials [2] and appear to be uncratered in Viking images, indicating surface ages of <100 Ka [4].

The older SPLD surface age may indicate that these higher-elevation surfaces largely ceased receiving deposits since the obliquity has been <40°, ~5 million years ago [4]. However, localized south polar (SP) deposition may account for mantles that cover (1) the residual ice cap, (2) broad, flat terrace surfaces on the planum, and (3) plains adjacent to Planum Australe (between ~330 to 30°W) [5]. It remains to be seen to what degree these young deposits may be layered.

Older polar deposits are preserved in the south polar (SP) region. The SP pitted material generally has been considered to be a deeply eroded, paleopolar dust and ice deposit [1,2,6]. The pitted material rises above the DAF, and the pits bottom out at about the surface level of the DAF. Thus the cavi material likely postdate or are coeval with the DAF and have an Late Hesperian crater density [6]. The pitting indicates local instabilities within the pitted material that might lead to collapse, such as concentrations of ice or more highly volatile ice mixtures. Pitted terrain underlies perhaps much of the SPLD adjacent to Cavi Angusti. Near the mouth of Chasma Australe, a 15-km crater having a pedestal ~100 km across overlies the DAF and is being exhumed from beneath SPLD. The crater apparently armors an intermediate, friable deposit. Plateaus at the mouth of Planum Boreale may form older polar deposits underlying NPLD, but this interpretation is highly conjectural.

No clear evidence for Noachian polar deposits has been discovered at either pole. This may be explained either by polar wandering or by perhaps climate conditions that did not promote concentrated polar ice-and-dust deposition. Noachian highland terrains across Mars appear to be ubiquitously layered and may in fact reflect highly voluminous but diffuse ice and dust deposition [7]. Alternatively, the SP Noachian terrain may include polar deposits that have been obscured by later activity.

Polar ice cap melting: Deposits with lobate flow margins and esker-like ridges surround both polar caps and have been interpreted in various ways, including melting of former ice caps [8-11]. Basal melting should occur if ice caps of sufficient thickness occur depending upon climate conditions and ice composition [12-13]. For example, sub-ice lakes may be present beneath Planum Australe if the SPLD is at least partly composed of CO_2 clathrate [12]. Water-ice layered deposits, however, may require thicknesses of several kilometers for basal melting to occur under present conditions.

If basal melting had occurred, the overlying layered deposits may have moved like warm-based glaciers on Earth. The sinuous ridges on the DAF have been interpreted as glacial eskers [11]; however, these features deviate in preservation and geomorphic associations in significant ways from terrestrial eskers. We find that the ridges also occur locally atop the pitted terrain. In any case, if the ridges are related to basal melting, then DAF actually may have formed by expulsion of water and sediment from beneath a former ice cap. The sinuous ridges mostly trend toward extant outcrops of pitted material and SPLD. Floods generated by ice-cap melting also have been proposed to explain the large chasma troughs that cut both polar plateaus [11, 14]. Sinuous ridges occur within Chasma Australe, but streamlined erosional landforms are not clearly observed in either chasma.

Long-term climate change: Like earth, the polar regions are the most sensitive regions of the planet to climate change. The polar layered deposits may record climate and atmospheric variations related to orbital changes, intense volcanic activity, impacts, and perhaps other phenomena. New MOC images show a

great diversity in the characteristics of individual layers in the polar layered deposits. Also, angular unconformities and trough structures within the deposits may also relate to periods of erosion or deformation controlled ultimately by climate. These changes may occur over times scales ranging from thousands to tens of millions of years during the Late Amazonian.

Older polar deposits differ in significant ways from the SPLD, and thus may have different compositions. In Viking images, except perhaps for a resistant cap in places, the SP pitted materials do not show layering. Also, the margin of the pitted materials locally has a lobate form suggestive of flow. Therefore, the pitted material may have been melted and may have been relatively more volatile (CO_2-rich?). The DAF may also have been derived from a highly volatile source; locally, its surface is covered by small pits that may have developed via volatile release.

Other geologic activity: Impacts, volcanism, and tectonism have likely affected the development and modification of layered deposits at both poles. Large impacts (>10 km) superposed on polar deposits are rare or obscure and limited to the SP region. Two types occur: (1) Those with well-developed secondaries; one each on both SPLD and DAF. One might expect that impact into icy material should produce fluidized ejecta morphologies instead. Instead, laboratory experiments demonstrate that impacts into porous target material tends to be ejected in large clumps, resulting in large secondary craters [see 5]. (2) The 15-km pedestal crater at the mouth of Chasma Australe that presumably is armoring some former, perhaps largely eroded deposit.

Possible volcanoes have been proposed in the vicinity of both polar layered deposits [2,15], raising the possibility that sub-layered deposit (and thus sub-ice) volcanism may have occurred. However, stronger evidence such as suites of tuya- (table mountain) related features have yet to be recognized.

Tectonic sagging of the underlying lithosphere has been proposed for both polar plateaus, based on their loading [16, 17]. Estimates range up to a few hundred meters of sagging, depending on the actual thickness of the deposits, their densities, and lithospheric rheology. In addition, catastrophic deposition in the northern plains associated with a mud or water ocean may have caused as much as a kilometer of regional sagging in the north polar basin. [18]

Summary: Both polar regions, while having similar-sized plateaus of layered deposits, differ markedly in related recent and long-term geologic activity, including both polar and non-polar geologic processes. New studies involving geologic mapping and geomorphologic and topographic analysis using MGS data are providing significant advances in unraveling the geologic histories of the polar regions, yielding potential insights into the polar climate records. We expected to see enhanced analyses, new interpretations, and continued debate of these largely enigmatic regions.

References: [1] Condit, C. D. and Soderblom, L. A. (1978) *USGS Map I-1076.* [2] Tanaka, K. L. and Scott, D. H. (1987) *USGS Map I-1802-C.* [3] Herkenhoff, K. E. (2000*) USGS Map I-2686* (in press). [4] Herkenhoff, K. E. and Plaut J. J. (2000) *Icarus* (in press). [5] Tanaka, K. L. et al. (2000) *this volume.* [6] Plaut, J. J. et al. (1988) *Icarus 73,* 357-377. [7] Tanaka, K. L. (2000) *Icarus,* in press. [8] Jöns, H.-P. (1987) *LPSC XVIII,* 470-471. [9] Jöns, H.-P. (1991) *The Planet Mars (map),* Lithographisches Institut, Berlin. [10] Howard, A. D. (1981) *NASA TM 84211,* 286-288. [11] Head J. W. (2000) *LPSC XXXI,* #1121. [12] Clifford, S. M. (1987) *JGR 92,* 9135-9152. [13] Kolb, E. J. and Tanaka, K. L. (2000) *this volume.* [14] Anguita, F. (1998) *First Intl. Conf. Mars Polar Sci. Exp., LPI Cont. 953,* 1. [15] Hodges, C. A. and Moore, H. J. (1994) *USGS Prof. Pap. 1534.* [16] Zuber, M. T. et al. (1998) *Science 282,* 2053-2060. [17] Smith, D. E. (1999) *Science 284,* 1495-1503. [18] Tanaka, K. L. and Banerdt, W. B. (2000) *LPSC XXXI,* #2041.

STRATIGRAPHY AND TOPOGRAPHY OF MCMURDO CRATER AREA, PLANUM AUSTRALE MARS: IMPLICATIONS FOR RESURFACING HISTORY AND POROUS CHARACTER OF THE SOUTH POLAR LAYERED DEPOSITS. K. L. Tanaka[1], P. H. Schultz[2], and K. E. Herkenhoff[1], [1]U.S. Geological Survey, 2255 N. Gemini Dr., Flagstaff, AZ 86001, ktanaka@usgs.gov, [2]Department of Geological Sciences, Brown University, Providence, RI, Peter_Schultz@Brown.edu.

Introduction: McMurdo Crater (84.5°S, 0°W) is the largest extant impact (~23 km diameter) that has scarred the south polar layered deposits (SPLD) of Planum Australe, Mars. It occurs along the margin of the SLPD and formed a broad field of secondary craters across the planum. These secondaries as well as other associated features serve as both (1) key stratigraphic markers that provide a basis for resolving stages in the resurfacing history of the SPLD, and (2) important indicators of the SPLD substrate character.

McMurdo Crater: Table 1 shows crater morphology parameters measured from Viking images (421B77-80) and 18 MOLA profiles currently available across the crater . The crater gouged the margin of Planum Australe, which is bounded by a scarp ~1.5 km high. The crater is only partly enclosed and opens out to the surrounding, lower-lying plains (Figs. 1 and 2). McMurdo includes a partly enclosed inner ring that is offset to the north of the center of the crater. This offset along with the lack of a northern rim may indicate that slumping associated with the impact event destroyed the northern rim and may be the cause of the apparent inner ring feature. No associated crater flows or ramparts have been detected. South of McMurdo, Planum Australe rises relatively rapidly; this rise may be due to uplift caused by the impact.

McMurdo's secondary craters are generally rimless (Figs. 3-4), except perhaps locally south of the crater. Because of imprecise locating of the MOLA tracks vs. the Viking images, we could not discriminate whether the dips seen in the profiles were secondary craters vs. other similar-scale topography (e.g., Fig. 4). In addition, the MOC image (Fig. 4) resolved lumps associated with the secondaries that may be piles of ejecta.

Table 1: Dimensions of McMurdo Crater and associated features.

Diameter	~23 km
Depth	1780 m
Maximum wall slope	18.4°
Rim height	0 to 51 m
Rim elevation	3031 to 3645 m
Inner ring diameter	~11 km
Inner ring depth	~600 m
Secondary size range	0 to 3 km
Depths of secondaries	< 25? m
Extent of secondaries	0 to 85 km
Lump widths	<400 m at 50 km range

Stratigraphy and Resurfacing: McMurdo's secondaries are unevenly distributed, apparently due to local burial and perhaps erosion [1,2]. On Planum Australe, a smooth mantle of variable albedo (unit Apm in Fig. 3) appears to bury the secondaries. This unit; mapped as SPLD (unit Apl) in previous mapping [3], might form the uppermost SPLD below the residual ice cap (unit Api) as well as deposits on broad, flat terraces southeast of McMurdo.

Peripheral to Planum Australe, the stratigraphy is less clear because of apparent eolian mantling. Hilly terrain may be made up of degraded ancient highland material (unit HNu), whereas as undulating, locally high-standing material may be an outlier of SPLD (unit Apl?). The smooth material filling in the low areas may also be younger SPLD material. McMurdo secondaries were obliterated by erosion at the perimeter of Planum Australe, which may account for the narrow trough in front of the planum east of McMurdo (Fig. 2), and (or) by deposition of unit Apm.

Post-McMurdo erosion of most of the SPLD on Planum Australe apparently has been relatively minor, perhaps on the order of meters to a few tens of meters at most to account for the preservation of secondary craters. Locally, ridges in the SPLD have crisp morphology and lack secondaries, and thus appear to have undergone greater erosion (Fig. 4). Deposition of the post-McMurdo SPLD-like mantle material (unit Apm) has been localized. These relations indicate that at least the flatter surfaces of Planum Australe have not changed significantly for what may have been a considerable period of time, consistent with surface age modeling based on crater statistics [4].

SPLD Character: McMurdo crater apparently formed in relatively unconsolidated layers on the basis of the following observations. First, the secondary craters are unusually large for the size of the crater. Laboratory experiments reveal that impacts into uncompacted, porous substrate produce large clumps of ejecta. This suppresses the role of the atmosphere [5], thereby minimizing the atmospheric effect on ejecta emplacement. Equally important it creates anomalously large and rimless secondary craters, which are largely the result of compression. Clumps and clouds of ejecta into porous materials have been observed experimentally to produce shallow, low-rimmed craters [6]. Moreover, anomalously large secondary craters around relatively small craters also have been found in the circum polar sedimentary plains and in craters on the Medusa Fossae Formation [5]. Second, the MOC-resolved lumps would be consistent as soft-captured primary ejecta debris analogous to large glass bombs

captured in the Argentine loess on Earth [7]. Third, the low rim height of McMurdo suggests that it has undergone extensive collapse (as indicated by the floor debris and slumps). Such collapse would be expected in an unconsolidated substrate due to the enhanced depth of the transient crater.

References: [1] Howard, A. D., *et al.* (1982) *Icarus 50*, 161-215. [2] Herkenhoff, K. E. (2000) *USGS Map I-2686* (in press). [3] Tanaka, K. L. and Scott, D. H. (1987) *USGS Map I-1802-C.* [4] Herkenhoff, K. E. and Plaut J. J. (2000) *Icarus* (in press). [5] Schultz, P. H. (1992) *JGR 97,* 11,623-11,662. [6] Schultz, P. H. and Gault, D. E. (1985), *JGR 90,* 3701-3732. [7] Schultz, P. H. et al. (1999) *LPSC XXX,* #1898.

Fig. 1. Digital terrain model looking southward into McMurdo Crater. [Vertical exaggeration 4X]

Fig. 2. MOLA tracks in 3D of McMurdo Crater looking southeastward across Planum Australe. Note shallow trough at base of Planum Australe (center left) and inner crater ring (dark green). [Vertical exaggeration 6X]

Fig. 3. Viking mosaic of McMurdo Crater. Api, residual ice cap; Apm, polar mantle material; Apl, SPLD; Amc, McMurdo crater materials; HNu, undivided highland material.

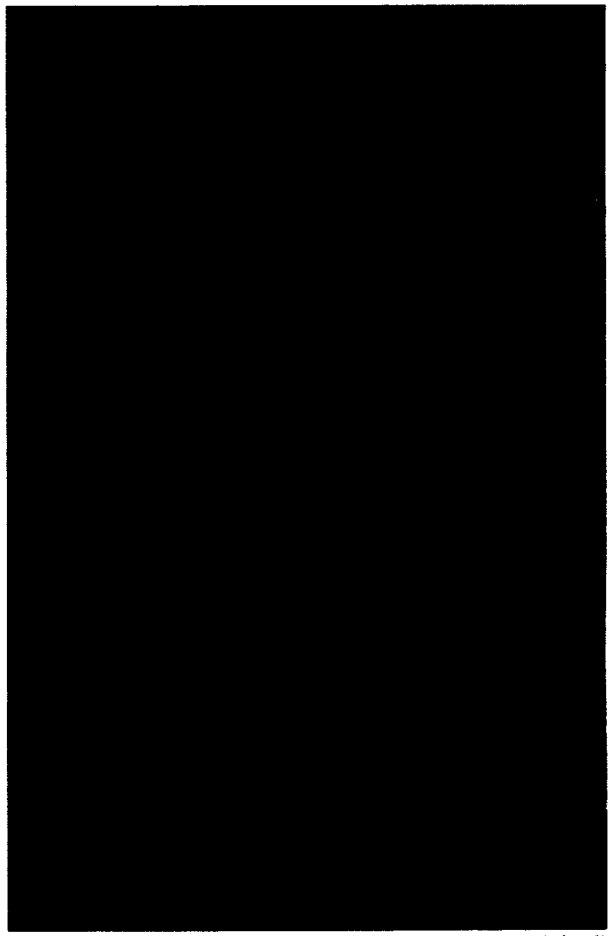

Fig. 4. Part of MOC image 06705 (32.5 m/pixel) showing SPLD on Planum Australe. Note secondary craters and lumps of ejecta from McMurdo crater (50 km to the east), which appear to be preferentially preserved in shallow troughs.

THE RESIDUAL POLAR CAPS OF MARS:GEOLOGICAL DIFFERENCES AND POSSIBLE CONSEQUENCES. P. C. Thomas[1],R. Sullivan[1], A.P. Ingersoll[2], B.C. Murray[2], G. E. Danielson[3], K.E.Herkenhoff[4], L. Soderblom[4], M.C. Malin[5], and K.S. Edgett[5], P. B. James[6], W. K. Hartmann[7], [1]Center for Radiophysics and Space Research, Cornell University, Ithaca NY 14853 USA, [2]Cal. Inst. of Technology, [3]Jet Propulsion Laboratory, [4]United States Geologic Survey, [5]Malin Space Science Systems, [6]Univ. of Toledo, [7]Planetary Sci. Inst. (Correspondence Email: Thomas@cuspif.tn.cornell.edu).

The Martian polar regions have been known to have thick layered sequences (presumed to consist of silicates and ice), CO_2 seasonal frost, and residual frosts that remain through the summer: H_2O in the north, largely CO_2 in the south. The relationship of the residual frosts to the underlying layered deposits could not be determined from Viking images. The Mars Orbiter Camera on Mars Global Surveyor has provided a 50-fold increase in resolution that shows more differences between the two poles. The North residual cap surface has rough topography of pits, cracks, and knobs, suggestive of ablational forms. This topography is less than a few m in height, and grades in to surfaces exposing the layers underneath. In contrast, the south residual cap has distinctive collapse and possibly ablational topography emplaced in four or more layers, each ~2 m thick. The top surface has polygonal depressions suggestive of thermal contraction cracks. The collapse and erosional forms include circular and cycloidal depressions, long sinuous troughs, and nearly parallel sets of troughs. The distinctive topography occurs throughout the residual cap area, but not outside it. Unconformities exposed in polar layers, or other layered materials, do not approximate the topography seen on the south residual cap.

The coincidence of a distinct geologic feature, several layers modified by collapse, ablation, and mass movement with the residual cap indicates a distinct composition and/or climate compared to both the remainder of the south polar layered units and those in the north.

ESTIMATING THE EVOLUTION OF CRYSTAL SIZE IN THE NORTH POLAR ICE CAP ON MARS.

Th. Thorsteinsson, Science Institute, Department of Geophysics, University of Iceland, Hofsvallagötu 53, IS-107 Reykjavik, Iceland. E-mail: ththor@raunvis.hi.is

Introduction: The drilling of deep ice cores to bedrock in Greenland and Antarctica has allowed the study of internal stratigraphy, crystal growth rates, fabric evolution and rheological properties of Earth's polar ice masses. We discuss the likely evolution of crystal size in the North Polar Ice Cap on Mars in the light of results obtained from Terrestrial ice sheets.

Glaciological Data: Estimated glaciological data for the North Polar Cap:

Thickness H = 3 km, based on new data obtained by the Mars Orbiter Laser Altimeter (MOLA) experiment on the Mars Global Surveyor spacecraft [1].

Accumulation rate estimates vary from 0.04 mm/yr to 3 mm/yr [2,3,4].

Surface temperature T_s = -100 °C. This value was used by Budd et al. [5] in a modeling study (citing data obtained by the Viking orbiters). Budd et al. argue that a simple steady-state form of the heat-transfer equation; $d^2T/dz^2 = 0$, is adequate, leading to a simple linear temperature profile of the form $T(z) = T_s + \gamma z$; where z is depth below surface and γ is the temperature gradient. Assuming a heat flux of 0.8 μcal/cm^2/s, Budd et al. calculated a bottom temperature of -50 °C. In the light of new constraints on ice thickness, this estimate appears realistic.

Age: Assuming a familiar, terrestrial flow pattern, the Nye and Dansgaard-Johnsen flow models of layer thinning with depth [6,7] can be used to estimate age versus depth. The maximum estimate of accumulation rates, a = 3 mm/yr, gives an age of 700000 yr at 1500 m depth and close to 5 million yr at 2700 m depth. This is a lower bound for the ages, which would be 10x higher assuming a = 0.3 mm.

Grain Growth in the North Cap: To estimate grain growth in the North Polar Cap, we use the basic relation

$$D^2=D_o^2 + k\,t \qquad (1)$$

where D is the average grain diameter at time t, D_o is the initial diameter at time t=0, t is time and k is the growth rate, which is governed by temperature by an Arrhenius factor according to the relation $k = k_o\exp(-Q/RT)$. Here k_o is a constant, Q is the activation energy, R is the gas constant and T is the temperature. The above relation successfully describes grain growth in polar firn undergoing metamorphism (sintering) to glacier ice [7], and is also useful for predicting increase in grain size with age in those parts of the polar ice sheets which are governed by normal grain growth but unaffected by other recrystallization processes. However, as discussed by Kieffer [8] in a theoretical study of grain growth in the uppermost 60 m of the North Cap, the rate of sintering is expected to be higher under Martian conditions in spite of the colder temperatures, due to a strong variation of the water vapour diffusion coefficient with atmospheric pressure. The transport coefficient determining the rate of sintering [9] thus needs to be scaled to Martian conditions, where average atmospheric pressure is only 7% of the Terrestrial average. Kieffer [8] found that this would lead to a growth rate two orders of magnitude higher in Martian firn than in Terrestrial firn, for the same temperatures. His results indicate that grain sizes of the order of 1 mm have evolved by a depth of 60 m in the North Cap, which is comparable to grain sizes at 100 m depth on the Greenland and Antarctic ice sheets.

Using Kieffer's scaling factor and the above glaciological data (with a = 3 mm/yr), the grain-growth relation has been used to estimate the evolution of crystal size below 60 m, starting with a diameter of 1 mm at this depth. A simple step calculation is performed, using time-averaged Arrhenius factors over each time step. Calculated grain-sizes at selected depths, as compared with measured GRIP and Vostok results are shown in Table 1. These preliminary results indicate that considerably larger crystals would grow in the uppermost 2.5 km of the Mars ice cap than in the terrestrial ones; the main reasons being the much higher age of the ice and the above mentioned Martian increase in sintering rate. Note that these are minimum crystal size estimates for the North Cap, since the maximum estimate of the accumulation rate is assumed.

Table 1. Crystal sizes in the Greenland and Antarctic ice sheets (measured on the GRIP and Vostok ice cores, respectively [10], [11]), and estimated for pure H_2O ice in the North Polar ice cap on Mars.

Depth	GRIP	Vostok	Mars North Cap
500 m	3	2	6
1000 m	4	3	15
1500 m	4	4	30
2000 m	3	5	70
2500 m	4	7	>100

Crystal diameters are given in mm

Discussion: A number of uncertainties are involved in this order-of-magnitude estimation. - Firstly, it must be questioned whether the Martian scaling factor for sintering is valid after pore-closeoff has occurred. - Secondly, the effect of polygonization, i.e. the subdivision of grains under increasing load, is not taken into account. This process counteracts grain growth and is the primary cause of the stop in grain growth in the interval 700-1600 m in the GRIP ice core [10]. It is, however, not unrealistic to assume that the effects of polygonization are minimal in the North Cap, since the vertical strain rate can safely be assumed to be very low. Polygonization is, for example, much less active at the Vostok site than at GRIP, indicating that the lower strain-rate and temperature leads to a lower concentration of intracrystalline dislocations forming sub-grain boundaries. - Thirdly and most importantly, the presence of dust in the ice has not been taken into account. There is ample evidence from ice core and ice margin studies that the presence of atmospherically transported dust and other insoluble impurities in significant concentrations can slow grain growth considerably, since the impurities tend to segregate to grain boundaries and retard their migration. Since the Martian ice caps seem to be heavily loaded with wind-transported dust, in much higher concentrations than those found in terrestrial ice sheets, this effect is likely to exert a strong controlling influence on the H_2O grain size.

In a theoretical study of the effects of microparticles on grain growth, Alley et al. [12] developed a model which predicts a 100% reduction in grain-growth rate for a dust volume percentage of only ~0.05%. But estimates of dust content in the Mars ice cap range from several % to perhaps higher than 50% [13], indicating a strong effect on grain-size evolution in this ice. The only terrestrial results which can perhaps be realistically compared to the Martian conditions are the ones obtained on debris-laden bottom ice from the various deep cores (GRIP, GISP2, Dye 3, Camp Century, Byrd). The weight percentages of bottom debris in such ice are typically 0.1-10% (see f.ex. Gow et al. [14] and Tison et al. [15]), and the dirtiest parts of such ice are fine-grained throughout (1-3 mm). This indicates extremely low grain-growth rates in the debris-laden ice, which is likely to be very old, perhaps dating from the initial stages of ice-sheet formation.

Summary: Our present state of knowledge of the Martian ice caps, in particular of their accumulation rates, dust content and age-depth profiles, is inadequate to allow for realistic estimates of crystal size variation. Factors such as high age and higher sintering rates would favour the formation of comparatively large crystals in the North Polar ice cap, whereas the high dust content is likely to exert a strong controlling influence on the crystal growth. Considerable variation in crystal size is likely to be superimposed on a downward increase, since the dust deposition is believed to have varied with long term climatic changes on the planet. If the general flow pattern is similar to that of Terrestrial ice sheets, layering exposed at the ice margin could reveal crystal size variations which have evolved in the interior regions of the ice cap over millions of years. Such crystal size variation, which would be an indirect indicator of past climatic variation, could be detected by orbiting spacecraft or measured directly by landers and rovers.s

References:

[1] M. Zuber et al. (1998) *Science*, 282, 2053-2060. [2] D.A. Paige & A.P. Ingersoll (1985) *Science*, 228, 1160-1168. [3] J. Pollack et al. (1979) *JGR*, 84, 2929-2945. [4] D.A. Fisher (1993) *Icarus*, 105, 501-511. [5] W.F. Budd et al. (1986) *Polarforschung*, 56, 46-63. [6] W. Dansgaard & S.J. Johnsen (1969) *J. Glaciol.*, 8 (53), 215-223. [7] W.S.B. Paterson (1994) *The Physics of Glaciers*, Pergamon, 480 pp. [8] H. Kieffer (1990) *JGR*, 95 (B2), 1481-1493. [9] P.V. Hobbs (1974) *Ice Physics*, Clarendon Press, 837 pp. [10] Th. Thorsteinsson et al. (1997) *JGR*, 102 (C12), 26583-26599. [11] V. Lipenkov et al. (1989) *J.Glaciol.* 35 (121), 392-398. [12] R.B. Alley et al. (1986) *J. Glaciol.* 32 (112), 415-433. [13] S. Clifford et al. (2000) *Icarus* (in press). [14] A.J. Gow et al. (1979) *J. Glaciol.*, 23 (89), 185-192. [15] J.L. Tison et al. (1994) *Earth Planet. Sci. Lett.*, 125, 421-437.

MESOSCALE SIMULATIONS OF MARTIAN POLAR CIRCULATION: I, POLAR CAP EDGE CIRCULATIONS AND DUST LIFTING. A. D. Toigo, and M. I. Richardson, Division of Geological and Planetary Sciences, MC 150-21, California Institute of Technology, Pasadena, CA 91125, toigo@gps.caltech.edu, mir@gps.caltech.edu

Introduction: Lifting of dust requires high near-surface winds. A major problem in understanding the Mars dust cycle centers on determining the mechanism(s) generating these winds. Potential mechanisms include small-scale convective vortices (dust devils), regional slope winds, albedo and/or thermal inertia contrast (seabreeze) winds, etc. The retreating edge of the south seasonal polar cap is the observed location of numerous local dust storms [1, 2]. Therefore the role of the strong temperature contrast between bare ground and the CO_2 ice has long been suspected of being an important generator of dust-lifting winds.

The acquisition of high quality topography for the south polar regions allows for the first time simulations of the south polar circulation to be undertaken. Of equal importance is the availability of high-resolution atmospheric models and high-speed computing facilities, which allow the circulation to be inferred from the topographic (and albedo and thermal inertia) data.

Mars mesoscale modeling: Mesoscale models of the earth's atmosphere have existed since the 1970's; however only recently have these models been applied to Mars. Mesoscale models represent a significant improvement over global models (general circulation models [GCMs]) in their ability to represent local processes, especially over the poles. The particular strength of mesoscale models for polar modeling results from the absence of a mathematical pole at the geographical pole, which is not the case for GCMs. Mesoscale models can define domains on a variety of map projections, allowing the pole to be included in a region of interest.

Model description: The Mars mesoscale model used in this study is a modified version of the Penn State/NCAR Fifth Generation Mesoscale Model (MM5). The original version of the model is described by [3] and [4]. The model solves the equations of motion in a regular, discretized domain (horizontal Arakawa B-grid, vertical sigma coordinates). Parameterization modifications include the Mars orbital parameters, Mars rotation and gravity, Martian atmospheric composition, CO_2 and dust radiative transfer schemes, the treatment of atmospheric condensation and sublimation, and injection and transport of atmospheric dust. Water processes are also included, but do not feed back on the rest of the simulation [5].

Simulations: We will discuss results from our simulations of polar circulations during the southern spring and summer seasons. Near-surface wind velocities and dust-lifting potential near the south pole will be analyzed to determine whether wind speeds and stresses ever become large enough for dust lifting, and if so, where those dust lifting locations are. We will assume a small amount of sand present everywhere to initiate the dust lifting as a result of saltation. Also we will discuss the nature of the polar circulations, including the role of small-scale and/or convective eddies.

References: [1] Peterfreund A. R. (1985) Ph.D. Thesis, Arizona State Univ. [2] Wells R. A. (1979) *Geophysics of Mars.* [3] Anthes R. A. and Warner T. (1978) *Mon. Wea. Rev., 106,* 1045-1078. [4] Dudhia J. (1993) *Mon. Wea. Rev., 121,* 1493-1513. [5] Richardson M. I. and Toigo A. D., (2000) this volume.

CATASTROPHIC FLOODS IN ICELAND. H. Tómasson, National Energy Authority, Grensásvegur 9, 108 Reykjavík, Iceland. (ht@os.is)

INTRODUCTION: Glaciers are a part of the solid earth, but they move much faster than other parts of "terra firma". Their movement in interply with subglacial volcanism causes rapid changes and release of energy hardly known elsewhere in nature. The fastest movement and release of energy takes place in ice covered calderas and ice dam lakes (Tómasson 1991). If we define catastrophic flood as one with a peak flow of hundreds of thousands m^3/s we probably have a few every century in Iceland. The most recent observed event to meet this definition, is the Grímsvötn jökulhlaup in 1996 (Haraldsson et al. 1997). Its peak flow is estimated at 50,000 m^3/s. The catastrophic floods dealt with in this paper are Katla 1918; a prehistoric jökulhlaup from Mýrdalsjökull about 1700 years old, a very large jökulhlaup in Jökulsá á Fjöllum occuring about 2500 years ago and finally a series of jökulhlaups from ice-dam lake in Hvítá about 9500 years old.

THE LAND FORMS AND PROCESSES BY CATASTROPHIC FLOODS: The landforms created by catastrophic floods are alluvial plains on a gentle slope and the canyons eroded at steeper slopes. The flood-deposited alluvial plains do not differ much from other alluvial plains, but canyons differ much from most other such formations in size and cross-sectional area. There are two types of parent rock, i.e. hard basalt and soft móberg (tuff, breccia or pillow-lava). The erosion occurs in two ways, through stones rolling or jumping in saltation over the bottom or the rock is broken up by cavitation which acts like explosions and is a function of velocity and rock form.. The energy of a rock particle in movement is:

$$0{,}5*mv^2$$

Where m is mass and v is velocity. Particles in fast flowing water are rapidly worn down. This process might lead to depletion i of the big particles in the fluid and decreasing erosional capacity. Cavitation can play a part in this process and add to the erosive capasity by breaking the rock into particles, which will then further erosion. There is considerable difference between canyons eroded in bsaltic lava flows on one hand and móberg on the other. The basalt lava flows are eroded into wide canyons but the móberg into narrow ones. In the basalt lava flows cavitation is more intense as the columnar jointing and horizontal cleavage create more sharp edges necessary for cavitation. The moberg is eroded more by particles in saltation. Cavitation is probably also active in subglacial tunnels increasing the critical cross-sections and thereby eroding glacier ice and rock.

KATLA AND MÝRDALSSANDUR: The Katla caldera has been very active in recent centuries. Many of the eruptions have been fairly well described by eyewitness. The most recent eruption occured the 12th of October 1918. A detailed description based on eyewitness accounts was published in 1919 (Jóhannson; Sveinsson 1919), The flood volume is estimated by comparing the difference between the maps of the Danish Ordinance Survey from 1904 and the map of U.S. Army Map Service from 1946. The difference between the contour lines of these maps is about 1 km^3 which corresponds to the ash deposited on land in the eruption. Measurement done by Einarsson (1979) indicates that 90 % of the material on the sandur plains is volcanic ash from the eruption. The rest of the material (Tómasson 1995) extended the shoreline 1 km seawards, was carried by the eastern branch of the flood and was also airborne. The estimated total quantity of ash is 2,5 km^3, which corresponds to 0,9 km^3 of solid lava and melted 8 km^3 of ice. The maximum discharge was estimated from flow velocity based on eyewitness accounts and measured cross-sectional area as inferred from flood marks. The flow velocity was calculated as 10 m/s, and the cross-section 2700 m^2. The the main channel carried 270,000 m^3/s. An approximation of the magnitude indicates that the catastrophic flood at peak discharge carried 300 000 m^3/s of liquid water, suspended sediments and ice.

MARKARFLJÓT CANYON: About 2500 years ago catastrophic flood burst on from below Mýrdalsjökull flowing towards north. This flood eroded the Markarfljót canyon (Sigurðsson 1988), among the largest canyons in the country. In this canyon the difference between erosion in móberg and basalt is obvious. A wide almost dry canyon eroded into basalt is to be found in Innri Emstur and at the lower end of Markarfljót canyon. In between these is the main canyon eroded in móberg, narrow, but up to 200 m deep. The dating of this event is based on thick sand layer found in the soil at Landeyjar (Haraldsson 1981).

JÖKULSÁ Á FJÖLLUM: The greatest catastrophic flood in postglacial time occurred in Jökulsá á Fjöllum. Traces of that flood are obvious all the way from the Vatnajökull glacier dawn to the sea shore about 170 km away. The bedrock is basaltic lava of various age. On the interior high plateau the slope is gentle and the flood path is markedby plucked and eroded rock surface, alternating with huge depositional gravel and sandbars. At the highland margin the canyons are eroded mostly into thick-bedded basalt lava flows. The total eroded volume is estimated $500+10^6$ m^3. The uppermost part is eroded into thick lava flows. the middle part is Svínadalur, a basin filled with postglacial lava now to a great extentl eroded; the lower canyon is eroded into lava flows. Parallel to the lower canyon is the erosion form Ásbyrgi. The landforms at Jökulsá á Fjöllum have strong resemblance to the channeled scabbland and canyons of the Columbia basalt plateau in the U.S. The Columbia plateau was flooded in catastrophic floods from ice dam lake Missula (Bretz 1959) in Montana.

The catastrophic flood in Jökulsá has been dated with tephrocronology. (Þórarinsson 1960). According to that all tepra layers older than H_3, which is 2800 years old, are lacking in the flood path, but a tephra layer about

2000 years old is found at the bottom of the soil layer. This indicates that the flood event is about 2500 years old. Since the colonization of Iceland 1100 years ago 8 jökulhlaup are documented in annals. These descriptions indicate jökulhlaups in the rance of some thousand m^3/s (Þórarinsson 1960). Whithin the watershed of Jökulsá in Vatnajökull there is a very active volcanic area. Most active and probably largest is Bárðarbunga volcano. Measurements have shown that under Bárðarbunga there is (Björnsson 1987) a huge caldera. South of Bárðarbunga is another well-known caldera, the Grímsvötn. In following table the two calderas are compared. All conditions favor a much bigger flood from Bárðarbunga than Grímsvötn.

	Grímsvötn	Bárðar-bunga
Drainage area km^2	160	80
Caldera km^2	24	48
Threshold ele. m a.s.	1200	1400
Bottom ele. m a.s.	1050	1100
Volume km^3	3,6	14,4

There are two types of Jökulhlaup. One type that increases slowly with low peak-flow and a considerable time lapse before reaching the peak. Such floods are cool and the conduit under the glacier is enlarged through frictional heat and erosion. The other type of jökulhlaups increases very fast. They have above zero water geting heat from geothermal activity or a volcanic eruption. A good example is jökulhlaup from Grímsvötn. The volume of the Grímsvötn jökulhlaup in 1940 to 1990 was in the order of magnitude 1-3 km^3, and the peak flow reached 1000-7000 m^3/s and lasted 2 weeks from outbreak to peak. The 1996 jökulhlaup (Haraldsson 1997) increased very fast, was hot in the beginning, but lasted only about a day. The total volume was 3,6 km^3 and peak flow 50,000 m^3/s. This flood was associated with a volcanic eruption. The same processes are responsible for the jökulhlaup from the caldera in Bárðarbunga. The present condition in the caldera is such that it is full of ice and there is no water accumulated at its bottom (Björnsson 1987). The melted water must leak out of the caldera through rock. Every now and then the geothermal heat or volcanic activity increases substantially and meltwater accumulates in the caldera and escapes in jökulhlaups, which are usually small in comparisation to the catastrophic floods. But occationally all conditions are favorable for catastrophic floods. The last time this occurred was 2500 years ago.

This catastrophic flood is calculated from slope and cross-sectional area to have been 500,000 m^3/s. Probably, big floods have often taken place and even some of them have been classified as catastrophic (Elíasson 1977). But the whole picture is of one catastrophic flood, much bigger than any previous or later floods. The simultaneous maximum volume of water in the flood channel was about 5 km^3, and it took the water 11 hours to flow in wetted channel from the glacier to the sea (Tómasson 1973). The probable total volume of the flood is 15 km^3 and it lasted 1-2 days.

HVÍTÁ Í ÁRNESSÝSLA AND KJÖLUR: The catastrophic floods in Hvítá were different from the one described above, which all came from volcanic calderas and a accompanied by volcanic activity. But the floods in Hvítá came from ice dam lakes created when the main inland glacier in Iceland retreated over the water divide at Kjölur gradually creating a very big ice dam lakes south of the water divide (Tómasson 1993). Conditions favorable for the creation of the big floods has probably lasted 100-200 years. This was at the final stage of the last glaciation of Iceland some 9500 years ago.

The ice dam lakes left shorelines at different levels. The uppermost are formed above the water divide towards north, but the clearest are at the level of the water divide. At that level a continuous flow has been towards north. Most of the shorelines are at a lower level. At the level of Bláfellsháls a fairly clear shoreline is found indicating a continuous flow of some duration. That period ended with the catastrophic flood east of Bláfell..

The flood channel is clear from elevation 300 to 50 m a.s.l. The most conspicuous part of it is the Gullfoss canyon. It is at the edge of the high plateau, and the total volume is $100*10^6$ m^3. Down stream of the canyon is a hugh gravel bar laid down by the catastrophic floods. The maximum discharge is estimated at 200,000 m^3/s and the volume of the lake was approximately 25 km^3. This has been a cold lake with the floods lasting 2-3 weeks.

References: [1] Björnsson, H. 1988. Hydrology of Ice Caps in Volcanic Regions. Reykjavík.[2] Bretz, J.H. 1959. Washington channeled scabland. The state of Washington, Division of mines and geology, Olympia. 1-57. [3] Einarsson, G. 1979. Mýrdalssandur pumice deposit. Reykjavík, Iðntækni stofnun. [4] Elíasson, S. 1977. Molar um Jökulsárhlaup og Ásbirgi. Náttúrufræðingurinn, 47.
[5] Haraldsson, H. 1981. The Markarfljót Sandur Area, Southern Iceland. Societas Upsalensis Pro Geologia Quarternaria v. 15. [6] Jóhannsson, G. 1919. Kötlugosið 1918. Reykjavík. [7] Sigurðsson F. et al. 1988. Fold og vötn að Fjallabaki. Árbók Ferðafélags Íslands 1988. [8] Snorrason, Á. et al. 1997. Hlaupið á Skeiðarársandi 1996. From Vatnajökull gos og hlaup 1996. Vegagerðin. [9] Sveinsson, G. 1919. Kötlugosið 1918 og afleiðingar þess. Reykjavík. [10] Tómasson, H. 1973. Hamfarahlaup í Jökulsá á Fjöllum. Náttúrufræðingurinn, 43. [11] Tómasson, H. 1993. Jökulstífluð vötn á Kili og hamfarahlaup í Hvítá í Árnessýslu, Náttúrufræðingurinn, 62. [12] Tómasson, H. 1996. The jökulhlaup from Katla in 1918. Annals of Glaciology 22 19. [13] Þórarinsson, S. 1960. Der Jökulsá-canyon und Ásbyrgi. Petermanns Geogr. Mitteilungen 104.

INITIAL 3-D MESOSCALE SIMULATIONS OF THE NORTH POLE MARTIAN SUMMER ATMOSPHERIC CIRCULATION. D. Tyler[1] and J. R. Barnes[2], [1]Affiliation (College of Oceanic and Atmospheric Sciences; Oregon State University; Corvallis, OR 97331 dtyler@oce.orst.edu), [2]Affiliation (College of Oceanic and Atmospheric Sciences; Oregon State University; Corvallis, OR 97331 barnes@oce.orst.edu).

Introduction: We are developing a computer model to simulate regional atmospheric circulations on Mars. The Fifth Generation Penn-State/NCAR Mesoscale Model (MM5) [1] has been modified for studying Mars (MMM5). We are using the NASA Ames Mars General Circulation Model (MGCM) to provide the initial and boundary conditions for our various simulations. The version of the MGCM that is being used in these simulations is described by [2]. The MMM5 is using the same atmospheric radiation code as developed for and used in the MGCM.

Pathfinder Simulations: At the time of this writing we are finishing our study of the diurnal variation of surface meteorology at the Sagan Memorial Site. We observe benefits in using the MMM5 to simulate the Pathfinder data, as the MMM5 does better reproducing the diurnal evolutions of wind direction and surface air temperature than does the MGCM. Our simulations to date have been dry and hydrostatic.

These modeling efforts take advantage of the newest data from the Thermal Emission Spectromenter (TES) and the Mars Orbital Laser Altimeter (MOLA), both flown on the Mars Global Surveyor mission. With data made available by [3], [4] and [5] we have developed maps for surface topography, surface thermal inertia and surface albedo for both the MGCM and the MMM5. Our modeling results have shown improvement by using these data. These results will be presented.

North Pole Simulations: At the time of this writing we have just begun our efforts to simulate atmospheric circulations for the Martian North Pole summer. The MGCM is again being used to provide initial and boundary conditions for the MMM5. In these modeling efforts we plan to study both the 3-d nature of katabatic flows from the polar ice cap and the sublimation and equatorward transport of water vapor during this season.

References:

[1] Dudhia J. (1993) *M. Wea. Rev.* 121 1493-1513. [2] Haberle R. M. et al. (1999) *JGR* 104 8957-8974. [3] Haberle R. M. (1999) personal communication. [4] Mellon M. (1999) personal communication. [5] Christensen P. (2000) personal communication.

A SUBSURFACE EXPLORER FOR DEEP UNDERGOUND EXPLORATION ON MARS. B. H. Wilcox[1], A.R. Morgan[2], Jet Propulsion Laboratory, California Institute of Technology, M/S 107-102, 4800 Oak Grove Dr. Pasadena, CA 91109, [1]Brian.H.Wilcox@jpl.nasa.gov, [2]Albert.R.Morgan@jpl.nasa.gov.

Abstract: A subsurface explorer (SSX) is being developed at the Jet Propulsion Laboratory which is suitable for exploration of the deep underground environments on Mars. The device is a self-contained piledriver which uses a novel "spinning hammer" technology to convert a small continuous power feed from the surface over a two-wire tether into a large rotational energy of a spinning mass. The rotational energy is converted to translational energy by a novel mechanism described here. The hammer blows propagate as shock waves through a nosepiece, pulverizing the medium ahead of the SSX. A small portion of the pulverized medium is returned to the surface through a hole liner extending behind the SSX. This tube is "cast in place" from two chemical feedstocks which come down from the surface through passages in the hole liner and which are reacted together to produce new material with which to produce the hole liner. The lined hole does not need to be the full diameter of the SSX: approximately 100 kilograms of liner material can create a tunnel liner with a 3 mm inside diameter and a 6 mm outside diameter with at total length of 4 km. Thus it is expected that core samples representing an overlapping set of 3-mm diameter cores extending the entire length of the SSX traverse could be returned to the surface. A pneumatic prototype has been built which penetrated easily to the bottom of an 8 meter vertical test facility. An electric prototype is now under construction. It is expected that the SSX will be able to penetrate through sand or mixed regolith, ice, permafrost, or solid rock, such as basalt. For pure or nearly pure ice applications, the device may be augmented with hot water jets to melt the ice and stir any sediment which may build up ahead of the vehicle. It is expected that an SSX approximately 1 meter long, 3-4 cm in diameter, and with a power budget of approximately 200 Watts will be able to explore up to ~5 kilometers deep at the rate of about 10 meters per day.

THE POLAR REGIONS AND MARTIAN CLIMATE: STUDIES WITH A GLOBAL CLIMATE MODEL. R. J. Wilson[1], [2]M. I. Richardson, and [3]A. V. Rodin, [1]Geophysical Fluid Dynamics Laboratory, Princeton, NJ 08542, rjw@gfdl.gov, [2]Division of Geological and Planetary Sciences, MC 150-21, California Institute of Technology, Pasadena, CA 91125, mir@gps.caltech.edu, [3]IKI, Profsoyuznaya 84/32, 117810 Moscow, Russia; rodin@irtn.iki.rssi.ru

Introduction: Much of the interest in the polar regions centers on the fact that they likely contain the best record of Martian climate change on time scales from years to eons. This expectation is based upon the observed occurrence of weathering product deposits and volatile reservoirs that are coupled to the climate. The interpretation of these records requires an understanding of the exchange of dust, water, and CO_2 between the surface and atmosphere, and the atmospheric redistribution of these species. Here we discuss a global climate model that incorporates these elements at some level and will allow examination of the coupling between polar deposits and global climate systems to begin in earnest.

Model: The GFDL Mars GCM simulates the circulation of the Martian atmosphere from the surface to roughly 90 km [1]. The GCM provides for the transport of an arbitrary number of aerosol tracers and includes parameterizations for the interactive calculation of heating rates at infrared and visible wavelengths due to aerosols. We have examined a range of assumptions about the injection of dust into the lowest atmospheric layer. The water cycle is addressed by including surface ice and regolith water reservoirs, atmospheric transport and ice cloud formation [2]. Recently, a cloud microphysical scheme has been implemented to explicitly track the growth of water ice on dust aerosol [3]. The optical properties of ice-coated dust aerosol are accounted for, allowing investigation of the potential radiative-dynamical-microphysical effects of water ice cloud formation to be examined in a Mars GCM for the first time.

Dust Cycle: Variations in the amount of suspended dust provides a primary control on atmospheric heating and the vigor of the resulting circulation. It is likely that the signature of the dust cycle and its varying intensity at different times is recorded in some fashion in the polar layered terrains. The fundamental issue is the determination of dust raising mechanisms.

To date we have focussed on simulating the evolution of the dust distribution following the onset of global dust storms. A substantial amount of data exist which provide constraints on the character and behavior of dust, including measurements of the surface pressure tide, atmospheric optical depths, measurements of atmospheric temperatures as a function of height, and extended seasonal and local time coverage of air temperatures in a deep layered centered at roughly 25 km. The model does exceptionally well in simultaneously fitting these diverse observations, suggesting that processes *after* dust injection into the lowest model level are now captured and understood [4].

The injection feedback is the most important individual piece missing. While stresses resulting from large-scale winds can be tuned to raise dust by arbitrarily scaling the lifting stress threshold, simulations have been unsatisfying due to a strong dependence on model resolution suggesting that the true processes are of smaller than resolved scales [5]. Determination of dust lifting processes will require study with higher resolution models, such as the Mars Mesoscale Model described by [6].

The modeled cycles of dust and air temperature do not currently show any significant interannual variability. As only the dust injection rate is specified, this suggests that the atmospheric side of the dust cycle (above the surface layer) possesses little internal variability and subseasonal memory. A possible mechanism for interannual variability is the spatial distribution of dust on the surface, supported by spacecraft and telescopic observations of interannual albedo variations. A future line of research will couple injection and sedimentation to surface budgets of dust to investigate their role in interannual variability.

Water Cycle: The water cycle has been incorporated in the GCM through the prescription of a northern residual ice cap, treatment of water vapor and ice atmospheric transport, regolith diffusion and adsorption, surface water condensation, and surface-atmosphere exchange. Studies of the water cycle to date have concentrated on an effort to determine those physical processes controlling the total atmospheric abundance of water and the annual cycle of water between reservoirs. An understanding of these mechanisms is a fundamental prerequisite for study of the paleo-water cycle. We have undertaken a number of multi-annual simulations of the water cycle with varying degrees of regolith activity and dust loading (differing air temperatures).

As discussed in [2], we find that the primary

"spigot" controlling the amount of water in the atmosphere is the northern residual water ice cap temperature. We describe a feedback control mechanism involving transport to and from the cap over an annual cycle. While the regolith plays a role in altering the distribution of vapor as a function of time, it is of secondary importance for controlling atmospheric water amounts. We also find that substantial amounts of water move between the hemispheres during the cycle, effectively "sloshing" between the seasonal caps with a small net loss of water annually to the southern residual CO_2 ice cap.

An important theoretical consequence of the control mechanism is the prediction of relative water ice cap stability. Simulations initiated with water ice caps at both poles result in a net transfer of water from south to north, and the elimination of the southern cap (the net transport of water in the *current* climate would be south-to-north were it not for the south polar cap cold trap). This occurs even when the cap surface temperatures are arbitrarily equalized. Transport asymmetries therefore destabilize water at the southern pole even in the absence of a cap temperature difference.

A major unresolved issue in our modeling of the water cycle involves the hemispheric asymmetry of water vapor mass observed by the Viking Mars Atmospheric Water Detector (MAWD). While MAWD suggests a rough doubling of vapor between southern and northern summers, the model shows a much smaller gradient (although the vast majority of water is always in the northern hemisphere). Regolith activity does not allow the model to be in any better agreement with the data. Nor do changes in cloud precipitation rate (although a more detailed treatment of clouds offers some modest hope of better agreement). However, southern spring and summer MAWD data are badly degraded by dust scattering due to two dust storms. Further, the model is in somewhat better agreement with telescopic observations.

Coupling of Cycles: The aphelion season (L_s~40-130°) is characterized by relatively cold temperatures, low dust loading, and a prominent tropical water ice cloud belt [7]. We have carried out simulations that reproduce the major observable features this period and have found that dust/water ice cloud interactions may be significant in suppressing the depth and amount of the dust aerosol. The predicted water condensation level is ~10 km in the tropics. The simulations show a realistic development and decay of both the tropical cloud belt in the aphelion season and the water ice cloud component of the North Polar hood that forms in autumn and decays in early spring. We suggest that the characteristics of the tropical cloud belt, and hence, the global dust loading and temperature, may be strongly linked to the physical conditions of the residual North polar water ice cap.

Response to Orbital Variations: We have begun using the model to examine surface wind patterns and their variation with orbital parameters and have found that surface winds are remarkably resilient to changes in orbital parameters and dust injection [8]. The wind speeds can vary by a factor of 2 between 15° and 35° obliquity. The phasing of the perihelion season modifies the relative intensity of northern and southern summer flows, however the strong zonally-averaged cross-equatorial topographical slope significantly favors the southern hemisphere summer circulation. At high obliquity there is the expectation of increased dustiness due to the intensified Hadley circulation and increased water column at the summer pole due to increased insolation. We are examining the possible influence of increased tropical water ice clouds in these circumstances.

References: [1] Wilson R J. and Hamilton K. (1996) *JAS* 53, 1290-1326. [2] Richardson, M. I. (1999) Ph.D. Thesis, UCLA. [3] Rodin, A. V. et al. (1999) *Adv. Space. Res.* 23, 1577-1585. [4] Wilson and Richardson (1999). Abstract #6234, 5th Int'l Conf. On Mars [5] Forget *et al.* (1999) 5th Int'l Conf. On Mars. [6] Toigo A. D. and Richardson M. I. (2000) this volume. [7] Pearl J. et al. (2000) *JGR.* in press [8] Fenton L. K. and Richardson M. I. (2000) LPSC XXXI 2072.

THE DETECTION OF COLD DESERT BIOMARKERS, ANCIENT AND MODERN: ANTARCTICA AND MARS? D.D. Wynn-Williams[1*], H.G.M. Edwards[2] and E.M.Newton[2], [1]British Antarctic Survey, Natural Environment Research Council, High Cross, Madingley Rd., Cambridge CB3 0ET, UK, e-mail: ddww@bas.ac.uk; Tel.: +44 (0)1223 221554; Fax: +44 (0) 1223 221259; * corresponding author, [2] Department of Chemical and Forensic Sciences, University of Bradford, Bradford, West Yorkshire BD7 1DP, UK, e-mail: h.g.m.edwards@bradford.ac.uk; Tel.: +44 (0)1274 233787; Fax: +44 (0)1274 235350.

Dry cold conditions preserve biomolecules, as exemplified by the standard freeze-dried preservation of microorganisms and frozen storage of biochemicals. The drying process is part of the successful fossilization of organisms and preservation of their organic derivatives. Fossil cyanobacteria and their kerogens are an example. Porphyrins from photosynthetic systems are found in oil-bearing shales (Huseby and Ocampo 1997) and hopanoids are found in some of the most ancient cyanobacterial stromatolites on Earth (Summons et al. 1999). Deamer (1997) puts the origin and fate of porphyrins into an astrobiological context. There are also reports of carotenoids as potential components of ancient kerogens (Damste and Koopmans 1997), whilst scytonemin has been detected in ancient lake sediments (Leavitt et al. 1997).

These photosynthetic and photoprotective pigments have distinctive structures with components which are efficient at interacting with photons. These components are frequently rings and similar complex structures (as in isoprenoids) which retain their core integrity even when their side chains are degraded by microbial decomposition or natural entropy. The cores of these molecules, such as the tetrapyrrole ring of porphyrins, are good biomarkers for extant surface life in extreme desert habitats, and their longevity is enhanced by very low temperatures which decrease the kinetic energy and slow down entropic decay. Antarctic deserts are therefore a good place to evaluate the longevity of such molecules under extremes of UV stress such as might have influenced the early evolution of microbial life on Earth and the putative development and survival of life on early Mars. Vorobyova et al. 1997) have evidence of viable bacteria in Antarctic permafrost for up to millions of years.

The third Epoch of McKay's hydrological model for Mars (McKay 1997) includes the potential survival of photosynthetic sulfur and non-sulfur bacteria and cyanobacteria in cold dry habitats including stromatolites in paleolake beds, evaporite crusts, and endolithic communities in translucent rocks. We have shown previously that it is possible to detect ecologically significant pigments such as cyanobacterial scytonemin in whole organisms and biofilms (Wynn-Williams et al. 1999). These findings, in a polar terrestrial context, poses the following question:

Is it possible to detect evidence of former photosynthetic microbial life at the surface of Mars by using non-intrusive remote techniques (e.g. laser technology) to probe the regolith profile below the zone of peroxide degradation into former stromatolitic or endolithic microbial strata of paleolake beds?

We believe that Raman spectroscopy, using near IR wavelengths to minimize autofluorescence, and applied on Mars using miniaturized CCD technology, would be a suitable technique (see Wynn-Williams et al 2000).

Raman spectroscopy is a technique based on the scattering of incident laser light at frequencies that are shifted by the vibration of component moieties of a compound dependent on its elemental composition and bonding. It has potential for analysis of Martian regolith *in situ* (Edwards and Newton 1999)

The use of near-IR lasers (1064 nm) for Raman spectroscopy avoids autofluorescence of a variety of ecologically important pigments. These include the UV screening pigment scytonemin (Wynn-Williams et al 1999), carotenoids which are UV quenchers (Edwards et al 1998), and the chlorophyll of photosynthetic systems.

Although the presence of numerous other biochemicals in a microbial community can affect the precise wavenumbers of the Raman bands corroborative groups of bands constitute a unique "fingerprint" for any compound. This approach has great potential for the remote detection of biomolecules, as the spectrum of a compound is a sum of its component chemical moieties, each of which gives a distinct band.

Table 1. Wavenumbers/cm^{-1} and selected band vibrational assignments for components of scytonemin

ν/cm^{-1}	Approximate assignment of vibrational mode
565	δ(CCN) aromatic ring indole system
677	δ(CCN) pyrrole ring-puckering mode
754	δ(CCC/CCN) indole ring puckering mode
1090	ν(C-O) phenolic
1163	ν(CC) ring breathing pyrrole
1172	ν(C=C-C=C) system (*trans*)
1245	ν(CC) aromatic ring; *p*-disubstituted benzenes
1384	ν(CCN) indole ring
1444	δ(C=CH)
1525	ν(N=C-C=C) ring mode
1549	ν(CCH) *p*-disubstituted aromatic ring
1590	ν(CCH) aromatic ring quadrant stretch
1605	ν(C=CH) attached to cyclopentene ring
3028	ν(CH) vinylic
3061	ν(CH) aromatic

We have accumulated an FTRS spectral database from a wide range of Antarctic desert habitats and communities as part of a research project on surface microbial communities near the limits of survival under extreme UVB, desiccation and low temperature stress in the Antarctic. We have diagnosed the FT Raman spectra for pure samples of several key protective pigments (including scytonemin and β-carotene). We can now identify them in natural microbial ecosystems such as desert crusts (Wynn-Williams et al., 1999) and endolithic microbial communities within translucent sandstone of the Trans-Antarctic Mountains (Russell et al 1998).

FTRS differs from techniques such as HPLC or TOFSIMS which give a single peak for a compound, dependent on the sum of its characteristics. The comparison of diagnostic Ra-

Raman spectroscopy of microhabitats and microbial communities: Antarctic deserts and Mars analogues

D.D. Wynn-Williams[1*], H.G.M. Edwards[2] and E.M.Newton[2]

man spectroscopy with these techniques for individual molecules would be a powerful combination.

Laser Raman spectroscopy has several advantages for remote planetary analyses: it is based in the scattering of light from the surface of a sample and is therefore independent of path length. The natural freeze-dried state of Antarctic desert microbial biofilms and mats resulting in highly concentrated biomass in an essentially 2-dimensional stratum (either as surficial mats or as light-delineated strata in endoliths or stromatolites), makes them an optimal target for precision laser spectrometry. Using microscopic objectives, the spot size can be as small as 5μm diameter. However, the signal is not affected by moisture, unlike IR spectroscopy, so that analyses can be made on field fresh samples, whatever their hydration state. It is non-intrusive and can be carried out *in situ* without sample transference. Although individual Raman bands can suggest the presence of a compound, corroborative patterns of bands are used to confirm its identity by the sum of the bands of its components and their interactive influence.

If anaerobic green bacteria such as *Chlorobium* (Steinmetz, Fischer 1981) photosynthetic sulfur bacteria , e.g. *Chromatium* (Overmann et al. 1993) or non-sulfur bacteria e.g. *Rhodobacter* (Mukidjanian and Junge 1997) or cyanobacteria-like organisms originated on early Mars, these productive and protective pigments functional moieties may well have been necessary for survival (Garcia-Pichel 1998). The Raman spectra of their functional cores (e.g. isoprenoid derivatives of the abundant carotenoids, see Grice et al 1996) may therefore be a good source of evidence for former life. They are likely to survive much of the fossilization process, especially in polar permafrost. Raman spectra of isoprenoids and cyanobacterial hopanoids, found in Apex cherts 3.5 billion years old (Summons 1999) may therefore be key signatures for future Mars missions with drill facilities for stratal scanning. Suitable strata might be expected in the beds of paleolakes (Doran et al. 1998; Cabrol et al 1999) that are residual from water bodies of the Martian Hesperian period (McKay et al., 1997).

We therefore recommend the evaluation of Raman spectroscopy in Antarctic deserts for pigment in paleo-strata beneath the regolith zone that is likely to be affected by peroxide oxidation (Zent 1998). This would increase our chances of asking the right scientific questions when we have an opportunity to include miniature systems on Mars landers. The advantages of FTRS with 1064 nm laser excitation with negligible pigment autofluorescence will have to give way to the shorter wavelength of c. 852 nm to utilize the light weight, rugged technology of CCD detection systems with long fibber optic probes capable of being lowered down drill holes.

References

Cabrol, N. A., E. A. Grin, H. E. Newsom, R. Landheim and C. P. McKay 1999. Hydrogeologic evolution of Gale Crater and its relevance to the exobiological exploration of Mars. *Icarus* **139**, 235-245.

Damste, J. S. S. and M. P. Koopmans 1997. The fate of carotenoids in sediments: An overview. *Pure and Applied Chemistry* **69**, 2067-2074.

Deamer, D. W. 1997. The first living systems: a bioenergetic perspective. *Microbiology and Molecular Biology Reviews* **61**, 239-261.

Doran, P. T., Wharton, R. A., Des Marais, D. J., McKay, C. P., Antarctic palaeolake sediments and the search for extinct life on Mars, *J.Geophys.Res.Planets* **103**, 8481-28494, 1998.

Garcia-Pichel, F. 1998. Solar ultraviolet and the evolutionary history of cyanobacteria. *Origins of Life and Evolution of the Biosphere* **28**, 321-347.

Grice, K., P. Schaeffer, L. Schwark and J. R. Maxwell 1996. Molecular indicators of palaeoenvironmental conditions in an immature Permian shale (Kupferschiefer, Lower Rhine Basin, north-west Germany) from free and S-bound lipids. *Organic Geochemistry* **25**, 131-147.

Huseby, B. and R. Ocampo 1997. Evidence for porphyrins bound, via ester bonds, to the Messel oil shale kerogen by selective chemical degradation experiments. *Geochimica et Cosmochimica Acta* **61**, 3951-3955.

Leavitt, P. R., R. D. Vinebrooke, D. B. Donald, J. P. Smol and D. W. Schindler 1997. Past ultraviolet radiation environments in lakes derived from fossil pigments. *Nature* **388**, 457-459.

McKay, C.P., The search for life on Mars, *Orig. Life Evol. Biosph.* **27**, 263-289, 1997.

Mukidjanian, A. Y. and W. Junge 1997. On the origin of photosynthesis as inferred from sequence analysis -A primordial UV-protector as common ancestor of reaction centers and antenna proteins. *Photosynthesis Res.* **51**, 27-42.

Overmann, J., G. Sandmann, K. J. Hall and T. G. Northcote 1993. Fossil carotenoids and paleolimnology of meromictic Mahoney Lake, British Columbia, Canada. *Aquatic Sciences* **55**, 31-39.

Russell, N.C., Edwards, H.G.M., Wynn-Williams, D.D. 1998. FT-Raman spectroscopic analysis of endolithic microbial communities from Beacon sandstone in Victoria Land, Antarctica, *Antarct. Sci.* **10**, 63-74.

Steinmetz, M. A., Fischer, U. 1981. Cytochromes of the non-thiosulfate-utilizing green sulfur bacterium *Chlorobium limicola*. *Arch. Microbiol.* **130**,31-37

Summons, R.E., Jahnke, L.L., Hope, J.M. and Logan, G.A. 1999. 2-Methylhopanoids as biomarkers for cyanobacterial oxygenic photosynthesis. *Nature (London)* **400**, 554-557.

Vorobyova, E., V. Soina, M. Gorlenko, N. Minkovskaya, N. Zalinova, A. Mamukelashvili, D. Gilichinsky, E. Rivkina and T. Vishnivatskaya 1997. The deep cold biosphere: facts and hypothesis. *FEMS Microbiology Reviews* **20**, 277-290.

Wynn-Williams, D.D., Edwards, H.G.M., Garcia-Pichel, F. 1999. Functional biomolecules of Antarctic stromatolitic and endolithic cyanobacterial communities, *Eur. J. Phycol.* **34**, 381-391

Wynn-Williams, D.D., Edwards, H.G.M. 2000. Proximal analysis of regolith habitats and protective biomolecules *in situ* by Laser Raman micro-spectroscopy: Overview of terrestrial Antarctic habitats and Mars analogs, *Icarus* **144**, 486-503

Wynn-Williams, D.D., Edwards, H.G.M., Newton. E.M., (2000) Raman spectroscopy of microhabitats and microbial communities: Antarctic deserts and Mars analogues. In *Lunar and Planetary Science XXXI*, Abstract **#1015**. Lunar and Planetary Institute, Houston (CD-ROM)

Zent, A.P. 1998. On the thickness of the oxidized layer of the Martian regolith, *J. Geophys. Res. Planets* **103**, 31491-31498.

POLAR CAP FORMATION AND EVOLUTION OF MARTIAN ATMOSPHERE. T. Yokohata, K. Kuramoto, *Division of Earth and Planetary Science, Hokkaido University, Sapporo, 060-0810 JAPAN (yokohata@ep.sci.hokudai.ac.jp)*, M. Odaka, *Graduate School of Mathematical Sciences, University of Tokyo, Tokyo, 113-0033 JAPAN*, S. Watanabe, *Division of Earth and Planetary Science, Hokkaido University, Sapporo, 060-0810 JAPAN.*

Introduction

Several lines of geological evidence strongly suggest that H_2O was once distributed globally over the Martian surface. At present, however, the surface H_2O is observed only at the polar caps. Under what climate conditions did H_2O gather to the polar caps? To shed light on this question, we construct a climate model including atmospheric transport processes of H_2O to polar cap.

Among the studies on Martian climate, widely accepted one is Gierasch and Toon (1973) (G&T). They suggested that the Martian atmospheric pressure is determined by the CO_2 vapor pressure on the polar cap because CO_2, the main atmospheric component, can condense onto the polar cap. In order to test this idea, they estimated the polar surface temperature by using a simple energy balance model which includes the effect of radiation, heat advection between polar surface and atmosphere, and that between equatorial and polar atmospheres. Assuming the vapor pressure equilibrium between the CO_2 polar cap and the atmosphere, this model can reproduce the present atmospheric pressure as a stable solution.

However, the G&T model has several problems. They assumed the equatorial temperature to be constant. In fact, the equatorial temperature should be determined by the energy balance. Furthermore, seasonal variation of the polar temperature is neglected. In addition, greenhouse effect is not taken into account.

Model

Our energy balance climate model is modified from G&T as follows: 1) Energy balance equations are formulated for the equatorial and summer and winter polar regions (3 box). The solar flux absorbed by the surface is given by the seasonally averaged value in each region. 2) The greenhouse effect is taken into account. The radiative fluxes at the top and bottom of the atmosphere are estimated by solving the radiative transfer for a gray atmosphere with radiative-convective structure. The absorption coefficient of the gray atmosphere is given as a function of the surface atmospheric pressure so as to fit the non-gray calculation by Pollack et al. (1987). 3) Our model includes the latent heat of CO_2 sublimation or condensation at the polar surface. The latent heat flux is given in proportion with the difference between CO_2 equilibrium vapor pressure and the atmospheric pressure. 4) H_2O is transported from the equatorial region to the polar region by advection of atmosphere. The process of the atmospheric advection is the same as G&T, which is by baroclinic waves. We assume that H_2O in the atmosphere is always saturated. The deposition rate of H_2O onto the polar caps is estimated from the mass flux of H_2O transport from the equatorial region to the polar region.

We consider two cases of the surface albedo: one is that only the polar regions are covered with ice (standard model), another is that the surface is entirely covered with ice (snowball model) assuming a past Mars with more surface H_2O.

Results and discussion

Figure 1 shows the surface temperature obtained from the standard model. The surface temperature increases with the atmospheric pressure (p_s) because of the greenhouse effect. When $p_s > 10^4$ Pa, CO_2 should sublime even at the winter pole. In this case, the atmospheric pressure is determined by the total mass of CO_2 which can sublime from Martian surface. When $p_s < 10^4$ Pa, on the other hand, CO_2 sublimes at the summer pole but condenses at the winter pole. This means that p_s could be determined by the balance between the CO_2 sublimation and condensation fluxes.

Taking into account the latent heat, the surface temperatures of the summer and winter poles become almost the same as the CO_2 condensation temperature. This is because the summer polar surface is effectively cooled down by the latent heat of CO_2 and the winter one is otherwise.

If we assume that the polar cap covers the latitudes higher than 45 degree, the sublimation and condensation fluxes of CO_2 are 6.70×10^8 kg s^{-1} and 8.29×10^8 kg s^{-1} under the present atmospheric pressure.

Figure 2 shows the surface temperature obtained from the snowball model. The surface temperature increases with p_s due to the atmospheric greenhouse effect. However, the temperature increase is smaller than that of standard model. This is because the absorbed solar flux is decreased at the equatorial region. However, when $p_s > 10^5$ Pa, CO_2 sublimation is expected to occur even in the winter pole. On the other hand, when 10^4 Pa $< p_s < 10^5$ Pa, CO_2 condensation occurs even in the equatorial surface. That is, this range of p_s could not exist stably due to global CO_2 condensation. When $p_s < 10^4$ Pa, CO_2 sublimes at the summer pole and condenses at the winter pole.

We estimate the polar cap formation time by dividing the observed mass of H_2O in the polar cap (1.2×10^{18} kg, Zuber et al., 1998) by H_2O deposition rate obtained from our climate model. As shown in Figure 3, the cap formation time decreases with p_s. This is because the mass of H_2O transport increases due to the rise of H_2O vapor content in the atmosphere. Under the present atmospheric pressure, the cap formation time is almost the same as that estimated from crater extinction rate (Plaut et al., 1988). On the other hand, when the surface is covered with ice globally, it takes very long time for the cap formation. In such circumstances, the present polar cap could

not form in 4.6 Gyr under the present atmospheric pressure.

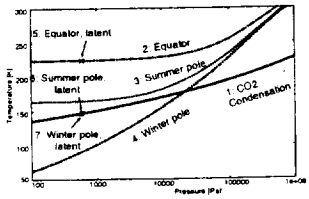

Figure 1: The surface temperature of equator (curve 2), summer pole (3), and winter pole (4) for various atmospheric pressure in standard model without considering the effect of CO_2 latent heat. The points 5 (equator), 6 (summer pole), and 7 (winter pole) represent a solution set for standard model including the effect of CO_2 latent heat.

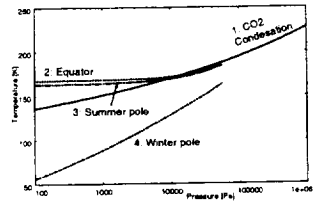

Figure 2: The result for snowball model. The curves from 1 to 4 represent as Figure 1.

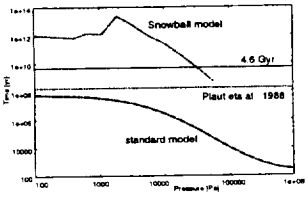

Figure 3: The timescale of the polar cap formation. The curves show the result for the standard and snowball models, respectively. The age of Mars, 4.6 Gyr, and the cap formation time calculated from the crater extinction rate on the polar cap surface (Plaut et al., 1988) are also indicated.

Conclusion

Sublimation and condensation of CO_2 on the polar caps could change the atmospheric mass over a time scale longer than seasons. Under the present albedo distribution, when $p_s < 10^4$ Pa, CO_2 sublimes from the summer polar cap and condenses onto the winter cap. The atmospheric mass could change over a long time because the sublimation and condensation rates are not necessarily the same. Supposing the initial condition of $p_s = 0$, the net sublimation (sublimation - condensation) is positive, so that the atmospheric pressure should increase. On the other hand, the net sublimation could be negative under the present atmospheric pressure. Thus, we vertually increase p_s from zero, there is a atmospheric pressure where net sublimation changes from positive to negative. We can consider this atmospheric pressure to be stable, which probably corresponds to the mean atmospheric pressure of present Mars. On the other hand, if $p_s > 10^4$ Pa, CO_2 sublimes globally. In this case, the atmospheric mass should continue to increase until all the surface CO_2 become released. The stable atmospheric pressure depends on solar flux absorbed by the polar cap surface and the areal extent of the polar cap. Therefore the changes in the obliquity, total mass of the surface volatiles, and frequency of the dust storm may shift the martian averaged atmospheric pressure to other stable points.

Under the present atmospheric pressrue and distribution of the surface albedo, our estimate of H_2O deposition rate on the polar cap is consistent with the value estimated from the crater extinction rate by Plaut et al.(1988). In this case the time scale over which the polar cap is renewed is estimated to be about 10^8 year.

Geological evidence suggests that H_2O was widespread on past Mars and the coverage of polar caps were larger than the present one. Large coverage of polar caps leads the climate colder. When the Martian surface is entirely covered with ice, global CO_2 condensation occurs under some atmospheric pressure range. Under such circumstances, H_2O mass flux is so small that it takes extremely long time for H_2O to gather to polar regions.

References

P. J. Gierasch and O. B. Toon, 1973, *J. Atmos. Sci.* **30**, 1502-1508.

J. B. Pollack *et al.*, 1987, ICARUS, **71**, 203-224. J. J. Plaut *et al.*, 1988, ICARUS, **75**, 357-377.

M. T. Zuber *et al.*, 1998, *Science*, **282**, 2053-2060.

CONTRACTION CRACKING AND ICE WEDGE POLYGONS IN MARS. K. Yoshikawa Water and Environmental Research Center, Institute of Northern Engineering, University of Alaska Fairbanks. POBox 755860 Fairbanks, AK 99775-5860, ffky@uaf.edu

Introduction: The Viking images reported gigantic polygonal patterns on the surface of Mars and, since then the origin of these polygons has been the subject of much discussion. The shape of these polygons are not only similar to terrestrial frost contraction crack polygons such as ice wedge polygons or soil wedge polygons, but the conditions under which these polygons develop also appears to be similar to those in permafrost regions of Earth. However, compared with terrestrial polygons, some of the Martian polygons are simply too big. In this paper we address the question, "How many of the Martian polygons developed by contraction cracking?" There is high potential for contraction cracks to form on the Martian surface. Thermal contraction cracking normally occurs in frozen, ice-rich materials with a high internal cohesive strength and generally produces polygonal patterns on the surface as the cracks intersect one another. A fracture is initiated when the surface soil contracts due to extreme cold causing a crack in the permafrost and ice growing there. In terrestrial polar regions, this cracking is commonly accompanied by growth of ice wedges or sand wedges as the contraction cracks reoccur along the same fracture plane every winter over hundreds or thousands of years. Many of the Mars Orbiter Camera (MOC) images of the polygonal patterns show a similar size and shape to the polygons in the tundra regions of the Arctic. Some of the Martian polygons probably developed through other means besides frost contraction cracking, such as magma cooling or desiccation. These pattern types can be distinguished by the size and shape of the polygons and the surface material characteristics.

Image analysis of the recent high resolution images from the Mars Orbiter Camera (MOC) [*1*] by the Mars Global Surveyor enables classification of the types of cracking in the polygonal pattern. Polygons are characterized by shape (form factor), size (equivalent to diameter), type of boundary (trough and/or ridge), and pattern of intersections (orthogonal or non-orthogonal systems). These polygonal characteristics respond to properties of the ground material, the temperature gradient, and the ice (water) content. It is possible to estimate the subsurface composition (soil properties) using thermal crack models.

Lachenbruch [2] used mechanics to develop detailed mathematical models that support the theory and provide a quantitative basis for amount of thermal tension, depth and rate of cracking, crack spacing, and origin of the polygonal network. He distinguished two polygonal systems: orthogonal and non-orthogonal. The ground material and thermal regime of polygons sites can be estimated by the space of the cracking and the pattern of the intersections of polygons and surface morphology. The goal of this study is to reveal the underground structure and the depth of the ice rich permafrost under the Martian polygons.

Image analysis: Martian polygons from MOC2 -150, -189, and Viking 538A08 images were used in this analysis. All of the polygonal patterns were digitized for calculating area, convex area, perimeter, equivalent diameter, form factor, roundness, aspect ratio, convexity, breadth, length, x-center of gravity, and y-center of gravity. Terrestrial polygons for an analogue study were obtained from aerial photographs of Barrow, Alaska and Longyearbyen, Svalbard, and Antarctic (Dry Valley) polygons. Three groups of polygons were classified (Figure 1). In the latter plot, the horizontal axis (size) is the equivalent circular diameter of the feature and the vertical axis (shape) is the form factor.

In both Arctic and Antarctic terrestrial contraction polygons, cracking is generally spaced from a few meters to about 20 meters apart. The two differentiating characteristics of Antarctic and Arctic polygons are the water (ice) content of the soil and the wedge materials. The material in Antarctic sand wedge polygons is fine sorted sand. On the other hand, Arctic tundra polygons are filled mainly with silt, clay, and peat. However, the sizes of the polygons (spacing of the cracks) are of a similar range. This uniformity in terrestrial polygons is caused by the similar temperature gradient in spite of various water contents and soil properties. The differences in ground materials have the greatest effect on the polygon shape (orthogonal or non-orthogonal). Non-orthogonal system polygons are those that have a preponderance of tri-radial intersections, commonly forming three obtuse angles of about 120°. It is suggested that they result from the uniform cooling of very homogeneous, relatively non-plastic media. In contrast, orthogonal systems of polygons are those that have a preponderance of orthogonal intersections. They are evidently characteristic of somewhat inhomogeneous or plastic media in which the stress builds up gradually with cracks forming first at loci of low strength or high stress concentration [2].

Conclusion: Three different sizes of the polygons have been classified on the Martian surface. The big-

ger diameter polygons (more than 10 km diameter) are unlikely to be formed through frost contraction cracking. Also, the shape of the bigger polygons is different from the mid size and smaller polygons. The mid size (100-200 m diameter) polygons developed on ice-rich permafrost under the dry surface material. The temperature gradient of the ice-rich permafrost layer is quite low, less than 1°K/m. The thickness of the dry surface materials is 2-3m at Martian arctic region (MOC2-150). The formation of the orthogonal system and double ridge geomorphology supports the theory that wedges consisting of ice or ice-rich materials form the boundaries of these polygons.

The smaller polygons are identical to terrestrial polygons in size and shape. The images from MOC2-189 are sand wedge polygons with nonorthogonal systems. Crater rims and inside craters support orthogonal systems that are likely to be ice-wedge polygons. The depth of the top of the ice-rich permafrost at MOC2-189 site starts at about 10m. The ejecta of the rampart crater have ice-rich materials and these polygons seemed to develop under current climate conditions.

The structure of the upper part of Martian ground has two different layers. There is dry material, which is never experiences contraction and expansion as a massive layer. The ejecta of the rampart crater has an ice-rich layer on the surface. There is also an ice-rich layer under the Martian dry surface layer. These ice-rich layers respond to thermal gradients by contraction cracking and developing polygonal patterns. The ground temperature fluctuation patterns will be similar to the terrestrial polar coastal region. The thickness of the dry surface material upon the ice rich layer will vary. Thinner sediments (< 3m) will support development of contraction polygons; however, thicker surface materials (> 8m) will not develop polygons in the Martian polar region.

References: [1] Malin, M.C., K. S. Edgett, M. H. Carr, G. E. Danielson, M. E. Davies, W. K. Hartmann, A. P. Ingersoll, P. B. James, H. Masursky, A. S. McEwen, L. A. Soderblom, P. Thomas, J. Veverka, M. A. Caplinger, M. A. Ravine, T. A. Soulanille, and J. L. Warren, (1999) NASA's Planetary-Photojournal. No. MOC2-150, 189. [2] Lachenbruch, A.H. (1962) Mechanics of thermal contraction cracks and ice-wedge polygons in permafrost.

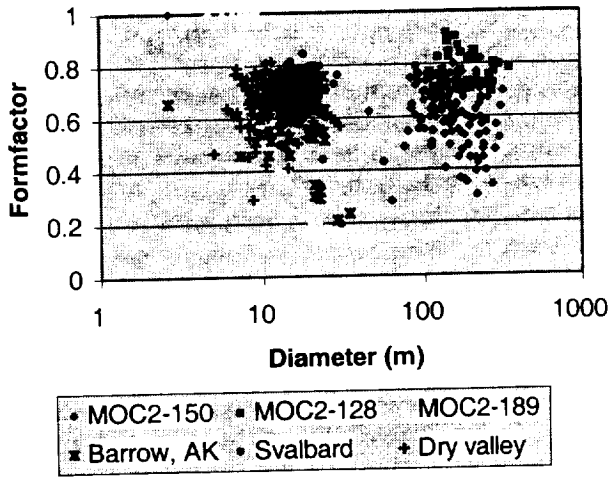

Figure 1. Size and shape of Martian and terrestrial polygons. Size is equivalent to diameter of area and shape is calculated from a form factor.

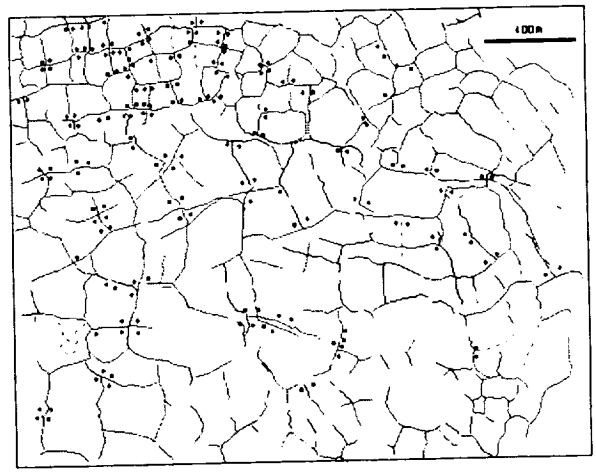

Figure 2. Interpretation of crack patterns of MOC2-150 image. Dots denote orthogonal intersections.

A SEARCH FOR UNCONFINED FLUVIAL OUTFLOW DEPOSITS ON MARS. J. R. Zimbelman and M. C. Bourke, Center for Earth and Planetary Studies, National Air and Space Museum, Smithsonian Institution, Washington, D.C. 20560-0315, U. S. A. (jrz@nasm.edu; mbourke@nasm.edu)

Introduction: Fluvial processes have been active during a large portion of Martian history, as evidenced by a variety of erosional features, ranging from concentrations of small channels to scour features generated by floods that affected enormous areas on Mars [e.g. 1]. Most research efforts prior to Mars Global Surveyor (MGS) focused on channelized reaches since these were some of the most convincing fluvial features on the planet [e.g. 2]. Since MGS reached its planned mapping orbit [3] in 1999, a new era of Mars exploration has been opened. The m-scale resolution of the Mars Orbiter Camera (MOC) [4], the precise elevation measurements of the Mars Orbiter Laser Altimeter (MOLA) [5, 6], and the compositional constraints derived from the Thermal Emission Spectrometer (TES) [7, 8] allows one now to search for deposits as well as erosional landforms. Here we describe our initial efforts at a search for deposits on Mars where flow was no longer confined within a topographic channel. We are using both new MGS and existing Viking data, in conjunction with field results of fluvial deposits in unconfined reaches from central Australia [9, 10] and elsewhere as analogues for the deposit characteristics to search for on Mars [11, 12].

Unconfined Fluvial Deposits: The arid interior of Australia has important similarities to the Martian landscape in terms of its arid climate, slow land surface process rates, the ancient history of its landforms, low overall relief, low sediment yield, occasional high magnitude floods, and extensive reworking of fluvial deposits by aeolian processes [11]. All catchments in the areas studied to date have unconfined channel reaches that terminate in the Simpson Desert [9-11].

The Australian deposits provide important information on what similar deposits on Mars might be like. Flood sediment is preserved in sediment stores along the channel bed and in marginal backwater areas, with textures varying from coarse gravel to mud with decreasing sediment size downstream [12]. Bedforms include large-scale (gravel and sand) longitudinal and expansion bar complexes and transverse bar fields [12] (Fig. 1). Suspended load deposits are emplaced in marginal areas where ponding occurred, preserved as clay pans in dune swales and slackwater deposits in tributary mouths [12]. The Australian floodout sediment characteristics are similar to deposits in braided streams, where discharge is variable and sediment load exceeds the local carrying capacity (Figs. 2, 3), and may also be comparable to the sandur plains of Iceland [13]. Such mixtures of particle sizes and depositional forms give us specific attributes to look for as we search the available Martian data sets for features potentially indicative of unconfined fluvial deposits.

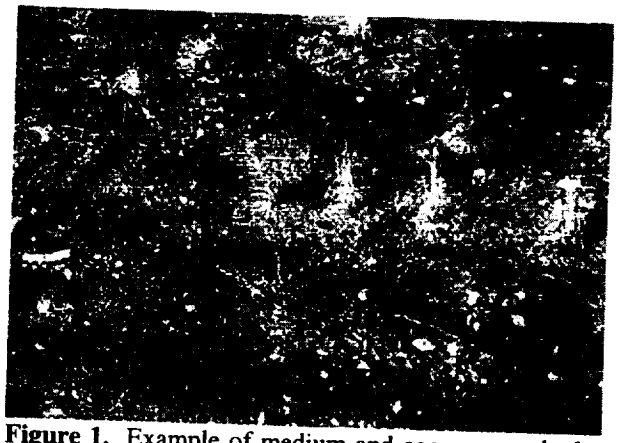

Figure 1. Example of medium and coarse gravels deposited by a large flood along the Simpson Desert margin by the Hale River, central Australia. MCB.

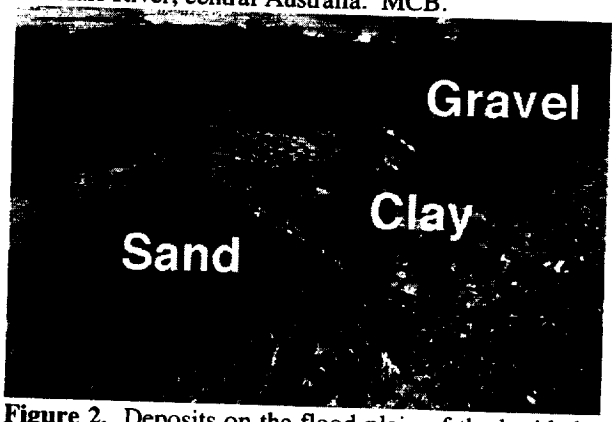

Figure 2. Deposits on the flood plain of the braided Gerstle River, Alaska, ~50 m from currently active channel. Deposits include gravel bars draped in places by sand and clay from subsequent low-energy flow. Scale is 20 cm long. N63°49.0', W144°55.43'. JRZ.

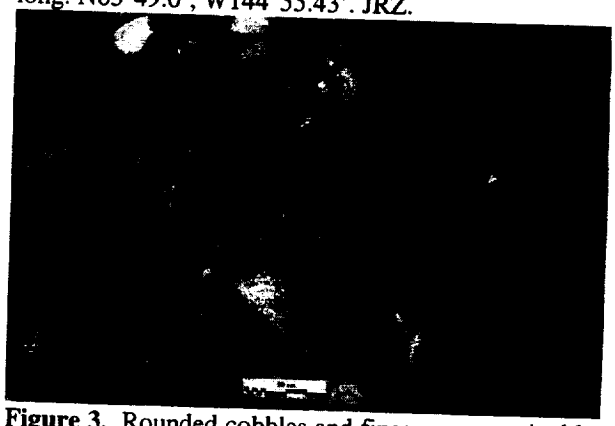

Figure 3. Rounded cobbles and fines on a marginal bar in the Matanuska River, Alaska. Scale is 20 cm long. N61°44.05', W148°41.98'. JRZ.

Searching for Unconfined Deposits on Mars: Viking data provide a global context in which we can look for candidate sites for unconfined deposits. Our preferred

locations are where visible channels terminate on a shallow slope and sediments are likely to occur, as the carrying capacity of the fluid decreases upon leaving the confined channel. An excellent site for this situation to occur is among the craters and isolated massifs in the Libya Montes (Fig. 4). The channel reaches in the Libya Montes were recently the site of a demonstration of the utility of combining Viking derived Digital Elevation Models (DEMs) with MOLA profile data, which allowed the morphometry of valley networks to be classified [14]. Unfortunately, Viking resolution is clearly insufficient to reveal the presence (or absence) of specific deposits beyond the mouths of channels like those in the Libya Montes.

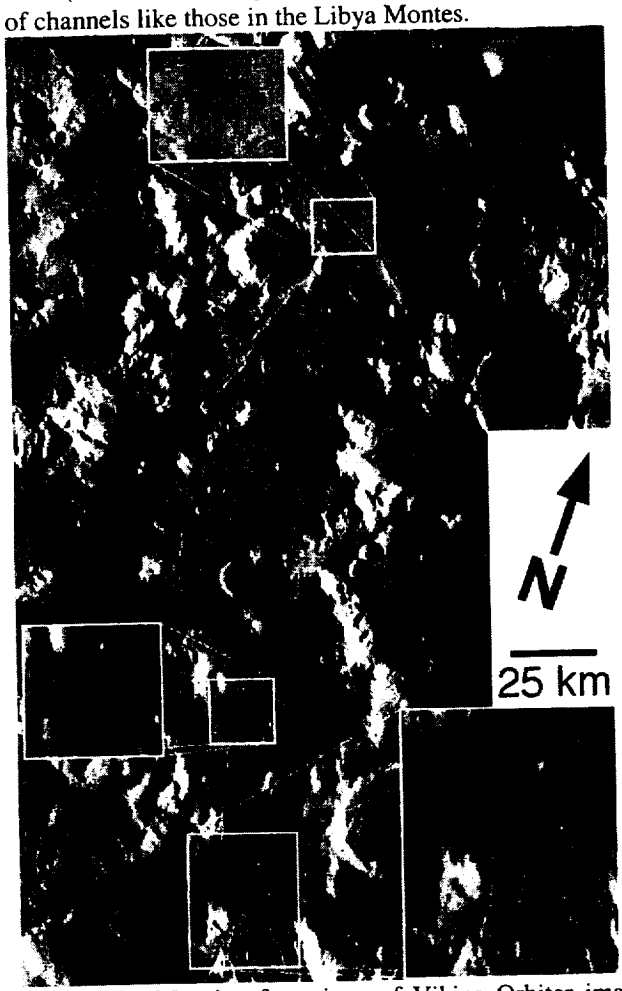

Figure 4. Mosaic of portions of Viking Orbiter images 377S77-78, showing an unnamed channel in the Libya Montes south of Isidis Planitia. 2X enlargements of two unconfined reaches are included. 230 m/pixel, centered near 0.5°N, 277.5°W.

We have yet to find a released MOC image that happens to cross the mouth of a small Martian channel like those in the Libya Montes. A new release of MOC images is scheduled to take place in April, 2000, when thousands of images from the mapping phase of the MGS mission become available. We are hopeful that these new images will include close-up views of areas beyond the mouths of Martian channels. However, we realize that the surface of Mars revealed to Viking and to MOC have very important differences [15], which will need to be factored in to the search.

The field analog characteristics of unconfined fluvial deposits provide additional clues as to what attributes might be detectable in other MGS data sets. The intimate mixture of particle sizes, ranging from gravel to clay within distance scales of only a few meters (e.g., Fig. 2), would not be resolvable even in the wonderful MOC images. However, such a particle size distribution may result in distinctive thermal emission properties, as were observed in the Viking Infrared Thermal Mapper (IRTM) data set [e.g., 16-18]. TES data are amenable to thermal inertia calculations [19, 20], and such data may prove helpful in identifying anomalous particle size abundances at the mouths of channels. Similarly, the meter-scale relief of the unconfined fluvial deposits also may produce MOLA pulse width scattering properties [e.g., 5] that could prove helpful in identifying candidate sites for such deposits. Our future efforts will involve looking for distinctive signals in all of the MGS data sets as they are released.

[This work is supported in part by NASA grant NAG5-1234 from the Mars Data Analysis Program.]

References: [1] Baker V. R. et al. (1992) *Mars* (H. H. Kieffer et al., Eds.), p. 493-522, U. of Arizona Press, Tucson. [2] Baker V. R. (1982) Univ. of Texas Press, Austin, 198 p. [3] Albee A. L. et al. (1998) *Science, 279*, 1671-1672. [4] Malin M. C. et al. (1998) *Science, 279*, 1681-1685. [5] Smith E. E. et al. (1998) *Science, 279*, 1686-1692. [6] Smith D. E. et al. (1999) *Science, 284*, 1495-1503. [7] Christensen P. R. et al. (1998) *Science, 279*, 1692-1698. [8] Bandfield J. L. et al. (2000) *Science, 287*, 1626-1630. [9] Bourke M. C. (1999) Ph.D. thesis, Australian Nat. Univ., Canberra. [10] Bourke M. C. and Pickup G. (1999) In *Fluvial Form* (A. J. Miller and A. Gupta, Eds.), pp. 249-271, Wiley. [11] Bourke M. C. and Zimbelman J. R. (1999) *LPS XXX*, Abs. #1804. [12] Bourke M. C. and Zimbelman J. R. (2000) *LPS XXXI*, Abs. #1393. [13] Rice J. W. and Edgett K. S. (1997) *J. Geophys. Res., 102(E2)*, 4185-4200. [14] Craddock R. A. and Cook A. C. (2000) *LPS XXXI*, Abs. #1625. [15] Edgett K. S. and Malin M. C. (2000) *LPS XXXI*, Abs. #1059. [16] Christensen P. R. (1982) *J. Geophys. Res., 87*, 9985-9998. [17] Ditteon R. (19820 *J. Geophys. Res., 87*, 10197-10214. [18] Christensen P. R. and Moore H. J. (1992) *Mars* (H. H. Kieffer et al., Eds.), p. 686-729, U. of Arizona Press, Tucson. [19] Mellon M. T. et al. (2000) *LPS XXXI*, Abs. #1898. [20] Pelkey S. M. et al. (2000) *LPS XXXI*, Abs. #1716.

STRUCTURE AND DYNAMICS OF THE POLAR REGIONS OF MARS FROM MGS TOPOGRAPHY AND GRAVITY. Maria T. Zuber[1,2], David E. Smith[2], Gregory A. Neumann[1,2] and Frank G. Lemoine[2]. [1]Department of Earth, Atmospheric and Planetary Sciences, Massachusetts Institute of Technology, Cambridge, MA 02139-4307 and [2]Laboratory for Terrestrial Physics, NASA/Goddard Space Flight Center, Greenbelt, MD 20771; zuber@tharsis.gsfc.nasa.gov.

MGS Topography and Gravity. The Mars Global Surveyor (MGS) spacecraft [1] has been engaged in systematic mapping of Mars since insertion into Mars orbit in September, 1997. The objectives of the MGS mission [1] are to globally map Mars as well as to quantify seasonal changes on the planet. MGS geophysical/geodetic observations of topography from the Mars Orbiter Laser Altimeter (MOLA) [2, 3] and gravity from the Radio Science investigation [4] are providing significant new insights on both static and time-varying aspects of the polar regions of Mars. These observeations have implications for polar processes on diurnal, seasonal and climatic timescales.

Thus far, MOLA has collected over 300-million precise measurements of Martian topography [5, 6] and cloud heights [7-9]. The instrument has also provided measurements of the width of the backscattered optical pulse and of the 1064-nm reflectivity of the Martian surface and atmosphere. The along-track resolution of MOLA ground shots is ~300 m and the across-track spacing in the polar regions is a maximum of about 4 km. The vertical accuracy of the topography is determined by the precision recovery of spacecraft orbits from the Radio Science investigation [10], which includes MOLA altimetry in the form of crossovers [11]. This accuracy is currrently ~1 m.

The gravity field is derived from X-band Doppler tracking with typical accuracy of 0.03 to 0.05 mm s^{-1} averaged over 10 s [10]. Current Mars gravity fields [6, 12, 13] are to approximately degree and order 80 but are interpretable to ~ degree and order 60 (spatial resolution <180 km), which represents an estimate of the approximate coefficient limit of a field that can be produced without a power law constraint [14] on the gravitational field inversion, which is commonly imposed for solution stability.

North Polar Region. The north polar cap (Fig. 1a) stands ~3 km above the surrounding terrain but lies within an ~5-km-deep hemispheric-scale depression that is contiguous with the northern lowland regions. The regional setting of the northern cap has significant implications for the global cycling of water [7] and the solar insolation [15] throughout Martian history. The northern cap displays complex structure, including deep spiral chasms that penetrate nearly to the level of surrounding terrains and are a sink for windblown dust. Small-scale layering visible at the margins of the cap from high-resolution imaging [16] is not resolved in MOLA altimetry.

Large areas of the ice cap are extremely smooth, with regional slopes over many tens of km of order 0.2°. Topography on spatial scales of kilometers has been observed in several areas to be smooth at the resolution of the instrument [3]. These surfaces also appear smooth at the spatial scale of the MOLA laser footprint (~100 m), as evidenced by the instrument's returned pulse width. Deposits outward of the main cap show regional slopes that are comparable to those observed in association with the central cap deposits, hut the outer terrains exhibit more small amplitude variation than the central cap deposits. Such topographic variance may be indicative of stagnant ice in the outlying deposits [7]. Gravity anomalies do not correlate well with the northern polar deposits [10], suggesting either a compensated load or complex subsurface structure [17].

South Polar Region. The southern ice cap (Fig. 1b) lies at an elevation 6-km higher than the northern cap due to the 3-km offset between Mars' center of figure and center of mass [5, 18]. The southern cap is visually much smaller than in the north, although south polar layered deposits extend much farther from the ice cap and exhibit a more asymmetric distribution than their northern counterparts [5]. The residual ice, which persists throughout the seasonal cycle, is offset from the present rotational pole toward 35° - 40° E such that the pole does not fall within the residual ice deposit. The topography is highest in the south polar region within the residual ice deposits (87° S, ~10° E), where a broad dome is present at one end of the cap (Fig. 1b). The relief of the southern polar cap is comparable to that of the northern cap [5].

The area of probable ice-rich material greatly exceeds the region of residual ice that is apparent from images. This conclusion is based first on the existence of distinctive plateau regions that correlate with layered terrain units (Fig. 1b), as would be expected if the layers were deposited on cratered terrain. A well-defined gravity anomaly correlates with the southern layered deposits [10]. In addition, impact craters within the plateaus share unusual geometric properties with counterparts in the north polar region [19] that are observed to have formed in an ice-rich substrate. This similarity suggests that significant portions of the south polar ice cap may be buried beneath mantling dust deposits.

Finally, profiles across the northern and southern caps (Fig. 2) show a correspondence in shape that argues for a similarity in composition and suggests that the southern cap may have a significant water ice component [20].

Volatile Inventory. The polar caps represent one of the two major reservoirs of present-day volatiles on Mars with the other being the subsurface regolith. The layered terrains are the only reservoir that can be reasonably be estimated on the basis of present-day observations. Best estimates for volumes, accounting for the possible effect of lithospheric flexure [5, 7, 17], are given in Table 1.

The CO_2 Cycle. Over the course of the Martian year as much as one-third of the atmosphere exchanges with the polar caps. This results in a change in polar topography, a re-distribution of planetary mass [21], and a change in the rotational angular momentum [22]. Effort is underway to measure these changes.

References: [1.] Albee A. A. et al. (1998) *Science, 279,* 1671-1672. [2.] Zuber M. T. et al. (1992) *J. Geophys. Res., 97,* 7781-7797. [3.] Smith D.E. et al., (1998) *Science, 279,* 1686-1692. [4.] Tyler G. L. (1992) *J. Geophys.. Res., 97,* 7759-7779. [5.] Smith D. E. et al. (1999) *Science, 284,* 1495-1503. [6.] Zuber M. T. et al. (2000) *Science, 287,* 1788-1793. [7.] Zuber M. T. et al., (1998) *Science, 282,* 2053-2060. [8.] Pettengill G. H. and P. G. Ford (2000) *Geophys. Res. Lett., 27,* 609-612. [9.] Neumann G.A. et al. (2000) *LPSC XXXI.* [10.] Smith, D. E. et al. (1999) *Science, 286,* 94-97. [11.] Rowlands D.D. et al. (1999) *Geophys. Res. Lett., 26,*1191-1194. [12.] Sjogren W. L. et al. (1999) *Eos Trans. Am. Geophys. Un. 80.* [13.] Lemoine F.G. et al. (2000) manuscript in preparation. [14.] Kaula W. M. (1966) *Theory of Satellite Geodesy*, Blaisdell, Waltham. [15.] Arrell J. R. and M. T. Zuber (2000) this issue. [16.] Malin, M. C. et al. (1998) *Science, 279,* 1681-1885. [17.] Johnson C. L. (2000) *Icarus,* in press. [18] Smith D. E. and M. T. Zuber (1996) *Science, 271,* 184-188. [19.] Garvin J. B. et al. (2000) *Icarus,* in press. [20.] Durham W.B. et al. (1999) *Geophys. Res. Lett., 26,* 3493-3496. [21.] Smith D. E. (1999) *J. Geophys. Res., 104,* 1885-1896. [22] Smith D. E. et al. (1999) *Eos Trans. Am. Geophys. Un. 80.*

Table 1. Polar Layered Terrain Volumes from MOLA

Mars Layered Terrain	Value*
North#	1.2 to 1.7 x 10^6 km^2
South&	2 to 3 x 10^6 km^2

* Ranges into account possible contribution of lithospheric flexure.

From [7 and 17]. & From [5]

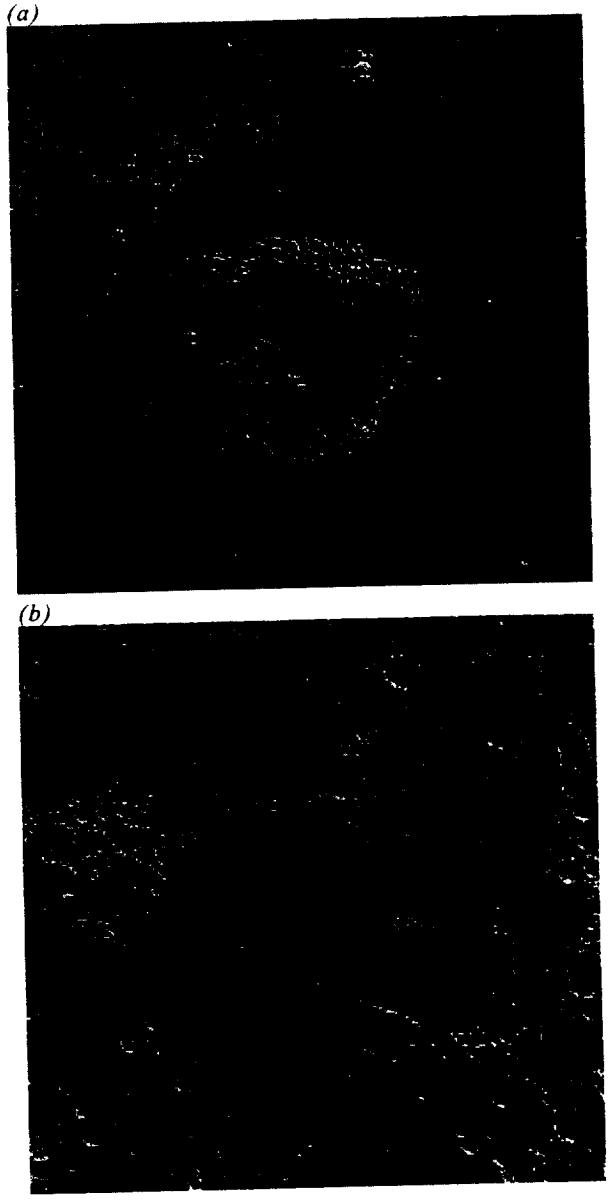

Figure 1. Topographical images of the *(a)* northern and *(b)* southern polar regions of Mars from MOLA. Images include regions from ±70• to the poles.

Figure 2. Topographic profiles across the *(a)* northern and *(b)* southern polar layered terrains from MOLA.

MORPHOLOGY OF MARS NORTH POLAR ICE CAP. H. J. Zwally[1], A. Fountain[2], J. Kargel[3], L. Kouvaris[1], K. Lewis[4], D. MacAyeal[5], T. Pfeffer[4], and J. L. Saba[1], [1]Code 971, NASA Goddard Space Flight Center, Greenbelt, MD 20771 (jay.zwally@gsfc.nasa.gov), [2] Portland State University, Portland, OR 97207, [3] U. S. Geological Survey, Flagstaff, AZ 86001, [4] INSTAAR, University of Colorado, Campus Box 450, Boulder, CO 80309, [5] Geophysical Sciences, University of Chicago, Chicago, IL 60637

The northern ice cap of Mars consists of a parabolic dome centered within 13 km of the pole, plus an arm-like ridge extending from the dome between about 135° and 225° E [1]. Chasma Boreale lies between the dome and the extended ridge. The base of the dome is approximately elliptical with a major axis of 1100 km along the 90° E to 270° E direction and minor axis of 700 km along 0° E to 180°. The heights of the dome and the extended ridge are respectively 2900 m and 1700 m above the surrounding basin (Figure 1.). Least-squares fitting of a parabola through height profiles of the dome along longitudes 90° to 270° and 0° to 180° gives an elliptic-paraboloid equation for the dome: $Z\,(m) = 2800 - (X-x)^2/113.6 - (Y-y)^2/50.3$, where X is the 90° to 270° axis, x = 9.90 km, y = 13.32 km, and the slightly-different fitted heights for the two axes are averaged. The center of the dome is shifted 13.32 km from the pole along 0° longitude and 9.90 km along 90° longitude. Typical mean surface slopes on the ice cap are the order of 1/100 (0.6°). A small central portion of the cap, about 100 km by 200 km, extends in elevation about 200 m above the parabolic shape of the cap.

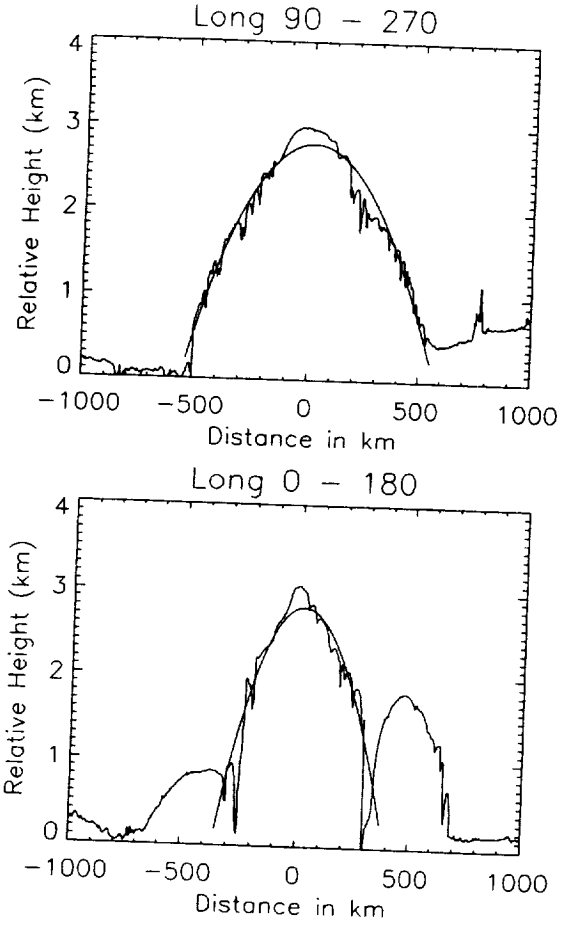

Figure 1. Elevation profiles of Mars North Polar ice cap from gridded Mola data with parabolic fit.

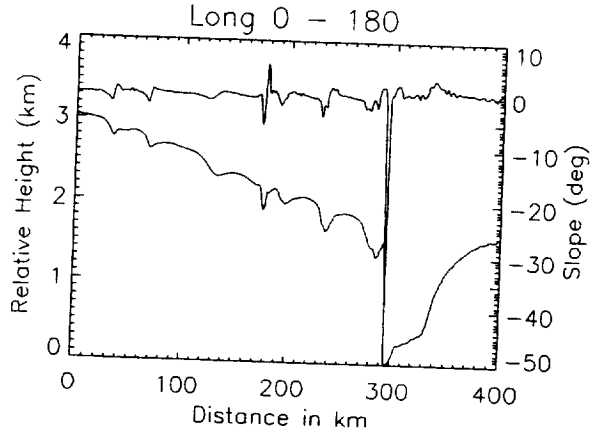

Figure 2. Elevation profile and surface slope along 180° longitude from the pole through Chasma Boreale.

Superimposed on the basic parabolic shape of the ice cap are troughs (Figure 2 and 3) with characteristic depths of 200 to 500 m and lengths of several hundred kilometers. The troughs in the ice cap have often been described as spiral features, but their orientation actually tends to be more concentric with respect to the center of the dome. Although the troughs do in places deviate by as much as 45° from being perpendicular to radial lines from the pole, particularly near the edge of the cap, some of the spiral-like appearance of the troughs is due to the basic elliptical shape of the dome. Therefore, the predominate direction of the troughs tends to be perpendicular to the large-scale surface slope. In addition, troughs on the inner part of the dome are typically closed depressions with inward-directed slopes at both ends.

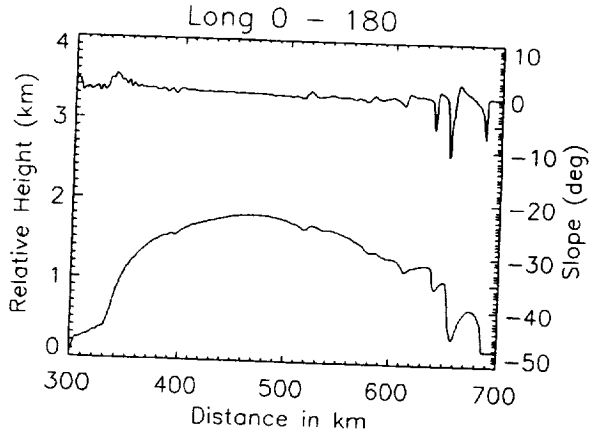

Figure 3. Elevation profile and surface slope along 180° longitude from Chasma Boreale to edge of ice cap.

MORPHOLOGY OF MARS NORTH POLAR ICE CAP. H. J. Zwally, et al

In contrast, the troughs on the arm-like extended ridge are oriented primarily across the ridge in a more north-south direction (azmuth about 135°). The higher elevations and the north-facing side of the of the ridge are the smoothest parts of the whole ice cap and relatively free of troughs (Figure 3). Typical slopes on the south-facing sides of the troughs are 5° to 20°, in contrast to 1° to 4° on the more rounded north-facing sides. The steepness of the north-facing slopes is consistent with enhanced ablation due to greater solar insolation from the south. In general, the morphology of the ice cap is consistent with a dynamic ice cap in which ice flow is balanced in part by ablation at the margins and net accumulation in the central regions.

References: [1] Zuber M. T. et al. (1998) *Science*, 282, 2053-2060.